Mass Spectroscopy in Physics Research

U. S. Department of Commerce

National Bureau of Standards

Circular 522

UNITED STATES DEPARTMENT OF COMMERCE • Charles Sawyer, *Secretary*
NATIONAL BUREAU OF STANDARDS • A. V. Astin, *Director*

Mass Spectroscopy in Physics Research

Proceedings of the NBS Semicentennial Symposium on
Mass Spectroscopy in Physics Research
Held at the NBS on September 6, 7, and 8, 1951

National Bureau of Standards Circular 522
Issued January 23, 1953

For sale by the Superintendent of Documents, U. S. Government Printing Office
Washington 25, D. C. – Price $1.75 (Buckram)

Preface

All the papers presented at the Symposium on Mass Spectroscopy in Physics Research are included in the present volume and in most cases a fairly complete record of the discussions following the papers is given. Professor A. O. Nier arranged the successful closing session on experimental methods; the informality, so effective at the time, made it difficult later to assemble for this volume a complete record of this session. Fortunately, many of the speakers edited the notes which were tape-recorded, inserting illustrations where necessary and in a few cases submitting complete manuscripts covering the subject matter of their talks. Those participating in the discussions did not have an opportunity to edit their remarks except in isolated instances and the reader should keep this in mind.

Many persons at the National Bureau of Standards and in other institutions aided by suggestions, by active participation in organizing the conference, and in preparing this volume for publication. Of course, the Mass Spectroscopy Symposium Committee was particularly active in this. The committee was composed of the following members: L. T. Aldrich, Department of Terrestrial Magnetism, Carnegie Institution of Washington, Washington, D. C.; A. O. C. Nier, University of Minnesota; V. H. Dibeler, F. L. Mohler, R. E. O'Dette, Hugh Odishaw and H. Sommer, of the National Bureau of Standards.

J. A. Hipple, *Chairman,*
Mass Spectroscopy Symposium Committee.

Contents

Page
Foreword ---- III
Preface ---- IV
1. Precision mass spectroscopy and theory of dispersion, by J. Mattauch ---- 1
2. A double-focusing mass spectrometer, by Alfred O. C. Nier ---- 29
3. Accuracy of mass spectrographic isotope mass measurements, by H. Ewald ---- 37
4. A discussion of masses derived from recent doublet and Q measurements, by K. T. Bainbridge ---- 47
5. The use of mass spectrography in the study of nuclear shell structure, by Henry E. Duckworth ---- 53
6. On the substandards of atomic mass, by K. Ogata and H. Matsuda ---- 59
7. Masses of hydrogen, carbon, and some nuclides of medium mass, by Thomas L. Collins ---- 67
8. New doublet measurements, by J. Mattauch and R. Bieri ---- 71
9. Some recent investigations in electron and ion optics, by N. Svartholm ---- 75
10. Increase of the sensitivity of mass spectrographs by concentration of all beams in one point, producing a spectral line, by Richard F. K. Herzog ---- 85
11. Improved focusing in combinations of radial electric and magnetic fields, by H. Hintenberger ---- 95
12. High resolution in conventional 180° mass spectrometers, by Clifford E. Berry ---- 99
13. The influence of the stray field on the focusing qualities of a magnetic sector field, by W. Paul ---- 107
14. The nonmagnetic radio-frequency mass spectrometer, by Willard H. Bennett ---- 111
15. Time-of-flight mass spectrometer, by E. E. Hays, P. I. Richards, and S. A. Goudsmit ---- 115
16. The mass synchrometer, by Lincoln G. Smith ---- 117
17. Work on cyclotron resonance at the National Bureau of Standards, by J. A. Hipple and H. Sommer ---- 123
18. Present status of isotopic abundances, by Alfred O. C. Nier ---- 131
19. Mass spectrometer for the measurement of small differences in isotope abundance ratios, by S. Epstein ---- 133
20. Instrumental problems encountered in mass spectrometer isotope analysis of water samples, by H. W. Washburn, C. E. Berry, and L. G. Hall ---- 141
21. The mass spectrometer as a tool for studying nuclear reactions, by Mark G. Inghram ---- 151
22. Electromagnetic separation of noble gas isotopes and their use in some nuclear and spectroscopic experiments, by Jørgen Koch ---- 165

Page
23. High-intensity electromagnetic isotope separator, by J. Kistemaker and C. J. Zilverschoon 179
24. Measurement of trace quantities of uranium and lead in minerals and meteorites, by David C. Hess, Harrison Brown, Mark G. Inghram, Clair Patterson, and George Tilton 183
25. Further results on the double beta decay of Te^{130}, by Richard J. Hayden and Mark G. Inghram 189
26. Ionization by electron impact, by Homer D. Hagstrum 193
27. Mass spectrometer effects at higher pressures, by Francis J. Norton 201
28. Observation of ion dissociation in a parabola spectrograph, by A. Henglein and H. Ewald 205
29. Direct measurement of appearance potential and ionization probability using a mass spectrometer, by R. E. Fox, W. M. Hickam, T. Kjeldaas, Jr., and D. J. Grove 211
30. Mass spectra of heavy hydrocarbons, by M. J. O'Neal 217
31. Space charge and error in mass spectrometric measurement, by E. W. Becker and W. Walcher 225
32. Mass spectrometric studies in solids, by R. H. Plumlee 229
33. The distribution of S^{34} in nature, by H. G. Thode and J. Macnamara 235
34. The influence of fractionizing and viscosity effects in mass spectrometric gas handling systems, by J. Kistemaker 243
35. The mass spectral patterns of isotopic molecules, by O. Schaeffer 249
36. Session on experimental methods 255

1. Precision Mass Spectroscopy and Theory of Dispersion

By J. Mattauch [1]

1. Introduction

As is well known, mass spectroscopy was established at about the same time (1918–19) by F. W. Aston [1] [2] and by A. J. Dempster [2]. Aston in his apparatus succeeds in getting velocity focusing of the ion rays by taking advantage in a very simple way of the *prism* effect of the deflecting fields, while Dempster, using rays of homogeneous energy, employs a special case (previously known) of the *lens* effect of a magnetic field. Progress in precision measuring of masses was next made by K. T. Bainbridge [3] (fig. 1) who inserted a velocity filter in front of a Dempster setup thereby admitting into the analyzing magnetic field only rays of homogeneous velocity. A similar arrangement with a rather huge magnet was built later by his pupil E. B. Jordan [4] (fig. 2). However, these and similar arrangements [5] have been abandoned today by reasons of intensity. A better solution has been found by making full use of the lens, as well as of

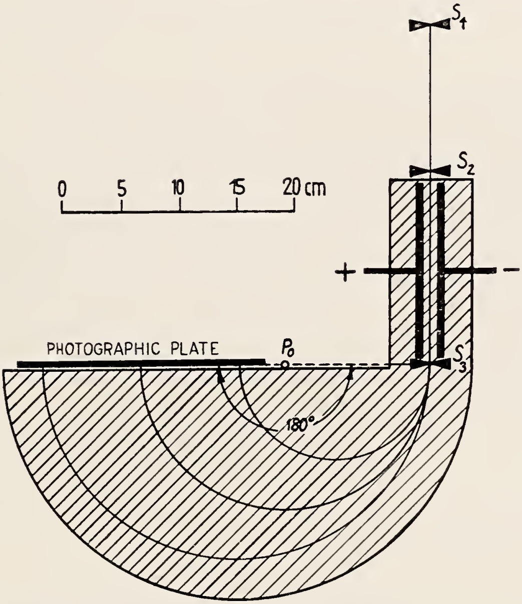

FIGURE 1. *Arrangement of K. T. Bainbridge (1933)*

---

[1] Max Planck Institut für Chemie, Mainz, Germany.
[2] Figures in brackets indicate the literature references on p. 27.

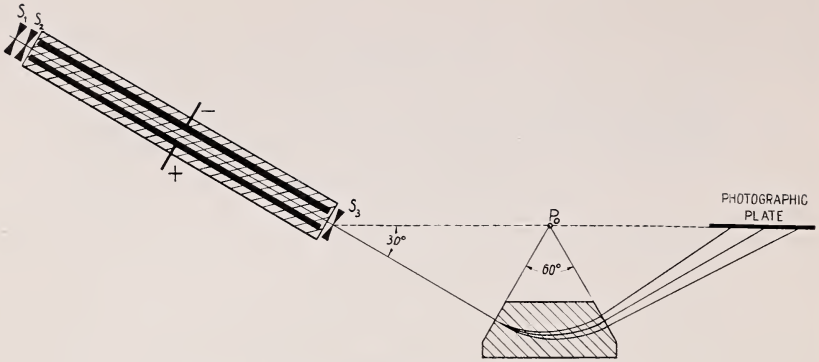

FIGURE 2. *Arrangement of E. B. Jordan (1941).*

the prism effect of the deflecting fields yielding the mass spectrographs with double focusing (as the term is understood by us [6]), of which up to now five different types have been realized. These shall be the main objects of our present consideration.

2. Lens and Prism Effect—Double Focusing

For deflection of the ion beam in double-focusing arrangements, only two different kinds of fields have been used up to now that will interest us here; they are (a) a homogeneous magnetic field of constant field strength B_0 having straight boundaries of the pole shoes, and (b) a radial electrostatic field for which the relation between radius vector r and potential $V(r)$ is $r\,[\partial V(r)/\partial r]=T_0$ where T_0 is a constant. The lens and prism effect of such fields was computed in a general way for the first time by R. Herzog [7] making the assumption that the angle of aperture of the pencil of rays is small so that it may be neglected in the second order; furthermore, only rays are considered which travel in the plane perpendicular to the magnetic and parallel to the electric fields (cylinder lenses); finally, the influence of the stray (edge) fields is disregarded [8].

In the following representation we differentiate quantities of the conjugate spaces of objects and images by ′ and ″ respectively; they may be exchanged in all image equations since it is always permitted to reverse the direction of the rays. Where it is necessary, quantities and equations relating to the magnetic or electric field shall carry the subscript m or e, respectively.

2.1. Lens Effect

We consider pencils of rays of ions having all the same mass M_0, the same charge e, and the same velocity v_0.

a. Magnetic Field

Within the field the orbits are circles of the same radius,

$$r_m=\frac{M_0 v_0}{eB_0}, \tag{1}$$

and outside of it they are the straight tangents of these circles. One finds the image point A'' of an object point A' according to a construction given by L. Cartan [9]; this is shown in figure 3 from which

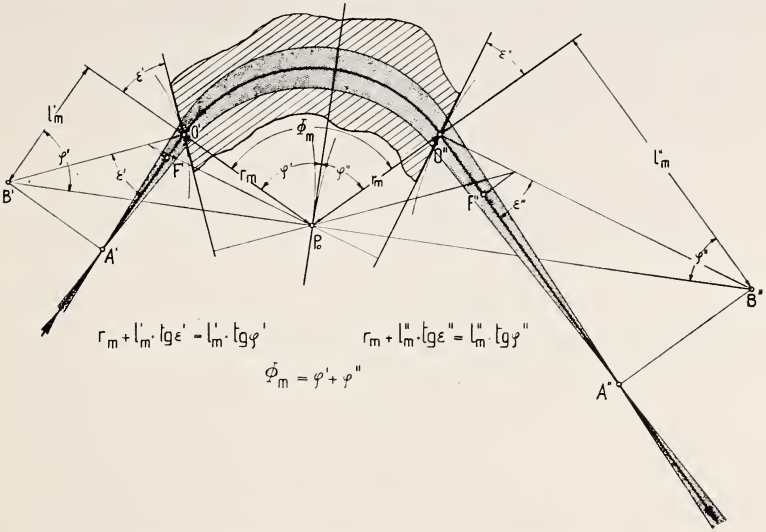

FIGURE 3. *Lens effect (Cartan's construction).*

also the denotations may be gathered. That a pencil of rays diverging from A' is reunited to a first degree of approximation at A'' is proved by a simple geometrical consideration based on the following facts: The centers of the circular orbits are lying to a first degree of approximation on the segments of arc with radii $B'P_0$ and $B''P_0$ touching each other at P_0; the segments of arc with radii $B'O'$ and $B''O''$ are touching the field boundaries, and the angles of intersection between the radii of these arcs and the tangent rays going into, and coming out of, the field are equal to a first degree of approximation to ϵ' and ϵ'' respectively; finally, the sine of the angle $O'A'B'=\pi/2$ and $O''A''B''=\pi/2$ does not change to a first approximation in the neighborhood of this value.

From figure 3 one easily reads the relations [10]:

$$\Phi_m=\varphi'+\varphi''; \quad \tan\varphi'=\tan\epsilon'+\frac{r_m}{l'_m}, \quad \tan\varphi''=\tan\epsilon''+\frac{r_m}{l''_m}. \qquad (2m)$$

Elimination of the auxiliary quantities φ' and φ'' yields the lens equation which one suitably writes in the form

$$(l'-g')(l''-g'')=f^2, \qquad (3)$$

from which then Herzog's formulas for f_m, g'_m and g''_m may be read directly. The meaning of the denotations is understood by looking at the schematic drawing of figure 4 from which one also gathers the lateral enlargement,

$$-\frac{b''}{b'}=\frac{a''}{a'}=\frac{f}{l'-g'}=\frac{l''-g''}{f}. \qquad (4)$$

Wherever one is concerned with the paths of rays in the field-free spaces only, one does not need to be disturbed by the fact that in figure 4 only one principal plane is drawn, though our fields in general are the analogs of "thick" lenses (two principal planes).

We shall need only the distances of the focal points F from the points of entrance and exit O' and O'' of the mean ray, which one gets easily from eq (2m). If, for instance, one moves A' into infinity ($l'_m \rightarrow \infty$, $\varphi' = \epsilon'$) then A'' lies in the focal point ($l''_m = g''_m$, $\varphi'' = \Phi_m - \epsilon'$) and one gets

$$\frac{r_m}{g''_m} = \tan(\Phi_m - \epsilon') - \tan \epsilon''. \tag{5m}$$

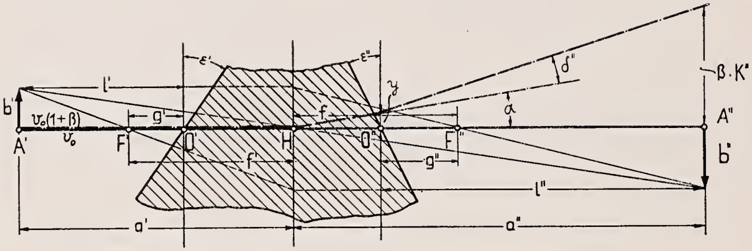

FIGURE 4. *Lens and prism effect (schematically).*

b. Electrostatic Field

We shall deal only with fields for which

$$\epsilon' = \epsilon'' = 0. \tag{6}$$

We obtain a singular radius $r = r_e$ by establishing the potential

$$V(r_e) = 0. \tag{7}$$

The equilibrium of forces states that

$$M_0 v_0^2 = re \frac{\partial V(r)}{\partial r} = e\,T_0. \tag{8}$$

Parallel rays of mass M_0, charge e, and velocity v_0 entering perpendicularly to the field boundary would therefore travel on concentric circular orbits if they would retain their kinetic energy. Lens effect comes about here by the fact confirmed by observation [11] that at the field boundaries the rays have to surmount a jump of potential which, if we limit ourselves to the "neighborhood" of r_e,

$$r = r_e(1+\xi), \quad \xi \ll 1 \tag{9}$$

reduces the kinetic energy and therefore lessens the velocity to

$$v = v_0(1-\xi). \tag{10}$$

Herzog's calculations show that one obtains the position of the focal points and focal length by replacing everywhere in the formulas valid for the magnetic field (for instance, eq (2m) and (5m))

$$r_m \text{ by } \frac{r_e}{\sqrt{2}}, \text{ and } \Phi_m \text{ by } \sqrt{2}\Phi_e. \tag{11}$$

In particular, one gets for the position of the focal points from eq (6)

$$\frac{r_e}{g_e''}=\frac{r_e}{g_e'}=\frac{r_e}{g_e}=\sqrt{2}\tan(\sqrt{2}\Phi_e). \tag{5e}$$

2.2. Prism Effect

One considers two parallel rays (mean rays of two pencils) the ions of which, though having the same mass M_0 and same charge e, show a proportional difference of velocity $\beta \ll 1$.

a. Magnetic Field

We denote by r and φ the polar coordinates of a particle of velocity $v=v_0(1+\beta)$, P_0 being the pole; $r=r_m$ then is the circular orbit of the particles of velocity v_0. If both rays enter the field with common tangent at the point O' (fig. 5), they won't be affected by the size of ϵ'. However, since according to eq (1) the radii of the two circular orbits differ by βr_m, the always positive distance y of corresponding points on the same radius vector will change with period 2π having a maximum $2\beta r_m$ at the polar angle $\varphi=\pi$ as is easily understood from figure 5. Therefore,

$$y=r-r_m=2\beta r_m \sin^2\frac{\varphi}{2}. \tag{12}$$

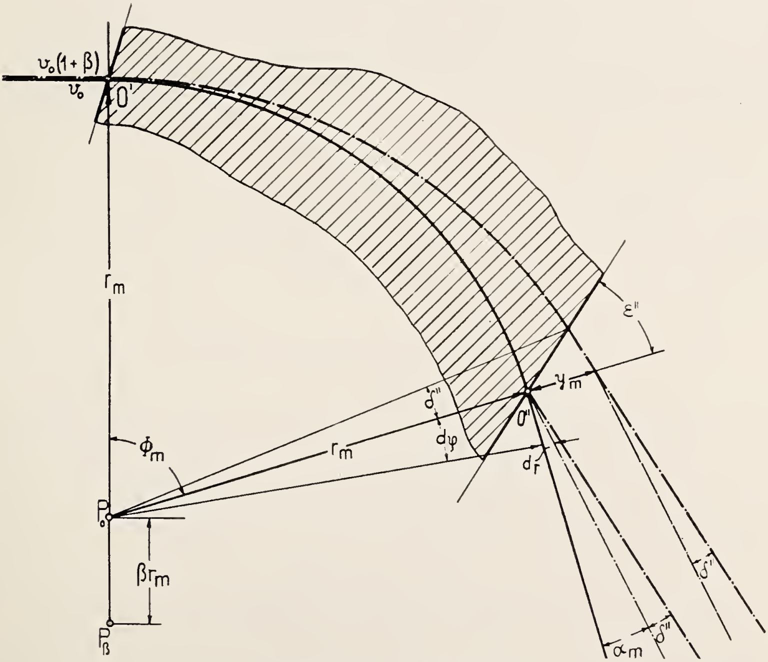

FIGURE 5. *Prism effect.*

At the exit of the field the distance between both rays is therefore

$$y_m = \beta r_m (1 - \cos \Phi_m). \tag{13m}$$

Were $\epsilon''=0$ the angle between the tangents of the two orbits would then be

$$\alpha_m = \frac{1}{r_m}\left(\frac{dr}{d\varphi}\right)_{\varphi=\Phi_m} = \beta \sin \Phi_m \tag{14m}$$

as is easily seen from figure 5. If $\epsilon'' \neq 0$ the angle

$$\delta'' = \frac{y_m \tan \epsilon''}{r_m} = \beta(1-\cos \Phi_m) \tan \epsilon'' \tag{15m}$$

has to be added as one sees from the same figure. In figure 4 this prism effect is shown schematically. We add that one can achieve by the special choice

$$\epsilon'' = \frac{1}{2}\Phi_m - \frac{\pi}{2}, \text{ i.e., } \tan \epsilon'' = -\operatorname{ctn} \frac{1}{2}\Phi_m \text{ that } \delta'' = -\alpha_m \tag{16}$$

so that both rays emerge parallel.

By velocity dispersion we understand the distance $\beta K''_m$ at which both rays hit a screen placed vertically to the direction of the rays at the position of the image. As one sees at once (fig. 4),

$$\beta K''_m = y_m + l''_m(\alpha_m + \delta''). \tag{17m}$$

b. Electrostatic Field

Besides the replacement of eq (11) one has to replace according to Herzog's calculations:

$$y_m \text{ by } \frac{y_e}{\sqrt{2}}, \tag{18}$$

since one is dealing with a length. One gets at once the corresponding formulas

$$y_e = \beta r_e [1 - \cos(\sqrt{2}\Phi_e)] \tag{13e}$$

$$\alpha_e = \frac{1}{r_e}\left(\frac{dr}{d\varphi}\right)_{\varphi=\Phi_e} = \beta\sqrt{2} \sin(\sqrt{2}\Phi_e). \tag{14e}$$

Since here, on account of eq (6), the additional prism effect vanishes,

$$\delta'' = 0, \tag{15e}$$

they yield the velocity dispersion

$$\beta K''_e = y_e + l''_e \alpha_e. \tag{17e}$$

2.3. Double Focusing

If, in front of the magnetic field analyzing the rays into the different masses, one inserts a radial electrostatic field as energy filter, one has to take the image by the electric lens (intermediate image) as object of the magnetic lens

$$b''_e = b'_m \tag{19}$$

in order to get on the photographic plate or on the receiving slit the final image b''_m of the entrance slit $s = b'_e$; furthermore one has to take care that

$$l''_e = \Delta - l'_m, \tag{20}$$

if Δ denotes the distance between the end of the electric and the beginning of the magnetic deflection. Moreover, to get the final image b''_m of the magnetic lens independent of a velocity difference β, the velocity dispersions of the two bundles thought of as originating from corresponding points of the slit and of the final image have to be equal at the position of the intermediate image, i. e.,

$$\beta K''_e = \beta K'_m. \tag{21}$$

According to eq (17e) and (17m) the condition for double focusing reads therefore explicitly

$$y_e + l''_e \alpha_e = y_m + l'_m(\alpha_m + \delta') \tag{22}$$

in which the values given by eq (13e), (14e), (13m), and (14m) are still to be inserted.

For the design of a double-focusing apparatus this condition is necessary but not sufficient. A series of data may be chosen at liberty; in the choice of the realized types, practical points of view or even historical reasons seem to have been decisive. In general, condition (22) can be fulfilled for one mass only since y_m depends on the radius r_m which in turn depends on mass. However, by a special choice of data to which we shall return later, one succeeds in getting it independent of mass.

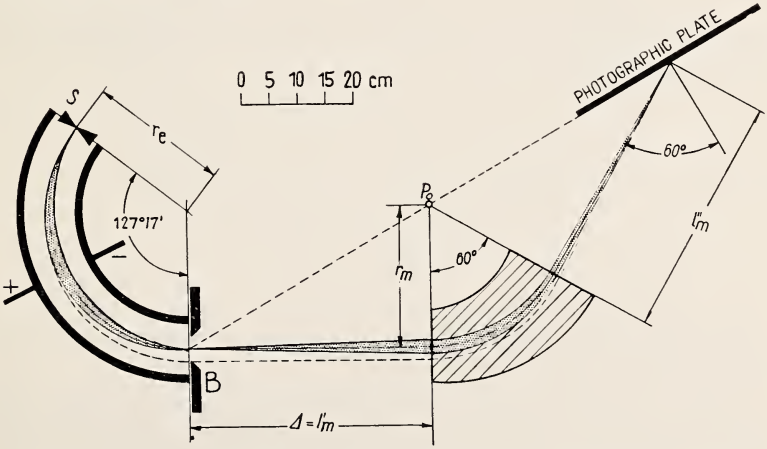

FIGURE 6. *Arrangement of K. T. Bainbridge and E. B. Jordan (1936).*

3. The Realized Types of Double-Focusing Mass Spectrographs

We turn now to a discussion of the actually completed mass spectrographs. To be able to compare them later with relation to their resolving power, mass dispersion, etc., we shall also compute for each one the expressions for K'_e and K''_m decisive for these properties.

3.1. Double Focusing for One Mass Only

For the sake of simplicity one has used here only magnetic fields for which, as with the electric fields, eq (6) is always fulfilled. Moreover, in all cases symmetrical image formation was chosen in one or both of the fields (i.e., $\varphi' = \varphi'' = \frac{1}{2}\Phi_m$ or $\varphi' = \varphi'' = \frac{1}{2}\sqrt{2}\,\Phi_e$). Therefore according to eq (2m) and (11),

$$l'_m = l''_m = \frac{r_m}{\tan\frac{1}{2}\Phi_m} \text{ respectively } l'_e = l''_e = \frac{r_e}{\sqrt{2}\tan(\frac{1}{2}\sqrt{2}\,\Phi_e)}. \tag{23}$$

Besides in this case according to eq (17m, e), (13m, e), (14m, e), and (15m, e),

$$K'_m = K''_m = 2r_m \text{ and } K'_e = K''_e = 2r_e. \tag{24}$$

One special case of each of these three possibilities has been realized:

Type 1. *K. T. Bainbridge and E. B. Jordan* (*1936*) [12] (fig. 6) select the most simple case of symmetrical image formation in both fields; in particular they chose $\Phi_e = \sqrt{2}\,\pi/2$ (i.e., according to eq (2m) and (11) $l'_e = l''_e = 0$), $\Phi_m = \pi/3$ and $l'_m = l''_m$.

Slit and intermediate image therefore are situated respectively at the beginning and at the end of the electric field; the distance between the two fields according to eq (20) is

$$\Delta = l'_m \tag{25}$$

With the help of eq (24) the condition (21) for double-focusing takes here the very special form

$$K'_e = K''_e = 2r_e = 2r_m = K'_m = K''_m. \tag{26}$$

The ratio of the singular radii is therefore 1 and according to eq (2m) one has to take care that

$$r_e = r_m = \frac{l'_m}{\sqrt{3}} = \frac{l''_m}{\sqrt{3}}. \tag{27}$$

The same set-up was copied in 1940 by T. Asada, et al. [13] and technically improved recently by K. Ogata and H. Matsuda [14] maintaining the original dimensions.

Type 2. *A. J. Dempster* (*1935*) [15] *and H. E. Duckworth* (*1950*) [16] (fig. 7) start from the well-known magnetic field of $\Phi_m = \pi$ for which according to eq (2m) $l'_m = l''_m = 0$ and which Dempster for a long time used for his mass-spectrometric research work; additionally they chose r_e as well as $\Phi_e = \pi/2$ with $\tan\varphi' = 1/(0.15\sqrt{2})$.

Therefore, according to (2m) and (11), the slit and intermediate image are situated at

$$l'_e = \frac{r_e}{\sqrt{2}\tan\varphi'} \text{ and } l''_e = \frac{r_e}{\sqrt{2}\tan\left(\sqrt{2}\frac{\pi}{2}-\varphi'\right)}. \tag{28}$$

Besides, the distance between the fields has to be

$$\Delta = l''_e. \tag{29}$$

With the help of eq (13e), (14e), (15e), as well as (24) and (28), the double-focusing condition (22) takes the special form

$$K''_e = r_e\left[\left(1-\cos\sqrt{2}\frac{\pi}{2}\right)+\sin\sqrt{2}\frac{\pi}{2}\operatorname{ctn}\left(\sqrt{2}\frac{\pi}{2}-\varphi'\right)\right] = 2r_m = K'_m = K''_m \tag{30}$$

yielding numerically

$$r_m = 1.146\ r_e \text{ or } r_e = 0.873\ r_m. \tag{31}$$

For K'_e one gets in the same way

$$K'_e = r_e\left[\left(1-\cos\sqrt{2}\frac{\pi}{2}\right)+\sin\sqrt{2}\frac{\pi}{2}\operatorname{ctn}\varphi'\right] = 1.775\ r_e. \tag{32}$$

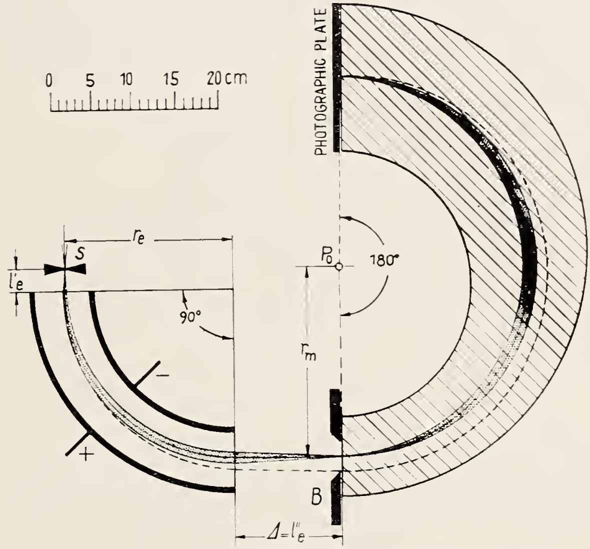

FIGURE 7. *Arrangement of A. J. Dempster (1935).*

J. A. Hipple, et al. [17], are working with an alteration of Dempster's set-up; however, the data chosen have not yet been published.

Type 3. *A. O. Nier, et al. (1949–51)* [18] (fig. 8) keep r_m constant for all masses using as a measure for the masses the voltage (that is, the constant T_0) on the radial electrostatic field by the change of which the masses are brought to the receiving slit one after the other. Simultaneous double focusing for all masses is rendered unnecessary

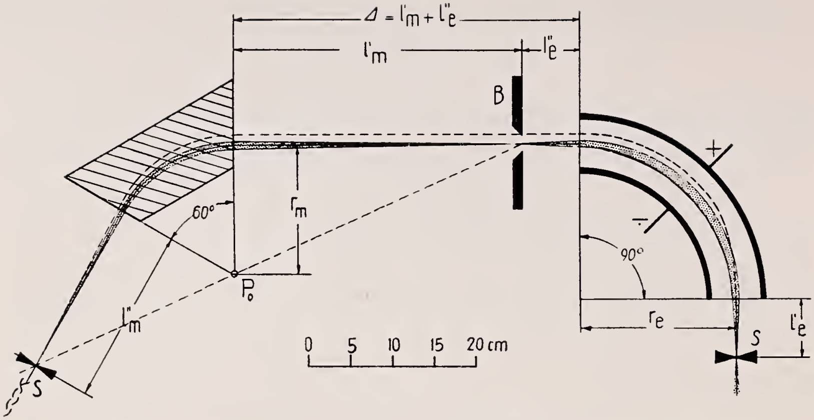

Figure 8. *Arrangement of A. O. Nier and T. R. Roberts (1949–1951).*

here. They chose $\Phi_e = \pi/2$ with symmetrical image formation $l'_e = l''_e$ and the angle of deflection $\Phi_m = \pi/3$ used by Nier in his mass-spectrometric work to which r_m and $\tan\varphi' = 0.438$ are being fixed. According to Nier this special choice of asymmetric image formation ought to yield direction-focusing of the second order (cf. the paper given at this symposium by H. Hintenberger, p. 95).

According to eq (23), the slit and intermediate image are positioned at equal distances from the beginning and from the end of the electric field:

$$l'_e = l''_e = \frac{r_e}{\sqrt{2}\tan\left(\sqrt{2}\,\frac{\pi}{4}\right)}. \tag{33}$$

Besides, one has to make

$$l'_m = \frac{r_m}{\tan\varphi'} \text{ and } \Delta = l'_m + l''_e. \tag{34}$$

In the same way one gets for the distance of the receiving slit from the end of the magnetic field

$$l''_m = \frac{r_m}{\tan\left(\frac{\pi}{3} - \varphi'\right)} = \frac{1 + \sqrt{3}\tan\varphi'}{\sqrt{3} - \tan\varphi'}\, r_m. \tag{35}$$

Using eq (13m), (14m), (15m) and (24), (34) one arrives at the following special form of the double-focusing condition:

$$K'_e = K''_e = 2r_e = \tfrac{1}{2} r_m (1 + \sqrt{3}\operatorname{ctn}\varphi') = K'_m, \tag{36}$$

which yields numerically

$$r_e = 1.238\ r_m \text{ or } r_m = 0.808\ r_e. \tag{37}$$

Finally, using in addition eq (33) one gets

$$K''_m = \tfrac{1}{2} r_m \left[1 + \sqrt{3}\operatorname{ctn}\left(\frac{\pi}{3} - \varphi'\right)\right] = 1.677 r_m. \tag{38}$$

3.2. Double Focusing for All Masses

As one perceives in (22), the influence of the term y_m hindering the realization of this wish is getting the smaller the larger l'_m is chosen. Dividing eq (20) and (22) by l'_m and proceeding to the limit $l'_m \rightarrow \infty$ one gets

$$\frac{l''_e}{l'_m} = -1 \text{ and } \alpha_e + \alpha_m + \delta' = 0 \tag{39}$$

where the radius r_m of the orbit in the magnetic field which depends on mass does not appear any more. Eq (39) thus makes its début at first as *one* condition the observance of which grants double focusing for all masses. It accomplishes, however, more than that.

Substituting the values of eq (14e), (14m) and (15m) one gets explicitly

$$-\sqrt{2} \sin (\sqrt{2}\Phi_e) = \sin \Phi_m + (1 - \cos \Phi_m) \tan \epsilon'. \tag{40}$$

Since Φ_e (the angle of deflection of a cylindrical condenser correspondingly cut up) and ϵ' (all rays enter the magnetic field in the "neighborhood" of O') are the same angles for all masses, the same has also to hold for Φ_m, the angle of deflection in the magnetic field. In figure 9 one sees at once that then by reasons of similarity ϵ'' also has to have the same value for all masses. The back boundary of the field, therefore, becomes a straight line through O' inclined to the direction of the incoming rays by the angle ψ. On it all points of exit O'' of the rays are lying. Introducing this angle ψ instead of Φ_m one reads from figure 9 that

$$\Phi_m = 2\psi = \text{constant and also } \psi - \epsilon'' = \frac{\pi}{2} \tag{41}$$

has to hold. Thus ϵ'' has become just the angle of eq (16) for which $\delta'' = -\alpha_m$, that is, rays differing in velocity only emerge parallel to each other just as do rays which differ only in mass. That one follows from the other is seen already from eq (1) because the radius of curvature is determined by the momentum Mv only.

The transition $l'_m \rightarrow \infty$ has the effect that the distance Δ from the end of the electric to the beginning of the magnetic field becomes indeterminate and may be chosen ad libitum. Above all it means that rays of the same mass M_0, charge e, and velocity v_0 are traveling parallel to each other between the two fields; there is, therefore, no real intermediate image. For this purpose the slit of which one wishes to construct the final image has to be placed at the focal point of the electric lens and the photographic plate must be lodged in the geometric locus of the focal points F, that is, in the focal line, of the magnetic lens. One has to take care that

$$l'_e = g_e = \frac{r_e}{\sqrt{2}} \operatorname{ctn} (\sqrt{2}\Phi_e) \tag{42}$$

and that

$$l''_m = g''_m = r_m \sin \psi \cos \psi \, [1 - \tan \psi \tan (\psi - \epsilon')]; \tag{43}$$

the special values are derived from eq (5e) and (5m) using eq (41). Since g''_m is proportional to r_m, all the focal points F are also situated

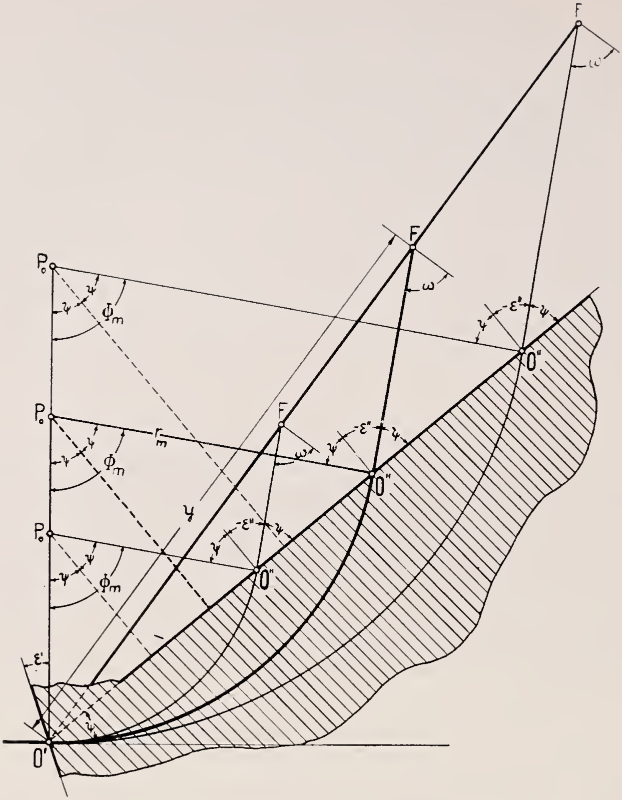

FIGURE 9. *Double-focusing for all masses (general case).*

on a straight line through O' in which the plate has to be lodged; that is also easily seen from figure 9 since with Φ_m constant the path of the rays repeats itself similarly for each mass. The position of the plate in a straight line through the entrance point O' of the rays into the magnetic field has, moreover, the advantage as we shall see later that it is the only one where the mass scale can be expressed in a finite form.

On the other hand, it is easy to see that the demand of double focusing for all masses with straight back boundary of the pole shoes and straight focal line can be fulfilled only if both straight lines go through O', if Φ_m is constant for all masses, and if the paths of homogeneous rays are parallel between the fields [19]. Therefore condition expressed in eq (39) or eq (40) is also the only one possible to grant double focusing for all masses if we use the two kinds of fields to which we have limited our considerations and if, simultaneously, we ask for a straight back boundary of the pole shoes and a straight focal line.

To characterize the position of the plate we introduce the angle ω (fig. 9) under which the oncoming rays are inclined to the perpendicular of the plate. The sine theorem applied to the triangles $O'O''F$ having the angles $\psi+\omega-(\pi/2)$, $\pi-\psi$ and $(\pi/2)-\omega$ yields

$$y:g''_m:2r_m \sin\psi=\sin\psi:-\cos(\psi+\omega):\cos\omega \tag{44}$$

if y denotes the distance $\hat{O}'F$. With the help of eq (43) we get thus the two relations

$$\frac{1}{2}\,y=\frac{\sin^2\psi}{\cos\omega}\,r_m \text{ and } \tan\psi\,\tan(\psi-\epsilon')+2\tan\psi\,\tan\omega=3. \tag{45}$$

With it we write our condition (40) in the form

$$-\sqrt{2}\sin\left(\sqrt{2}\Phi_e\right)=2\sin\psi\cos\psi\,(1+\tan\psi\,\tan\epsilon')=\frac{\tan\psi}{2-\tan\psi\,\tan\omega}, \tag{46}$$

which, when choosing a special apparatus, makes it easier to dispose of two of the three constant angles, ψ, ϵ', and ω in any way desired.

For all mass spectrographs of this kind

$$K_e'=r_e \tag{47}$$

and

$$K_m''=2r_m\sin^2\psi=y\cos\omega, \tag{48}$$

as one sees at once from eq (17e), (13e), and (14e) taking notice of eq (42), and from eq (17m), (13m) taking notice of eq (16) and (45) respectively.

Type 4. *C. Reuterswärd (1943)* [20] (fig. 10) chooses $\epsilon'=\psi$ and wishes an angle of incidence not larger than $\omega=65°$ whereby $\operatorname{ctn}\omega=0.467$ is fixed. Then it follows from eq (45) that

$$\tan\psi=\frac{3}{2}\operatorname{ctn}\omega \text{ or } \psi=\epsilon'=35°,\ \Phi_m=70°. \tag{49}$$

The condition (46) for double focusing of all masses thus becomes:

$$-\sqrt{2}\sin\left(\sqrt{2}\Phi_e\right)=2\tan\psi=3\operatorname{ctn}\omega \text{ whence } \Phi_e=-58° \tag{50}$$

follows. Finally one computes from (48) and (49)

$$K_m''=\frac{18\operatorname{ctn}^2\omega}{4+9\cdot\operatorname{ctn}^2\omega}\,r_m=0{,}658r_m. \tag{51}$$

The special case $g_m''=0$ may lay claim to particular interest because the rays emerging from the magnetic field do not have to pass the stray field; the photographic plate may be placed in the homogeneous part of the field. For this purpose there must be:

$$\tan\psi\,\tan(\psi-\epsilon')=1, \text{ i. e., } 2\psi-\epsilon'=\frac{\pi}{2} \tag{52}$$

as one sees from (43). Furthermore, according to (45) also

$$\tan\psi\,\tan\omega=1, \text{ i. e., } \psi+\omega=\frac{\pi}{2} \tag{53}$$

has to be fulfilled. With that the condition (46) becomes

$$-\sqrt{2}\sin(\sqrt{2}\Phi_e)=\tan\psi=\operatorname{ctn}\omega=\frac{1+\tan\frac{\epsilon'}{2}}{1-\tan\frac{\epsilon'}{2}}. \tag{54}$$

Now one has a free choice of only one of the three angles, ψ, ω, and ϵ'. For instance, if one wishes to build the apparatus having the steepest angle of incidence of the rays onto the plate, one sees at once from (54) that ctn ω reaches its maximum value if one chooses

$$\sqrt{2}\Phi_e=-\frac{\pi}{2},\ \Phi_e=-\frac{\pi}{2\sqrt{2}}. \tag{55}$$

With that condition, (54) determines the angles ψ, ω, ϵ'. Thus

$$\tan\psi=\operatorname{ctn}\omega=\sqrt{2},\ \tan\frac{\epsilon'}{2}=\frac{\sqrt{2}-1}{\sqrt{2}+1}. \tag{56}$$

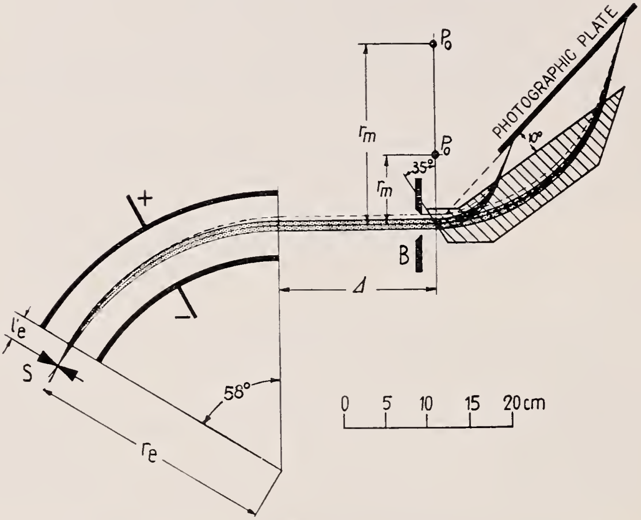

FIGURE 10. *Arrangement of C. Reutersward (1943).*

Type 5. *J. Mattauch and R. Herzog (1934–36)* [21] (fig. 11) in the apparatus built by them choose $g_m''=0$ and also $\epsilon'=0$. The condition (54) of double focusing for all masses then simplifies thus:

$$-\sqrt{2}\sin(\sqrt{2}\Phi_e)=\tan\psi=\operatorname{ctn}\omega=1. \tag{57}$$

Whence follows

$$\psi=\omega=\frac{\pi}{4},\ \Phi_m=\frac{\pi}{2},\ \sqrt{2}\Phi_e=-\frac{\pi}{4},\ \Phi_e=-\frac{\pi}{4\sqrt{2}}. \tag{58}$$

With that we get from eq (48) very simply

$$K_m''=r_m. \tag{59}$$

The same set-up was copied in the original dimensions by H. Lichtblau [22] for H. Wahl and by H. Ewald [23], the latter improving it technically a great deal. It was rebuilt on a smaller scale by A. E. Shaw and W. Rall [24] and is at present being built on a larger scale by J. M. Delfosse and by K. T. Bainbridge, the latter employing a linear enlargement of about eight times.

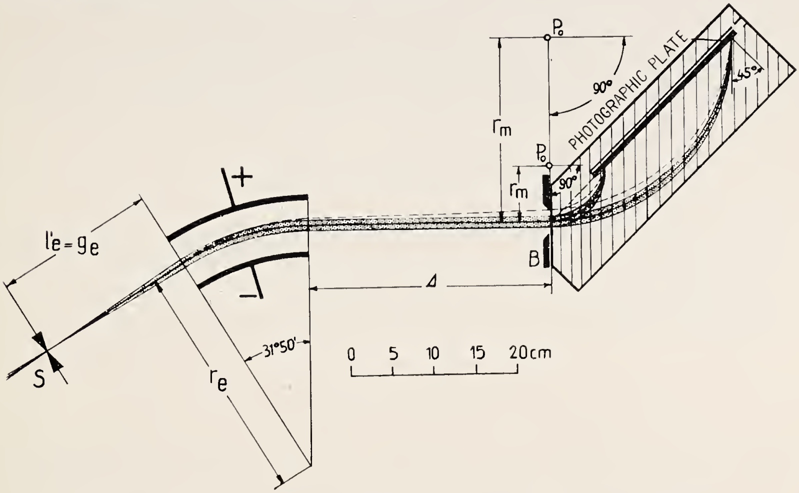

Figure 11. *Arrangement of J. Mattauch and R. Herzog (1934).*

4. Comparison of the Double-Focusing Mass Spectrographs

If we compare the different arrangements discussed in the preceding section under types 1, 2, 3, 4, and 5, the lateral enlargement, the mass-dispersion, and the resolving power are decisive above all. One obtains them all at once from the notions of velocity dispersion introduced in the first section. If the condition for double focusing required the equality of the velocity dispersion *after* the electric and *before* the magnetic field, it is the same quantities *before* the electric and *after* the magnetic field which will matter now. For our considerations these intuitive notions therefore prove to be of great usefulness and applicability.

(a) *The lateral enlargement* we get at once if we start from the intermediate image and follow up in both directions (i. e., towards the electric field and towards the magnetic field) the paths of the mean rays (lying so to speak one upon another) of two pencils of velocity v_0 and $v_0\,(1+\beta)$. In the cases where the intermediate image is removed to infinity, any point between the two fields may be taken as the starting point. Both these rays have by definition the distance $\beta K_e'$ at the slit of width s and the distance $\beta K_m''$ at the final image of width b_m''. Now, if we chose β such that $\beta K_e' = s$, it is exactly the purport of double focusing that with the proportional velocity difference chosen in this way $\beta K_m'' = b_m''$ has to hold also. To achieve just this, velocity focusing with simultaneous focusing of ray directions (i. e., double focusing) was introduced. For all double focusing arrangements, the lateral enlargement, therefore, is given generally by

$$\frac{b''_m}{s}=\frac{K''_m}{K'_e}. \tag{60}$$

In table 1 it is entered for the types with intermediate image in terms of the ratio r_m/r_e (here constant), as well as with its absolute value, using the corresponding equations (26), (27), and (30), (32), (34) and (36), (38), (37), respectively.

With arrangements having double focusing for all masses, r_m may have any value, and one states here better the range of y which is covered by the photographic plate. Using eq (47) and (48), for these types we have

$$\frac{b''_m}{s}=\frac{r_m}{r_e}(1-\cos\Phi_m)=\frac{y}{r_e}\cos\omega. \tag{61}$$

Table 1 contains the corresponding entries for both the realized types of this kind using eq (51) and (59) respectively; for the absolute values the numerical values of table 2 have been anticipated.

(b) *The line-width dy* on the photographic plate is given by

$$dy=\frac{b''_m}{\cos\omega}=\frac{K''_m}{K'_e\cos\omega}s \tag{62}$$

and with the arrangements having double focusing for all masses by

$$dy=\frac{r_m}{r_e}\frac{(1-\cos\Phi_m)}{\cos\omega}s=\frac{y}{r_e}s. \tag{63}$$

The corresponding values for the different types realized may be gathered from table 1 where, for type 3, $\cos\omega=1$ is assumed.

(c) *The mass-dispersion.* By that one understands (similar to the notion of velocity dispersion) the distance of two lines on the plate due to two rays of the same velocity v_0 which, however, possess a proportional mass difference $\mu=(M-M_0)/M_0$. For $\mu\ll1$ this distance will be equal to μD where D, which we are going to compute, is called the dispersion coefficient. Frequently the dispersion for 1 percent mass difference ($\mu=0.01$) is stated and denoted by $D_{1\%}$. It is, therefore, to a close approximation:

$$D_{1\%}=0.01\ D. \tag{64}$$

It is a matter of perfect indifference whether the proportional change of the radius of curvature in the magnetic field (which in section 2.2 led to the prism-effect and to the derivation of eq (17m) for K''_m) is caused by a proportional change β of velocity or by a proportional change μ of mass. We therefore get the corresponding expressions for the mass dispersion as is seen immediately from eq (1) and (8) by putting $\beta=\mu$ in the case of a velocity filter in front of the magnetic field or by putting $\beta=\frac{1}{2}\mu$ in the case of an energy filter in front of the magnetic field and, of course, dividing by $\cos\omega$. For all double-focusing mass spectrographs possessing an energy filter in the form of a radial electrostatic field, therefore, quite generally,

$$D=\frac{K''_m}{2\cos\omega}. \tag{65}$$

For the arrangements having double focusing for all masses we have especially

$$D = \frac{(1-\cos \Phi_m)}{2 \cos \omega} r_m = \frac{1}{2} y. \tag{66}$$

This relation holds also for type 2 described in section 3 (fig. 7) since here also the two straight lines for the back boundary of the field and for the position of the plate (which coincide here just as they do in type 5) go through the point of entrance O' of the rays into the magnetic field (fig. 9). However, sharp lines are to be found in this type at *one* position on the plate only as determined by eq (31) and (45).

The mass dispersion is fixed, as is seen from eq (65) and (66), by the size of the available magnet, according to which r_m, Φ_m, and ω have to be adjusted. The attainment of large dispersion is, therefore, mainly a question of money. In table 1 the mass dispersion is entered for the different types in terms of r_m.

(d) *The resolving power M/dM* is defined as that value of $1/\mu$ for which the distance of the lines on the plate is equal to the line-width. From eq (65) and (62) one gets thus for all double-focusing mass spectrographs

$$\frac{M}{dM} = \frac{K_e'}{2s} \tag{67}$$

and substituting the value of eq (47) especially for arrangements with double focusing for all masses

$$\frac{M}{dM} = \frac{r_e}{2s}. \tag{68}$$

The resolving power is, of course, the larger the smaller one is able to make the width s of the slit. Otherwise, as is worthy of note, it depends on the dimensions of the radial electrostatic field only and, especially in arrangements with double focusing for all masses, it is simply proportional to the singular radius r_e. Since in the latter cases r_e may be chosen independently of r_m, the attainment of large resolving power is here mainly a question of skill and of the size of the grains of the photographic plates which forms a lower limit for the width of the lines. In table 1 we note it for the different types in terms of r_e/s.

(e) *The energy filtered.* We still wish to compute the percentage dW/W_0 of the mean kinetic energy $W_0 = \frac{1}{2} M_0 v_0^2$ of the ions which passes a diaphragm of opening d placed at the position of the intermediate image. If the one edge of the diaphragm is hit by a ray of velocity v_0 then all rays may pass that have a proportional velocity difference smaller than a maximum value β_m with which the other edge of the diaphragm is hit. Here is by definition

$$\beta_m K_e'' = d \text{ and } \beta_m = \frac{1}{2} \frac{dW}{W_0}, \tag{69}$$

whence follows the percentage in question,

$$\frac{dW}{W_0} = \frac{2d}{K_e''}. \tag{70}$$

TABLE 1.

Type of apparatus	Lateral enlargement ($b''_m s$)	Line-width (dy)	Dispersion-coefficient (D)	Resolving power (M/dM)	Energy filtered (dW/W_0)	Length of ion path (L)
Real intermediate image:						
1. *Bainbridge and Jordan (1936)*	$1.000\, r_m/r_e=1$	$2.000s$	$2.000\, r_m$	$1.000\, r_e/s$	$1.000\, d/r_e$	$6.733\, r_e=6.733\, r_m$
2. *Dempster (1935)*	$1.127\, r_m/r_e=1.291$	$1.291s$	$1.000\, r_m$	$0.887\, r_e/s$	$0.873\, d/r_e$	$5.144\, r_e=4.490\, r_m$
3. *Nier et al. (1949/51)*	$0.839\, r_m/r_e=0.677$	$0.677s$	--------	$1.000\, r_e/s$	$1.000\, d/r_e$	$6.059\, r_e=7.502\, r_m$
Double focusing for all masses:						
4. *Reuterswärd (1943)*	$0.658\, r_m/r_e=0.20\text{–}0.48$	$(0.47-1.14)s$	$0.776\, r_m$	$0.500\, r_e/s$	$1.143\, d/r_e$	$2.21\, r_e = 7.37\, r_m$ to $2.95\, r_e = 4.02\, r_m$
5. *Mattauch and Herzog (1934/36)*	$1.000\, r_m/r_e=0.23\text{–}0.87$	$(0.33-1.23)s$	$0.707\, r_m$	$0.500\, r_e/s$	$1.505\, d/r_e$	$2.67\, r_e = 11.36\, r_m$ to $3.74\, r_e = 4.22\, r_m$

TABLE 2.

Type of apparatus	r_e	r_m	y	Δ	s	d	dy	D	M/dM	dW/W_0	L
Real intermediate image:	*cm*	*cm*	*cm*	*cm*	*microns*	*mm*	*microns*	*cm*		%	*cm*
1. *Bainbridge and Jordan (1936)*	25.4	25.4	--------	44.0	5–8	0.08	10–16	50.8	50,800–31,750	0.32	171.0
2. *Dempster (1935)*	20.07	22.99	45.98	12.2	25.4	(1.0)	33	22.99	7,010	(4.35)	103.2
3. *Nier et al. (1949/51)*	18.87	15.24	--------	41.4	25	2.5	17	--------	7,550	13.3	114.3
Double focusing for all masses:											
4. *Reuterswärd (1943)*	30.0	9.0 –22.0	14.0–34.2	19.0	34	2.0	16–39	7.0 –17.1	4,410	7.6	66.3– 88.4
5. *Mattauch and Herzog (1934/36)*	28.00	6.58–24.26	9.3–34.3	29.0	2	0.5	0.7–2.4	4.65–17.25	70,000	2.7	74.7–102.5

In the cases where the intermediate image is removed to infinity (arrangements with double focusing for all masses), the position of the diaphragm may be chosen arbitrarily. However, one will place it most suitably at the point of entrance O' of rays into the magnetic field. The computation of K_e'' for the purpose of eq (69) can then also be made according to eq (17e), if, instead of l_e'', the arbitrary value Δ of the distance between the electric and the magnetic field is used. In table 1 dW/W_0 is given in terms of d/r_e; again for the last two lines the numerical values of Δ/r_e of table 2 had to be anticipated.

(f) *The total length* L of the path of the rays from the slit to the plate or to the receiving slit,

$$L=l_e'+r_e\Phi_e+\Delta+r_m\Phi_m+l_m'', \tag{71}$$

may be of some interest, lastly. It is entered in table 1 in terms of r_e and of r_m, as it is easily computed with the help of the relation given in section 3, types 1, 2, and 3 for the last two lines again the values of table 2 had to be used.

If, as was done in table 1, the properties used for comparison are related to the same size of the radii r_m and r_e, then, especially with regard to dispersion and resolving power, type 1 seems the best choice. When we compare them in this way, the types with real intermediate image do better than those having double focusing for all masses. In particular, the resolving power seems to be cut to one-half with the latter types. However, in paragraph (c) of this section we saw that by surrendering arrangements with velocity filter to those having double focusing, a factor of 2 was lost in the dispersion to be achieved since here an energy filter had to be employed. In this respect especially the arrangements shown in figure 1 and figure 6 (type 1) and those in figure 2 and figure 7 (type 2), respectively, can be compared with each other directly. Nevertheless, one has taken into account this seeming disadvantage when abandoning velocity filters in favour of double focusing, because the latter granted a higher resolving power (at least when one relates to the same intensity) on account of the better defined sharpness of the lines. Similarly, one gathers now from table 1 that double focusing for all masses also has its price. Judging, however, from the reproductions, especially of type 5, which are being built at some places even today, one seems to be willing to pay it. As we will see in the last section type 1 is not a happy choice with respect to the mass scale at least if one is concerned with the higher terms in the development of it. As will be shown, it is important to have sharp lines along the hole plate when making precision measurements of doublets. Only by measuring neighbouring lines of the same exposure used as dispersion lines does it seem possible to determine experimentally the dispersion-coefficient at the position of the doublet as well as the higher coefficients in the development of the mass scale. Furthermore, for purposes of control and in order to avoid systematic errors, it is desirable to be able to change the dispersion within certain limits by placing the doublet on different positions of the plate.

Among the 3 realized types having a real intermediate image, type 2 seems to be the one least luckily chosen. Besides the advantage of the favourable mass scale (plate through O') which it shares with the types having double focusing for all masses, it can, at best, point to the advantage (not carrying too much weight) of having a shorter path length of the rays. Even here it is not superior to the latter two types.

Table 2 gives an idea of the values of dispersion, resolving power, etc., actually achieved by, or within reach of, the different mass spectrographs. The numerical values of the various dimensions interesting us here are entered in the first 6 columns for the 5 different types that have been constructed. (For type 2 the data of H. E. Duckworth [16] were used and the opening of the diaphragm not given by him was assumed to be $d=1$mm. In the last line, the data used in the measurements of the author and R. Bieri were entered.) From these the values of the last five columns were computed for the properties used here for comparison. The theoretical resolving power was in fact achieved very closely wherever the effort was made. It is striking, to be sure, that for this purpose with type 1 [3] apparently only a small amount of filtered energy could be admitted for focusing in the magnetic field. The data given by the different authors are somewhat uncertain, especially when dealing with a very high resolution, since with extremely narrow slit-width neither this nor the width of the lines may be measured very accurately. Anyhow, one will be inclined to mistrust statements of resolutions achieved which exceed the theoretical values of the tables above. A. O. Nier, et al. (type 3), have not yet made the effort to attain the theoretical value of their resolving power given in table 2 apparently because they prefer to work with an unusually high percentage of the energy filtered.

5. The Mass Scale—Theory of Dispersion

A property important for the comparison of different types of mass spectrographs is the mass scale. Only by its help can the measured quantity which may be a length, a voltage or a resistance, a frequency or a time (time of flight) be expressed in mass units. Denoting the measured quantity by y and the mass by M, we shall call the function,

$$y=f(M) \tag{72}$$

the mass scale. Above all one is interested in its development in powers of $\mu=(M-M_0)/M_0$ in the "neighbourhood" of the point $y_0=f(M_0)$ at which the mass difference (doublet) to be measured has been placed (e. g., the point where double focusing is taking place). For this purpose we write:

$$y-y_0=F(\mu)=D\mu(1+a_1\mu+a_2\mu^2+\ .\ .\ .). \tag{73}$$

Here D is the dispersion coefficient defined in paragraph (c) of the preceding section, and the following relations hold:

$$D=M_0f'(M_0)=\left(\frac{dy}{d\mu}\right)_0=F'(0) \tag{74}$$

. . . .

$$a_i=\frac{M_0^i}{(i+1)!}\frac{f^{(i+1)}(M_0)}{f'(M_0)}=\frac{F^{(i+1)}(0)}{(i+1)!D}. \tag{75}$$

---

[3] Here the last data of the Japanese authors (cf. reference [14]) were used.

It will be our problem (1) to compute the theoretical values of these coefficients for the different types of mass spectrographs whereby our considerations are easily extended to the modern set-ups using the measurement of voltage, time or frequency; (2) to show how D and at least a_1 can be determined experimentally by measuring suitable "lines" of known mass (dispersion lines) which have to be present on the same exposure or run (by "lines", maxima resulting from the variation of voltage, time, or frequency are to be understood as well as lines on a photographic plate).

Solving eq (73) for μ we get what we shall call the "inverse form" of the mass scale (or "inverse function" for short)

$$\mu=\Phi(y-y_0)=\frac{y-y_0}{D}\left[1+\alpha_1\left(\frac{y-y_0}{D}\right)+\alpha_2\left(\frac{y-y_0}{D}\right)^2+\ldots\right] \tag{76}$$

$$\text{where } D=\frac{1}{\Phi'(0)} \text{ and } \alpha_i=\frac{\Phi^{(i+1)}(0)D^{i+1}}{(i+1)!}. \tag{77}$$

It is this form which enables us to compute the proportional mass difference μ (or very closely the difference of packing fractions of a doublet) from the measured "distance" $y-y_0$ between a "line" of unknown mass and the one of the known mass M_0 (doublet width). One convinces oneself by continuous differentiation according to μ of the identity

$$F'(\mu)\Phi'(y-y_0)\equiv 1 \tag{78}$$

that the coefficients of the two forms of the mass scale defined by eq (75) and (77) are connected by the following relations:

$$\left.\begin{aligned}
\alpha_1&=-a_1\\
\alpha_2&=2a_1^2-a_2\\
\alpha_3&=-5a_1^3+5a_1a_2-a_3\\
\alpha_4&=14a_1^4-21a_1^2a_2+3a_2^2+6a_1a_3-a_4\\
&\ldots\ldots\ldots\ldots\ldots\ldots\ldots\ldots
\end{aligned}\right\} \tag{79}$$

5.1. Theoretical Values of the Coefficients D, a_1, a_2, Etc.[4]

In mass spectrographs as a rule the ion beam consisting of particles of mass M, charge e and velocity v is analyzed in the magnetic field the field strength of which is to be constant $B=B_0$ and where they are traveling on circular orbits of radius r. We write once more (1) in the form

$$\frac{Mv}{r}=eB_0. \tag{80}$$

At first we consider r as the quantity to be measured and introduce in analogy to μ the proportional difference of radii $\rho=(r-r_0)/r_0$:

(a) *A velocity filter* in front of the magnetic field has the effect that for all ions v is constant, $v=v_0$. Then according to eq (80)

---

[4] This section is an extract of a paper to be published soon by the author and L. Waldman.

$$\frac{M}{r}=\frac{eB_0}{v_0}=\frac{M_0}{r_0}, \tag{81}$$

or

$$\rho=\mu. \tag{82}$$

(b) *An energy filter* in front of the magnetic field means according to eq (8) that

$$Mv^2=eT_0=\frac{eX_0}{ln\, r_a/r_i} \tag{83}$$

and therefore the kinetic energy is the same for all ions; here X_0 denotes the voltage between the two plates of the cylindrical condenser and r_a and r_i the radii of the outer and inner plate respectively. According to eq (80) and (83) we have here

$$\frac{M}{r^2}=\frac{eB_0^2}{T_0}=\frac{M_0}{r_0^2} \tag{84}$$

and therefore

$$\rho=(1+\mu)^{1/2}-1=\tfrac{1}{2}\mu(1-\tfrac{1}{4}\mu+\tfrac{1}{8}\mu^2-\tfrac{5}{64}\mu^3+\tfrac{7}{128}\mu^4-+\ldots). \tag{85}$$

However, the measured quantity y which occurs in the mass scale is not the radius r or the proportional deviation ρ but the distance of a line on a photographic plate from a suitably chosen zero-point, at least in the arrangements (the mass spectrographs proper) which we shall consider here first. Fortunately, for the relation between ρ and y we have to differentiate again only two cases in order to cover all mass spectrographs used for precision measurement of masses, with the exception of Aston's.

I. The plate (or its straight extension) passes through the point of entrance O' of the mean ray into the magnetic field (the left part of fig. 12) through which also the extension of the straight back boundary of the magnetic field is going. We choose O' as zero-point of y.

From reasons of similarity it follows at once that here

$$y-y_0=y_0\rho \tag{86}$$

II. For the magnet (the right part of fig. 12) a sector field ($\epsilon'=\epsilon''=0$) with an angle of aperture $\Phi_m=\pi/3$ is chosen, the straight boundaries of which are perpendicular to the mean ray at the side of entrance and perpendicular to the ray of mass M_0 at the side of exit. In the magnetic field therefore the ions of mass M_0 describe a circular orbit of radius r_0 the center of which lies in the vertex P_0 of the sector. The straight extension of the plate goes through P_0 and is inclined to the back boundary of the field by the angle $\pi/3$. P_0 is chosen as zero-point of y.

The result of a somewhat lengthy calculation employing the application of the sine theorem to the triangles $PO''P_0$ and $P_0O''Y$ and neglecting terms of higher order than ρ^3 is

$$y-y_0=2y_0\rho\left(1+\frac{9}{16}\rho+\frac{9}{16}\rho^2+\ldots\right). \tag{87}$$

The two arrangements of magnetic field and plate defined by I and II combined with one of the two possibilities (a) and (b) of filtering result in four types of apparatus which differ with reference to the mass scale. Elimination of ρ from the equations above gives these scales. Thus one gets:

(Ia) the case of K. T. Bainbridge's [3] old arrangement (fig. 1) with the linear mass scale

$$y-y_0=y_0\mu \tag{Ia}$$

(Ib) the case of the types 2, 4, and 5 described in section 3 (figs. 7, 10, and 11) with

$$y-y_0=y_0[(1+\mu)^{1/2}-1]=\frac{y_0}{2}\mu\left(1-\frac{1}{4}\mu+\frac{1}{8}\mu^2-\frac{5}{64}\mu^3+\frac{7}{128}\mu^4-+\cdots\right) \tag{Ib}$$

where the measured quantity is proportional to the square root of the mass,

(IIa) the case of the apparatus of E. B. Jordan [4] (fig. 2) with

$$y-y_0=2y_0\mu\left(1+\frac{9}{16}\mu+\frac{9}{16}\mu^3+\cdots\right), \tag{IIa}$$

and finally

(IIb) the case of type 1 of section 3 (fig. 6) with

$$y-y_0=y_0\mu\left(1+\frac{1}{32}\mu+\frac{1}{8}\mu^2+\cdots\right). \tag{IIb}$$

The special arrangement II of plate and magnetic field was originally chosen by K. T. Bainbridge and E. B. Jordan [12] among other reasons because with energy filter one gets a nearly linear mass scale (coefficient a_1 small) which at the time was thought an advantage. With velocity filter (case IIa) this advantage was lost again. We also don't want to forget that with this arrangement of plate and magnetic field the two developments (IIa and IIb) given above are valid for the neighborhood *of point* Y_0 *only* (the right part of fig. 12) whereas with arrangement I (the left part of fig. 12) the mass scales (Ia) and (Ib) are valid for *every point* of the plate.

III. Here we want to summarize all the new arrangements (mass spectrometers) which are *not* using a photographic plate but which are characterized by a fixed receiving slit behind which the ions are recorded electrometrically (mostly with the help of an electron multiplier).

(a) A. O. Nier et al. (type 3 of section 3, fig. 8) vary as was mentioned the voltage X of the electric field keeping the radius r of eq (80) constant, $r=r_0$. Therefore with the help of eq (83) one gets

$$MX=eB_0r_0^2\ln\frac{r_a}{r_i}=M_0X_0. \tag{88}$$

The form of this relation is not changed by the fact that the resistance R of a potentiometer is measured instead of X. Identifying X or R respectively with y, we get thus for this case the mass scale

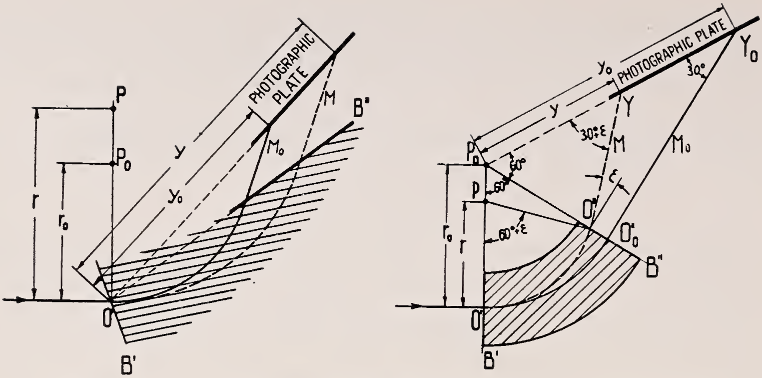

FIGURE 12. *Arrangement of photographic plate and magnetic field.*

$$y-y_0=y_0[(1+\mu)^{-1}-1]=-y_0\mu(1-\mu+\mu^2-\mu^3+\mu^4-+\ .\ .\ .) \qquad \text{(III)}$$

i. e., the measured quantity is inversely proportional to mass.

(b) S. A. Goudsmit [25] has proposed a "time-of-flight" mass spectrometer which he has set up with his coworkers [26]. The ion source is pulsed, which means that the voltage of acceleration is acting only a fixed time shorter than the time the lightest ions need to cover the distance of acceleration. The momentum Mv, therefore, is constant, and an analysis of masses in the usual sense cannot take place in the magnetic field. Nevertheless, such a one is used for reasons of focusing. The ions travel on helical paths and hit the receiver placed vertically below the ion source after n complete revolutions. The time of flight $\tau=2n\pi r_0/v$ between ion source and receiver is measured for which

$$\frac{M}{\tau}=\frac{eB_0}{2n\pi}=\frac{M_0}{\tau_0}. \qquad (89)$$

Writing y instead of τ one gets again the linear mass scale (Ia).

(c) J. A. Hipple, et al. [27], in their arrangement known as the "omegatron" employ the cyclotron principle according to which only ions are admitted to the receiver for which $v/r=\omega$ where ω, the cyclotron frequency, is the circular frequency of an alternating voltage applied to a suitable system of accelerating electrodes. According to eq (80) we have therefore

$$M\omega=eB_0=M_0\omega_0. \qquad (90)$$

If the measured quantity y were given by the cyclotron frequency ω then mass scale (III) would be valid. Actually, however, when dealing with small mass differences ω is kept constant, $\omega=\omega_0$, and instead the field strength B is varied by varying the current in an auxiliary coil.

We have therefore

$$\frac{M}{B}=\frac{e}{\omega_0}=\frac{M_0}{B_0} \qquad (91)$$

which, when identifying B with y, gives again the linear mass scale (Ia).

In table 3 the theoretical values of the coefficients of both forms of the mass scale are summarized for the different types of apparatus.

5.2. Experimental Determination of D and a_1

To determine at least these two coefficients, two measured quantities (i. e., the "distances" between the "lines" of three different but known masses) are necessary. One can determine D and a_1 independently of one another by choosing as dispersion lines besides M_0 two other neighboring lines of the same exposure (or run) which are lying symmetrically to M_0 with reference to mass number. We differentiate by the subscripts r and l, respectively, all quantities relating to the "right" line (corresponding to the heavier mass) and to the "left" line (corresponding to the lighter mass). Here we are making the further assumption that

$$\mu_r = -\mu_l = \bar{\mu} \tag{92}$$

which is always fulfilled if, for example M_l, M_0, M_r are of a hydride series. We also introduce the abbreviations

$$\Delta y = y_r - y_l, \quad \kappa = \frac{y_r - y_0}{y_0 - y_l}, \quad \Delta M = M_r - M_l. \tag{93}$$

1. of the Mass Scale: $y - y_0 = D\mu(1 + a_1\mu + a_2\mu^2 + a_3\mu^3 + a_4\mu^4 + \ldots)$

Type of Mass Spectrograph	I. Plate through O'		II. Plate through P_0		III.
	a) velocity f.	b) energy f.	a) velocity f.	b) energy f.	Nier, Hipple
Dispersion Coëff. D	y_0	$\frac{1}{2}y_0$	$2y_0$	y_0	$-y_0$
Coëfficient a_1	0	$-1/4$	$+9/16 \approx +1/2$	$+1/32$	-1
a_2	0	$+1/8$	$+9/16 \approx +1/2$	$+1/8$	$+1$
a_3	0	$-5/64 \approx -1/13$	?	?	-1
a_4	0	$+7/128 \approx +1/18$	?	?	$+1$

2. of the Inverse Function: $\mu = \frac{y-y_0}{D}\left[1 + \alpha_1\left(\frac{y-y_0}{D}\right) + \alpha_2\left(\frac{y-y_0}{D}\right)^2 + \alpha_3\left(\frac{y-y_0}{D}\right)^3 + \ldots\right]$

$-a_1 = \alpha_1$	0	$+1/4$	$-9/16 \approx -1/2$	$-1/32$	$+1$
$2a_1^2 - a_2 = \alpha_2$	0	0	$-9/128 \approx +1/14$	$-63/512 \approx -1/8$	-1
$-5a_1^3 + 5a_1a_2 - a_3 = \alpha_3$	0	0	?	?	$+1$

TABLE 3. *Numerical values of the coefficients.*

We imagine now that eq (73) is written down twice, once for the right and once for the left dispersion line. Subtracting one from the other gives, with the assumption (92), the equation

$$\Delta y = D\frac{\Delta M}{M_0}(1 + a_2\bar{\mu}^2 + a_4\bar{\mu}^4 + \ldots) \tag{94}$$

where the odd coefficients do not appear any more; solving it for D one obtains the value of the dispersion coefficient at the point y_0. If the mass-number of M_0 is larger than 10 one is calculating D to an accuracy better than 0.01 percent by retaining the quadratic term of the parenthesis only.

Dividing the two equations written down according to (73), we get, if we neglect $\bar{\mu}^3$ and higher powers,

$$\kappa=(1-2a_1\bar{\mu}+2a_1^2\bar{\mu}) \tag{95}$$

where neither D nor a_2 appear. The solution is

$$a_1=-\frac{(1-\kappa)}{2\bar{\mu}}, \tag{96}$$

if one neglects $(1-\kappa)^2$ and higher terms. When dealing with mass-numbers larger than 10, eq (96) gives a_1 with an accuracy better than one percent.

With the coefficients determined in this way, one can then with the help of eq (76) compute the unknown mass difference $\mu\cdot M_0$ with an accuracy corresponding to the precision of the measurement within reach today. In practice one must suitably work with the deviations of the experimentally determined coefficients from their theoretical values. That besides D at least a_1 ought to be determined experimentally is shown, for example, by the work of S. A. Goudsmit et al [26], who, by measuring at least three dispersion lines, allow for higher terms, though in their case theoretically the linear mass scale (Ia) ought to be valid. It is true though that here, where one is working with very slow ions, disturbing influences have a rather large effect.

With the exception of the mass spectrographs employing arrangement II of plate and magnetic field (the right part of fig. 12) one is able to undertake the following important control. One varies y_0 by placing the doublet together with its dispersion lines at different positions of the plate. That is easily done in the types of apparatus having double focusing for all masses and in a figurative sense as well in type 3 of section 3 having the mass scale (III). By differentiating (74) with respect to M_0 and y_0 and using eq (75) for a_1 one sees easily that the relation

$$\frac{dD}{dy_0}=\frac{D'}{f'(M_0)}=1+M_0\frac{f''(M_0)}{f'(M_0)}=1+2a_1 \tag{97}$$

ought to be fulfilled which connects the slope of the experimentally determined D-curve or the curve of $(D\text{-}D_{\text{theor.}})$ with the experimentally determined value of a_1 or with the deviation from its theoretical value. Besides, in these cases, curve (97) easily enables one to get the value of the dispersion coefficient at the point y_r or y_l, i. e., at the position of the right or of the left dispersion line; this is important if only on one side of the doublet to be measured suitable dispersion lines are to be found. In the mass spectrographs using arrangement II of plate and magnetic field, the execution of the control above cannot be done very easily because, as was mentioned before, the developments of the mass scale (IIa) and (IIb) are not valid if y_0 is varied.

6. References

[1] F. W. Aston, Phil. Mag. **38,** 707 (1919); **39,** 611 (1920); F. W. Aston and R. H. Fowler, Phil. Mag. **43,** 514 (1922).

[2] A. J. Dempster, Phys. Rev. **11,** 316 (1918); **18,** 415 (1921); Proc. Am. Phil. Soc. **7,** 45 (1921); Phys. Rev. **20,** 631 (1922).

[3] K. T. Bainbridge, Phys. Rev. **39,** 847; **40,** 130 (1932); Franklin Inst. **215,** 509 (1933).

[4] E. B. Jordan, Phys. Rev. **60,** 710 (1941).

[5] W. R. Smythe and J. Mattauch, Phys. Rev. **40,** 429 (1932); J. Mattauch, Physik. Z. **33,** 899 (1932).

[6] J. Mattauch and R. Herzog, Z. Phys. **89,** 786 (1934).

[7] R. Herzog, Z. Phys. **89,** 447 (1934).

[8] How this influence can be practically removed by placing suitable diaphragms at the field edges has been shown by R. Herzog, Z. Phys. **97,** 596 (1935).

[9] L. Cartan, J. Phys. radium **8,** 453 (1937).

[10] H. Hintenberger, "Habilitation" treatise (Berne, 1950).

[11] J. Mattauch, Phys. Z. **33,** 899 (1932).

[12] K. T. Bainbridge and E. B. Jordan, Phys. Rev. **50,** 282 (1936).

[13] T. Asada, T. Okuda, K. Ogata, and S. Yoshimoto, Proc. phys. math. Soc. Japan [3] **22,** 41 (1940).

[14] K. Ogata and H. Matsuda, Phys. Rev. **83,** 180 (1951).

[15] A. J. Dempster, Proc. Am. Phil. Soc. **75,** 755 (1935).

[16] H. E. Duckworth, Rev. Sci. Instruments **21,** 54 (1950), rebuilds Dempster's set-up with some technical improvements and a linear enlargement of 1:2, 3.

[17] J. G. Gorman, E. J. Jones, and J. A. Hipple, Anal. Chem. **23,** 438 (1951); H. Sommer and J. A. Hipple, Phys. Rev. **83,** 229 (abs.) (1951).

[18] A. O. Nier, T. R. Roberts, and E. G. Franklin, Phys. Rev. **75,** 346 (abs.) (1949); A. O. Nier and T. R. Roberts, Phys. Rev. **81,** 507 (1951); T. L. Collins, A. O. Nier, and W. H. Johnson, Jr., Phys. Rev. **84,** 717 (1951).

[19] A. Klemm, Z. Naturforsch. **1,** 137 (1946).

[20] C. Reuterswärd, Arkiv Mat. Astron. Fysik [30A] **7** (1943).

[21] J. Mattauch and R. Herzog, Z. Phys. **89,** 786 (1934); J. Mattauch, Sitzber. Akad. Wiss. Wien, Klasse [IIa] **145,** 461 (1936); Phys. Rev. **50,** 617 (1936).

[22] J. Mattauch and H. Lichtblau, Z. Phys. **111,** 514 (1939).

[23] H. Ewald, Z. Naturforsch. **1,** 131 (1946).

[24] A. E. Shaw and W. Rall, Rev. Sci. Instruments **18,** 278 (1947).

[25] S. A. Goudsmit, Phys. Rev. **74,** 622 (1948).

[26] P. I. Richards, E. E. Hays, and S. A. Goudsmit, Phys. Rev. **84,** 824 (1951); **85,** 630 (1952).

[27] J. A. Hipple, H. Sommer, and H. A. Thomas, Phys. Rev. **76,** 1877 (1950); H. Sommer, H. A. Thomas, and J. A. Hipple, Phys. Rev. **82,** 697 (1951).

2. A Double-Focusing Mass Spectrometer

By Alfred O. C. Nier [1]

Several years ago we at Minnesota became interested in the possibility of measuring atomic masses using a mass spectrometer rather than a mass spectrograph. You can see it would be quite natural that we should be thinking along this line since all of the work which my associates and I have done in the past has been with instruments which measured ion currents electrically. While we hoped that our instrument could compete with conventional mass spectrographs, we always reconciled ourselves with the thought that if it could not measure masses to the highest precision, it would at least be valuable to have an instrument with extremely high resolving power in the laboratory. The instrument might then be used for making special gas analyses or for studying the isotopic composition in solids.

The machine which we designed and constructed worked as well as we secretly hoped it would—better than we would openly admit—and it has been possible to obtain some definite results. It is my intention to discuss the machine.

The considerations in designing the instrument were, for the most part, simple. Although we are now thinking about the construction of a large instrument, in the past I have never believed in becoming involved in large construction projects. Thus, our philosophy has been to use existing equipment or facilities wherever possible. In the instrument which I will describe it was decided that the magnetic analyzer should be a 60° one with a radius of 15 cm. This construction would enable us to use the various jigs and fixtures already available in the laboratory from the construction of our numerous single-focusing mass spectrometers.

The construction of an electrostatic analyzer led to some complications. It turned out that we could house the analyzer in a standard 90° elbow made of Inconel. Inconel is an alloy which is practically nonmagnetic, will withstand high temperatures, and may be hard soldered and machined readily.

We felt that there would be some advantages in an instrument which would record the ion currents electrically. First of all, there was the possibility that we could employ an electron multiplier for measuring the ion currents and, hence, obtain extremely high sensitivity. Our first measurements with the new instrument did not employ an electron multiplier, but during the past year all of our measurements have been made with the use of an electron multiplier. The extremely high sensitivity obtained enabled us to work with very rare isotopes. Moreover, if a furnace is used in the source for evaporating a particular element, the temperature may be relatively low with the result that very little material condenses on the slits and other parts of the apparatus. Thus, the time between clean-ups of the apparatus is materially increased.

Use of an electrical recording method requires that focusing in the

---

[1] University of Minnesota, Minneapolis, Minn.

instrument be obtained at one point only. This gives us some advantages in arriving at a more perfect focusing condition.

We were quite familiar with the process of producing ions by electron impact. This is the kind of work which has been done in our laboratory for many years. Also, with an instrument of our design it is quite easy to use a thermal ionization source.

Another real advantage, that we felt would be associated with an instrument of our design, was that it would be relatively easy to make frequent checks on the performance of the instrument while we were in the process of obtaining actual data. One could check on the double focusing, the calibration of the mass scale, and other factors which one must know about in making precise measurements.

The use of our new instrument, however, raises problems which do not exist in conventional mass spectrographs. Because we cannot measure the two parts of a mass doublet simultaneously, the instrument may drift during the time a doublet measurement is made. It is essential to have conditions as steady as possible. As we produce our ions by electron impact of gases or vapors at low pressure or by thermal ionization, we do not obtain as many of the interesting combinations of atoms in ion fragments or as many multiply charged ions as are found in mass spectrographs using sparks or electric discharges for producing ions. All in all, we felt that the systematic errors in our instrument should be different from those found in mass spectrographs. If we were able to check results with others, we might all feel gratified; if not, the disagreement would stimulate work with all kinds of instruments.

Figure 1 is a schematic diagram of the instrument in its present form. This diagram supersedes the one shown by Dr. Thomas Roberts and myself in our publication last spring. The present diagram shows the instrument in the form in which it has been used during the past year. Let me now briefly review the operation.

In the main mass-spectrometer tube there is an ion source employing electron impact of gases or vapors. After the ions have fallen through a potential difference of approximately 6,000 v, they pass through a 90° electrostatic analyzer. An energy spectrum is produced at the position of the slit, S_3. The ions continue through the magnetic analyzer, through the narrow slit, S_4, and on to the first plate of the 10-stage electron multiplier. The output current of the multiplier is amplified with a conventional inverse feed-back electrometer tube amplifier. The final signal is then recorded on one channel of a two-channel Brush high-speed recorder. The single-focusing auxiliary mass-spectrometer tube shown mounted in the magnet is used for stabilizing the circuit and for providing a means for conveniently scanning the mass spectrum. The radius of curvature of the ions in the auxiliary tube is one-half that in the main tube, and the energy is approximately one-fourth. Thus, we employ a gas in the auxiliary tube having ions whose mass is approximately the same as that of the mass doublet to be studied in the main tube.

In normal operation the beam in the auxiliary tube strikes the pair of collectors symmetrically, one-half of the current going to each one. The differential amplifier, which is actually a distinct pair of conventional inverse feed-back amplifiers, measures the difference in the signal between the two collectors. This difference appears as a voltage, V, at the output of the differential amplifier.

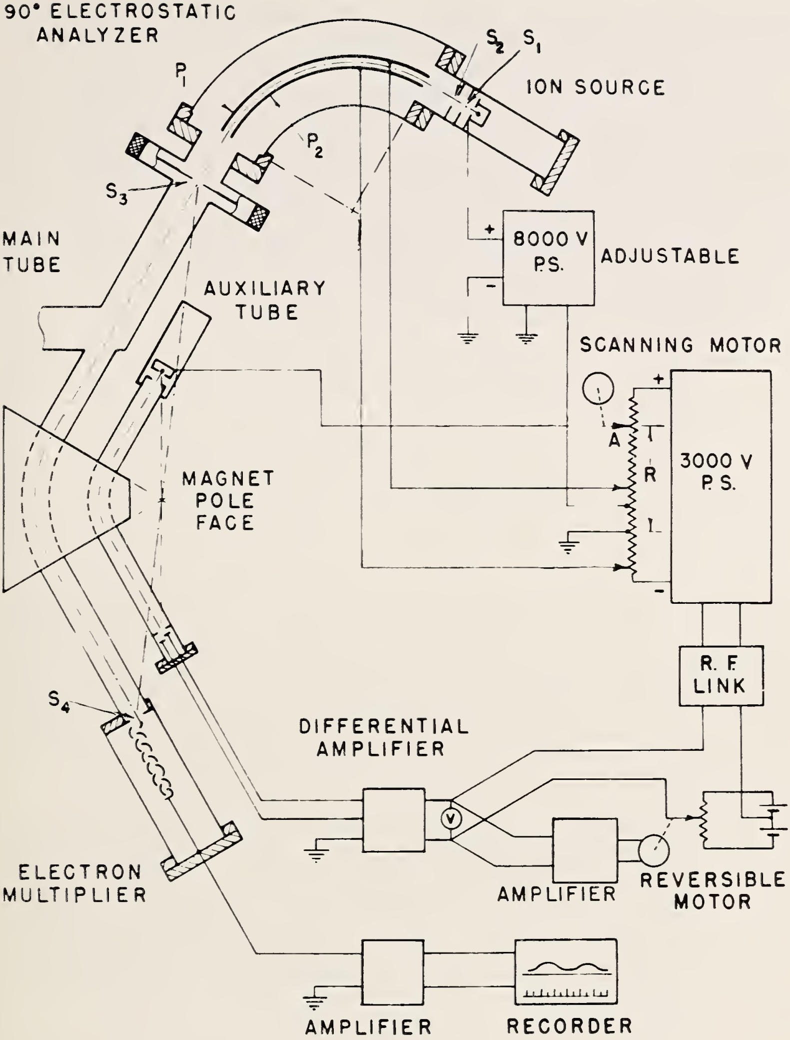

Figure 1.

Before saying more about the control system, I would like to say a few more words about the focusing arrangement in the main tube. We are attempting to eliminate the second-order angular aberration by having the proper combination of electric and magnetic fields, and object and image distances. In the case of the electrostatic analyzer, everything is symmetrical, that is, the distances from S_1 and S_3 to the 90° cylindrical condenser are the same. The magnetic analyzer is not symmetric. As may be seen from the diagram, the distance from S_3 to the magnet is greater than the distance from S_4 to the magnet. Although we are not as yet employing a wide enough divergence angle in the source to make full use of what we believe might be described as third-order focusing, we expect in time to take real advantage of the possibilities of the instrument. Even today we are using a wider divergence angle in the source than is normally employed in double-focusing mass spectrographs.

Let us return now to a discussion of the control system. The 3,000-v power supply has a voltage divider across it. The output voltage of the power supply may be changed by changing the input signal entering at the lower edge. The voltage divider provides the voltages for the electrostatic analyzer plates and the voltage for accelerating the ions in the auxiliary tube. It also provides, in an indirect way, the voltage for accelerating the ions in the main tube. As may be seen in the diagram, this voltage is actually provided by the 8,000-v power supply. However, by means of a tap on the voltage divider discussed above, the output voltage of the 8,000-v power supply is made to follow in a linear fashion, the output voltage of the 3,000-v power supply. The relation is rather accurate since an inverse feed-back circuit is used in the 8,000-v power supply. The purpose of the second-power supply is to prevent leakages or other extraneous effects in the ion source of the main tube from disturbing the voltage distribution in the voltage divider under discussion. For purposes of visualization in discussion, one could think of the accelerating voltage in the main tube as being supplied directly by the voltage divider.

How, then, does our regulating circuit perform? The output signal V from the differential amplifier is fed into the 3,000-v power supply. However, because the 3,000-v power supply and the output of the differential amplifier cannot have a common ground, a small radio-frequency link is used to separate the circuits. This link may be thought of as a direct-current transformer since this is its function in the circuit. A discussion of a single link of this kind was given by Prof. Otto Schmitt in the Review of Scientific Instruments several years ago.

For the moment, let us disregard the reversible motor and circuitry associated with it. If, now, the voltage applied to the ions in the auxiliary tube or the magnetic field changes for some reason, the differential amplifier notes the shift in the beam in the auxiliary tube, and the divider on the 3,000-v power supply is instructed to shift the accelerating voltage applied to the ions of the auxiliary tube in such a manner as to compensate for the effect. In the process a similar compensation takes place for the shift of the beam in the main mass spectrometer tube.

As in any feed-back loop, it is not possible to have an infinite gain, because the system will oscillate. In the particular circuitry which must be employed here, there are many opportunities for phase shifts in different places. The result is that oscillations take place with the gain in the loop as low as approximately 100.

An examination of the circuit shows that a mass spectrum may be swept by merely moving the tap A on the voltage divider. A simple calculation shows that if ΔR represents the difference in resistance corresponding to the two parts of a mass doublet, then the difference in mass for the doublet may be computed by the equation $\Delta M/M = (\Delta R/R)\ (G/G+1)$. In the measurements reported by Dr. Roberts and myself early this year, it was necessary to measure the gain, G, of the loop for each run. It turns out that it is actually more difficult to measure the gain than the value $\Delta R/R$. The use of a second control device eliminates the need of measuring the gain of the loop since, in effect, it is infinite for slow changes in the system such as those which one has as one scans the spectrum with the motor-driven tap A.

The second control device is the reversible motor and associated equipment, neglected in the discussion above. The output of the differential amplifier is fed into the amplifier which provides power for the reversible motor. If V is not zero, the motor will rotate, the direction of rotation depending upon the polarity of V. As may be seen from the circuit, if the tap on the potentiometer driven by the reversible motor is not at the center, a signal is added to V and the sum fed into the r-f link. Thus, whenever V has any value other than zero, the reversible motor will run until the signal V is reduced to zero. In practice, the "dead spot" of the amplifier is so small that we may think of V being reduced completely to zero. This is equivalent to having an infinite gain in the circuit as one sweeps the mass spectrum. Thus, in effect, the equation which we use in computing the value for a mass doublet reduces to the simple form $\Delta M/M = \Delta R/R$.

Figure 2 shows a chart obtained under typical operating conditions by scanning a mass doublet having a value of $\Delta M/M$ of one in 1,000. The sweep was started in the normal way, and at the steepest point on the side of the second peak the scanning motor was stopped. If the stabilization were perfect, one should obtain a smooth horizontal line. In practice, one obtains a line with slight imperfections in it. That the stabilization is very good may be seen, if one makes a deliberate change in voltage of one part in 100,000 as shown. One notes that this change produces a fluctuation four or five times as great as the ones normally present. Thus, our auxiliary tube not only provides a convenient way for scanning the mass spectrum, but also makes the power supplies in the system equivalent to having been stabilized to within a few parts in a million.

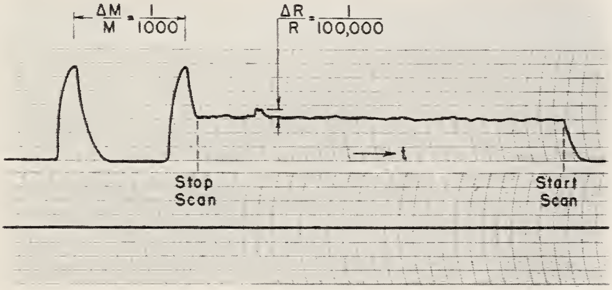

Figure 2.

There are other tests which may quite readily be made on the performance of the instrument. One question which arises is whether or not $\Delta R/R$ really measures the fractional change in voltage on the deflecting plates of the electrostatic analyzer. If there were a leakage current in the source of the auxiliary mass-spectrometer tube, this would contribute to the current in the divider, and the potentials applied to the deflecting plates would not vary as we assume in our formula. A test for leakage can easily be made by inserting a galvanometer in the grounding lead to the voltage divider. Since the normal current in the divider is approximately 4 ma, it is quite easy to detect a current which would be large enough to affect the accuracy of the measurements.

The energy focusing may be checked quite easily. The procedure is to run a spectrum of a single peak and then, after changing the accelerating voltage applied to the ions in the main tube by an arbitrary amount (approximately 40 v), to repeat the spectrum. A third run is then taken with the accelerating voltage restored to its original value. When the energy focusing is working properly, the three charts, when laid upon one another, will coincide exactly. If the energy focusing is not correct, the second chart will deviate from the first and third. Correction for a steady drift in the instrument may be made by comparing the first and third charts. If the energy focusing is not working properly, it may sometimes be corrected by merely moving the main mass-spectrometer tube in the magnetic field. Sometimes the difficulty is due to insulated coatings found on the plates of the electrostatic analyzer. If this happens to be the case, the analyzer is taken apart and cleaned.

Figure 3 shows a typical spectrum of the type we are now obtaining. This one was taken at mass-28 position and shows the three common gases: carbon monoxide, nitrogen and ethylene. The mass difference between carbon monoxide and nitrogen is approximately one part in 2,500. It is seen that the peaks are almost perfectly resolved. Actually, the figure shown here is obsolete, better resolution being obtained at the present time.

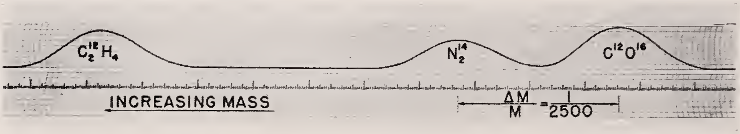

Figure 3.

The matter of determining the dispersion is one of great importance. We have already indicated the formula which one should use for calculating the difference of mass in a doublet. Is this formula really correct, or must some correction factor be employed in using it? A convenient test of the formula is made by using adjacent fragments in a hydrocarbon as a doublet. A test of our formula is made whenever measurements are undertaken. Table 1 shows the calculated hygdroen-mass values computed from our data and the formula

Table 1. *Hydrogen mass doublets*

Date (1951)	Mass numbers	Difference	Date (1951)	Mass numbers	Difference
April 17	28–27	[a] 1.00809	June 11	81.80	1.0081
April 20	28–27	[a] 1.00836	June 15	44–43	1.0077
April 23	28–27	[a] 1.00892	July 3	44–43	1.0076
April 24	28–27	[a] 1.00834	July 6	42–41	1.0082
April 30	28–27	[a] 1.00835	July 6	44–43	1.0080
May 8	50–49	[a] 1.00788	July 9	44–43	1.0080
May 14	44–43	[a] 1.00783	July 19	44–43	1.0079
May 28	44–43	[b] 1.0075	July 24	54–53	1.0079
May 30	44–43	[b] 1.0072	July 26	54–53	1.0079
June 1	44–43	1.0086	July 27	54–53	1.0082
June 2	44–43	1.0078			
June 4	44–43	1.0079			
June 5	44–43	1.0081	Average [c]		1.00808
			Difference (%) from 1.00814		0.006

[a] Taken during H^1 and C^{12} determinations. Average, 1.00832.
[b] Low results discarded. Tube found twisted.
[c] Neglecting the values referred to in footnote b.

$\Delta M/M = \Delta R/R$. Whenever the results deviate by more than a few parts in 10,000 from the proper value, i. e., 1.00815, the apparatus is examined for misalinement or is cleaned. Thus, we always use the formula without a correction term. You will note that the data taken around May 28 and May 30 appeared systematically low. A readjustment of the apparatus brought the values back into line.

Figure 4 shows a typical mass spectrum of the sort used in obtaining data. A run consists of 10 consecutive spectra of the sort shown here. As indicated in the figure, the procedure is to measure from one half height to the corresponding one on the adjacent ion current peak. Thus, for each doublet one obtains two measurements, and a run consists of some 20 measurements. In practice, runs taken on the same day agree somewhat closer than ones taken at different times. Thus, before considering a value for a given doublet as final, a number of runs (perhaps four or more) may be taken over a period of some weeks or even months. While the peaks may not be exactly symmetric; when everything is right, they do have the same shape. To the best of our knowledge, this is a satisfactory criterion for obtaining correct answers. As the resolution of our instrument is rather low when compared with some of the modern mass spectrographs, the problem of correcting for carbon 13 in hydrocarbon fragments sometimes arises. This comes about because often when a given hydrocarbon is used as a comparison peak in a doublet, there will be a hydrocarbon fragment having one less hydrogen atom. A C^{13} atom in the lighter fragment will give a fragment of the same mass number as the fragment undergoing measurement in the doublet, and the C^{13} containing fragment will not be resolved from the one being measured. The procedure in such instances is first of all, to use hydrocarbon gases in which the effect will be as small as possible, and secondly, when it exists, to make a correction for the unresolved peak after computing the amount of the correction from the amount of the lighter fragment present. For example, in the case of figure 5 there will be superimposed on the $C_2^{12}H_4$ a small amount of $C_2^{12}C^{13}H_3$.

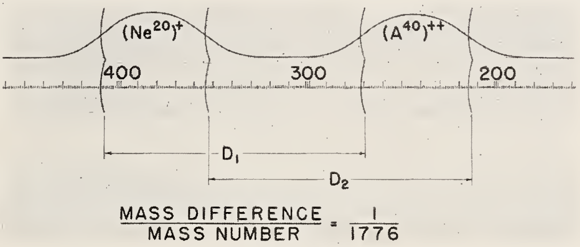

FIGURE 4.

There is one other point which should be made in discussing the method of measurement. It is to be noted in figure 5 that a calibration scale is printed in the second channel of the two-channel recorder. Permanently connected to the shaft of the 40-turn helical potentiometer used for scanning the spectrum is a system of gears. Riding on the teeth of these gears is a system of little switches which open and close as the gear teeth go by. Different gears give different size pulses, and, hence, it is possible to record on the chart precisely the position of the potentiometer at the time the spectrum was scanned. Corrections for the linearity of the potentiometer may be made by reference to a calibration chart for the potentiometer.

Discussion

H. E. Duckworth: I would like to ask if there is any appreciable correction for carbon 13 when you are working with hydrocarbons having two atoms of carbon as you show here.

A. O. C. Nier: This varies. If you go up to three or four or more carbon atoms, the effect is more pronounced. This is a matter which concerns us a great deal. For instance, an example of a particularly difficult case would be that at mass 40. For most hydrocarbons C_3H_3 is a very pronounced fragment. Thus, the C^{13} containing C_3H_3 will give a large addition to the $C_3{}^{12}H_4$. All I can say is that we do the best we can in cases of this kind. The unwanted combination may amount to only a few percent of the total peak. In some cases it amounts to much more.

Duckworth: You do make corrections in the C_2 range?

Nier: Yes.

R. E. Honig: What determined the choice in the electrostatic analyzer which you used?

Nier: 90° is easy to construct in the machine shop, and one can readily purchase 90° elbows for a housing. The considerations in our case were actually simple. I do not pretend this has any great advantages over any other dimensions. I had hoped that in this conference I would learn of some angle that would be better.

Honig: Are there some advantages in using a 127° analyzer?

Nier: In the 127° analyzer the focal points lie in the entrance and exit planes of the analyzer. One of the considerations we had was that we wanted to take the source and exit slit of the electrostatic analyzer away from the analyzer for mechanical reasons.

J. Mattauch: Would there be any advantage in having 127°? As I showed in the table, Dr. Nier actually approaches the resolution found in the 127° case. I would like to ask Dr. Nier—I do not have your *R* and *S* figures—how close have you approached the theoretical calculations?

Nier: Our slits are about one-thousandth of an inch wide. We approach the theoretical resolutions to within about 10 percent, and our number is on the low side, indicating that we are not doing as well as the theory would predict.

Mattauch: Did you ever think of trying Dr. Hintenberger's method? He has set up a similar sort of thing. In order to shorten the path, he accelerates the ions in two steps and is able to use a smaller electrostatic analyzer.

Nier: No; we have not done anything like that.

3. Accuracy of Mass Spectrographic Isotope Mass Measurements

By H. Ewald [1]

The accuracy of mass spectrographic doublet measurements is dependent upon four important preliminary conditions: (1) resolution, (2) mass dispersion, (3) line shapes, (4) mass scale. We shall discuss in detail these different conditions and the limits which they impose upon the attainable accuracy. The resolution of the mass spectrograph used should be as high as possible, which means that the width of the lines should be as small as possible compared with the distances of the lines. The resolution of the mass spectrographs focusing for all masses is given by the relation

$$M/\Delta M=(a_e/2s_e)\left[1+\frac{l'_e-g_e}{f_e}\right]=\rho/2d\rho$$

where a_e is the median radius of curvature of the electric field, s_e is the width of the entrance slit, ρ is the distance of the line in question from the entrance point of the rays into the magnetic field, which is also lying in the plane of the plate, and $d\rho$ is the width of the line. The bracket contains only ion-optical constants of the electric field and is of the order 1. From this relation we can see that the width of the lines is of the same order as the slit width.

The hitherto existing apparatus has values of a_e of 10 to 30 cm and values of s_e of some 10^{-3} mm or more. With such values one should be able to realize a resolution of 10^4 to 10^5. A value of 50,000 could be reached in practice. Supposing that we were able to measure the distances of two mass lines with an accuracy of about 1/10 of the line width, then we would have an accuracy for the mass comparison of about 10^5 to 10^6. By increasing a_e, this maximum resolution and accuracy could be increased, perhaps by a factor of 10 where a practical limit will be reached.

Now we ask for the conditions which must be fulfilled in order to reach the highest resolution. It stands to reason that the whole apparatus should be adjusted in the best possible manner, corresponding to the theoretical conditions. This is a very laborious task, and we shall not speak about it in the whole, but shall restrict ourselves to the adjustment of the entrance slit.

It is necessary to have a specially constructed entrance slit, which permits us to use and to maintain slit widths down to some thousandths of a millimeter in spite of the bombardment and the soiling by the ion rays. The best slit has proved to be one formed between two steel rolls which are held exactly parallel to each other at a distance of some tenths of a millimeter in a special frame. This frame may be turned as a whole around an axis passing through the slit and vertical to the incident ion beam. In this manner the effective slit width can be adjusted to the value wanted. The effective slit width

---

[1] Max Planck Institut für Chemie, Mainz, Germany.

is controlled best electrically by comparing the ion current coming through the slit with the ion current at maximum slit width. We thus assume a rough proportionality between slit width and ion current.

By means of four rods we can move the slit into the wanted position relative to the whole ion optical system while in operation. Figure 1 shows the system installed in the apparatus. The different adjustments are to be made by the five upper revolving rods. Figures 2 and 3 show pictures of the apparatus.

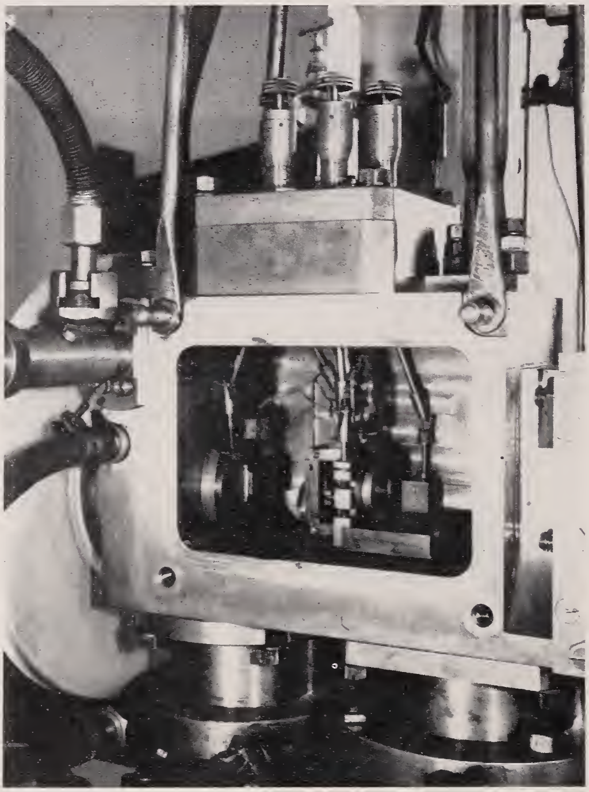

FIGURE 1. *Slit adjusting mechanism.*

Returning to the adjustment of the slit, it is necessary to adjust it exactly vertical to the field lines of the electric field. That means vertical to the median deflection plane of the apparatus. The requirements in this relation are very high, because the length of the slit, in general, is very large compared with the width of the slit. Even small deflections from the vertical position can give rise to a considerable broadening of the effective slit width. The effective slit width is given by the projection of the slit into the median plane corresponding to the relation $s=s_0+h \sin \gamma$; s_o is the real slit width and h the length of the slit and γ its deviation from the vertical position. If we have $s_0=0.005$ mm, $h=4$ mm, $\gamma=0.35°$, this will result in $s=0.025$ mm which is 5 times s_0. From this follows the condition that the slit be adjusted to 0.1° or better.

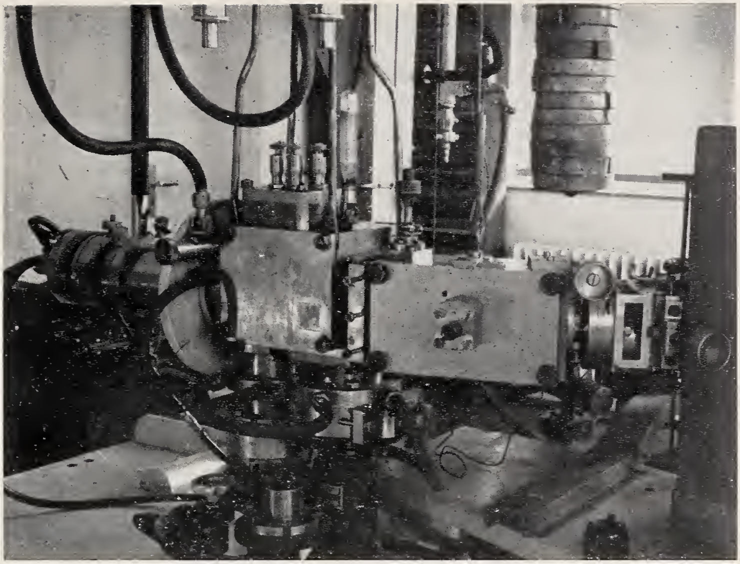

Figure 2. *View of spectrograph.*

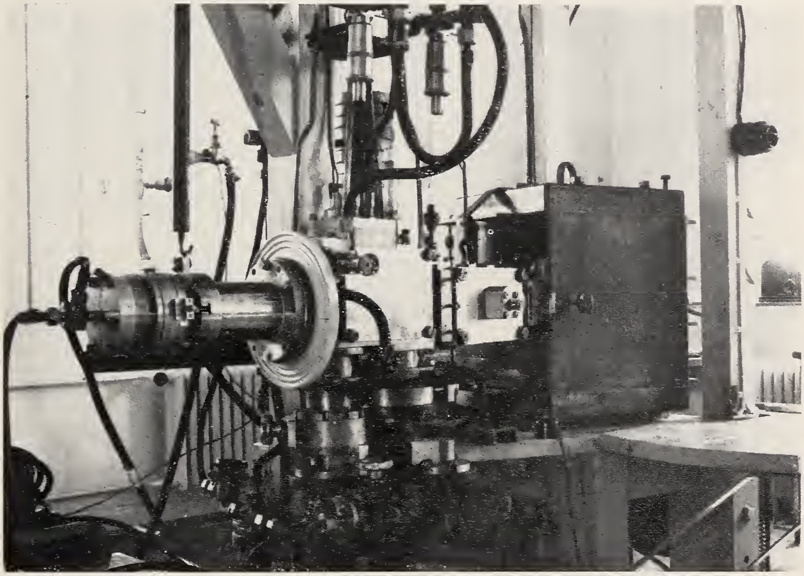

Figure 3. *Another view of spectrograph.*

In practice this can be done in the following manner. We arrange a double diaphragm in front of the slit and crossed to it. If the slit is not adjusted exactly vertically, we shall observe a double line, so to speak an artificial doublet instead of a broadened line, because only two little parts of the slit are used, the projections of which do not fall into the median plane together but act as a double slit. From the width of these artificial doublets and from the distance of the diaphragms, we may compute the angle γ and then correct the adjustment of the slit. In this manner the attainable accuracy of adjustment is 0.1°. We can then reduce the length of the slit by a factor of about 10, to be sure that the effective slit width will not be greater than the real width of the slit.

There is another reason for such a shortening of the slit. It has been observed that the two lines of the mentioned artificial doublets in general are not exactly parallel to each other (fig. 4). For instance, we measure the distance 0.026 mm at the top and 0.019 mm at the bottom. Even if the slit is adjusted in the best possible manner, the two lines do not fall together exactly but cross over a little. That means that the rays coming from the different points of the slit give rise to slightly different elementary lines of slightly different direction. If we are working without the mentioned double diaphragm, or a corresponding single diaphragm in front of the slit, then these different elementary lines corresponding to the different points of the slit will overlap each other and give rise to a broadened summation line and in this manner reduce the resolution. The cause of such an effect may be found in little inhomogeneities of the fields. It may be overcome by the shortening of the slit by means of a single diaphragm.

The mass dispersion of the mass spectrograph used should be as high as possible for the following reason. The line widths on the one hand should be as narrow or thin as possible compared with the distances

Figure 4. *Artificial "doublet" caused by nonvertical slit.*

of the lines, but on the other hand should remain wide compared with the grain size of the photographic plates and also compared with the lowest accuracy limit of the Abbe-comparator, the optical measuring instrument used to measure the plates.

The existing mass spectrographs of highest resolution do not very well fulfill these conditions. They have line widths of some thousandths of a millimeter compared with grain sizes of about one thousandth of a millimeter and an accuracy limit of the measuring instrument of about 3/10000 mm.

Errors in the measurements of the line distances arising from the sizes and the density fluctuations of the grains in the emulsion have to be eliminated by measuring a great number of the same doublets and equalizing the results. As to the accuracy limit of the measuring instrument, it is not reasonable to give the final results more accurately than to some ten thousandths of a millimeter corresponding to about a tenth of the line width in the best case.

The grain size of the plates and the accuracy of the measuring instrument are principal limits of the accuracy of the doublet measurements. This can only be overcome by increasing the mass dispersion, that is, by increasing the dimensions of the magnetic field of the mass spectrograph. As mentioned above, such an increase will now reach a practical limit.

Apart from the resolution and the mass dispersion, the attainable accuracy of the mass comparisons is essentially dependent upon the shapes of the mass lines. In general we have to suppose that the intensity will be distributed asymmetrically across the lines. There are many causes for such asymmetries.

Even if we may suppose that the ion current falling onto the plate is distributed symmetrically across the line width, asymmetrical lines may be created by a very small change of the deflecting fields during the exposure time. Such a changing of the order of 1 to 10 ppm also may be caused by a slightly variable polarization effect of the plates of the electric field.

However, even with constant fields and an ideal adjustment of the apparatus, asymmetrical lines in general have to be expected because of the second-order aberrations of the field combinations. These aberrations become more important as the resolution is increased. The broadening of the lines and the intensity distributions coming from them in general are asymmetrical. By non-ideal adjustment of the apparatus these asymmetries may be increased.

Measurements of the distances of asymmetrical lines are acceptable only if the lines have the same intensity. This is because the primary intensity distributions across the lines may be changed by the blackening-function of the photographic plate in a manner that results in displacements of their centers of gravity. This displacement can be different for lines of different intensity. Therefore we demand the same intensities of the doublet lines.

Asymmetrical intensity distributions across the mass lines may also be produced if the entrance slit of a few millimeters of length is not adjusted exactly vertical to the median deflection plane of the apparatus and if this slit is not illuminated homogeneously by the ion rays. The slit may be illuminated at its one end by an ion ray of high intensity while the other parts of it may be illuminated only by a relatively low intensity. The corresponding effective slits have a large inhomogeneity of illumination and therefore the lines have a considerable displacement of their centers of gravity.

Furthermore, there may be very different broadening and asymmetry of the different lines. That means that the illumination of the slit by the different ions delivered at the same time by the ion source may be very different. This results in different sizes of the displacements of the centers of gravity of the lines and therefore in considerable errors in the measurements of the distances of the lines. By a very exact adjustment of the slit, and by its shortening, these errors may be avoided.

Similar asymmetries and errors will result in consequence of the fact that in the second approximation the width of the lines are also dependent upon the angle of divergence of the rays coming through the entrance slit if the intensity is distributed inhomogeneously across this angle of divergence in the median plane. Such one-sided broadenings of the lines may be much increased if the apparatus is not well adjusted. From the different width of the lines one may conclude again, that the different ions coming from the ion source at the same time have a different angle of divergence. Therefore the corresponding displacements of the centers of gravity of the lines are of different size again. The resulting errors in the doublet measurements can only be overcome in a sufficient manner by reducing the possible angle of divergence to 0.1° or less.

Finally, we have to speak about the mass scale, which may be calculated theoretically and determined practically for each apparatus. The mass scale can be expressed as a function which relates the masses M of the observed lines and their positions ρ on the photographic plates $M=f(\rho)$. In mass spectrographs which have double focusing for all masses, we have the relation $M=k\rho^2$. In reality, these functions are only approximately valid. We have to make small corrections, therefore, when calculating the mass differences from the measured distances of the doublet lines.

In mass spectrographs which have double focusing for all masses, we also have the following relation

$$\delta M = M_2 - M_1 = M_2 \left[1 - A \left(1 - \frac{\delta\rho}{\Delta\rho} \frac{\sqrt{M_2} - B\sqrt{M_0}}{\sqrt{M_2}} \right)^2 \right].$$

M_1 and M_2 are the masses of the doublet lines, and M_0 is the mass of a dispersion line of another mass number. M_o and M_2 need to be known only approximately. $\delta\rho$ and $\Delta\rho$ are the exact measured distances of the doublet lines M_1 and M_2 and the dispersion lines M_0 and M_2 respectively. This relation with $A=B=1$ holds for magnetic fields of ideal homogeneity.

If this latter condition is not fulfilled exactly, the ions of the three masses M_0, M_1 and M_2 will traverse, in their passage through the magnetic field, regions differing in field strength. Then we have to add two correction factors

$$A = 1 + 2\epsilon_1 - 2\epsilon_2 \text{ and } B = 1 - \epsilon_0 + \epsilon_2$$

into the above relation. The quantities ϵ are of the order 10^{-4} in our own apparatus, and may be determined empirically as suggested by Professor Mattauch and undertaken finally by Mr. Bonisch at Vienna and later by myself. The results of the measurements of a doublet obtained in such a manner are independent of the position of the doublet on the photographic plate.

Considering the present-day accuracy, this correction is only necessary if the dispersion lines M_0 and M_2 have a relatively large mass difference, namely, 10 percent or more. For instance, this is the case for the doublets H_2-D, D_2-He and D_3-C^{++}.

If we now summarize once more the different conditions which must be fulfilled, we have to request

(1) high resolution and mass dispersion,
(2) a narrow, short, and well adjusted slit,
(3) fine grain of the photographic plate,
(4) high accuracy of the optical measuring instrument,
(5) equal intensity of the doublet lines,
(6) small angle of divergence of the rays,
(7) corrections for inhomogeneities of the magnetic field

After recognition of these conditions, a great number of new measurements have been made in the last years. The results seem to be in better agreement than the former ones. Figure 5 shows some graphs of these new plates. I shall mention only the good agreement we have found in calculating the masses ^1H, ^2D, ^{12}C compared with the new calculations of the same masses by Li, Whaling, Fowler and Lauritsen from Q-values of nuclear transformations (see table below).

Isotope	Calculations of author	Calculations of Li, Whaling, Fowler, and Lauritsen
^1H	1.008141±2	1.008141±3
^2D	2.014732±4	2.014734±6
^{12}C	12.003807±11	12.003803±17

So we assume that our new measurements are now without considerable systematic errors. Nevertheless, we must not cease looking for any further errors. At all events, we should make all possible cross checks in order to assure especially the masses of the substandards, for instance, by measurements of the doublets $C^{+++}-O^{++++}$, He_2-O^{++}, D_2-C^{+++}, and so on.

An attempt of such a cross check of quite another type has failed as yet, but I shall mention it briefly. Commonly the masses of ^1H, ^2D, and ^{12}C are calculated from the doublets H_2-D, D_3-C^{++} and CH_4-O. Now we intended to omit the second of these doublets and to replace it in the following manner. We adjusted the gas inlet system of the apparatus in such a manner that the four lines DH^+, D_2^+, C^+, O^+ were simultaneously observed in the same intensity as shown in figure 6. At a fixed position of the plate we made an exposure and then quickly changed the electric field by a factor of about 1.33 and made another exposure without moving the plate (fig. 7). So we obtain two artificial doublets which we may write

$$xDH-D_2=\beta_1$$

$$xC-O=\beta_2.$$

We obtained without difficulty a greater number of these artificial doublets with best resolution. They can be measured in the usual way. In combining the results with those of the doublets H_2-D and

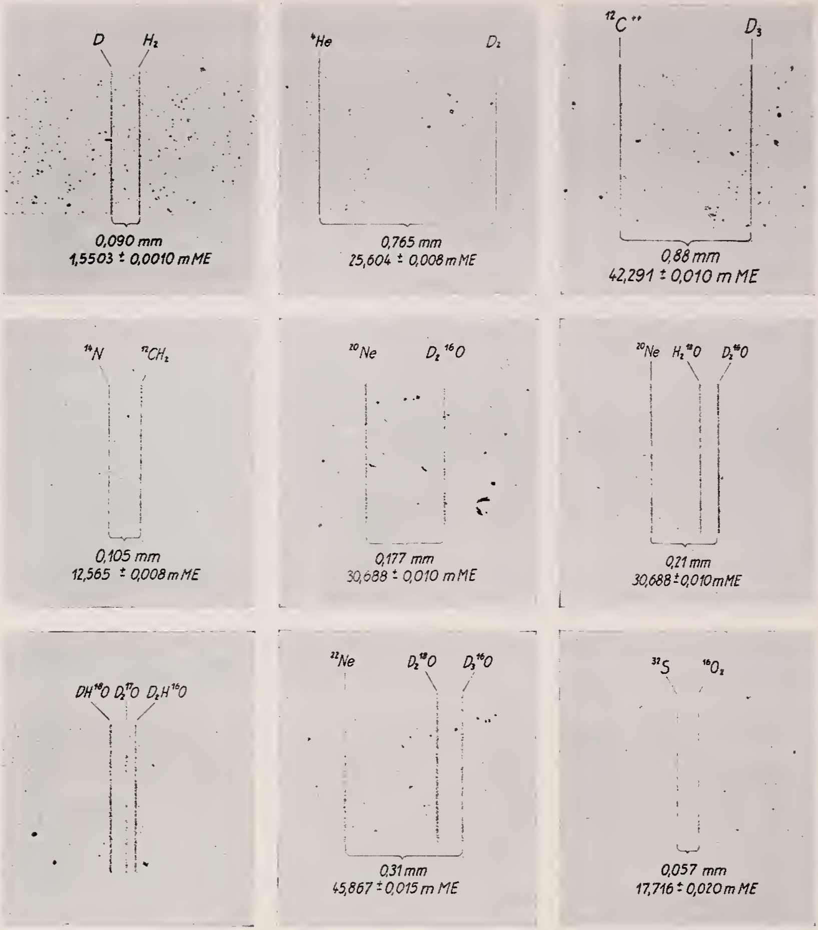

FIGURE 5. *Some typical multiplets.*

CH_4-O, we can eliminate the unknown factor x and solve for the masses of substandards. So we got the result $^{1}H=1.008165\pm0.000005$ *ME*. This does not agree with our new value of 1.008141, which is nevertheless considered to be the best value. We are obliged, therefore, to assume that some systematic error, till now unknown, may affect our method of control of the two artificial doublets. Perhaps it may be a little magnetic stray field in the region of the electric field. We shall look for the source of any such error in the near future in order to remove the above discrepancy.

It should be mentioned that this method of artificial doublets may also be valid in cases where there is a lack of the second doublet line of a known mass. For instance, we have determined in this way the mass of ^{23}Na by measuring the artificial doublets $x^{20}Ne-ODH$ and $^{22}Ne-x^{23}Na$.

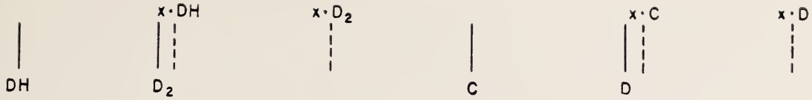

FIGURE 6. *Method of making artificial doublets.*

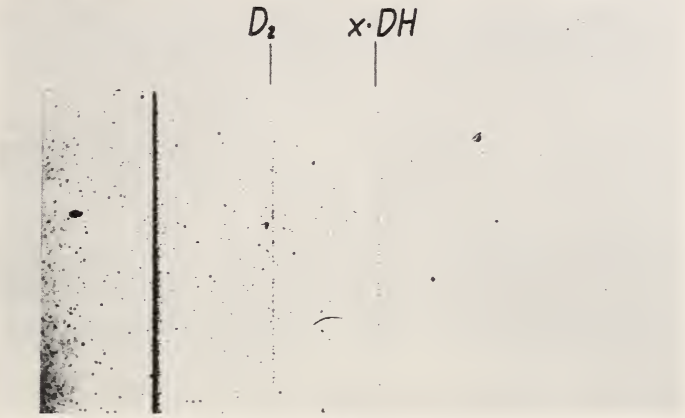

FIGURE 7. *Artificial doublet.*

Discussion

A. O. NIER: I should like to ask how long are the slits you use in practice in your work?

H. EWALD: One- or two-tenths of a millimeter.

J. MATTAUCH: You see the slit width is only two or three thousandths.

NIER: So it is really a long slit though it doesn't sound like it.

MATTAUCH: It is surprising how little intensity you lose. You don't have to have such a long slit. May I perhaps make just one of my comparisons? At first I had great doubt that Dr. Nier's measurement compared with our case. We obtained 50,000 compared to the 2,500 he mentioned. I don't see any easy way to compare the dispersion in millimeters in the different measurements. We don't have them on the same plate in the microscope. May I ask, Dr. Ewald, which you think is more advantageous to use, one dispersion line or two?

EWALD: Sometimes it is difficult to find the other dispersion line.

MATTAUCH: But it isn't in the doublets you and we measured in Bern.

EWALD: I think the corrections are accurate enough to eliminate errors. The corrections are so little and are so definitely measured that I think they will eliminate these errors.

MATTAUCH: Well, most mass spectrographic measurements show that it comes out a little bit here. That is mainly determined by the doublet shown there on the table. I think we can defer this discussion until this afternoon.

Chairman W. BLEAKNEY: Those are certainly very beautiful doublets.

H. E. Duckworth: Dr. Ewald, I would like to ask you what the pressure is in your mass spectrograph.

Ewald: I think it has to be better than 10^{-5} mm of Hg, and it is better to have 10^{-6}. We have to evacuate every one or two hours. If we make one exposure after another every ten minutes, you can see in what manner the lines grow sharper and sharper. After one or two hours they do not get any sharper.

Duckworth: You remember that Professor Dempster and Dr. Shaw showed that the sharpness of the line wasn't a reliable criterion. They had sharp lines and yet the doublet spacing changed and I was wondering if you had noticed any shifting of the doublet.

Ewald: I have not observed any such varying of the distance in connection with the pressure, but I think it would be good for us to examine this question. Have I understood you in the right manner?

Duckworth: Yes, I will look forward to talking with you.

Bleakney: Are there any others?

Mattauch: If you have on your plate, say for instance—now, I never had any trouble getting lines like this. (Illustrating on board.)

Duckworth: I am not questioning the sharpness of the lines. My point was that sometimes, as Dempster and Shaw showed, sharp lines do not mean that the pressure is low enough.

Nier: That is not a good enough criterion.

Mattauch: I see.

Ewald: May I ask if the work of Dempster and Shaw has been continued in the meantime?

Duckworth: Well, Dr. Shaw is here, or he was.

A. E. Shaw: Several spectra have been taken under different fixed conditions, and it has been found that it shifted the result when the pressure was high enough, probably due to energy changes.

Mattauch: Do you think that was a space charge effect?

Shaw: It was probably an energy change and hence a shift of the lines when the pressure is high enough.

Mattauch: Why should it affect one doublet line and not the other?

Duckworth: It is a differential effect. It affects both, presumably, but one more than the other.

H. D. Hagstrum: The comparisons were a very heavy type. The explanation was that this is slowed down more than the small ones, and hence the energy in the magnetic field was different and hence the doublet spacing changed as they changed pressure.

Mattauch: If you have 10^{-6} in there, I think that even you would—

Shaw: If the pressure is below 10^{-6} the pressure effect is very small.

Mattauch: I should say so.

4. A Discussion of Masses Derived From Recent Doublet and *Q* Measurements

By K. T. Bainbridge [1]

The proper time to present a table of masses is, certainly, after a conference is over and everyone has had a chance to discuss discrepancies and come to some mutual agreement as to what is right and what is wrong. This is particularly important for the light isotopes, as the higher masses in a mass table depend directly at the present time on knowing the secondary standards of mass, hydrogen, deuterium, and carbon to a high precision. These are the masses which provide the most widely used links between oxygen, the standard, and heavier masses.

Instead of presenting a mass table, I should like your permission to talk about a comparison between the mass spectroscopic mass table and that derived from disintegration measurements.

Last November Bill Buechner at M. I. T. was good enough to give me a list of a great many Q values which his group had measured with their Van de Graaff generator and analyzing equipment. Included among these Q values was the one involving oxygen, from the O^{16} (d,α) N^{14} reaction. This is the key reaction of the group. It was the first time that it had been measured with any great accuracy by deflection methods, and the measurement makes it possible to relate all of the lighter masses to oxygen.

When, in December, I had constructed a disintegration mass scale and started comparing it with the mass spectroscopic scale, I found considerable discrepancies, as a result of which I looked for the presence of possible systematic errors in one system or the other.

If such errors were present, they would not be subject to the ordinary laws of distribution of error. One cannot just pile weighted data into a machine and turn the crank. The matter comes down to a more subjective choice.

C, H, D, and also He, which enters into the Q scale, form the classical links to higher masses. Of these masses, that of carbon is the one which has given the most trouble, having been in dispute from the earliest days. Between the low values for $C^{12}H_4-O^{16}$ of 360 and 363×10^{-4} mass units of Aston and the value of 364.9×10^{-4}mu that Jordan and I reported from early work no agreement was ever reached, at least not between those two camps.

It is pleasing to see that there are now new approaches, that radically different instruments are under development (particularly those of Nier and Goudsmit), and that there are new methods of relating carbon to oxygen. Besides the recent experiments of Nier, Roberts, and Collins, relating C and O via S^{32}, we have Duckworth's work in which O, for example, can be referred to trebly ionized Ti^{48}, and C to quadruply ionized Ti^{48}. Further up the scale, singly ionized Ti^{48} can be referred to doubly ionized Mo^{96} and to quadruply ionized Pt^{192}.

---

[1] Harvard University, Cambridge, Mass.

These results yield a link to the higher masses, but one which is not firm as long as C^{12} is in dispute between the mass system based on Q values and the one based on mass doublets.

In addition to the new methods of approach using mass spectroscopes, we have completely different new instruments: the omegatron of Hipple, Sommer, and Thomas, the time of flight spectrometers of Goudsmit, Hays, and Richards and of L. G. Smith and his associates; and the cyclotron studies of Bloch and Jeffries. Even though not all of these instruments were designed specifically for the comparison of masses, they are very useful in measuring the H/D ratio, and in some cases they have particular applicability to heavier masses.

There are points of similarity between the methods of measurement of masses by spectrographs and by disintegration studies. Those who measure Q values most accurately are using deflection methods. They are applying the ion optics theories of Herzog and Mattauch, Stephens and Hughes, and others who have worked in this field in order to determine the momentum and energy of the products of nuclear disintegrations.

There is also an important similarity in the methods by which masses are obtained from the input Q data or the doublet data. In each system an expression is set up for $(M-A)$ which is equal to the mass excess referred to the mass number A of any particular isotope under consideration. For mass spectroscopic data $(M-A)$ is equal to the sum of some doublet measurements, where each one is multiplied by an appropriate simple numerical coefficient. In the case of disintegration work, the mass excess $(M-A)$ is equal to the sum of some Q values multiplied by simple numerical coefficients. The three classical doublets which relate H, C, and D to O are:

$$2\mathrm{H}-\mathrm{D}=a$$

$$3\mathrm{D}-\mathrm{C}/2=b$$

$$(\mathrm{C}+4\mathrm{H})-\mathrm{O}=c \text{ mass units.}$$

The simultaneous solution of these equations yields the familiar equations:

$$\mathrm{H}-\frac{\mathrm{O}^{16}}{16}=\mathrm{H}-1=\frac{3}{8}a+\frac{1}{8}b+\frac{1}{16}c$$

$$\mathrm{D}-\frac{\mathrm{O}^{16}}{8}=\mathrm{D}-2=-\frac{1}{4}a+\frac{1}{4}b+\frac{1}{8}c$$

$$\mathrm{C}-\frac{3}{4}\mathrm{O}^{16}=\mathrm{C}-12=-\frac{3}{2}a-\frac{1}{2}b+\frac{3}{4}c$$

In Nier's method, where C is related to O by means of S^{32},

$$4\mathrm{C}-(\mathrm{S}+\mathrm{O})=d$$

$$2\mathrm{O}-\mathrm{S}=e$$

and

$$\mathrm{C}-12=\frac{d-e}{4}$$

Similarly, if we designate by Q_1 the Q value for the reaction $O^{16}(d,\alpha)N^{14}$, Q_1 appears in the expressions for the mass excess of C, H, D, and He as follows:

$$C-12=\left(-\frac{3}{4}Q_1+\sum a_iQ_i\right)1.074\times10^{-3}$$

$$H-1=\left(-\frac{1}{16}Q_1+\sum b_jQ_j\right)1.074\times10^{-3}$$

$$D-2=\left(-\frac{1}{8}Q_1+\sum c_kQ_k\right)1.074\times10^{-3}$$

$$He-4=\left(-\frac{1}{4}Q_1+\sum d_eQ_e\right)1.074\times10^{-3}$$

where the Q values are in millions of electron volts and 1.074×10^{-3} is the conversion factor to mass units.

The results for $(M-A)$ can be compared for the two mass systems, or the directly measured mass spectrograph doublets can be compared with the sum of a set of Q values cast to give the equivalent doublet measurements.

At an informal conference held in March 1951, the following comparison of the two systems was made from data then available:

Doublet	Difference (Q—M.S.)
2H-D	~0.
3D-C/2	M.S. value greater
CH_4-O	M.S. value greater
2D-He	~0.

The differences which occur are well outside the probable errors of the individual results.

It was of interest to see whether, on the basis of this comparison, one could uncover evidence of systematic errors in one or the other of the two sets of measurements. For example, Q values are all measured relative to some standardization energy. Could an error in this value be the source of the discrepancies in the mass differences of the doublets listed above?

Standardization energies are supplied from several sources. Q values are measured relative to the energies of alpha-particles from Po, RaC′ and Th C, and relative to absolute calibrations of (p, n) thresholds obtained at the University of Wisconsin [1] and at the Research Laboratory of the Westinghouse Company.[2]

The alpha-particle energy values go back to 1928, and might be suspect simply because of the difficulty in making accurate magnetic field intensity measurements at that time. Richards has pointed out, however, that when Sturm [3] at Wisconsin measured the energy of RaC′ and Po alpha-particles in an absolute cylindrical condenser analyzer, he found excellent agreement with the earlier results of Briggs and Lewis and of Bowden. Thus the alpha-particle standardization energies have been checked by the same analyzer which had established the (p, n) threshold values in general use.

---

[1] R. G. Herb, S. C. Snowdon, O. Sala, Phys. Rev. **75**, 246 (1949).
[2] W. E. Shoupp, B. Jennings, W. Jones, Phys. Rev. **76**, 502 (1949).
[3] W. J. Sturm, V. Johnson, Phys. Rev. **83**, 542 (1951).

In any case, it is easy to see that an error in the standardization energies could not account for the discrepancies in mass values. For instance, if the standardization energies were off by some factor, say β, then since all doublet mass differences obtained from Q values represent the sum of a set of Q values, all of these differences would have to be corrected by the same factor, $1/\beta$. A correction of the (3D−C/2) and (CH_4−O) mass differences would result in a large disagreement between the Q and M. S. systems for (2D−He).

A second consideration for Q data is the question as to exactly what is measured as a Q value. Can the published Q values be taken over directly for calculations of atomic masses involving Q_{atomic}? The answer, which is that $Q_{\text{observed}}=Q_{\text{atomic}}$, is not immediately obvious.

Q is defined for the reaction 0 (1, 2) 3 as

$$Q_{\text{obs}}=Q=E_2+E_3-E_0-E_1 \tag{1}$$

where (0) is the target, (1) is the bombarding particle, (2) is the product particle whose energy is analysed in the experiment, and (3) is the residual nucleus.

In some books and articles Q, heat of reaction, is defined as

$$(M_0+M_1-M_2-M_3)C^2 \tag{2}$$

where the masses are nuclear and M_iC^2 is in millions of electron volts. The Q of equation (2) is really Q_{nuclear}, which must be corrected for the binding energy of the electrons when Q_{nuclear} is converted to Q_{atomic}. For example in a (d,α) reaction, the electrons are more tightly bound to the target nucleus (0) than to the residual nucleus (3), and the difference in binding energies between atoms (0) and (1), and between (2) and (3) ranges from a few hundred to approximately a thousand electron volts in the low **Z** region. This difference, although small. is close to some of the assigned probable errors of the measurements,

Fortunately Q_{observed} does equal Q_{atomic}, and no correction need be made to the observed Q in order to apply the Q measurements to atomic mass calculations. The explanation lies in a factor, suggested independently by Purcell, which had previously been considered by Hebb in connection with β-decay. The Hartree-Fock electronic field distribution surrounding the nucleus of the target (0) and residual atoms (3) increases the energy of the bombarding particle (1) and decelerates the outgoing particle (2) by just the amount needed to make $Q_{\text{observed}}=Q_{\text{atomic}}$.

The probability of other energy losses by excitation and ionization is small and can be neglected.

The large discrepancies which existed last March between the C. I. T. disintegration mass scale [4] and the mass spectrograph scale disappeared with the arrival of Ewald's [5] most recent results in April. However, there is still a considerable difference between Nier's value for CH_4−O and the equivalent in the Q mass scale. Most of this difference lies in the value for C^{12}.

---

[4] C. W. Li, W. Whaling, W. A. Fowler, C. C. Lauritsen, Phys. Rev. **83,** 512 (1951).

[5] See paper in this volume by H. Ewald.

I have made a second attempt to see whether I could point to one Q value or one doublet and say that it is responsible for the discrepancy in the CH_4-O values. There is indeed one Q value, that for the $O^{16}(d,\alpha)N^{14}$ reaction, which if changed by the huge amount of 48 kev would improve the agreement between Nier's mass spectograph scale of masses and the Q scale. In fact, the agreement on H^1, D^2, He^4, and (CH_4-O) would all be improved.

This possibility looked so intriguing that I spoke to Buechner about it. Although he was confident of the accuracy of his earlier measurements, he agreed to measure the reaction again under different conditions from those of the prior runs. He did so by a method which unequivocally identified this target nucleus as O^{16}, and obtained again the same Q value which he had measured prior to November, 1950, and which had been confirmed by later measurements at C. I. T.

Accordingly, I do not believe that the discrepancy between Nier's value for C^{12} and the Q derived value can be attributed to an error in the $O^{16}(d,\alpha)N^{14}$ reaction value, Q_1. Even though it is one of the two reactions in the entire mass structure which is unsupported, i. e., there are no alternative paths from O^{16} to N^{14} by means of other reactions, the $O^{16}(d,\alpha)N^{14}$ reaction is too firmly established to be considered in error by the gross amount of 48 kev.

Anyone seeking to compare mass tables must try out such arithmetical digressions, and there are many instances in the history of physics where interesting developments have resulted from surveys of available data. In the present instance, however, it seems clear that the answers must come from the laboratory.

5. The Use of Mass Spectrography in the Study of Nuclear Shell Structure[1]

By Henry E. Duckworth [2]

It has been known since the discovery of the mass defect by Aston in 1923 that a precise knowledge of atomic masses would yield significant information about nuclear stability. The desire to obtain this knowledge led to the design and construction of precision mass spectrographs and spectrometers. With these it is now possible to measure atomic masses with very great accuracy.

Most of the work in precision mass spectrography has been concerned with the measurement of the masses of certain of the lighter nuclides such as H^1, D^2, He^4, C^{12}, and N^{14}, the so-called secondary standards. Among the heavier nuclides, not only has less work been done, but also there has been very poor agreement among the results obtained in different laboratories. At least, such was the situation a couple of years ago when our group at Wesleyan University undertook to measure a number of the heavier masses with a view to determining the main features of the packing fraction curve. The state of knowledge of the heavier masses at that time is fairly well represented by Professor Dempster's celebrated packing fraction curve, first published in 1938. It is true that work done subsequent to 1938 indicated that the minimum in Dempster's curve should be somewhat lower than he had believed it to be, but there was no reason to doubt that the general shape of his curve was not correct.

An important feature of Dempster's curve was the experimentally observed fact that the slope in the mass region 90–104 was twice that in the mass region 180–208. This called for a point of inflection between the two regions which Dempster chose to locate at mass 180, giving rise to a semiplateau in the W–Pb region. In 1949 Feenberg suggested that this plateau be shifted to the tin region, which could be done, steepening the packing fraction curve in the zirconium-palladium (90–104) area and making the slope from wolfram to lead equal to one-half of this new value. This suggestion had also been implied by Mattauch in a packing fraction curve appearing in one of his isotope reports. We were interested in checking the existence of such a plateau in the neighborhood of tin, and became considerably more interested when it was realized that the break in the packing fraction curve at zirconium, resulting from the steep slope between zirconium and palladium, might be associated with the completion of the 50 neutron shell, which had recently been pointed out by Maria Mayer, Feenberg, Nordheim, and Hazel, Jensen and Suess, as constituting a particularly stable nuclear configuration. Measurements which were subsequently made of the masses of some of the isotopes of Sr, Zr, Mo, Pd, Cd, and Sn gave evidence that there was a marked effect associated with the closure of this 50 neutron shell, and resulted

---

[1] The experimental work described in this paper was done at Wesleyan University under Contract At(30-1)-451 with the Atomic Energy Commission.

[2] Hamilton College, McMaster University, Hamilton, Ontario, Canada.

in similar effects being sought in the neighborhood of other alleged "magic" numbers. Before describing the present status of this work I should like to speak about a couple of related topics.

It would be a tremendous undertaking to attempt to measure directly by mass spectroscopic methods the masses of all the stable isotopes. Fortunately, there are transmutation and other data available which can be used to compute from mass-spectrographically known masses the masses of many nearby nuclides. Foremost among the transmutation data are those obtained from (d, p), (n, gamma) and (gamma, n) experiments, which give directly the mass difference between adjacent isotopes of an element. If the product nucleus is unstable, its decay scheme is frequently known, so that the mass difference between two stable nuclides differing by one mass unit may still be calculated. In this connection, although it is not too difficult to keep posted on current (d, p), (n, gamma) and (gamma, n) experiments, one who is not a specialist in the field cannot hope to follow the beta-decay work without the help of Katherine Way's indispensable compendium and Mitchell's list of approved decay schemes. It frequently develops that an unstable nuclide decays by K-capture, in which case there is no way of directly measuring the energy which is carried off by the demure neutrino. In some instances of this type the daughter (p, n) threshold has been measured and furnishes the means of measuring the desired mass difference. This field of the measurement of (p, n) thresholds is one in which a great deal of work has yet to be done, particularly among the heavier nuclides where positron emission can seldom successfully compete with the K-capture process.

Recently a new type of mass datum has become available, arising from microwave absorption studies of the pure rotational spectra of certain linear molecules. This work, abetted chiefly by Townes and his group at Columbia, has resulted in relative mass differences for the isotopes of several elements, examples of which are germanium and selenium. In the case of these elements one is able, by measuring the masses of two of the stable isotopes by mass spectrographic means, to combine these results with the microwave data to obtain masses for most, if not all, of the other stable isotopes. Thus, as a result of our determinations of the masses of Ge^{70} and Ge^{72}, we have been able to compute masses for Ge^{74} and Ge^{76}. Furthermore, since the Ge^{74}-Se^{74} and Se^{77}-Se^{76} mass differences are known, it is possible to extend the germanium results and obtain absolute masses for all the stable selenium isotopes. This help from the microwave spectroscopist is very welcome to the mass spectroscopist, especially where it concerns elements which possess many isotopes.

It is now possible with the aid of auxiliary data of the sort I have just described to list masses for approximately 120 of the stable nuclides with Z greater than 21, or approximately half of the stable nuclides in this region. During the past summer I have made an attempt to examine this list for internal consistency in the following way: For elements for which a number of isotopic masses are experimentally known, the binding energy per nucleon, B.E./Nucleon, has been plotted against mass number and compared with the predictions of the semiempirical mass formula, as shown in figure 1 for the elements nickel and cobalt. The semiempirical curves (using the values computed by Metropolis), shown as dotted lines, have been displaced vertically by an arbitrary amount so as to facilitate the

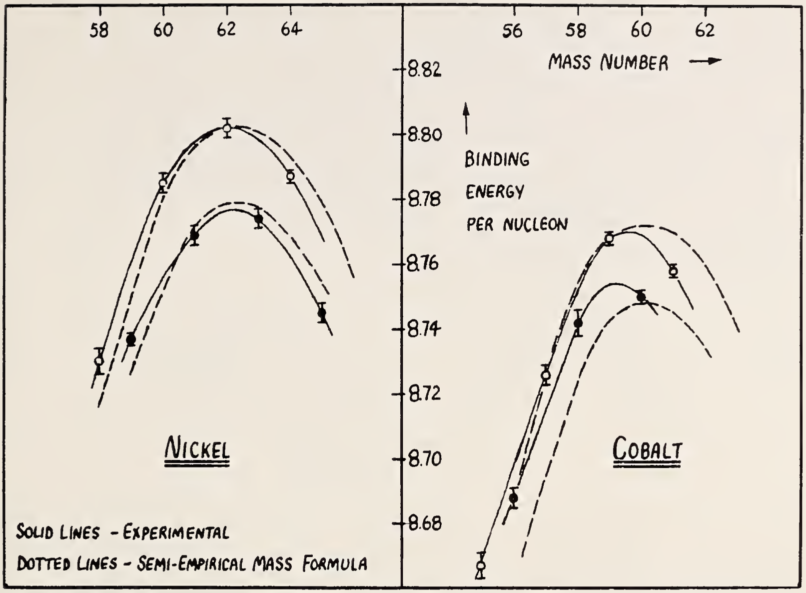

FIGURE 1. *Comparison of the experimental with the semiempirical mass formula calculation of the binding energy per nucleon for nickel and cobalt isotopes.*

comparison. In the cases shown in figure 1, and in others not shown, it appears to be possible to draw a smooth pair of parabolic-like curves through the experimental points, of the same general shape as those predicted by the mass formula. In fact, on the basis of this sort of study of many elements, the condition that two such curves exist appears to be a necessary one, and the use of the criterion of smoothness of the curves seems to be a valid means of detecting inconsistencies among the masses. Furthermore, the curves for a given element may be used to estimate masses for some isotopes which are otherwise not known. A few examples of the use of these will now be given.

In figure 2, the three known masses for gallium are shown with their respective probable errors. Also, as indicated on the plot in figure 2, one knows from the Ga^{71} (gamma,n) threshold of 9.05 Mev that Ge^{71} is 0.005 Mev/nucleon more stable than Ga^{70}. It is now an easy matter to sketch the curves shown, being guided with respect to their sharpness of curvature by the known curves for copper (with atomic number 2 less than Ga) and arsenic (with atomic number 2 greater than Ga). In a similar manner, using a number of experimental masses together with the measured Br^{79} (gamma,n) threshhold, the curves for bromine can be drawn, as is also shown in figure 2. The third example in figure 2, that of strontium, is an example of how the criterion of two smooth curves can be used to mass assign a reaction. Sherr, Halpern, and Mann have measured (gamma,n) thresholds for three strontium isotopes, tentatively assigning 11.15 Mev to the Sr^{88} (gamma,n) and 9.50 Mev to the Sr^{86} (gamma,n) thresholds. It seems logical to assign the larger threshold to Sr^{88}, a 50-neutron configuration, until one realizes that such an assignment leads to the situation shown by the dotted curves in figure 2, where the even-even curve intersects the even-odd, a most unlikely situation.

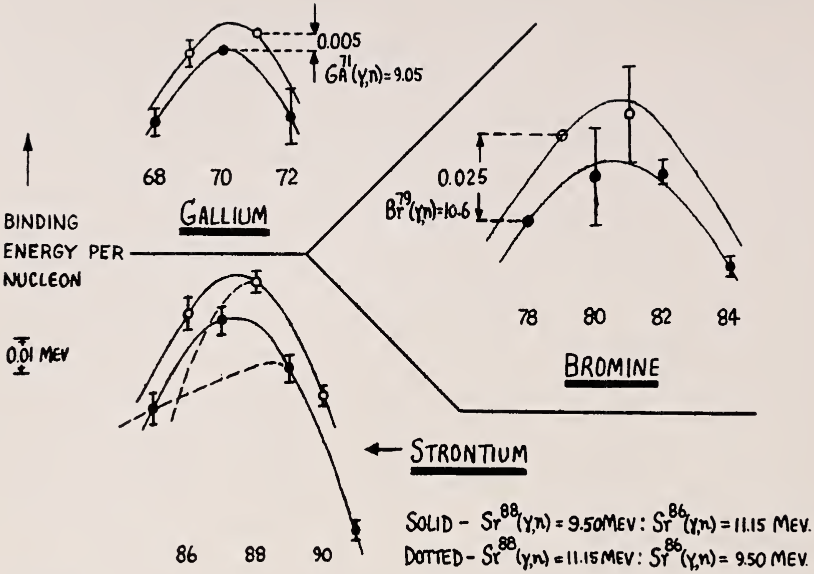

FIGURE 2. *Use of binding energy per nucleon curves to predict and confirm masses.*

This inconsistency is removed if one associates the 11.15 Mev threshold with Sr^{86} and the 9.50 Mev threshold with Sr^{88}, since then, as is shown in figure 2, two smooth curves of the type expected are obtained.

By means of this type of empirical consistency check, we have satisfied ourselves that the mass-spectrographically obtained values for the heavy masses, plus the other masses derived from these, constitute a reasonably consistent set, and should give a correct picture of the main features of the binding energy curve in the regions where masses are available. As is to be expected, we have discovered some notable inconsistencies, as for example, in the masses of Cr^{50}, Sn^{117}, Sn^{122}, Te^{128}, and Pt^{192}. It is our intention to remeasure these and other suspected values.

The present status of the work is shown in figure 3, in which the B.E./Nucleon is plotted against mass number for all the known heavy nuclides. I should like to draw your attention to certain features of this curve which have special significance:

(a) There is a well-known break in this curve occurring at mass number 208, presumably due to the completion of the 82-proton shell and the 126-neutron shell.

(b) Clearly shown is the sudden break in the region of mass 90, which is to be associated with the closure of the 50-neutron shell. This sudden change in slope appears to occur at Sr^{88} (rather than at Zr^{90} as we had earlier suggested).

(c) There is an unmistakable break in the 82-neutron region, probably located at Ce^{140}.

(d) The stabilizing effect of the 50-protron configuration has a pronounced effect on the B.E./Nucleon, giving rise to a definite plateau which breaks off at or in the neighborhood of Sn^{120}.

(e) The maximum of the binding energy occurs at Ni^{62}. It may or may not be significant that the maximum is located at this particular isotope of nickel, but it is undoubtedly significant that it is an isotope of nickel, the element whose proton number is 28.

These five features of the B.E./Nucleon curve for the heavy masses are now well authenticated. In addition to these, as can be seen from figure 3, there are faint suggestions of other fine structure which need further study, and there are also whole unexplored regions.

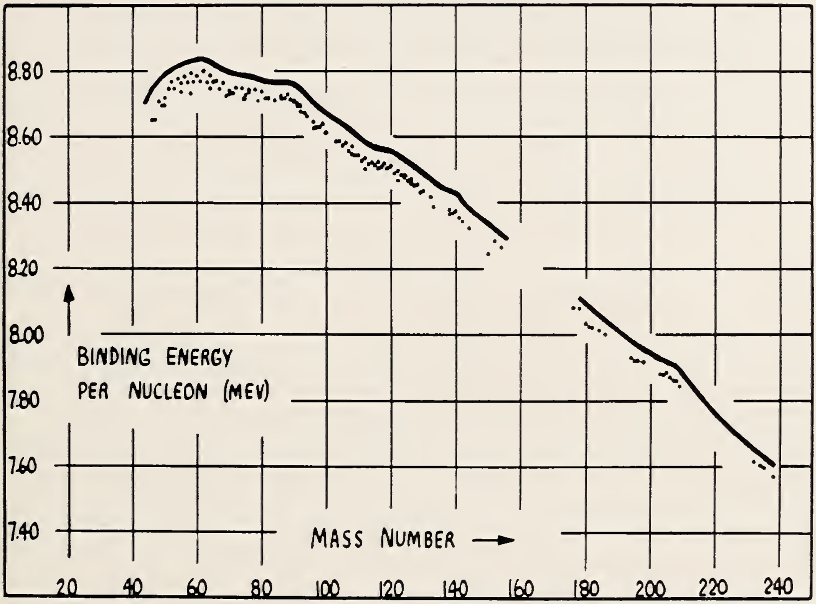

Figure 3. *Binding energy per nucleon curve for nuclides with $Z>21$.*

6. On the Substandards of Atomic Mass

By K. Ogata and H. Matsuda[1]

1. Introduction

In 1936, immediately after Bainbridge-Jordan's paper appeared in the Physical Review, we were intending to construct the double-focusing mass spectrograph of their type under Prof. T. Asada in Osaka University. The features of this apparatus were quite similar to those of Bainbridge-Jordan's; the angle of electric field and magnetic field were $\pi/\sqrt{2}$ and $\pi/3$ respectively, and the radius of the center beam in both fields 25 cm. The construction of the apparatus was completed in 1938 and mass determination by means of this apparatus was started at the beginning of 1939. After that we continued our mass measuring work until the beginning of 1943. During that time, we obtained the masses of about 31 isotopes. However, the evacuating system of this apparatus was not very good, so the gas pressure at the operating condition was about 5 to 6×10^{-5} mm of Hg. The collimating system consisted of two slits, the widths of which were 0.05 mm and 0.02 to 0.03 mm, respectively, the length about 5 mm, and the distance between them 40 mm. The photographic plate was located on the line through the apex of magnet pole piece and the double-focusing point. Under these conditions, we obtained spectral lines with breadth of about 0.07 to 0.08 mm, and so the resulting experimental resolving power was roughly estimated as 7,000 to 8,000, though its calculated resolving power was about 17,000.

At the beginning of 1943, our work was suspended and this apparatus was dismantled, and we evacuated from Osaka. After the war, in 1947, we began the reconstruction and improvement of our apparatus and this work was completed towards the end of last year.

2. Apparatus

The main points of the improvement were aimed at the evacuating system and the collimating system in order to get sharper lines than those in our old mass measurements mentioned above. The evacuating system now used consists of one 6-in. fractionating oil diffusion pump, its pumping speed being about 280 liters/sec at 10^{-4} mm of Hg, and two $4\frac{1}{2}$-in. oil diffusion pumps and one mercury diffusion pump with liquid air trap. These pumps are backed by 80 liters/min mechanical pumps. The evacuating leads are made as large as possible in diameter and as short as possible in length. The 6-in. pump is connected to the electric field, one $4\frac{1}{2}$-in. pump to the magnetic field and the camera, and the other $4\frac{1}{2}$-in. pump and the mercury pump to the collimating chamber. The collimating chamber is separated into two parts by a canal, the diameter of which is about 1 cm, the length about 7 cm. The part before this canal is evacuated by the mercury pump and the part behind by the $4\frac{1}{2}$-in. pump.

The ions are created by ordinary gas discharge in a cylindrical glass discharge-tube with a diameter of about 5 cm, and a length of

---

[1] Department of Physics, Faculty of Science, Osaka University, Japan.

about 50 cm. A stable electric discharge is maintained by using a 20 kv transformer with a rectifier and a 2 μF smoothing condenser. Two 20 k-ohm resistors are used in series to anode, and stable discharge current of 2–4 ma is obtained during the operating time. The gas or vapour to be examined is introduced into the discharge-tube near the cathode through an adjustable leak of needle type. Under the operating condition, the gas pressure in the deflecting fields and the camera is about 7 to 8×10^{-6} mm of Hg measured by a Fogel-type ionization gage. With the pumping system and vacuum material now used, we could not decrease the pressure less than that.

The second point improved is in the collimating system. It consists of a hole and a principal slit. The hole has a diameter of about 0.5 mm and is positioned at one end of the canal which is bored through the center axis of the cathode. The diameter of the canal is 1.5 mm and the length 10 mm. The front surface of the cathode is flat. The principal slit is located at the entrance of the electric field, its width is 0.005 to 0.008 mm and its length about 0.2 mm. The distance between the hole and the principal slit is about 45 cm and the resulting aperture angle α becomes between 1/1800 and 1/1100. The energy selecting slit which is placed at the exit of the electric field is 0.08 mm wide and so the energy aperture is about $\beta = 1/6000$. At this aperture condition, the theoretically expected increase in the line breadth caused by 1 mm vertical shift of the plate from the velocity focal plane is about 5/10000 mm and is 5/1000 mm for the same shift from the directional focal plane, that is, about ten times larger than that for velocity. So the plate is located nearer to the directional focal plane than to the velocity one. The angle of the photographic plate against the center beam is about 24°, according to Herzog's calculation.

Other parts of the apparatus, the electric field and the magnetic field, are quite similar to that used in the earlier stage of our mass measurement. The electric field potential is obtained from twenty-six 90-v dry batteries connected in series, and the center point is grounded. For the magnet current supply, a 6 to 18 v storage battery of 100 amp/hr capacity is used. Both the electric field and the magnetic field are sufficiently stable during the exposure time, which is usually a few minutes. The photographic plates used in our experiment are of the Schumann-type and of our own making. The schematic diagram of the apparatus used now is shown in figure 1.

3. Resolving Power

For the rough determination of the experimental resolving power, we took the photograph of the proton line on several positions of a photographic plate by changing the strength of the magnetic field, and roughly measured the total line breadth by a comparator. Figure 2, shows the line breadth and the dispersion curve for 1 percent mass difference. From these curves, we can roughly calculate the experimental resolving power at any point of photographic plate. The resolving power thus obtained is also shown in the figure. The maximum resolving power obtained from these results is about 60,000. For mass determination we can use a region of about 8 cm on the photographic plate without decreasing the accuracy, 3 cm on the heavier mass side and 5 cm on the lighter side, from the double-focusing point.

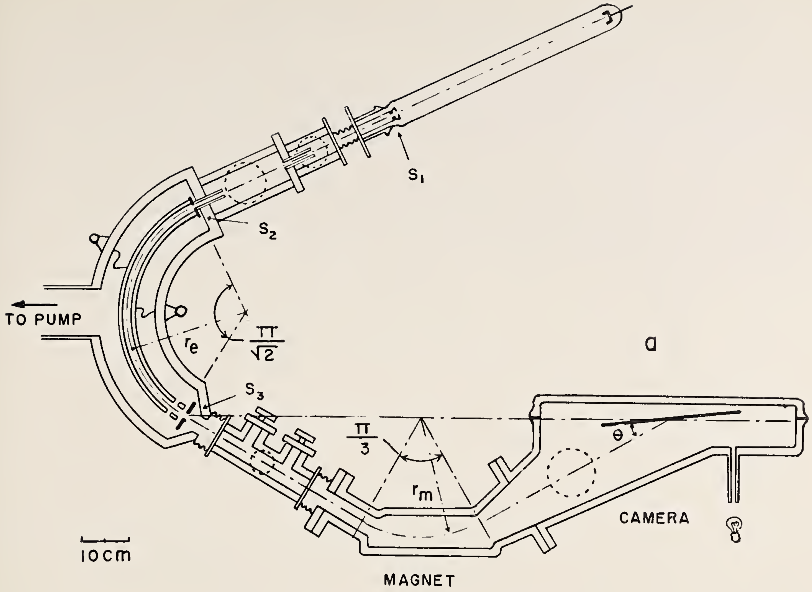

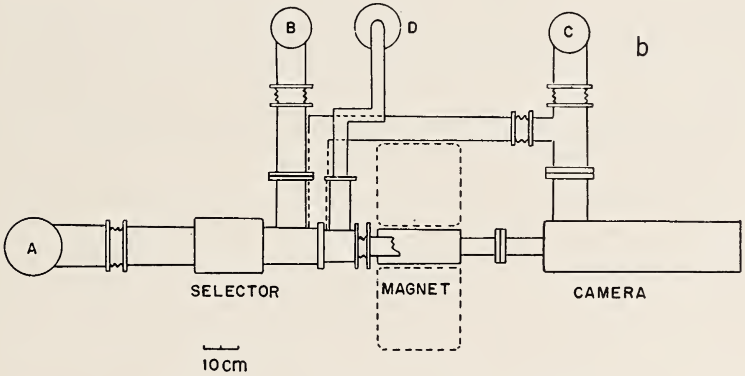

FIGURE 1a. *Diagram of mass spectrograph.*

$s_1=0.5$ mm, $s_2=0.005$ mm, $s_3=0.08$ mm, $r_e=25$ cm, $r_m=25$ cm, $\Theta=24°$.

FIGURE 1b. *Details of vacuum system.*

A, 6 inches oil diffusion pump; *B. C*, 4.5 inches oil diffusion pump; *D*, mercury diffusion pump.

4. Mass Scale Calibration

In such a narrow region where the doublet is photographed, as mentioned above, the following linear relation probably will hold for two doublets of different kind on the same position of a plate;

$$\frac{\Delta M_1}{M_1}\bigg/\frac{\Delta M_2}{M_2}=\frac{\Delta D_1}{\Delta D_2} \tag{1}$$

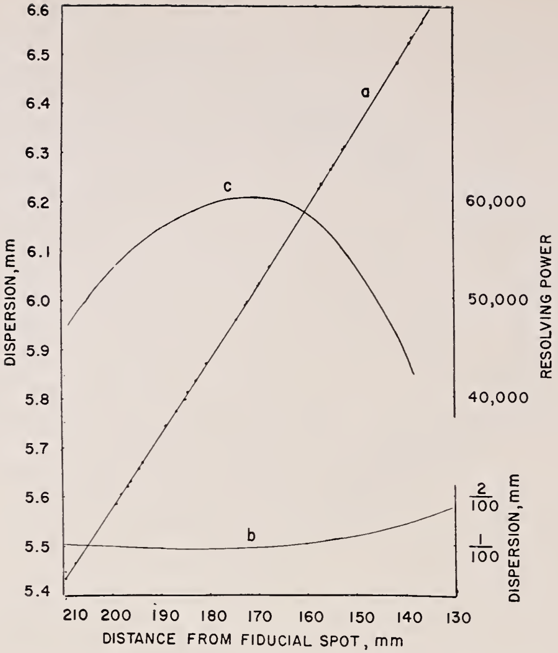

FIGURE 2. *Study of performance of the mass spectrograph using the proton line.* *a*, Dispersion for 1 percent mass difference; *b*, line breadth; *c*, resolving power.

where

ΔM=mass difference between the component of doublet

M=mass at the center of the doublet

ΔD=line separation of the doublet.

In order to check the limit of the breadth of the doublet separation at which the above relation holds, we used the Br-BrH (its separation is about 7 mm), C_3-group components (15 mm), C_2-group components (24 mm), and C_1-group components (38 mm). The dispersion of C_3-group components are in agreement with that of Br-BrH within 0.01 percent error in the region on the photographic plate usually used, and for C_2-group the agreement is satisfactory near the double-focusing point, but in the distant region about 0.05 percent discrepancy appears. On the other hand, for the C_1-group even near the double-focusing point, the disagreement becomes 0.03 percent. According to these investigations, the mass scale linearity in the region usually used seems to hold unless the doublet separation does not exceed that of C_3-group components (about 15 mm). So we can adopt as the calibration standards the separation of Br-BrH or that of C_3-group components. In our present case we use the Br-BrH separation for the calibration standards; the reason is that the Br and BrH lines are very easily photographed by the electric discharge through the vapour of methylene-bromide. The masses of ^{79}Br, ^{81}Br and ^{1}H are assumed as 78.943, 80.941, and 1.0081, respectively, the masses of Br being the mean values of Aston's and ours, while the mass of ^{1}H is taken from the Mattauch-Flammersfeld's table. This mass scale calibration was made for each plate.

5. The Determination of Doublet Mass Difference

In 1947, Dr. H. Ewald reported on the causes of systematic errors occurring in the mass measurement by a mass spectrograph. We investigated (with our apparatus) whether or not the mass differences measured were affected by the following factors, some of which were considered in his paper.

1. The center potential of the electric field was shifted about ±400 volts from that of the earth. Under such condition we measured the mass difference of $^{12}CH_4$-^{16}O doublet, and we obtained the following results:

Center potential	$^{12}CH_4-^{16}O$ Mass difference	Number of doublets measured
+400 v	364.59±0.1	3
0	364.47±0.05	75
−400 v	364.31±0.21	5

From these results, the mass difference seems to be not affected by such shifts of center potential from that of the earth.

2. We investigated whether the measured mass differences were influenced by their location on the photographic plate, that is, by the location of ion beam in the magnetic field. As an example, we show the variation of the mass difference of $^{12}CH_4-^{16}O$ as a function of position on the photographic plate in figure 4. This fluctuation is quite at random, and so we think that it is not necessary to make any correction for the measured mass differences according to their positions on the plate. Therefore, as the mass difference of a doublet, we adopted the mean value of the mass differences calculated from the doublets situated on several positions of the photographic plate.

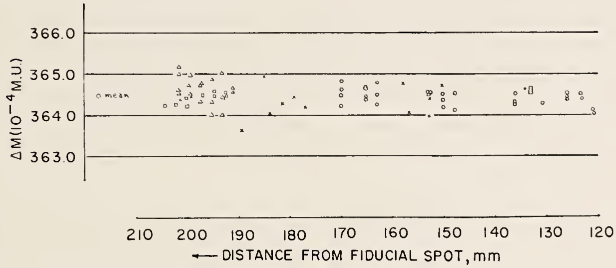

Figure 3. *Variation of measured CH_4-O mass difference with a position on photographic plate.*

□, plate I; △, plate II; X, plate III; ○, plate IV.

3. The influence of the intensity difference between the component lines of a doublet on the measured mass difference was investigated.

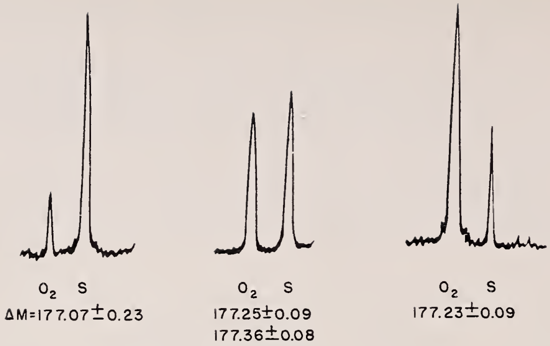

FIGURE 4. *Study of effect of intensity.*

For example, the mass differences of ${}^{16}O_2-{}^{32}S$ were determined under the following intensity relations (shown in fig. 4) and the results obtained are

${}^{16}O_4-{}^{32}S$ Mass difference ($\times 10^{-4}$amu)

Intensity	Mass difference	Number of doublets measured
${}^{16}O_2<{}^{32}S$	177.07±0.23	8
	177.25±0.09	14
${}^{16}O_2={}^{32}S$	177.36±0.08	32
${}^{16}O_2>{}^{32}S$	177.23±0.09	18

Considering these results, we may say that the difference between the intensities of the component lines of doublets can not be a serious cause of systematic errors.

4. Finally, we investigated under our present collimating condition whether or not any difference was found between the mass difference which was calculated from the separation of molecular-atomic doublet and that from the separation of molecular-molecular doublet. For example, the mass differences of ${}^{12}C^{1}H_4-{}^{16}O$ and ${}^{12}C_2{}^{1}H_4-{}^{12}C^{16}O$ and that of ${}^{12}C^{1}H_2-{}^{14}N$ and ${}^{12}C_2{}^{1}H_4-{}^{14}N_4$ were determined, and the results are shown as follows:

$$
\begin{aligned}
{}^{12}C^{1}H_4-{}^{16}O&=364.43\pm0.05\\
{}^{12}C_2{}^{1}H_4-{}^{12}C^{16}O&=364.51\pm0.06\\
{}^{12}C^{1}H_2-{}^{14}N&=125.94\pm0.02\\
{}^{12}C_2{}^{1}H_4-{}^{14}N_2&=251.99\pm0.05
\end{aligned}
$$

From these results, no discrepancy between them can be found beyond their experimental errors, and so we adopt the weighted means of each pair as ${}^{12}C^{1}H_4-{}^{16}O$ and ${}^{12}C^{1}H_2-{}^{14}N$ mass differences.

6. Results and Discussion

Under the condition mentioned just now, we determined the mass differences of several doublets, and these results are summarized in table 1. On the determination of mass difference of each kind of doublet, about ten or twenty doublets of the same kind were photographed on several positions of a plate, and two or four photographic

TABLE 1. *Mass differences* ($\times 10^{-4}$ *amu*)

A	Doublet	Source of ions	ΔM	Number of doublets measured
2	$^{1}H_2-^{2}D$	D_2 gas	15.525±0.006	62
6	$^{2}D_3-\frac{1}{2}{}^{12}C$	D_2+CH_4	423.46 ±0.07	35
14	$^{12}CH_2-^{14}N$	Air+CH_4	125.94 ±0.02	36
28	$^{12}C_2H_4-^{14}N_2$	Air+$(CH_2Br)_2$	251.99 ±0.05	18
14	$^{12}C^{1}H_2-^{14}N$		125.97 ±0.03	(Weighted mean)
15	$^{12}C^{1}H_3-^{15}N$		233.95 ±0.05	45
16	$^{12}C^{1}H_4-^{16}O$	O_2+CH_4	364.43 ±0.05	75
28	$^{12}C_2{}^{1}H_4-^{12}C^{16}O$	Air+$(CH_2Br)_2$	364.51 ±0.06	36
16	$^{12}CH_4-^{16}O$		364.47 ±0.04	(Weighted mean)
32	$^{16}O_2-^{32}S$	$O_2+H_2S_{16}$	177.27 ±0.05	72
34	$^{32}S^{1}H_2-^{34}S$	H_2S	199.02 ±0.03	37
36	$^{12}C_3-^{34}SH_2$	$H_2S+C_7H_{16}$	165.56 ±0.03	21
48	$^{12}C_4-^{32}S^{16}O$	$SO_2+C_7H_{16}$	331.27 ±0.07	32

Atomic Masses (amu)

$^{1}H=$ 1.008 151 4±12	$^{15}N=$15.004 905 ±6
$^{2}D=$ 2.014 754 2±21	$^{32}S=$31.982 273 ±5
$^{12}C=$12.003 845 4±21	$^{34}S=$33.978 676 ±7
$^{14}N=$14.007 551 ±4	

plates were used. The tabulated mass differences are the weighted means of the mean values which were calculated from the doublets of each plate, and the errors given were estimated from the probable errors based on the internal consistency of the data, and also that which may probably be caused from the mass scale calibration. These mass differences seem to be in fair agreement with Nier's recent values. For $^{1}H_2-^{2}D$, the agreement with Robert's 15.519±0.017 is excellent, and this mass difference is in good agreement with that calculated from nuclear reaction, 15.494±0.024 (Whaling's value). However, the $^{12}CH_4-^{16}O$ mass difference has a great discrepancy with that from transmutation, 363.72±0.12 (Whaling's value). For $^{16}O_2-^{32}S$, the present value is in good agreement with values obtained by other investigators, especially with that calculated by H. T. Motz as the best fit value, 177.2±0.5. We have found the value obtained in our earlier research to be utterly incorrect, but now we can not make clear the cause of such a mistake. On the other hand, the mass difference $^{32}S^{1}H_2-^{34}S$, which was measured at the same time, is in fair agreement with our present one.

From these doublet mass differences, we calculated the atomic masses of ^{1}H, ^{2}D, ^{12}C, ^{14}N, ^{15}N, ^{32}S, and ^{34}S. At first, we calculated the atomic mass of ^{12}C and ^{1}H from the three different cycles of doublets illustrated in table 2. These three values of ^{12}C and ^{1}H are unfortunately not in complete agreement with each other, but the discrepancies between them are not so much, so we adopted the weighted means of them for ^{1}H and ^{12}C. The atomic mass of ^{2}D was calculated from cycle I. These ^{1}H, ^{2}D, and ^{12}C are summarized in table 1 with ^{14}N, ^{15}N, ^{32}S and ^{34}S. The ^{12}C thus obtained agrees well with the Nier's value which was calculated from $^{12}C_4-^{32}S^{16}O$ and $^{12}C^{16}O_2-^{12}C^{32}S$, but not so well with Robert's, and disagrees with that calculated from transmutation data.

The agreement among the atomic masses which were measured by different methods (transmutation, mass spectrometer, mass spectrograph, synchrometer, etc.) is not so good. Now, we can not understand the cause of these discrepancies between the mass differences or the atomic masses determined by transmutation and by mass spectograph. However, nowadays, many different methods of mass determination are being carried on, so I hope that the accurate and correct values of atomic masses will be determined before long. We now intend to determine the mass differences again by using a different type of ion source, such as the electron bombarding type, and also by using different cycles of doublets.

TABLE 2.

I	II	III
$^{12}CH_4-^{16}O$ (a)	$^{12}CH_4-^{16}O$ (a)	$^{12}CH_4-^{16}O$ (a)
$^{2}D_3-\frac{1}{2}{}^{12}C$ (b)	$^{16}O_2-^{32}S$ (d)	$^{16}O_2-^{32}S$ (d)
$^{1}H_2-^{2}D$ (c)	$^{12}C_4-^{32}S^{16}O$ (e)	$^{12}C_3-^{34}S^{1}H_2$ (f)
		$^{32}S^{1}H_2-^{34}S$ (g)
$^{12}C=12+\frac{1}{4}(3a-2b-6c)$	$^{12}C=12+\frac{1}{4}(e-d)$	$^{12}C=12+\frac{1}{4}(a+f-d-g)$
$=12.003833\pm5$	$=12.003850\pm2$	$=12.003843\pm3$
$^{1}H=1+\frac{1}{16}(a+2b+6c)$ $=1.008153\pm1$	$^{1}H=1+\frac{1}{16}(4a+d-e)$ $=1.008149\pm1$	$^{1}H=1+\frac{1}{16}(3a+d+g-f)$ $=1.008151\pm1$

Weighted mean: $^{12}C=12.003\ 845\ 4\pm21$; $^{1}H=1.008\ 151\ 4\pm12$.

7. Masses of Hydrogen, Carbon, and Some Nuclides of Medium Mass

By Thomas L. Collins [1]

The design and operation of the Minnesota mass spectrograph has been described by Dr. A. O. Nier. I should like to describe the results which we have obtained from this instrument during the last six months. The work is divided into two separate topics: the measurement of secondary mass standards, and the measurement of some medium masses.

In April, 1951, we completed a series of measurements on doublets leading to masses for hydrogen and carbon (H^1 and C^{12}, the symbols H, C, O, and S will be used for the abundant isotopes). The results of these measurements have already been widely circulated although they are still in the process of publication.[2] I believe a review of the history of these measurements is instructive.

Early this year we received simultaneously the results of Dr. Ewald's mass measurements and a table of masses computed from nuclear reactions by Li, Whaling, Fowler, and Lauritsen.[3] The agreement was striking. Measurements by Nier and Roberts [4] were in marked disagreement with their masses for hydrogen and carbon. In view of the radical design of our mass spectrograph, it was imperative that we investigate the discrepancies before we could believe any of our measurements. It must be noted that the instrument underwent considerable revision after Roberts completed his work. We were not successful in completely removing the disagreement.

Because one of the "fundamental" mass doublets is not readily available with our type of source, we had to choose another set of doublets. We decided to concentrate on the sulfur doublets introduced by A. O. Nier. Thus, if

$$C_4-SO=a\text{(at mass 48)}$$

$$\text{and } O_2-S=b\text{(at mass 32)}$$

$$\text{then } C^{12}=12+\tfrac{1}{4}(a-b).$$

Hydrogen may then be computed from $C_3H_8-CO_2=c$(at mass 44), a doublet difference just twice the value of CH_4-O. There are several advantages in this set. Although the doublets are measured at high masses and hence have large absolute errors, the simplicity of the equations gives a very favorable compounding of errors. All doublets are measured in a relatively restricted mass range, requiring but small readjustment of the instrument; we feel this allows a better control of systematic error. Indeed, it is difficult to postulate systematic errors which would not largely cancel in the computation of the mass of carbon.

---

[1] University of Minnesota, Minneapolis, Minn.
[2] Collins, Nier and Johnson, Phys. Rev. **84**, 717 (1951).
[3] Li, Whaling, Fowler and Lauritsen, Phys. Rev. **83**, 512 (1951).
[4] A. O. Nier and T. R. Roberts, Phys. Rev. **81**, 507 (1951).

Our investigation disclosed an important possible source of error. It is possible to check and adjust readily the energy (velocity) focusing of our instrument. As Dr. Nier has outlined, this is accomplished by moving the ion tube in the magnet gap until a peak does not shift by more than 1 part in 10^5 when the 6,000-v accelerating potential is varied by about 40 v. To obtain consistent results, it was necessary to make this adjustment at least every day. The mass difference O_2-S is particularly sensitive to a lack of energy focus when the source of sulfur ions is SO_2 gas. When H_2S gas is used, much of this sensitivity disappears. The same doublet difference is found only when the energy focusing is adjusted in the manner outlined. Our preference for the C_3H_8-CO_2 doublet is based largely upon a similar sensitivity exhibited by the CH_4-O doublet.

After we had investigated each step of our method, we started a series of measurements. Each day we adjusted the energy focusing and obtained one run of each of the doublets and of a hydrogen mass doublet. A run consists of at least five forward and five backward traces of the two peaks. The large number of readings allows the computation of a statistical error for each run and the variations from day to day were consistent with these errors. From these statistics we compute the probable errors quoted. The results are

$$C_4-SO=33.132\pm 0.013 \text{ mmu.}$$

$$O_2-S=17.764\pm 0.007$$

$$C_3H_8-CO_2=72.854\pm 0.015\ (2\times 36.427)$$

giving $H^1=1.008146\pm 3$, $C^{12}=12.003842\pm 4$.
During the period when these measurements were being made, we frequently checked the operation of the instrument by measuring the mass difference between two hydrocarbon peaks differing by one hydrogen mass. We felt that an agreement within 0.1 percent of the accepted value of hydrogen was a good check on the operation of our machine. The average value of these measurements was 1.0083 with a standard deviation of 0.0003.

These masses are larger than those found by Dr. H. Ewald and those computed from nuclear reactions. The O_2-S difference is in reasonable agreement with Ewald's measurement. To obtain the same mass for carbon the C_4-SO difference would have to be less than 33.0 mmu! The fundamental CH_4-O difference is also high; however, if Dr. Ewald were to increase his value for this one doublet to agree with ours all masses would be essentially in agreement.

Because the disagreement was beyond statistical doubt, there was little profit in taking more measurements which would only improve the statistics. We therefore communicated our results to other mass spectroscopists with the request that they attempt to measure this set of doublets and proceeded with our work in the higher mass range.

A survey of the history of mass doublets will show that mass spectroscopy must be plagued by systematic error. Under similar circumstances prior knowledge of the "correct" answer has affected the results of careful experiments. It is probable that in our admitted endeavour to find why our instrument did not give "correct" answers we unknowingly controlled some factor in the direction of agreement. The probable errors which we quote do not allow for this possibility, and I would not be able to argue strongly against slightly higher masses.

Primarily this instrument is used for the measurement of higher masses where its great sensitivity allows the measurement of almost every stable isotope. In the last few months we have measured the masses of all isotopes of titanium, vanadium, chromium, manganese, and iron with the exeption of V^{50} (table 1). The work in this region now includes 31 nuclides between S^{32} and Fe^{58}. In addition it is possible to compute the masses of many unstable isotopes from nuclear reaction energies. We have also measured the masses of the krypton isotopes.

Table 1. *Atomic packing fractions*

Isotope	Packing fraction times 10^4	Comparison mass
Ti^{46}	7.181 ± 10	CH_2S
Ti^{47}	7.088 ± 20	CH_3S
Ti^{48}	7.673 ± 12	C_4
Ti^{49}	7.432 ± 11	C_4H
Ti^{50}	7.846 ± 8	C_4H_2
V^{51}	7.741 ± 9	C_4H_3
Cr^{50}	7.580 ± 13	C_4H_2
Cr^{52}	8.256 ± 18	C_4H_4
Cr^{53}	7.978 ± 15	C_4H_5
Cr^{54}	8.09 ± 4	C_4H_6
Mn^{55}	8.035 ± 20	C_4H_7
Fe^{54}	8.140 ± 9	C_4H_6
Fe^{56}	8.444 ± 18	C_4H_8
Fe^{57}	8.142 ± 18	C_4H_9
Fe^{58}	8.27 ± 7	C_4H_{10}
Kr^{78}	7.027 ± 23	C_3H_3
Kr^{80}	7.193 ± 14	C_3H_4
Kr^{82}	7.365 ± 13	C_3H_5
Kr^{83}	7.00 ± 5	C_3H_5
Kr^{84}	7.338 ± 11	C_3H_6
Kr^{86}	7.186 ± 9	C_3H_7

$H^1 = 1.008146 \pm 3$, $C^{12} = 12.003842 \pm 4$, $S^{32} = 31.982236 \pm 7$.

As the packing fraction curve is filled in, it shows an increasingly complex shape. There is great interest in discontinuities at "magic numbers", which are related to a nuclear shell structure. In this mass region both 20 and 28 have been separately suggested as magic numbers. We now have masses for four stable 20-neutron nuclei, five stable 20-proton nuclei, and five stable 28-neutron nuclei. It is interesting to look for an effect from nuclear shell structure.

Unfortunately, the odd-even fluctuations characteristic of the lighter nuclei are still present in this mass region. It is difficult to see discontinuities in the packing fraction curve or binding energy surface which could be associated with magic numbers. An initial approach to the problem of allowing for these fluctuations was to compare the masses with those predicted by the Bohr-Wheeler formula. The formula does not fit well although it does predict much of the fluctuation in mass. We have found that a more satisfactory fit can be obtained using Wigner's mass formula.[5]

Wigner expresses the binding energy as the sum of a coulomb, a kinetic, and a potential energy. The radius constant in the coulomb energy has been evaluated from mirror nuclei and the kinetic energy is expressed in terms of the same constant. The potential energy is expressed in terms of two potential functions L and L′ and the number of possible symmetric and antisymmetric couplings in the nucleus. Theory indicates that AL and AL′ should be constant. Comparison

---

[5] G. Gamow and C. L. Critchfield, Atomic Nucleus and Nuclear Energy Sources (Oxford Press, 1949).

with masses has shown that a fit over a wide range can be obtained by the addition of a surface effect. Thus we assumed

$$L = a_1 A(1 - a_3/A^{1/3})$$

$$L' = a_2 A(1 - a_3/A^{1/3}),$$

and obtained the constants a_1, a_2 and a_3 empirically by fitting the formula to our data.

TABLE 2. *Wigner mass formula minus observed masses for the 28-neutron region, 10^{-4} amu*

N	Ca	Sc	Ti	V	Cr	Mn	Fe
32	Fitted region						−2
31						−3	5
30					−3	0	8
29				−7	−1	3	1
28	−1		8	−8	−2		−6
27		−3	−17		−21	−20	−32
26			−25		−29		
25		−39	−27	−39	−52		
24	−46	−56	−49				

As an illustration table 2 presents the differences between the observed masses and the formula with constants fitted to nuclei having more than 28 neutrons. When the formula is extrapolated to the five stable nuclei with 28 neutrons, it also fits the data. For nuclei with less than 28 neutrons the errors become progressively larger. When the formula is fitted to nuclei with less than 28 neutrons a reverse pattern is found. The 28-neutron nuclei again fit, but nuclei with more neutrons do not. This shows a discontinuity of slope at 28 neutrons which may be associated with nuclear shell structure. In a similar manner, it can be shown that 20 neutrons are associated with a discontinuity in masses; however, the pattern suggests that the discontinuity is somewhat different in form. From this analysis it would appear that both 20 and 28 neutrons are magic numbers. This work is continuing.

8. New Doublet Measurements

By J. Mattauch and R. Bieri [1]

By careful adjustment, it is possible to obtain in the mass spectrograph used by us (type 5 of section 3 of the introductory paper of this symposium) sharp lines and with them nearly the theoretical resolution along the whole plate. Proof of it is figure 1 showing enlargements of multiplets at mass numbers A=4, 14, $14\frac{1}{2}$, 15, 17 and 29. They are all taken from the same plate and, with the exception of figure 1b, from the same exposure. These exposures were made with a mixture of air and a higher freon compound in the discharge tube in an attempt to get highly charged ions, e. g., the doublet $({}^{4}\text{He}-{}^{12}\text{C}^{3+})$ (fig. 1a). Indeed, with the highly ionizing effect of fluorine and the exposure of $17^{m}9^{s}$ even the rare isotopes of all the elements were obtained with which the gas come into contact. Multiplets at half-integral mass numbers caused by many doubly charged molecular ions provide a series of interest. Figure 1c shows a sample. The exposure of $17^{m}9^{s}$ covering the mass range from A=3 to A=33 shows doublets and multiplets at not less than 28 positions.

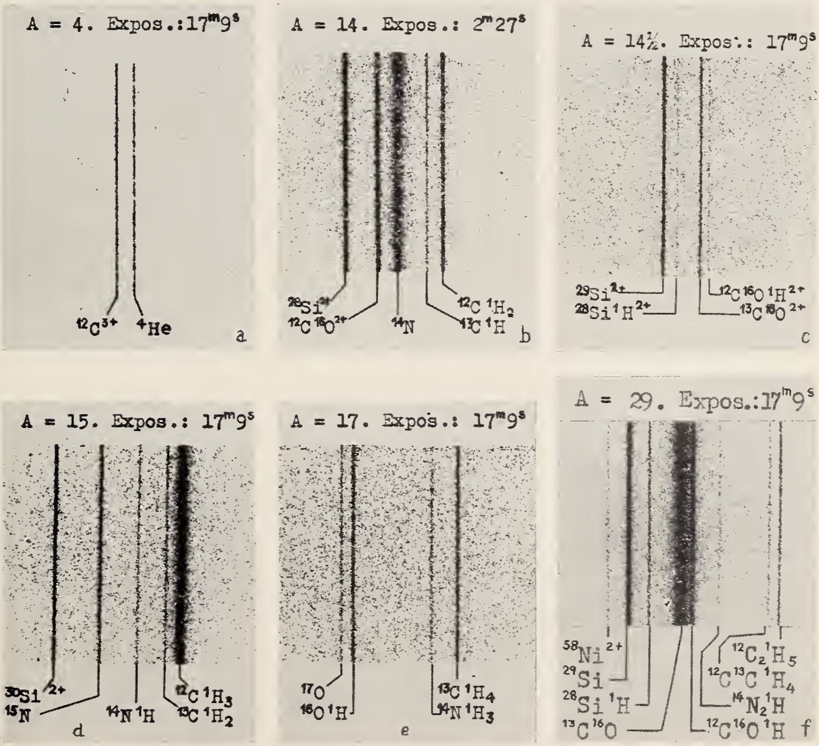

FIGURE 1. *Multiplets at six different mass numbers from a single exposure of 17 minutes, 9 seconds, except for b.*

---

[1] Max Planck Institut für Chemie, Mainz, Germany.

For the purpose of measurement, it is of course necessary to match the intensity of the doublet lines. This was done with the doublets $({}^1H_2-{}^2D)$, $({}^2D_2-{}^4He)$, $({}^2D_3-{}^4He{}^2D-\frac{1}{2}{}^{12}C)$, $({}^4He_2-{}^{16}O)$, $({}^{12}C{}^1H_2-{}^{14}N)$, $({}^{12}C{}^1H_4-{}^{16}O)$ and $({}^{14}N{}^1H_3-{}^{16}O{}^1H)$. Figure 2 shows a few examples. Twenty to thirty exposures of each have been obtained, together with suitable dispersion lines and with a resolving power of 30,000 to 50,000 and in the best cases of 70,000. By changing the magnetic field strength the position y_0 of the doublet was varied between exposures. Therefore the dispersion coefficient D was changed each time. It is hoped that in this way systematic errors, introduced by slight inhomogeneities of the magnetic field and other causes, may cancel as far as possible. Furthermore, D and the first coefficient α_1 in the development of the mass scale can now be determined experimentally in the way shown in the last section of the introductory paper. Up to now, this was done for the doublets at A=2 and A=16. Figure 3 shows the results for $\eta=(D-D_{\text{theor.}})$ and for α_1 plotted against y_0. In order to obtain $D_{\text{theor.}}$ one has, of course, to measure the distance of lines from a fiducial point. Since it is not possible to insert the plate every time in exactly the same position, the rows of points belonging to the same plate sometimes show systematic displacements from each other. The general slope of the η–curve agrees well with the theoretical slope (entered as a straight line) which one obtains according to eq (97) of the introductory paper from the deviation of the mean of the experimentally determined values of α_1 from its theoretical value which in our case is minus one quarter. The upper plot shows the deviations v. of the individual doublets from their mean value. As expected, they do not show a trend with y_0 though the dispersion coefficient has been changed by more than a factor of 2. We cannot maintain any longer the provisional values of the mass differences of these two doublets given at the time of the Symposium. At that time we relied on a calibration factor given to us by the Office of Weights and Measures in Berne where the measurements were made and which in the meantime was found to be slightly erroneous.

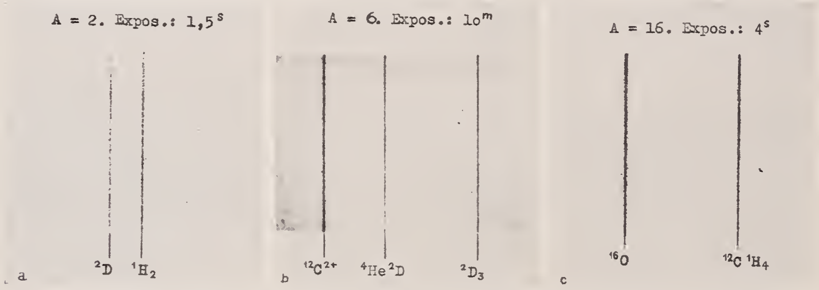

FIGURE 2. *Examples of doublets of matched intensity.*

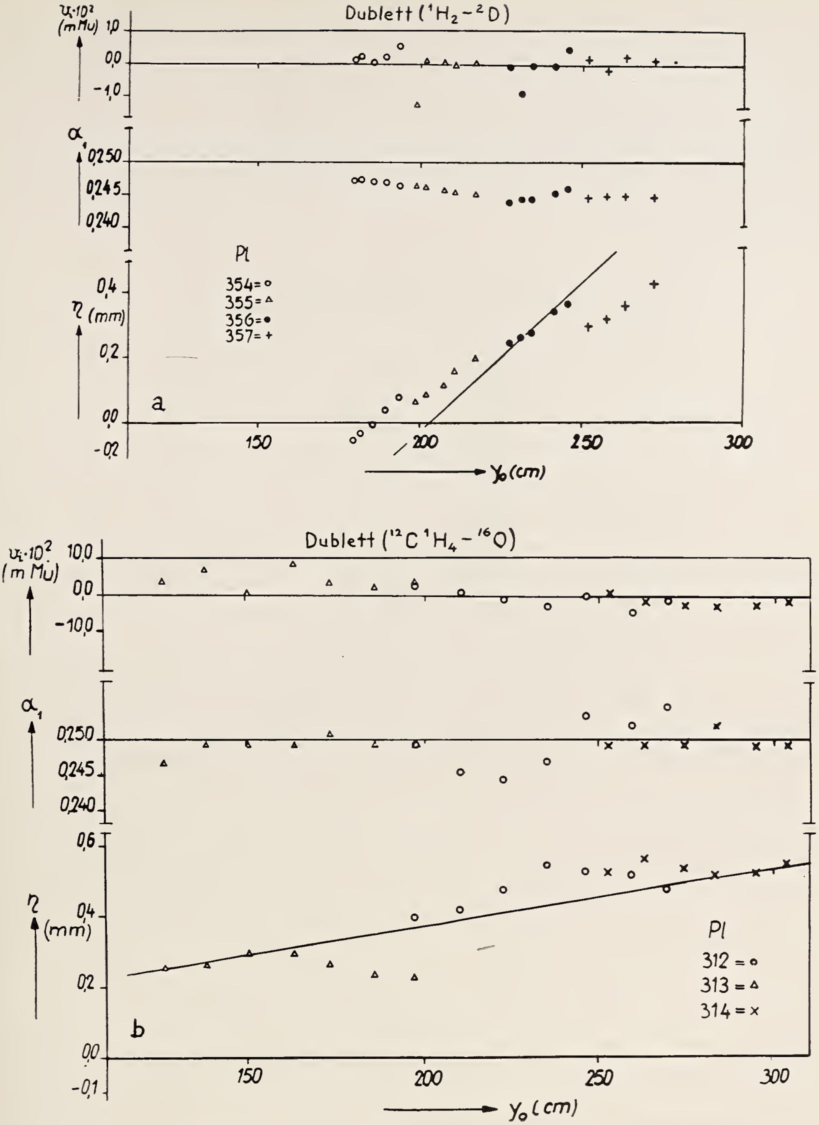

FIGURE 3. *The deviations v_i from the mean doublet value, the experimentally determined values of α_1 (theoretical value $\alpha_1 = -0.250$), and the differences η between the experimentally determined values of D and its theoretical value $\left(D_{\text{theor}} = \frac{1}{2} y_0\right)$ are plotted for each individual doublet against its position y_0 on the plate.*

Between the system of eight doublets that leads to the masses of the five substandards, ^1H, ^2D, ^4He, ^{12}C and ^{14}N, three checking relations must hold of which a least squares solution is to be obtained. Moreover, multiplets like ($^{12}C\,^1H_4 - ^{12}C\,^2D\,^1H_2 - ^{12}C\,^2D_2 - ^{14}N\,^1H_2 - ^{14}N\,^2D - ^{16}O$), of which a not yet matched example is shown in figure 4 will provide still another check because they permit expressing with high accuracy the mass difference ($^{12}C\,^1H_4 - ^{16}O$) or ($^{12}C\,^1H_2 - ^{14}N$) in terms of the doublet ($^1H_2 - ^2D$) without any knowledge of the dispersion coefficient.

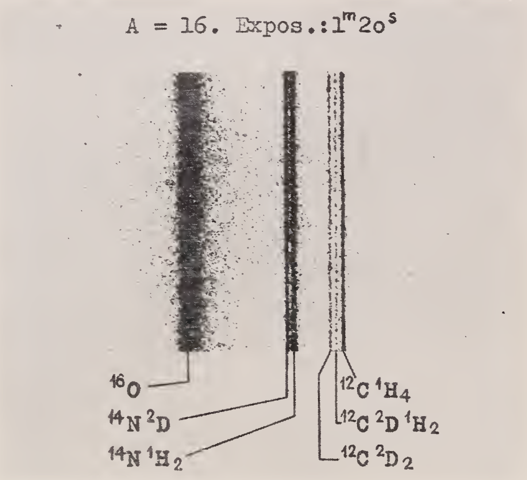

FIGURE 4. *Multiplets at mass 16.*

9. Some Recent Investigations in Electron and Ion Optics

By N. Svartholm [1]

Instruments that are intended for work in the spectroscopy of charged particles, which includes energy spectroscopy as well as mass spectroscopy, must have both dispersion and focusing properties.

It is certainly justifiable to regard the focusing properties as the secondary consideration. This can be shown, for example, by the principle of Aston's mass spectrograph, where geometrical focusing is completely absent and where resolution with respect to mass is obtained by means of collimation. In other systems which include some kind of geometrical focusing, resolution can be improved by collimation, at least in principle. Collimation has, however, the disadvantage of reducing the intensity of a beam. Thus the problem of improving a dispersing system can be put in the following way:

The resolution of a system being given, how can the intensity be increased? Putting the problem in this way indicates that geometrical focusing is, after all, a most important property.

Taking as a first example the magnetic prism, we find that there are two ways of improving the focusing properties: The shaping of the boundaries of the field and the shaping of the field itself. Both ways can be followed up in a great number of ways and it is not here feasible to give an exhaustive treatment of this question. I understand that Dr. Herzog is going to speak about the first group of problems. I will speak about some improvements of focusing in magnetic and electric fields which can be achieved by using shaped instead of uniform fields, and especially about the conditions for the so-called two-directional focusing as opposed to the one-directional focusing in uniform fields.

In order to explain this principle, let us take a magnetic field of any type and shape. Assuming that one single ion path is given, which may be any curve, even a twisted one, we search for the conditions to be fulfilled by the field for all neighboring paths to be focused equally towards the given path, which hereafter is called the central path of the system.

The answer to this problem is simply the following. Take an arbitrary point P of the central path and an osculatory plane at that point. The component of the magnetic field B perpendicular to this plane must have a gradient in the direction of the principal normal ν which is expressed by

$$\frac{\partial B}{\partial \nu} = -\frac{1}{2}\frac{B}{R}$$

where R is the radius of curvature at P.

The simplest case to which this principle can be applied is obviously

---

[1] Atomic Energy Laboratory, Stockholm, Sweden.

that of a plane central path of constant curvature. This was done in the construction of a beta-ray spectrometer at the Nobel Institute in Stockholm by Kai Siegbahn and myself about six years ago [1].[2] A small model magnet was first built with a radius of 12.5 cm and with a linear aperture angle, both axial and radial of about 0.1 radians. The instrument was used only for testing the focusing principle. In 1947 a bigger instrument was built [2] which has a radius of 50 cm, and a maximum linear aperture angle in both directions of about 0.4 radians. The resolution corresponding to that aperture was 1.3 percent. In beta-ray spectroscopy the conditions are such that in general the intensity requirements are most urgent. In exceptional cases, however, where strong sources are available, it is possible to decrease the apertures and to obtain resolutions of the order 0.1 percent. Experience in this field might be of some value in mass spectroscopy, too. It was found that relative measurements of momenta over a wide range can be made with an accuracy of one part in 10,000: For magnetic fields produced by electromagnets with iron this figure represents, I believe, an approximate limit of what is possible. The situation is a little more favorable for a uniform 180° field than for a shaped field, since it is easier in the former case to measure the field very precisely along the path of the particles, as has been done by Lindström [3] in his absolute determinations of beta-energies. It is even necessary to measure the field distribution for each setting of the field to make sure that the hysteresis of the iron does not disturb the results. The hysteresis effect is a more intricate question for the nonuniform field. Measurements made with the big beta-ray spectrometer show that the field gradient is slightly affected by the premagnetization of the iron and has to be measured continuously by means of rotating coils.

I mentioned that the condition for two-directional focusing is given by a relation between the field gradient and the field itself. If one makes calculation in more detail one finds that the resolution of the instrument, expressed as the line width of the image of a point source, is, in general, of the same order of magnitude as in the case of a uniform field, being proportional to the square of the (linear) angular aperture. A refinement of the focusing, involving a further gain in intensity, can be obtained by giving a prescribed value also to the second derivative of the field at each point of the central path. Writing the field strength B in the symmetry plane as a power series in the relative distance $\rho=(r-r_0)/r_0$ from the central path

$$B=B_0\ (1+\alpha_1\rho+\alpha_2\rho^2+\ \ldots\ )$$

the coefficient α_1 determines the gradient at points on the central path and the focusing angles, while α_2 determines the line width. In fact, it is possible to choose α_2 so that the line width vanishes for a beam of rays with either axial or radial angular aperture, but not, however, for a beam with simultaneous axial and radial aperture. The two cases mentioned correspond to the two values $\alpha_2=\frac{3}{8}$ and $\alpha_2=\frac{1}{8}$ respectively. In Stockholm we choose ⅜, while Shull and Dennison [4] at Michigan preferred ⅛. Which one chooses is not very important but has some bearing upon the actual design of the instrument.

When the demand for high resolution is less urgent, the coefficient α_2 may have any value close to the figures ⅛ and ⅜. The mean value

---

[2] Figures in brackets indicate the literature references on p. 82.

$\alpha_2=\frac{1}{4}$ has a special interest since the magnetic field is then easy to realize. It can be represented, apart from terms of higher order, by

$$B=2B_0r_0/(r_0+r)$$

which is the field between two conical pole faces. A beta-ray spectrometer has recently been built according to this principle at the University of Uppsala [5]. It was designed with a mean radius of 18 cm and a maximum angular aperture about four times bigger than that of the Stockholm instrument (fig. 1).

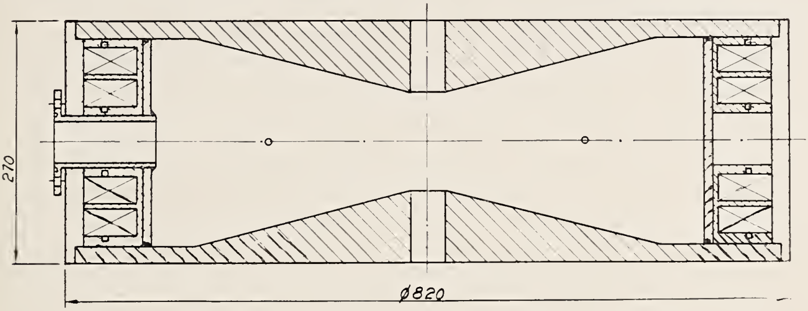

Figure 1. *Cross section of the Uppsala beta-ray spectrometer.*

It is obvious that the same types of fields can be applied to instruments intended for the energy spectroscopy of positive ions. From a constructional point of view it is more convenient to use a sector field instead of the complete 255° field. Here much stronger fields are needed, while the intensity requirements can be set lower in favor of a better resolution. It was shown by Lauritsen and collaborators [6] in the Kellogg Radiation Laboratory at Pasadena that a sector field of 180° is especially suitable for this kind of work. The resolution attainable is of the order 0.1 percent or better.

Also in mass spectroscopy similar focusing principles should be applicable. Some figures for the resolution which I have mentioned would be considered rather good if they were obtained in an ordinary spectrometer. Here the intensity question is much less important, so the resolution wanted can be obtained by collimating the incident beam. There are special cases, however, where focusing in shaped fields might have some advantages. In the separation of radioactive isotopes for nuclear investigations it is desirable to have a good total yield, which might be obtained by means of some type of focusing.

Finally, I will speak about the focusing in combined magnetic and electric fields for application in instruments with very high resolution. First a few words about instruments with the two fields in cascade. Such instruments have been used with uniform fields mostly for the measurement of atomic masses by the photographic doublet method. They can be grouped into (a) instruments which give energy focusing for one single mass, or, approximately, for two masses in a doublet, and (b) those giving energy focusing for all masses. When photographic recording is used, instruments of type (b) are preferable, while scanning and electrical recording can be applied in any type. To group (a) belong all instruments, such as Dempster's and Bainbridge-Jordan's, in which an intermediate image is formed at a point between the electrostatic field and the magnetic field. Here the essential point is that the radii of the fields are adjusted so that the energy dispersion of the two fields compensate. This can be achieved in any type of nonuniform field, too. Combined geometrical and energy focusing with the formation of an intermediate image can in fact be obtained in a great variety of ways. In order to get two-directional focusing in the electrostatic field one has to cut out a sector of a spherical condenser. The sector angle of the electric field as well as that of the magnetic field is immaterial in this connection. The inclusion of the principle of two-directional focusing would, no doubt, be advantageous for increasing the intensity in instruments for very high resolution.

In instruments belonging to group (b) no intermediate image is formed. It is well known from the work of Herzog and Mattauch that focusing for all masses is obtained if the sector angle of the electric field is $\pi/4\sqrt{2}$ ($\sim 32°$) and the sector angle of the magnetic field 90°. In the case of photographic recording, for which this focusing is so well suited, it seems natural, if not indispensable, to stick to the uniform magnetic field, while the electrostatic field can be shaped at will in order to improve the geometrical focusing. One such case suggests itself, namely the spherical condenser. It can be shown that energy focusing occurs for all masses if the sector angle amounts to 30°. The distance between the source or defining slit and the edge of the electric field has to be $r_e\sqrt{3}$, where r_e is the mean radius of the field (fig. 2). All paths which initially have radial as well as axial aperture angle, and belong to ions with the average energy, are parallel in the region between the two fields, which fact makes the edge effects less serious. The length of the image at the plate equals the maximum width of the beam.

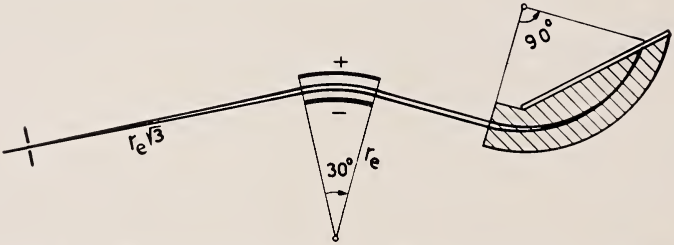

Figure 2. *The spherical condenser in a Mattauch-Herzog arrangement.*

The next question concerns the combination of electric and magnetic fields as simultaneous, or more exactly, as crossed fields. I mentioned that the second-order aberration of a nonuniform magnetic field can not be eliminated for paths with both radial and axial angular aperture. The same is true for a purely electrostatic field. By combining the two fields it is possible, however, to eliminate the second-order terms in a great number of ways. Moreover, energy focusing is achieved by an appropriate balancing of the fields. The following table summarizes some of the most important focusing cases, including both single-field and crossed-field systems. The first row gives the coefficient α_1 for a magnetic field and the corresponding focusing angle in the case of pure radial focusing, pure axial focusing and two-directional or stigmatic focusing, respectively. The second row gives the coefficient β_1, for an electrostatic field and the corresponding focusing angle. Finally, the last row refers to that particular case of crossed electric and magnetic field which gives energy focusing. For uniform fields the conditions for focusing were found by Bartky and Dempster in 1929 [7]. The principle is well known from the work of Dr. Shaw, who applied it to the determination of e/m for electrons. It was also used in a mass spectrometer built in Vienna by Bondy, Popper, and Johannsen [8]. It is indicated in the table that the same type of focusing occurs in nonuniform fields where the gradients are coupled together by the relation $\beta_1=2\alpha_1-1$. Similar relations exist for the two other cases quoted, the purely axial focusing, which has minor practical importance, and the two-directional focusing, where the relation is $\beta_1=2\alpha_1$ and the focusing angle π instead of $\pi/\sqrt{2}$ for the radial focusing. The last equation can be satisfied in various ways. First by the value $\alpha_1=-\frac{1}{2}$, which is the same as in the purely magnetic case, combined with the uniform electric field between two cylinders $\beta_1=-1$. This combination was applied in a model instrument which was constructed in 1948 in order to test the principle [9]. A uniform magnetic field $\alpha_1=0$ can also be used if combined with an electric field having $\beta_1=0$. In order to eliminate the second-order line width [10] for all directions one has to choose a third alternative $\alpha_1=\frac{1}{4}$, $\beta_1=\frac{1}{2}$. Furthermore, the next coefficients α_2 and β_2 must fulfill the relation $\beta_2=2\alpha_2+\frac{1}{2}$ which leaves one parameter free. Here, again, one special choice $\alpha_2=\frac{1}{4}$, $\beta_2=\frac{5}{8}$ is preferable. One reason for this is that the magnetic field can be realized by means of an electromagnet with conical pole pieces, which facilitates the accurate machining work considerably. The electric field is obtained by using deflectors with a radial section having a radius of curvature of $\frac{2}{3}$ r_o, where r_o is the radius of the central path.

TABLE 1.

Field	F	Directional focusing								
		Radial			Axial			Two-directional		
		α_1	β_1	Φ	α_1	β_1	Φ	α_1	β_1	Φ
Magnetic	1	0	------	π	-1	------	π	$-\frac{1}{2}$	----	$\pi\sqrt{2}$
Electric	0	----	-1	$\pi/\sqrt{2}$	----	-3	$\pi/\sqrt{2}$	----	-2	π
Crossed (velocity focusing) $f=eBr/mv$.	2	α_1	$2\alpha_1-1$	$\pi/\sqrt{2}$	α_1	$2\alpha_1+1$	$\pi/\sqrt{2}$	α_1	$2\alpha_1$	π

We decided, three years ago, to build a larger instrument according to these principles for measuring atomic masses and by using the techniques of the ordinary mass spectrometry, including electron impact ion sources, electric ion current measurements and some sort of scanning. The reasons for building such an instrument were certainly very similar to those which Professor Nier spoke about this morning with the very important difference that we had almost no experience in mass spectrometry in Stockholm. The magnet (figs. 3 and 4) is again of the ring type with a mean radius of 50 cm and a maximum field of 3,500 gauss, a central yoke and two exciting coils.

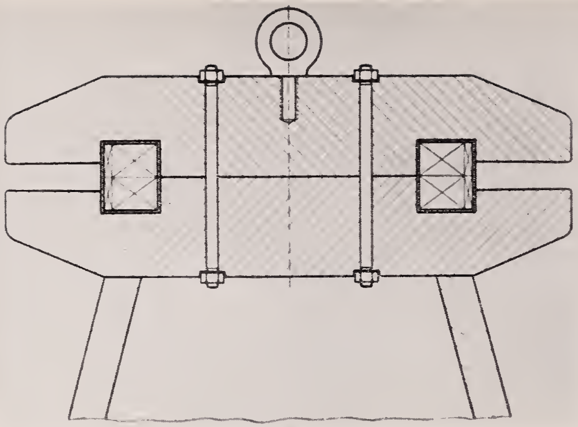

Figure 3. *Cross section of the mass spectrometer magnet.*

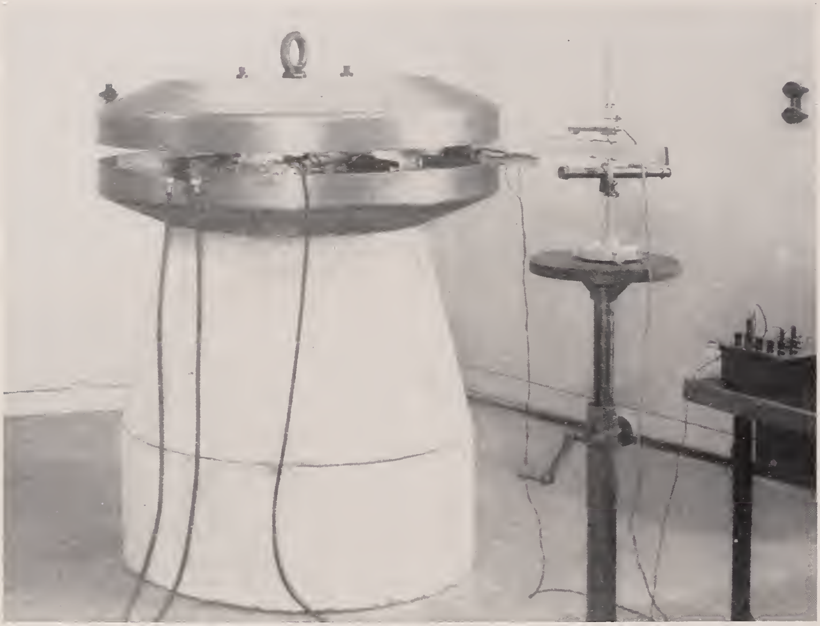

Figure 4. *The mass spectrometer magnet.*

Figure 5 shows a cross section of the pole faces, the vacuum chamber, and the deflectors.

Finally, I would say a few words about a method intended for the measurement of the relative mass difference in a mass doublet. Let us forget for the moment everything concerning the focusing and take the condition for the balance of the forces acting upon an ion moving in a circular path of radius r in crossed magnetic and electric fields, B and E, respectively. On the one hand there is the magnetic force evB directed towards the center of curvature, and on the other hand

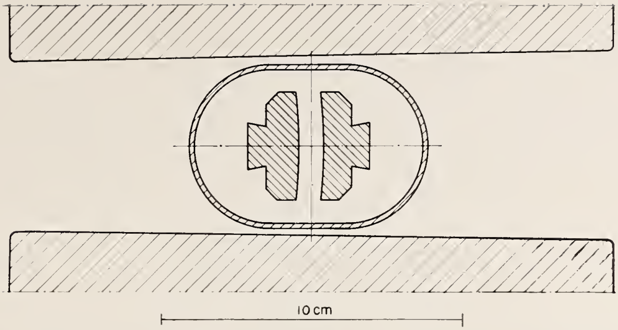

Figure 5. *Radial cross section of the mass spectrometer showing the pole faces, the vacuum chamber, and the deflectors.*

the electrostatic force eE and the centrifugal forces, directed outwards, or

$$evB=eE+mv^2/r$$

which shows that the relation between the velocity v and the magnetic field B for a given value of E, is represented by a branch of an hyperbola with a minimum of B, corresponding to energy focusing. For lower values of B no ions will describe the path considered, while for higher values of B there are two different values of v for ions with the same path. This means that scanning of the accelerating voltage V gives two peaks for each ion species. This was demonstrated in the model instrument mentioned earlier for hydrogen molecule ions (fig. 6). In figure 7 the deviation of the magnetic field from the value at exact velocity focusing in relative units is plotted versus the accelerating voltage for two different mass values m and $m+\Delta m$. If they do not differ very much from each other, one can show that, if the heavier mass gives a single peak at the voltage V_0 corresponding to exact energy focusing, and if the lighter mass gives two peaks at the voltages $V_0-\Delta V$ and $V_0+\Delta V$, then the simple relation

$$\frac{\Delta V}{V_0}=2\sqrt{\frac{\Delta m}{m}}$$

exists. A similar relation can, of course, be derived for the more general case where the magnetic field is sufficiently big to give two peaks for each kind of ions. From an experimental point of view, it is satisfactory that these relations do not contain values of the electric and magnetic fields, but they do include ratios between voltages, which have to be measured with an accuracy of about 0.1 percent. These ratios are rather big even for narrow doublets; for example, $\Delta m/m=10^{-4}$ gives $\Delta V/V_0=0.02$. This fact appears to be an advantage. On the other hand, the considerations just referred to apply to the central path of a beam only. When the accelerating voltage is varied, the conditions for geometrical focusing are also changed, which is a disadvantage. For small mass differences this effect will not be too big. Therefore, if sufficiently high resolution can be obtained, the apparatus would be most useful for close doublets.

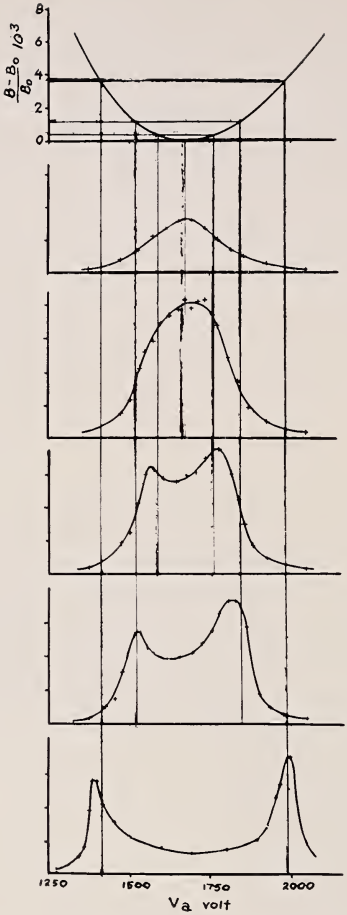

FIGURE 6. *The effect of varying the accelerating voltage in a crossed-field spectrometer.* From a model experiment

---

[1] N. Svartholm and K. Sieghahn, Arkiv mat. astron. fysik [A] **33**, 21 (1946); N. Svartholm Arkiv mat astron fysik [A] **33**, 24 (1946).
[2] A. Hedgran, K. Siegbahn, and N. Svartholm, Proc. Phys. Soc. **63**, 960 (1950).
[3] G. Lindstrom Phys. Rev. 83, 465 (1951).
[4] F. Shull and D. Dennison, Phys. Rev. **71**, 681 (1947); **72**, 256 (1947).
[5] Not yet published.
[6] C. W. Snyder, S. Rubin, W. A. Fowler, and C. C. Lauritsen, Rev. Sci. Instruments **21**, 852 (1950).
[7] W. Bartky and A. J. Dempster, Phys. Rev. **33**, 1019 (1929).
[8] H. Bondy, G. Johannsen, and K. Popper, Z. Physik **95**, 46 (1935).
[9] Not published.
[10] N. Svartholm, Arkiv fysik **2**, 195 (1950).

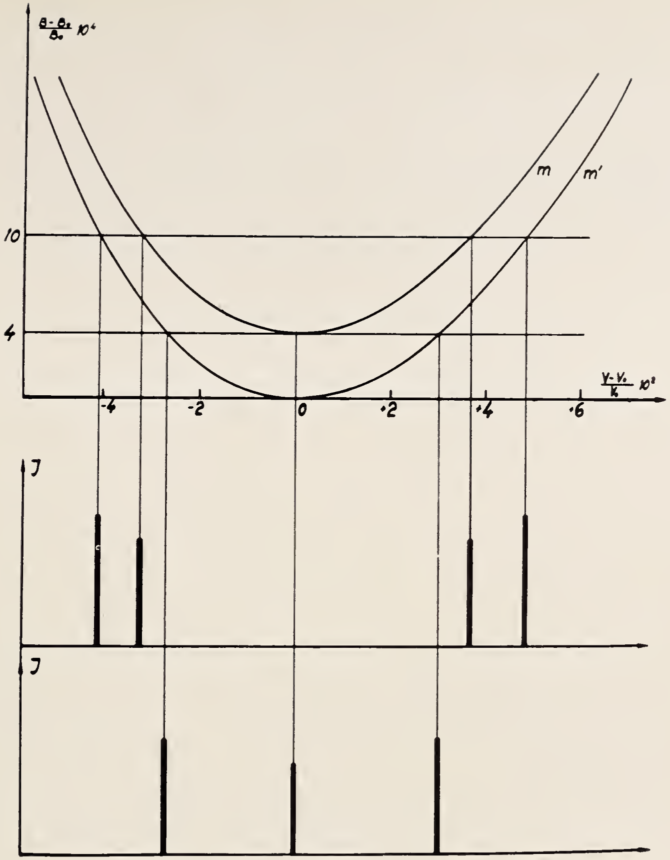

FIGURE 7. *The electrical doublet principle.*

Discussion

A. O. C. NIER: In the case where you use the shaped magnetic fields such as the one where the air gap changes with the radius, what about the actual practical situation as the field saturates; that is, if you are going to use this over a range of values, have you figured how this will affect the operation?

N. SVARTHOLM: We have some experience of this problem, first of all from the big beta-ray spectrometer where we can measure the field gradient over a fairly large area. We found that the bad properties of the iron are most pronounced for the lowest fields at which the spectrometer can operate, namely 10 gauss. Even at the highest fields (400 gauss), the iron of the pole pieces are so very far from saturation that the pole faces can be considered equipotential surfaces. In the mass spectrometer, on the other hand, we have a much higher field. Here again we found hysteresis effects in the gradient at fields of about 1000–2000 gauss. The effect was, however, very small, less than 0.1 percent.

Nier: It would seem that if you went to high field strength this might be a serious difficulty as the iron begins to saturate.

Svartholm: We intend to use a maximum field of only 3500 gauss. Even in the yoke the iron is then still far from saturation. The big radius of the instrument makes it possible to focus 2 kev ions of mass 200 in this field. The fact that the gradient shows a small hysteresis effect might be useful for the finer adjustment of the gradient by recycling the magnet according to some suitable scheme.

Nier: One other remark. I was going to say in the case of our machine, where we put two mass spectrometers in the same magnetic field, that, as the iron saturates, the fields don't go up together in the two positions. Of course, that is rather an extreme case where we have that wedge-shaped pole face and not too good a pole behind it, but we clearly detect this effect, if we try to change the magnetic field by very much. The machine won't completely compensate for such things and it is going to be important in our small machine that we now use as we go to very high field strength. We will have to hold them more constant than we will for the weaker fields, so it occurred to me that there is a connection here.

Svartholm: That is true, but I think there is an important difference. The effect of the stray fields should be more serious for such changes compared with the case of our 360° magnet, where the ions don't pass through any field boundaries. If the iron is very uniform, one should not expect any such big effects.

L. L. Marton: Mr. Svartholm, you mentioned for a magnet with two-directional focusing only the case of focusing at the $r\pi\sqrt{2}$ In this institution last year Peter Sturrock calculated the focusing properties of such shaped fields in general and found that focusing at $r\pi\sqrt{5}$ has added advantages. In particular, at equal transmission it has higher resolution.

Svartholm: That is an interesting possiblity, too. I suppose that is a case where an intermediate node is formed for one direction.

Marton: Yes, it has an intermediate node for the axial focusing.

10. Increase of the Sensitivity of Mass Spectrographs by Concentration of All Beams in One Point, Producing a Spectral Line

By Richard F. K. Herzog [1]

With most of the mass spectrographs at present in use, the electric and magnetic fields operate like cylindrical lenses. That is, the image of a point source of rays is a line whose length is dependent upon the divergence of the rays and upon the limitation of the pencil of rays.

The main object of the investigations which I am about to describe has been to obtain as the mass-spectrum image, a point instead of the usual line. In this way, the radiation density is increased and hence the blackening of the plate is considerably intensified. A mass spectrograph constructed in this way ought to be especially useful for detecting minute traces, or when work with rare or radioactive isotopes is contemplated.

How can this be attained? There are three possibilities: (1.) Already in the year 1943 I obtained an image of this kind by inserting into the ray path of the mass spectrograph an electron-optical accelerating lens (see Austrian patent No. 162363). Thereby, however, the ray path was considerably lengthened and the desired increase of intensity was partly lost again. (2.) Inhomogeneous magnetic fields have been employed by various other investigators, which, if properly produced, may bring about the additional focusing desired. However, it is experimentally difficult to obtain the exact degree of inhomogeneity. (3.) Not very long ago, I was able to demonstrate (Acta. Phys. Austriaca IV, 431, 1951, received April 27, 1950) that homogeneous magnetic fields, too, are applicable for this purpose if the angle between the beam and the edge of the pole piece is correctly chosen. I will first speak about this novel property of homogeneous magnetic fields, which should be of some importance for the further development of mass spectroscopy.

Figure 1 shows the two pole pieces in horizontal and upright projection, as well as a line of force at the fringe of the field. We now follow the path of a particle which, before entering the field, was moving parallel to the symmetry plane between the pole pieces, but not in this plane. This ion will travel in its known circular orbit within the field. On leaving the homogeneous field, the ion passes through the fringe field, which possesses a component H_1 perpendicular and another one H_2 parallel to the symmetry plane. Furthermore, we will resolve H_2 into a component H_3 parallel to the path and H_4 perpendicular to the path. It is this component H_4 which causes the deviation towards the symmetry plane as well as the novel focusing. I was able to show that, in the simplest way, this property may be described by means of a thin cylindrical lens, situated near the center

---

[1] University of Vienna, Vienna, Austria.

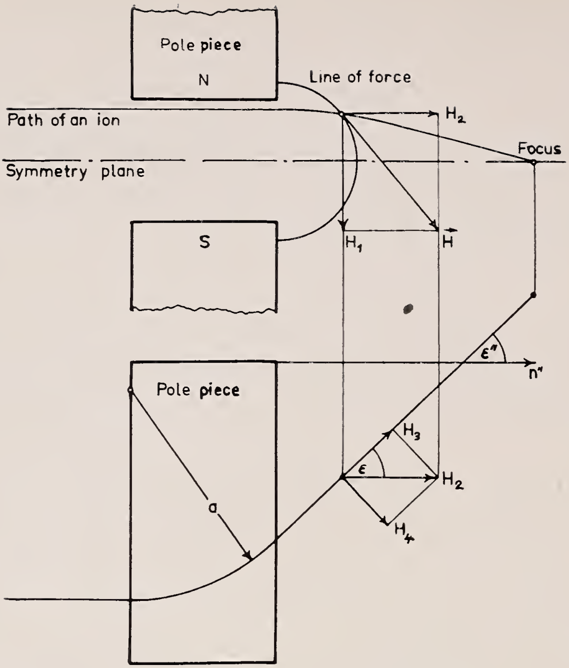

FIGURE 1. *Influence of magnetic fringe field on ion path.*

of the fringe field. The generators of this cylindrical lens are perpendicular to the magnetic lines of force. The focal length of this lens is

$$f = a/\tan \epsilon, \tag{1}$$

where a denotes the radius of curvature of the orbit within the homogeneous field, and ϵ stands for the angle between the direction of the beam and a line normal to the edge of the pole pieces.

Since the fringe field produces some deviation of the beam and since it is itself varying rapidly in intensity, it is evident that the value of ϵ will depend upon the distance traveled along the path. Hence we let ϵ denote this angle in the center of the fringe field, while ϵ'' is this angle at a point sufficiently far away so the field is negligible. Actually, as will be seen later, it is necessary to limit the fringe field very carefully by means of adequate shields in order to make the difference between ϵ and ϵ'' as small as possible.

Figure 2 shows some typical examples of magnetic lenses of this kind, in which the pairs of drawings show the field in plan and elevation. It was supposed that a parallel beam enters the magnetic field perpendicularly to the pole pieces, and is deviated by an angle of 50°. The angle of exit, ϵ'', was varied from plus 70° to minus 20°.

The lower drawings show the well-known lenticular effect, while the upper drawings show the novel lenticular effect. It will be observed that in the former case the focus is at first negative, becomes infinite, and finally becomes positive with steadily decreasing focal length. In the latter case, the opposite situation is encountered. However, the center drawing, with $\epsilon''=31°$, represents the extremely important case where the two foci coincide. This arrangement evidentally corresponds to a spherical lens.

Morton Camac has also studied this type of focusing (see Rev. Sci. Instruments *22*, 197, 1951, received Aug. 25, 1950). His paper, which was done entirely independently, was submitted for publication four months after mine was submitted. He did not calculate the focal length of the lenses, but rather the position of the image; his final formula is, therefore, considerably more complicated. However, I was able to derive and to confirm his results by means of my formulas.

I will now deal more closely with the employment of this novel focusing in mass spectroscopy. It has been my object to construct a double-focusing spectrograph, where the novel focusing in the longitudinal direction of the spectral lines is additionally apparent.

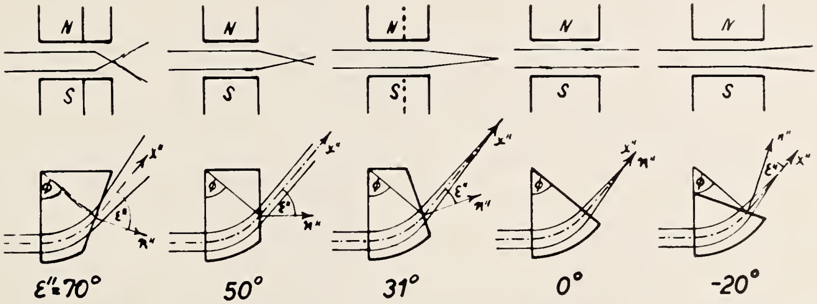

FIGURE 2. *Variance of fringe field focusing with magnetic pole face angle.*

A mass spectrograph with velocity focusing consists of an electric and a magnetic deviation field. The angles of deviation, however, must be chosen in such a manner that the velocity dispersion of the two fields will be compensated. Moreover, the two fields operate as electron-optical lenses, producing an image of the slit on the photographic plate. An especially important special case arises when the slit is at the front focal point of the electric field. In this case the rays coming from one point of the slit emerge from the electric field and enter the magnetic field parallel to one another, and the image appears in the focus of the magnetic field. The parallel beam is united into one point by the action of the magnetic field under the following conditions: If the incidence angle ϵ' is 26° and the angle ϕ of deviation 116°, the image is to be found just at the edge of the field. If we increase ϵ' and decrease ϕ correspondingly, the image may be produced at any point outside the field. It is especially gratifying that the angles are independent of the mass of the particles. That means that, on the plane photographic plate, the images of the slit, produced by all masses, will turn out to be sharp in both directions.

A serious difficulty, however, will manifest itself if one wishes also to obtain velocity focusing with a magnetic field of this kind. The velocity dispersion of such a magnetic field is greater than the greatest velocity dispersion of a cylindrical condenser. Therefore a cylindrical condenser is useless for this purpose.

I, therefore, investigated the properties of a spherical condenser and found that it provides the great velocity dispersion required (see Austrian patent No. 162365, Nov. 27, 1946). Moreover, a spherical condenser possesses the properties of a spherical lens: The image of a point object is also a point. I succeeded in demonstrating that the object, the center of the sphere, and the image must be on a straight line. (fig. 3). It is possible to choose the angle of deflection ϕ_e of the spherical condenser in such a manner that compensation of the velocity dispersion just takes place. The condition for this is as follows:

$$2 \sin \phi_e = \sin \phi + (\tan \epsilon')(1 - \cos \phi). \tag{2}$$

if we substitute the values for ϕ and ϵ', given before, we shall find $\phi_e = 53°$.

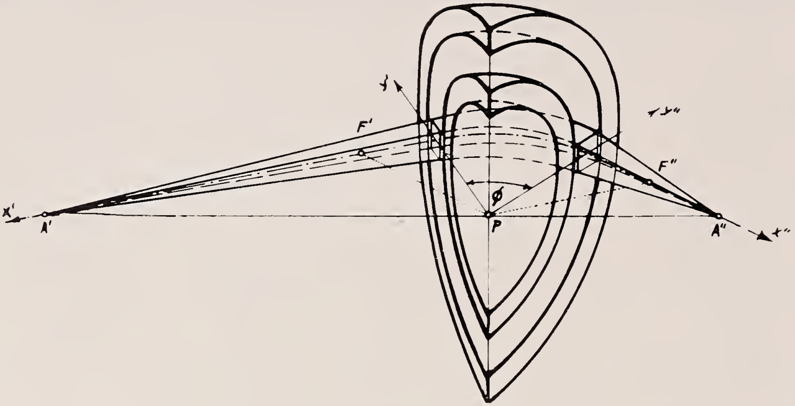

FIGURE 3. *Focusing properties of a spherical condenser.*

Figure 4 shows the entire ray path in the mass spectrograph. The bundle of rays, diverging from a point of the object diaphragm, leaves the spherical condenser as a parallel beam and is again united to one point by the magnetic field. Particles of the same mass, but of different velocities, arrive at the same point. The images produced by the different masses are formed on a straight line.

When deriving the simple results mentioned just now, I was obliged to resort to some suppositions considerably simplifying the calculation. I was eager to see how far the results derived theoretically would coincide with those arrived at experimentally. Today, I am not in the position to refer you to any completed work, but I can tell you about the experiences I have had in the construction of a mass spectrograph of this kind. I believe, however, that these experiences will be particularly useful to you, should any of you be thinking of constructing a similar apparatus.

First, I wished to attain my end as soon as possible and I, therefore, immediately constructed the entire spectrograph. The spectra I obtained were entirely blurred and therefore useless. This initial failure was not to be wondered at. As nobody is able to construct a microscope, consisting of a great number of lenses, without being familiar with the properties of a single lens, it is just as impossible to build a mass spectrograph without knowing the precise behavior of the electric and the magnetic lenses. It was necessary, therefore, to go back and investigate thoroughly the properties of the novel magnetic lens and I wish to give you a detailed report of this work.

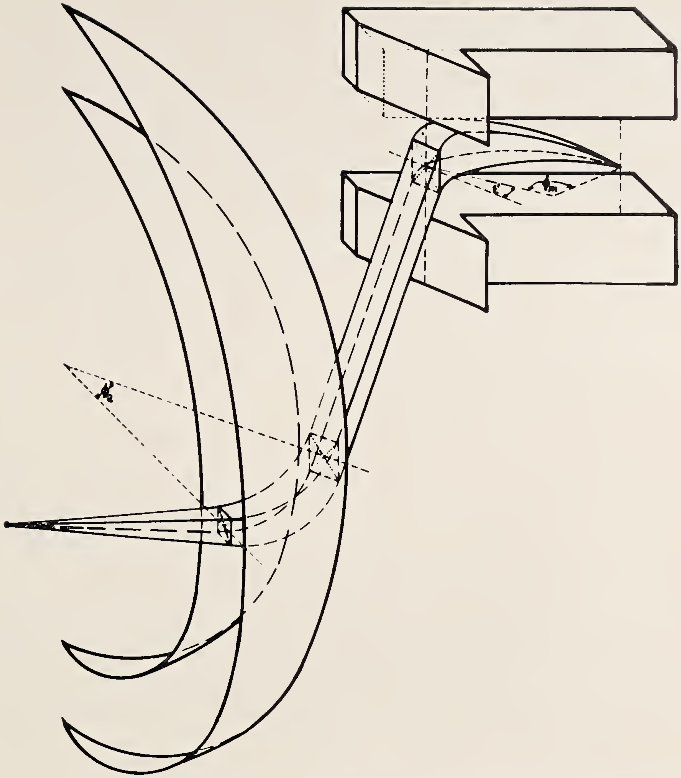

Figure 4. *Arrangement providing both velocity and two-directional focusing.*

For this investigation I employed the same magnetic field that was to be used with the mass spectrograph (fig. 5). The testing conditions, too, were made as similar as possible. Since the ray path must be parallel before entering the magnetic field, I removed the spherical condenser, and examined the image of a hole in the center of a diaphragm. This diaphragm I fixed as far from the magnetic field as possible, actually 120 cm. The diameter of the hole may be adjusted between one-tenth millimeter and 2 millimeters. The photographic plate or the fluorescent screen may be moved, and the focusing is effected in a similar way as it is with a photographic camera. In front of the magnetic field there is an aperture diaphragm, with the diameter of the aperture adjustable between 1 and 8 mm which limits the width of the beam of rays. It corresponds to the diaphragm of a photographic camera, and influences the intensity allowed to pass.

The experiments were made partly with electrons and partly with alkali ions. A constant accelerating voltage was of major importance, because the arrangement possesses a great energy dispersion. A voltage fluctuation of one part in a thousand would have blurred the image. Unfortunately, I had no electronic voltage regulator at my disposal, and so I could only work after midnight, when conditions proved to be much steadier. I made my initial experiments without any magnetic shielding but failed to obtain a useful result when the

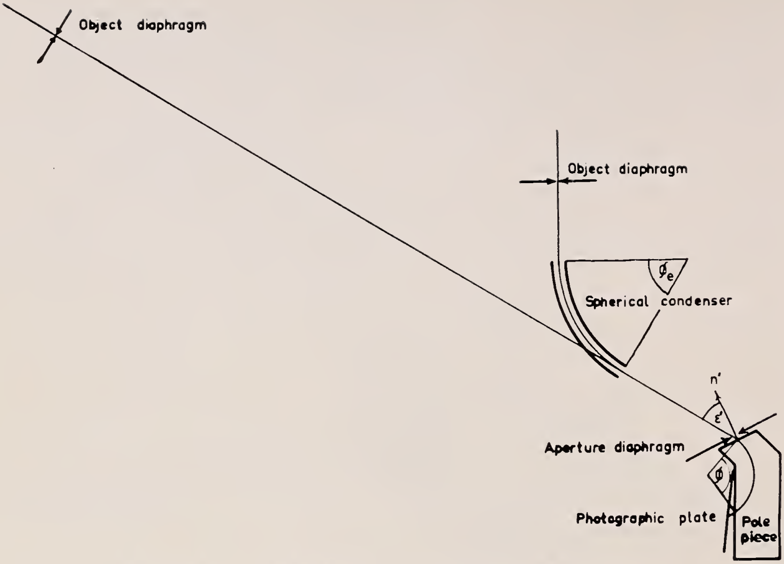

Figure 5. *Arrangement for testing magnetic focusing.*

incidence angle had the value calculated. There were two reasons for this: (1) The powerful and most extensive fringe field deflects the beam before the middle of the fringe field, and the difference between the angle ϵ' before the field and ϵ in the middle of the field becomes so great that the image is entirely destroyed. (2) The surfaces of equal intensity of field are not plane, as was assumed in the calculation, but curved.

It was these two causes which were responsible for the failure of the entire mass spectrograph.

In order to obtain the best coincidence possible with the theoretical assumptions, I decided to try shielding the fringe field by means of an iron screen (fig. 6). This screen consists of two iron plates, connected with each other by means of two stout iron blocks. Figure 7 shows the

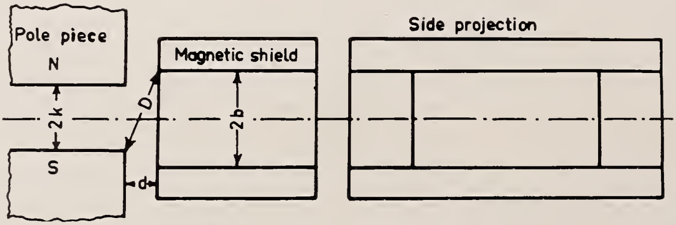

Figure 6. *Shielding arrangement.*

course of the field strength with and without the shield. One is able to see that, by use of the iron shield, the field falls off much more rapidly toward the outside, and that the fringe field becomes negligible even at a short distance from the homogeneous main field. Moreover, definite and accurately reproducible field configurations are obtained through the shielding. These field configurations are independent of the shape of the framework of the apparatus. Nevertheless, the difference between ϵ' and ϵ was found to be about 5°.

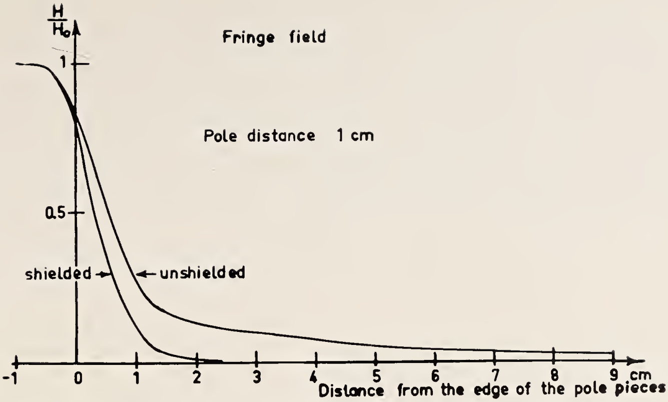

FIGURE 7. *Effect of shielding fringe field.*

The initial experiments were made with electrons, for the sake of better observation on a fluorescent screen. During these experiments the remanence of the iron shield was, at first, most disturbing. Unfortunately, I had no iron free from remanence at my disposal; I was, therefore, compelled to demagnetize most carefully or to anneal the shield, and I had to avoid any magnetization stronger than absolutely necessary during the experiment. When all these precautions were strictly observed, the coincidence between the theoretical calculation and the experimental results was excellent, and the quality of the image was better than had been expected.

Figure 8 shows a number of greatly enlarged photographs of the images obtained with electrons, where the aperture diaphragm had an opening variable between 1 and 8 mm in diameter. With an aperture of 1 mm the image defects are still negligible and the size of the image comes up to my expectations on the basis of Gaussian optics. With the increasing size of the aperture, the image defects increase as well. But even with an 8 mm aperture, usable focusing is still possible. You will notice this by comparing the diameter of the aperture with the diameter of the image.

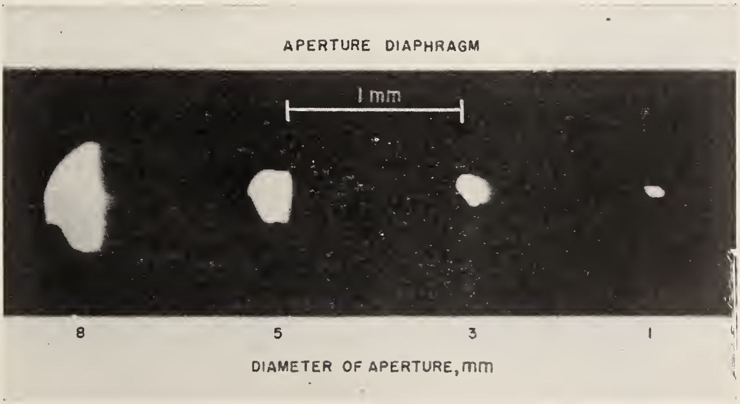

FIGURE 8. *"Point" images with various apertures.*

This result is more remarkable if we consider that the distance between the pole pieces was not more than 10 mm. The marginal rays, therefore, approach the edge of the pole pieces up to 1 mm. The theoretical assumption of rays near the optical axis is no longer fulfilled in this case. But the focusing is still sufficient in all those cases where a separation of doublets can be dispensed with, as, for instance, with a mass spectrograph for isotope separation. Since a small resolving power is sufficient in such an apparatus, one is able to utilize, for the beam of rays, almost the entire space between the pole pieces.

In these experiments with electrons the density of rays was increased twentyfold through the novel focusing compared with a similar arrangement with the customary cylindrical lenses. The magnitude of this increase is greatly dependent upon the special shape of the apparatus and on the special kind of ray source.

The rays must enter the magnetic field at a given angle, so that the image may be anastigmatic. A slight change of this angle of about 2° will considerably impair the image. On the other hand, the adjustment of the mass spectrograph is considerably simplified, because only the ordinary image, producing the width of the spectral lines, need be absolutely sharp. For the new image producing the length of the spectral line, the requirements can be considerably relaxed. In practice, a slit is used as the object in most cases, and its image is somewhat lengthened through the insufficient focus. There is no loss of intensity worth mentioning.

I next wished to test the magnetic lens by means of ions. For this purpose I used a hot anode source with Pyrex glass from which all alkali ions are emitted with the same energy. Unfortunately, the magnet at my disposal is too small, so that I cannot employ accelerating voltages greater than 4000 v if, for instance, I wish to get the rubidium isotopes onto the photographic plate. The great drawback is that the image on the fluorescent screen is so dull that it cannot be used for focusing any more. For the time being I dispensed with adjustment of the focusing altogether and I fixed the photographic plate at the place which had proved most favourable during my experiments with electrons. It is a gratifying proof of the correctness of the calculations that, nevertheless, the images turned out rather sharp. This also shows that the change in the field configuration of the fringe field, through the great saturation of the iron, has but little influence upon the lenticular effect. In later experiments, however, we shall obtain the best focus only through a number of trial exposures with the photographic plate in different positions.

As an example, figure 9 shows a mass spectrum of the lithium isotopes 6 and 7. The hole in the object diaphragm was 1 mm in

Figure 9. *Mass spectrum of lithium.*

diameter and that in the aperture diaphragm 3 mm. The distance between the two isotope spots is 7 mm. Thereby you are able to see that also with ions the focusing is rather good in both directions.

As the sharpness in the longitudinal direction of the spectrum is a trifle less than in the transverse direction, a slight correction of the position of the photographic plate or of the angle ϵ' will be necessary.

The experiments, described just now, confirm the correctness of the calculations of the novel focusing of magnetic deflecting fields, if the fringe fields are properly shielded. The focusing with its diverse advantages, being obtainable without any additional employment of apparatus, will be applied with ever increasing frequency, both in mass spectroscopy and in the spectroscopy of the α and β rays.

11. Improved Focusing in Combinations of Radial Electric and Magnetic Fields

By H. Hintenberger [1]

What I have to report today is not the full theory of second-order aberration, but only a few incomplete steps in this direction. We consider a uniform magnetic field, perpendicular to the plane of the table and cut off by the field boundaries k_1 and k_2 as shown in figure 1. A beam of ions all of the same mass and velocity emerging from P_1 with the angle of divergence $2\alpha_1$ will be focused in the image point P_2. However, the focusing is not perfect. The second-order aberration ΔB_m is given by the expression [2]

$$\Delta B_m = -\mathrm{K} r_m \left\{ c_1 + c_2 - \gamma_1 \frac{r_m}{R_1} - \gamma_2 \frac{r_m}{R_2} \right\} \alpha_1^2$$

with the abbreviation

$$\mathrm{K} = \frac{1}{2} \frac{l_1^2 l_2}{r_m^3} \left[1 + \left(\frac{r_m}{l_1} + \tan \epsilon_1 \right)^2 \right] \left[1 + \left(\frac{r_m}{l_2} + \tan \epsilon_2 \right)^2 \right]^{1/2}$$

and with the definitions of c and γ being given in figure 1. The other notations used are also illustrated in figure 1: l_1 and l_2 are the object and the image distances; ϵ_1 and ϵ_2 the entrance and the exit angles (in this figure ϵ has negative values); r_m is the radius of the ion path in the

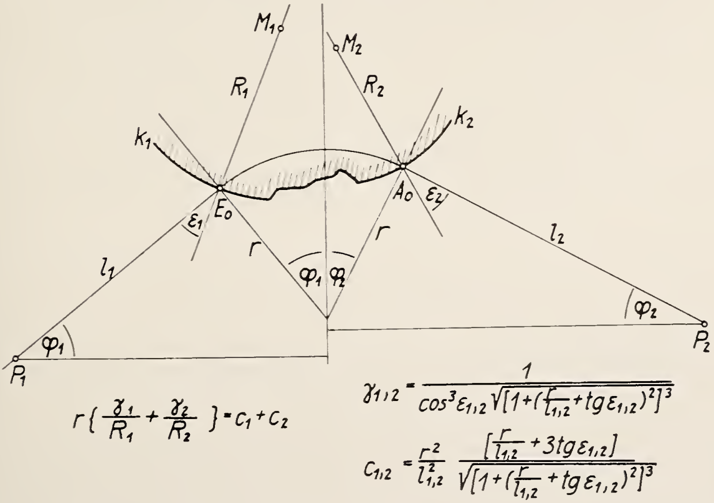

FIGURE 1. *Focusing by uniform magnetic field with boundaries of radii R_1 and R_2*

---

[1] Max Planck Institut für Chemie, Mainz, Germany.
[2] H. Hintenberger, Z. Naturforsch. 6a, 275 (1951).

magnetic field and R_1 and R_2 are the radii of curvature of the field boundaries on the entrance and exit points of the central beam. ΔB_m can be varied in a wide range by altering l_1 ϵ or R; in particular, it is possible to make $\Delta B_m=0$ if the condition is fulfilled

$$c_1+c_2=r_m\left(\frac{\gamma_1}{R_1}+\frac{\gamma_2}{R_2}\right)$$

In case of an electrostatic radial field this is not possible in such a simple manner. Here also cases can be found in which the second-order abberation $\Delta B_e=0$. For $\varphi_e=2\left(\frac{\pi}{\sqrt{2}}\right)$ and $l_{e1}=l_{e2}=0$, this is, for example, fulfilled, but in these cases the energy dispersion D_e is also zero and they can not be used in mass spectroscopy. Let us put

$$\Delta B_e=-Ar_e\alpha_1^2.$$

I have calculated A for the general case but the expression is complicated and not ready for publication.[3] One cannot get zero for any useful case. But in a combination of an electrostatic radial field and a magnetic field in which the electrostatic analyzer gives an image of P_0 at P_1 (fig. 2) and the magnetic field gives an image of P_1 at P_2, the second-order abberation of the magnetic field ΔB_m can be adapted to the second-order abberation ΔB_e in such a way that the second-order abberation of the combination of both fields at P_2 is zero. Then

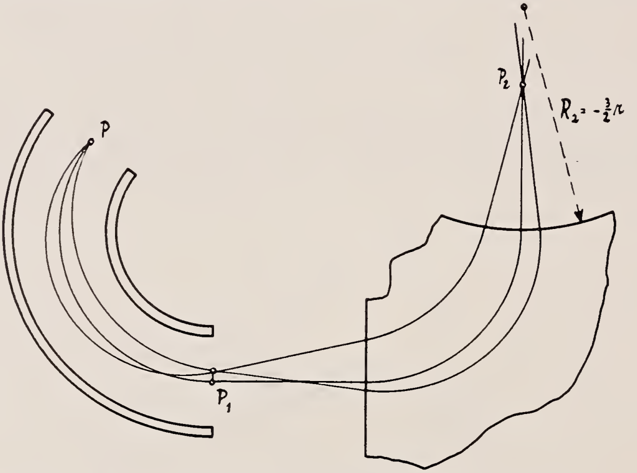

FIGURE 2. *An arrangement for velocity focusing in the first order and direction focusing in the second order.*

$$\Delta B_e=\Delta B_m^*$$

where the asterisk indicates that ΔB_m must be calculated for ions going in the opposite direction, that is from P_2 to P_1, and the subscripts 1 and 2 must be changed. The condition for second-order focusing in the combination of both fields is therefore

---

[3] A detailed report on the subject will be given in the Zeitschrift für Naturforschung.

$$A r_e \alpha_1^2 = \mathrm{K}^* r_m \left\{ C_1 + C_2 - \frac{\gamma_1}{R_1} r_m - \frac{\gamma_2}{R_2} r_m \right\} \alpha_2^2$$

where α_2 is the angle of divergence on the image side of the magnetic field which is given by $\alpha_2 = [l_1 \gamma_2 \cos{}^3 \epsilon_2 / l_2 \gamma_1 \cos{}^3 \epsilon_1]$. α_1. We can simultaneously require that velocity focusing in the first order must be fulfilled. For a symmetrical radial field this condition is the following: [4]

$$r_e / r_m = \frac{1}{2} \left\{ 1 - \cos \varphi + \frac{l_1}{r_m} \left[\sin \varphi + (1 - \cos \varphi) \tan \epsilon \right] \right\}.$$

We consider three typical cases in which both conditions for velocity focusing in the first order and for direction focusing in the second order simultaneously are fulfilled.

1. We choose rectilinear field boundaries and normal entrance and exit of the central beam in the magnetic field. Then we have $\frac{1}{R_1} = \frac{1}{R_2} = \epsilon_1 = \epsilon_2 = 0$ and by the two equations the object and image distances l_1 and l_2 and the radii r_e and r_m are determined. This leads to the case which Nier has used in his famous double-focusing mass spectrometer which he described in his lecture today.

2. In the second case we choose rectilinear field boundaries and a symmetrical magnetic field but $\epsilon \neq 0$. In this case $\frac{1}{R_1} = \frac{1}{R_2} = 0$, $l_1 = l_2 = l$, $\epsilon_1 = \epsilon_2 = \epsilon$. The two equations determine then the entrance and exit angle ϵ and the ratio of the radii $\frac{r_e}{r_m}$. We get in this case

$$\tan \epsilon = \frac{A-1}{2} \tan \frac{\varphi}{2} \text{ and } \frac{r_e}{r_m} = \frac{2}{3-A}.$$

This gives, for example with

$$\varphi_m = 60^\circ \text{ and } \varphi_e = \frac{\pi}{\sqrt{2}}, \epsilon = 5^\circ\, 30_0''$$

and $\frac{r_e}{r_m} = \frac{6}{5}$.

3. In the third case we put $\epsilon_1 = \epsilon_2 = \frac{1}{R_1} = 0$ and $l_1 = l_2$. This means normal entrance and exit, symmetrical position of object and image, and one rectilinear and one curved boundary of the magnetic field. Then we have $r_e = r_m$ and get for R_2 the following expression $R_2 = -\frac{\cot^3 \frac{\varphi_m}{2}}{2(A-1)} r_m$

With $\varphi_e = \frac{\pi}{\sqrt{2}}$, $\varphi_m = \frac{\pi}{2}$ we get $R_2 = -\frac{3}{2} r_m$. This is shown in figure 2.

These are only a few of the possibilities of realizing the same focusing properties which Nier has realized in his new instrument. As we have seen r_e was always of the same magnitude as r_m. Therefore the ion path in a double focusing instrument in the cases mentioned above is always longer than in a simple sector field instrument by a factor of nearly two.

---

[4] J. Mattauch and R. Herzog, Z. Phys. 89, 786 (1934).

It may be of interest to find a device which gives improved focusing in a mass spectrometer with less experimental expenditure. I think this can be achieved in the following manner. We accelerate the ions in two steps, at first with V_1 volts and then with $V-V_1$ in the second step. If the radial field is working after the first step the radius r_e can be reduced by a factor $\frac{V_1}{V}$ without altering the energy dispersion D_e of the electric field. We have only to pay attention to the fact that D_e is not altered in the second step. The second acceleration can take place in a tube lens. The image of the radial field must be brought into the one principal plane of this immersion lens.

We have such a device now under construction, but we have not yet got experimental results.

12. High Resolution in Conventional 180° Mass Spectrometers

By Clifford E. Berry [1]

The use of the mass spectrometer as a tool for quantitative and qualitative gas analysis has been developed within the past decade to a high degree. At the present time the techniques and instruments available are well suited to work with materials having vapor pressures above about 0.1 mm at room temperature and having molecular weights below about 200. In an effort to extend the present techniques to other materials, various groups have been working on the problem of handling low vapor pressure materials. One such group is that led by Mr. M. J. O'Neal, who will speak Saturday on the "Mass Spectra of Heavy Hydrocarbons." At the same time, our group has been working on the problem of increasing the resolving power of the mass spectrometer, since resolution up to about mass 700 is desired.

Most of what I have to say will apply generally to any single-focusing sector-type instrument, and will apply specifically to the 180° type instrument. I intend first to discuss briefly the various factors which influence the resolving power of the mass spectrometer; second, to describe an ion-optical method of varying the resolving slit width; and third, to present some experimental results.

The inherent resolving power of a mass spectrometer depends on the relation between the ion beam width at the focal plane and the dispersion of the instrument. The effective resolving power depends on these two factors and on the width of the resolving slit, i. e., the slit that is placed in front of the collector electrode.

Since an ion beam tends to "tail off" in a more or less exponential fashion on either side, one must adopt some sort of definition of ion beam width. For the purposes of this discussion, we will define the ion beam width as that width within which 98 percent of the ions of a given m/e lie, with 1 percent of the ions lying on each side. It will become clear as we proceed how this definition can be modified to meet any requirement.

Figure 1 shows the elements of a simple ion source. Ions formed within the confines of the electron beam are accelerated by a more or less uniform field toward the first slit. Once through the slit, the ions are accelerated by a much stronger uniform field. According to the well-known laws of electron and ion optics, the first slit behaves as a strong condensing lens, causing the ions to pass through a crossover point close to the first slit. Throughout most of the distance between the first and second slits, the ions are again in a uniform field, and thus move in parabolic paths. The second slit collimates a fraction of the ions impinging upon its plate and passes these through to the analyzer. In passing ions, however, the second slit acts as a diverging lens. Thus the combined effect of the two lenses is to

---

[1] Consolidated Engineering Corporation, Pasadena, Calif.

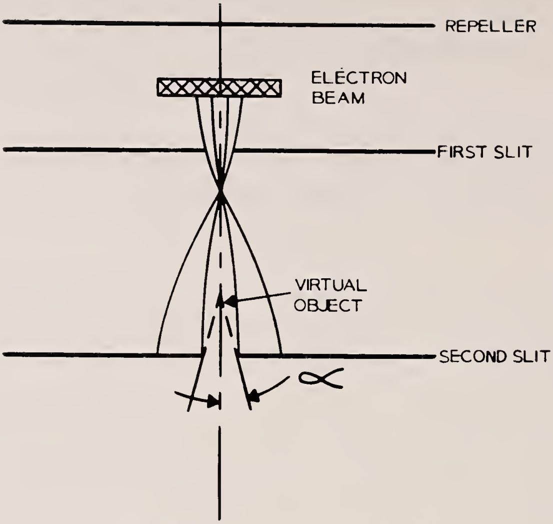

FIGURE 1. *Optics of ion source.*

produce a divergent beam of half angle α, which appears to originate from a point midway between the two slits, as indicated by the dotted lines. We call this point the virtual object.

The exact position of the virtual object, of course, depends upon the slit spacings and the relative field strengths. If the lenses were aberration-free, the virtual object would actually be a line of no breadth. Actually, the lenses possess various aberrations, so that the virtual object has a finite size. However, by proper design, it is easily possible to make the width of the virtual object appreciably smaller than the size of either of the slits in the source.

Figure 2 illustrates the well-known partial refocusing action of a magnetic field on a divergent ray. Below I have listed the various factors which contribute to the width of the ion beam b at the focal plane. The basic beam width, of course, is just the width of the virtual object. To this we must add the term $r\alpha^2$ due to the incomplete magnetic focusing. The remaining principal contributions arise from energy spread. The beam is broadened by an amount $r\Delta/V$, where ΔV is the energy spread in electron volts and V is the ion accelerating voltage. For a first approximation we need only to consider velocity components directed parallel to the forward direction of the ions. Components crosswise affect principally the size of the virtual object. The third component has little influence on the beam width. We can list four distinct contributors to ΔV, as follows:

(a) Thermal kinetic energy of the molecules.

(b) Excess kinetic energy arising from a fragmentation process.

(c) The potential difference across the electron beam.

(d) Rapid fluctuations or a-c ripple in the ion accelerating voltage. (This latter effect, of course, is not a true energy spread, but if the period of the ripple is short compared with the time constant of the ion detecting means, the observed effect is an apparent widening of the ion beam.)

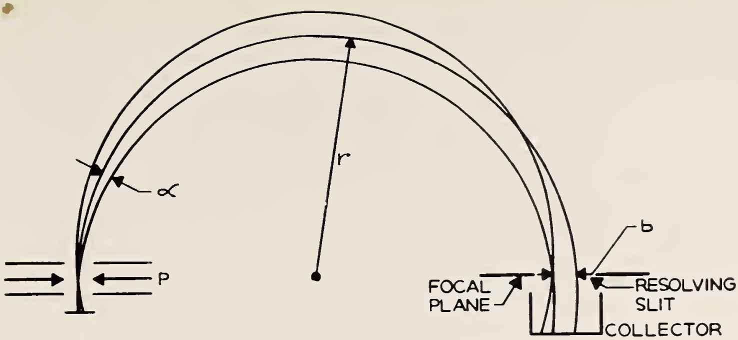

Figure 2. *Contributions of ion beam width.*

Beam width $b \simeq P + r\alpha^2 + r\frac{\Delta V}{V} + \text{misc.}$

A. ΔV includes:
- (1) Energy spread across electron beam
- (2) Thermal energy of molecules
- (3) Excess fragmentation energy
- (4) a-c ripple in the accelerating voltage

B. Miscellaneous factors include:
- (1) Space charge effects
- (2) Nonuniformity of magnetic field
- (3) Scattering at slit edges and by ion-molecule collisions

In addition, we may list a number of miscellaneous factors which are somewhat more elusive in character, such as

(a) Nonuniformity of the magnetic field.

(b) Scattering of some ions through ion-molecule collisions in the analyzer and scattering at the slit edges.

(c) Space charge effects.

Figure 3 illustrates some relations between the ion beam width, the dispersion, the resolving slit width, and the observed peak shape. I have shown two adjacent ion-beam current distributions. The dispersion of the beams is, to a close approximation, $r\Delta m/m$, where Δm is the mass difference and m the mean mass. I have indicated the points corresponding to the 98 percent beam width. Below is indicated a resolving slit of width greater than the beam width, which is shown in four different positions relative to the left hand beam. The four positions correspond respectively to collection of 1 percent of the current on the leading edge of the beam, 99 percent on the leading edge, 99 percent on the trailing edge, and 1 percent on the trailing edge. It is obvious from the diagram that the width of a peak between the 1 percent points at the base is equal to the slit width plus the beam width, and that the width at the top of the peak between the 99 percent points is equal to the slit width minus the beam width. If the slit width is equal to the beam width, then the top of a peak will be pointed, and 2 percent of the intensity will be lost. Furthermore, at that mass at which the dispersion of unit mass difference is equal to the beam width plus the slit width, a 2 percent valley will appear between adjacent peaks of equal height. A further conclusion that can be drawn from such reasoning is the following: If at mass m, a 2 percent valley exists between adjacent peaks of equal height, then at mass $2m$ each beam contributes 1 percent of its intensity to its neighbor.

Of course, the same reasoning can be applied using any definition of beam width, such as 90 or 99.8 percent.

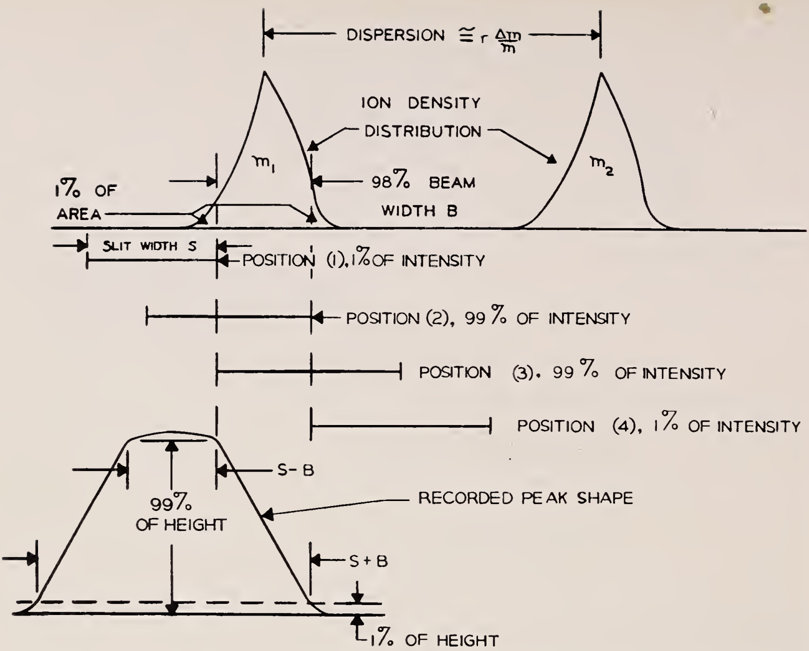

FIGURE 3. *Relation of recorded peak shape to beam width, dispersion, and resolving slit width.*

Figure 4 is an actual recording of a spectrum of *n*-butane, showing the 57, 58, and 59 peaks. The beam width can be calculated in either of two ways. First, if the beam is enough narrower than the resolving slit, measurements can be made both at the base and at the top. The ratio of the difference to the sum of these two measurements is just b/s. If s is known, as is usually the case, since it can be measured prior to assembly, then b is easily calculated.

The second method involves measuring the separation between centers of two peaks, preferably those bracketing the one to be measured. This measurement, together with the known dispersion of the instrument, enables a scale factor to be determined, which when applied to the base measurement gives $b+s$. If this sum is used in conjunction with the ratio of b/s, then both the beam width and apparent slit width can be calculated.

If the width of a peak is measured midway between its base and top, and provided the beam is appreciably narrower than the slit, then the slit width alone can be determined. If the result of this calculation is different from that obtained from the previous ones on the top and base measurements, it is a good indication that the resolving slit is twisted.

It is clear that the width of the resolving slit is important in determining useful resolving power. In quantitative analytical work it is important to use a slit that is wider than the ion beam in order that the intensity of the beam can be indicated by the reading of a peak height. At the same time, a relatively wide slit, giving flat topped peaks, allows a higher rate of scan before the recording system becomes a limiting factor. In an instrument that is to be used both for light

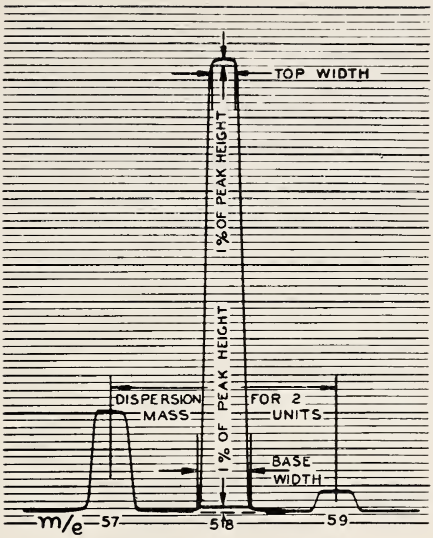

COMPUTATION OF BEAM WIDTH:

FIGURE 4. *Distance from center of 57 to center of* $59 = 59.5$ *mm, width of base of peak*$=14.5$ *mm;* $K = 14.5/(59.5/2) = .487$, $K = (b+s)/D$, $b+s = .487\ (5/58) = .042$, $s = .030$ *in.,* $b = .012$ *in.=beam width at resolving slit.*

gases and heavy, it is thus desirable to be able to narrow the resolving slit for the high mass work, but to leave it wide for low mass work. Figure 5 shows a method of doing this by ion-optical means.

At the top of the left-hand figure is shown the principal resolving slit, which is at ground potential. Following this is an insulated plate containing a somewhat wider slit. A third grounded plate containing another fairly wide slit follows the insulated plate, serving as a partial electrostatic shield. Below this is the ion collector.

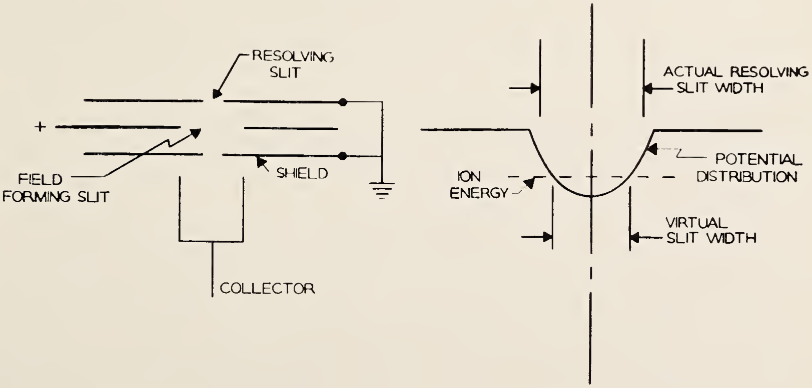

FIGURE 5. *Virtual resolving slit.*

Now, if a positive potential is placed on the insulated plate, a saddle-shaped potential distribution is produced in the region of its slit. The right-hand diagram shows the approximate shape of such a distribution taken in the direction normal to the ion bead and to the magnetic field. If the potential of the plate is sufficiently low, all ions that pass the main resolving slit can pass the potential barrier. If the potential is raised sufficiently high, so that the potential minimum is higher than the ion energy, no ions can get through the barrier.

At intermediate values of potential, ions which pass through near the edges of the main resolving slit cannot pass through the barrier, while those which pass through near the center are able to. Thus we can think of the potential barrier as a virtual slit, the width of which varies continuously as a function of applied voltage.

Obviously, the slit also acts as an energy filter, so that what I have just said applies strictly to mono-energetic ions. However, it is found that, over a range of potentials, the principal action is one of narrowing the slit rather than that of retarding low energy ions. This is borne out by the experimental observation that considerable narrowing can be achieved before any appreciable loss of intensity occurs. Beyond this point, as the slit is narrowed further, energy discrimination causes a simultaneous loss in intensity.

Figure 6 illustrates a series of scans of the nominal mass 44 peak in a mixture of CO_2 and propane, which have a mass difference of about 1 in 600. The instrument used was a standard commercial analytical instrument of the 180° type, with a radius of 5 in. The only modifications were a smaller than normal resolving slit, and a more careful adjustment of the operating potentials applied to the source so as to produce a minimum beam width. We see that as the potential on the slit-forming plate is increased, the first effect is to narrow the slit without much loss in intensity. Finally, the intensity drops sharply.

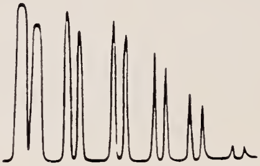

FIGURE 6. *Nominal mass 44 CO_2-propane mixture effect of narrowing virtual slit.*

For these records, the 98 percent ion beam width was about 0.0055 in., and the 90 percent beam width was 0.003 in. The mechanical resolving slit was 0.0065 in. The first peak on the left in figure 6 was obtained with no action from the virtual slit, i. e., only the mechanical slit was effective.

Figure 7 shows the peak shapes obtained when using various pairs of compounds having small mass differences. In each case the peaks on the left were obtained without use of the virtual slit, and those on the right were obtained using the virtual slit. The relative peak heights in each case show the intensity loss.

For the CO_2-propane mixture, the peaks at nominal mass 28, arising from fragments, are also shown. These peaks illustrate the fact that excess kinetic energy causes a broadening of the beam with consequent impairment of resolution.

COMPOUNDS	NOMINAL MASS	MASS DIFFERENCE (%)	SLIT WIDTH .0065 IN.	VIRTUAL SLIT WIDTH <.0065 IN.
CO_2 PROPANE (PARENT)	44	.165		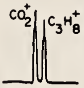
(FRAGMENT)	28	.13	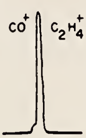	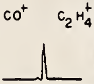
N_2 ETHYLENE (PARENT)	28	.09	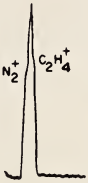	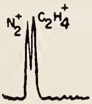
ACETONE n-BUTANE (PARENT)	58	.062	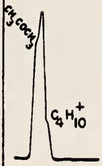	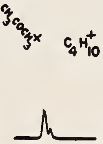
CO N_2 (PARENT)	28	.04	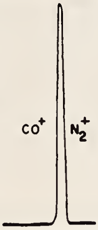	

FIGURE 7. *Resolution of ion pairs.*

Resolution obtained on 180° analytical mass spectrometer, using narrow resolving slit (0.0065 in.). Improvement obtained by use of ion-optical means of reducing slit to virtual width less than 0.0065 in. is shown in column at right.

13. The Influence of the Stray Field on the Focusing Qualities of a Magnetic Sector Field

By W. Paul[1]

Sometime ago we started to measure the abundances of lead isotopes for different minerals, but experienced difficulties concerning the resolving power of our 60° spectrometer. According to calculations by Walcher, we suspected that in our special case the trouble originated from the stray field of our 60° magnetic sector field. Because we did not find a previous work along this line, my coworker Bucka and I studied the influence of the stray field on the focusing qualities of the magnetic sector field by experiment. Our experimental arrangement is simple. It is shown in figure 1. We are using a common 60° mass spectrometer, the radius of curvature is 20 cm. The exit slit is movable along the optical axis within a wide range, about 40 cm. It is hanging on a counterpoise, which can be moved by a magnet. As test object we used the Rb ions of a hot tungsten anode. The ion beam could be moved across the exit slit by a sawtooth voltage superimposed on the high voltage. In this way it is possible to measure the width of the beam in any position by means of an oscilloscope.

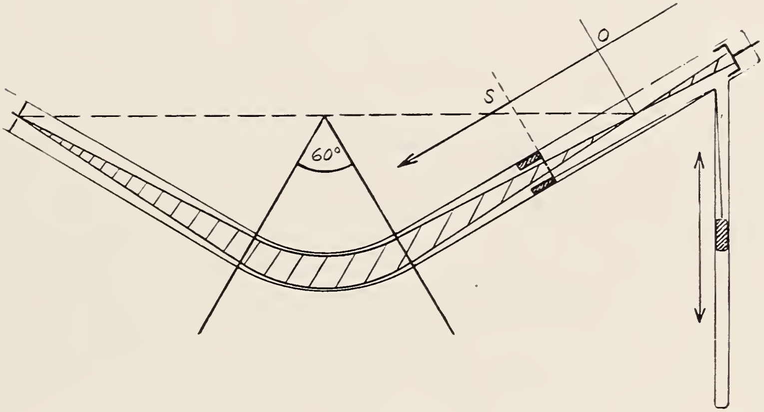

FIGURE 1. *Experimental arrangement for determining the focus.*

The usual way to adjust a spectrometer is to displace the magnet relative to the vacuum tube. If we disregard the stray field, a displacement by h cm will shift the image along the optical axis by $s_x = 4\ h$ cm (fig. 2). However, experiment showed that the shift is 20 h. In figure 3 the measured shift of the image is plotted as a function of the position of the magnet. h is the distance of the magnet from that point, where without stray field the optical path should be symmetric. The dotted line shows the calculated shift for this case. The expla-

---

[1] Institut f. Physik, Göttingen, Germany.

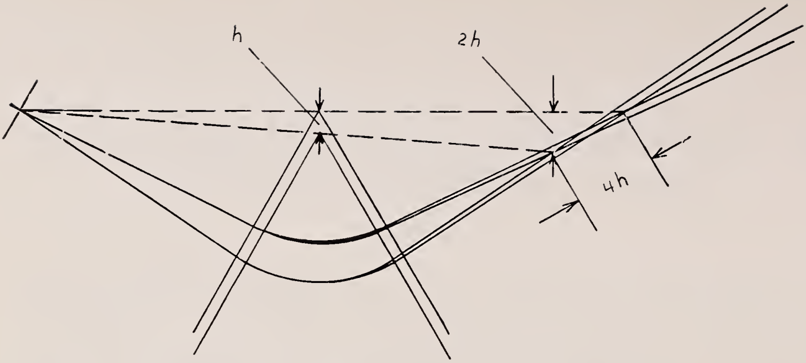

FIGURE 2. *Shift in focal point according to theory.*

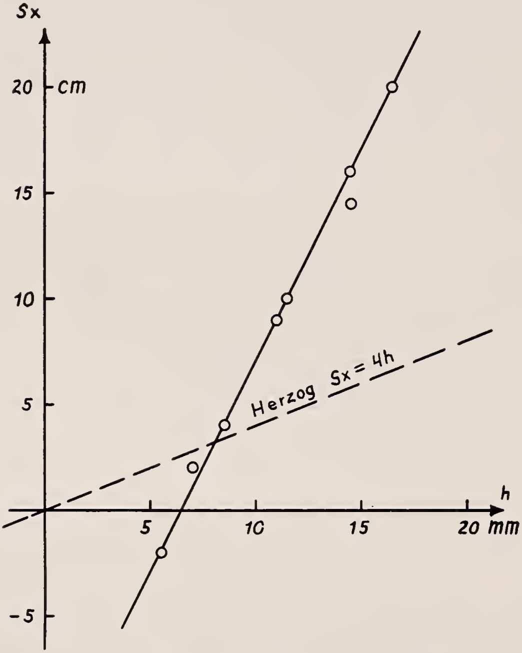

FIGURE 3. *Position of focal point determined experimentally as a function of magnet position.*

nation for this discrepancy between calculation and experiment is given by the stray field. Walcher, who treated the influence of the stray field on the focusing qualities theoretically, substituted the real field distribution, given by the iron pole pieces with stray field, by an idealized cut-off field. The boundary lines of that cut-off field have neither the actual position nor the actual shape as the edges of the iron pole shoes. If the boundary lines are curved, as in our case, the effective angle ϕ of the sector field varies with h. Therefore, the focal length is changed and the position of the image is shifted by an amount considerably bigger than can be accounted for by the Herzog case (fig. 4). The same occurs if the beam enters the field

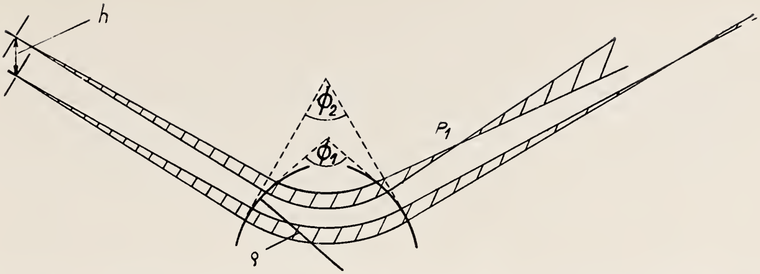

FIGURE 4. *Change of focal length as h is varied for curved boundaries of field.*

under different angles. If the aperture of the ion beam is large, we therefore get a high aperture error.

To study this fact we have shot a narrow beam into the field at different angles (fig. 5). With a small condenser the beam could be deflected. Now we measured the shift of the image as a function of the angle of incidence and found that $(\Delta s_x/\Delta\delta)=690$ cm for pole shoes 8 cm high. This means that a change in the angle of incidence of 1° shifts the image along the optical axis 12 cm. The relation between $\Delta s_x/\Delta\delta$ and the radius ρ of the curvature of the effective field bound is given by

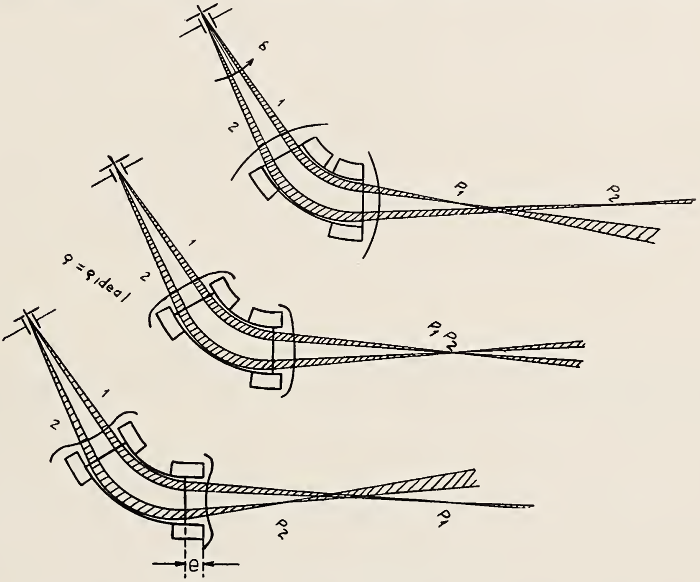

FIGURE 5. *Adjustment of the fringing field by means of shims.*

$$\Delta s_x/\Delta\delta = 2r\left[\left(r \operatorname{ctn}^3 \frac{\varphi}{2}\right)/\rho - 1\right] \qquad (1)$$

where r is the radius of curvature of the ion path. From the experimental value for $(\Delta s_x/\Delta\delta)$ we got $\rho=8$ cm. For another spectrometer tube with small pole pieces $\rho=4$ cm. If the aperture angle of the incident beam is α, the width of the beam on the most narrow place for infinitely small entrance slit is

$$b_\alpha = (\alpha^2/8)(\Delta s_x/\Delta\delta) = (\alpha^2 r/4)(\rho_{\text{ideal}}/\rho - 1) \tag{2}$$

To avoid this error ρ must be ρ_{ideal}, as Bainbridge has shown some years ago. Now, we put iron shims on the edges of the magnet. Therefore the lines of equal field strengths are adjustable. This is shown in figure 5. In the first case they are convex with the images lying at P_1 and P_2; in the second case, P_1 and P_2 fall together; in the third case, the boundary line is concave, P_2 has passed P_1 and lies now on the left. We measured the value $\Delta s/\Delta\delta$ for different positions of the shims. The result is shown in figure 6. Here $\Delta s/\Delta\delta$ is plotted as a function of position e of the shims as defined in figure 5. At the point e_0 the shift is zero and no aperture error exists. The dotted lines give the calculated radii of the corresponding cut-off fields. The best value is not $\rho = \infty$. The true value of ρ at the point e_0 can not be determined exactly. From equation $\rho_{\text{ideal}} = r\,\text{ctn}^3\,\frac{\phi}{2}$, ρ_{ideal} should be 105 cm. Furthermore, we proved equation (2) for different values of ρ experimentally and found that it is quite correct. With the shims in the right position we ascertained, in spite of the small pole shoes and wide aperture, that in the valley between isotopes 207 and 208 less than 1 percent of the abundant isotopes remains.

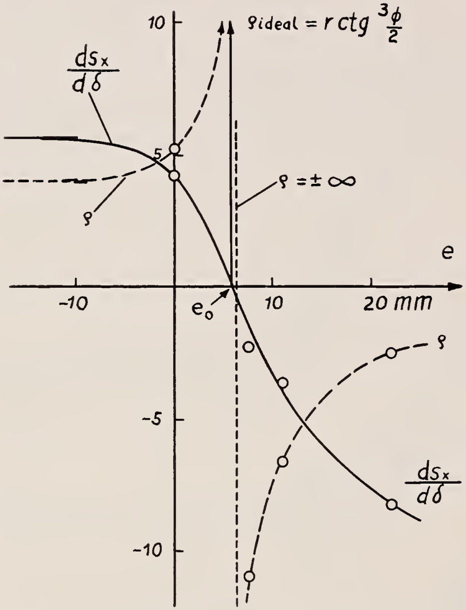

FIGURE 6. $\Delta s/\Delta\delta$ *as a function of shim position e.*

The dotted lines indicate the calculated radii of the corresponding cut-off fields.

It is worth mentioning that the calculation by Hintenberger and Bainbridge for the best shape of the pole shoes, to avoid aperture errors of second and higher orders, are only of theoretical interest, as long as the influence of the stray field is not taken into consideration. On the contrary, by shaping of the stray field these errors can be compensated.

14. The Nonmagnetic Radio-Frequency Mass Spectrometer

By Willard H. Bennett [1]

The nonmagnetic radio frequency mass spectrometer grew out of some work which was originally done in order to separate negative ions of quite different masses. That negative-ion work was originated at the National Bureau of Standards in 1946 and continued until 1950.

The arrangement originally used consisted of three grids, the middle one of which had applied to it a radio frequency alternating potential. A retarding potential was applied at the collecting electrode which lay beyond the three grids and turned back all ions except those of a particular mass which could pass through the three grids while the radio-frequency potential on the middle grid was changing phase so that those ions could pick up sufficient energy from the radio-frequency fields to overcome the retarding potential and reach the collector.

There seems to be a rather widespread impression that in such a system the ions will pick up a maximum of energy if they pass the successive grids at half-period intervals. This impression perhaps has carried over from experience with linear accelerators used in nuclear disintegration work. It can be shown, however, that the ions acquire a maximum of energy if they pass the first of the three grids at a 46½° phase angle, and the second grid at 180°.

More recently the design of tubes using three stages has been worked out. One such tube is shown in figure 1.

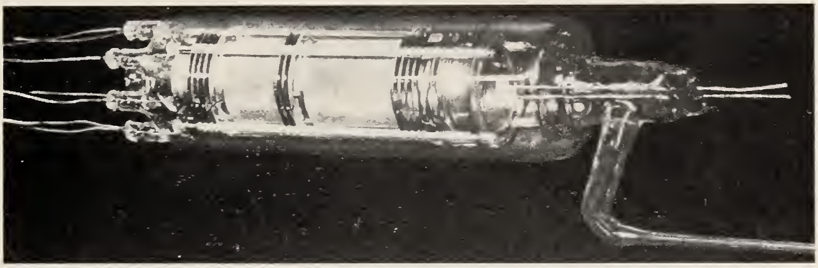

Figure 1.

The operation of the three-stage tube can best be understood in terms of the relationships which must apply in order that an ion can pick up a maximum of energy from each of the three stages. In order for the ion to acquire a maximum of energy while passing through the middle stage, it is necessary for the ion to pass the middle grid of that stage at a 180° phase angle of the radio-frequency potential, and the energy acquired by that ion in passing through the second stage varies with the frequency of the radio-frequency potential in accordance with the middle curve of figure 2. This same ion which

---

[1] University of Arkansas, Fayetteville, Ark.

passes the middle grid of the middle stage at a 180° phase angle acquires energy from the first stage according to the upper curve of figure 2, if the number of cycles traversed by the radio-frequency potential while the ion passes from the first to the second stage is 5 cycles. Similarly, the lower curve of figure 2 shows the energy acquired by that same ion while passing through the third stage. The total energy acquired from all three stages is shown in figure 3 and it is observed that since the numbers of cycles for the two drift spaces are different, the harmonics are substantially suppressed. By using a retarding potential in the collector sufficient to turn back all ions which have not acquired at least 80 percent of the maximum energy acquirable, there will be only one frequency for any particular ratio of e/m for which that value of e/m can reach the collector.

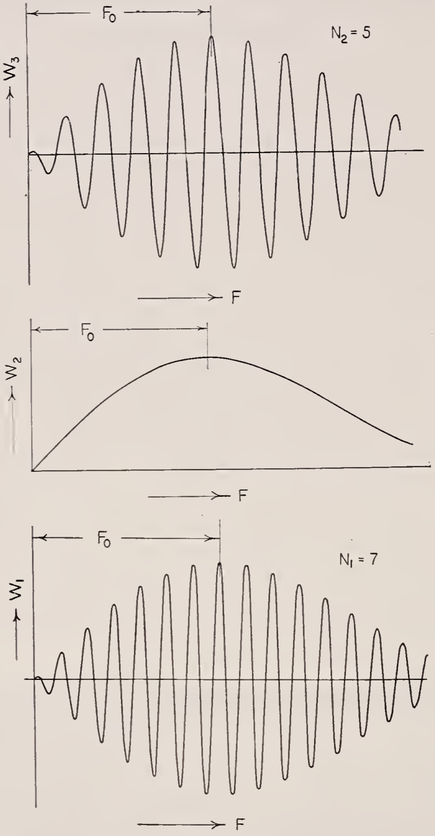

FIGURE 2.

If the distance between grids in each of the three stages is S, the frequency of the radio-frequency alternating potential in megacycles is F and the d-c potential through which the ions are accelerated between the ion source and the first stage of the analyzer in volts is V, then the mass of the ion which can reach the collector in atomic units (or, in case of multiply charged ions, the ionic mass divided by the number of charges) is $M=(0.266V)/(S^2F^2)$.

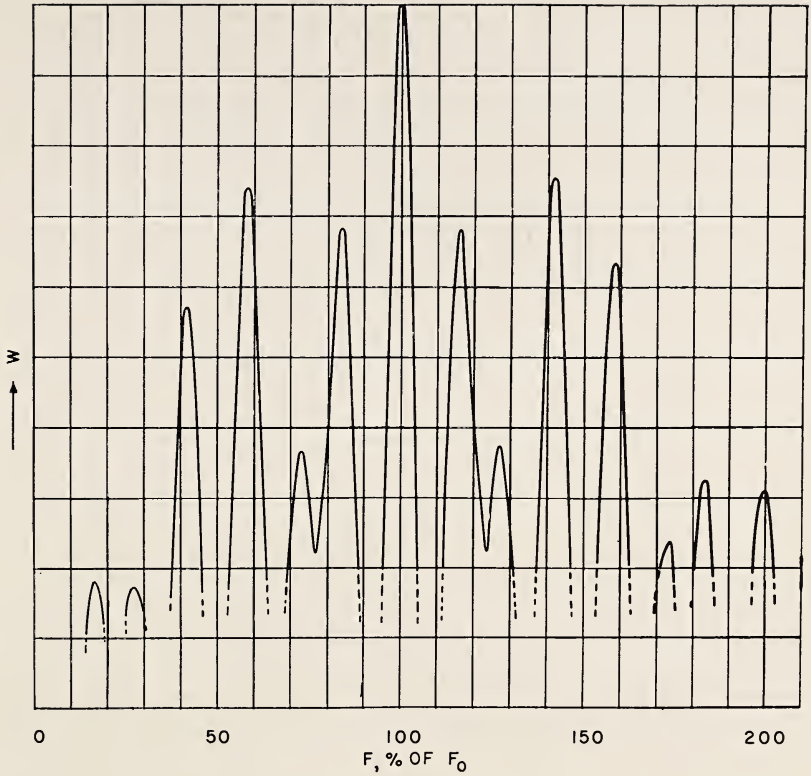

FIGURE 3.

A typical spectrum observed some time ago is shown in figure 4. This spectrum was observed before recent improvements were worked out whereby the background current could be suppressed. It will be observed that the base line is appreciably different from zero. This spectrum was taken by holding all voltages constant and varying the frequency. The data are plotted on semilogarithm paper which results in all lines having the same width except for effects of velocity spread due to different conditions in the ion source for the different kinds of ions.

During the past year considerable advances have been made toward improving this instrument, principally in the simplification in the structure of the tube, suppression of background currents, improvements in the resolution, and improvements in the sensitivity. This work is continuing. It is evident that much can still be done to improve this instrument with respect to the electronic circuits needed for operating it. One laboratory already has been able to advance the circuit development so that the complete mass spectrometer, including the tube and all electronic circuits and power supplies suitable for use in a rocket for the direct measurement of the composition of the upper atmosphere, weighs less than 25 lbs.

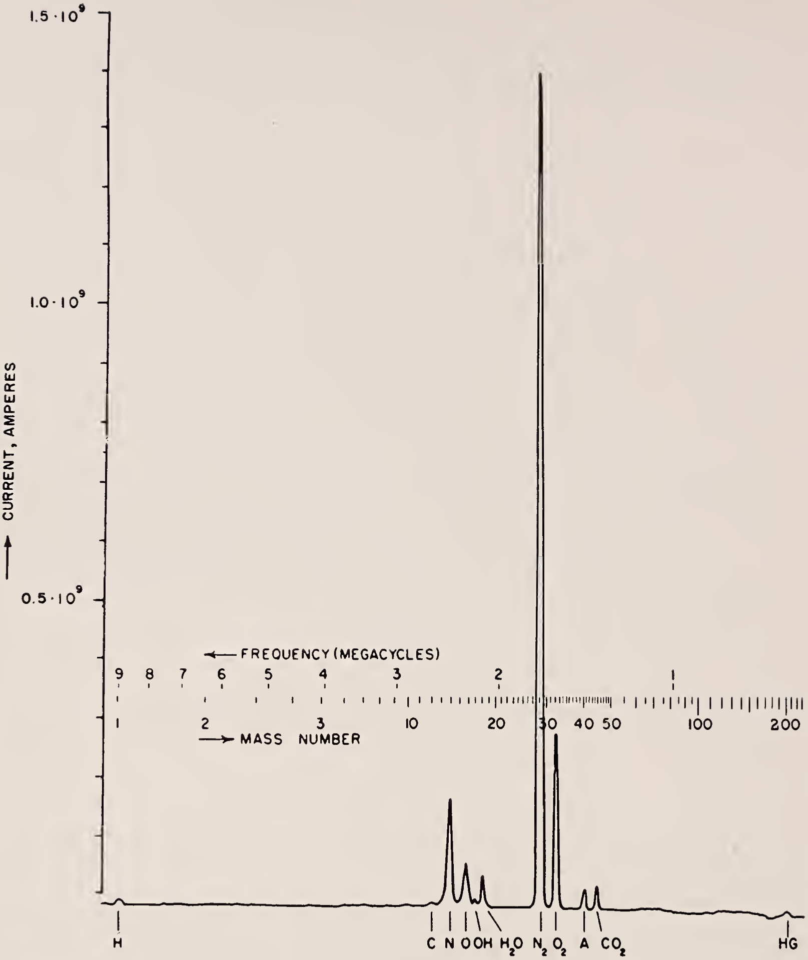

Figure 4.

A project has been started at the University of Arkansas to see what can be done by way of developing a leak which will admit gases directly into the ionization chamber from a chamber where a chemical reaction is proceeding. If it were possible to get these partially reacted gases to enter by a direct path into the region where ions are being formed, a means would be provided for studying the progress of the chemical reaction. This seems to be a feasible experiment because this instrument does not require the ions to pass through any narrow slits.

15. Time-of-Flight Mass Spectrometer

By E. E. Hays, P. I. Richards, and S. A. Goudsmit [1]

A mass spectrometer of the type originally proposed by Dr. S. A. Goudsmit has been built with the intention of evaluating the precision and usefulness of time-of-flight methods for mass measurement. The present communication has somewhat the nature of a final report on our work in this field.[2]

The machine measures the period of the cyclotron resonance frequency for the ion in question. This period, as is well known, is independent of energy and direction of motion and is given in microseconds by $T=652M/H$, where M is the ionic mass in atomic mass units, and H is the magnetic field in gauss. The mass scale of the machine is thus linear, and the precision in ΔM will be constant over the entire mass range. The machine is thus especially useful for heavy masses but, in its present embodiment, at least, practically useless for very low mass numbers.

The present machine employs the following ideas: A large volume of uniform magnetic field (about 600 gauss) is produced by a spherical aircore magnet [3] of 20-in. diameter. On a single magnetic-field line are located a pulsed ion source and, about five inches below, an electron-multiplier detector.[4] Pulsed ions having various thermal-velocity components along the H field travel in spirals of various pitches and reach the detector after various numbers of spiral turns. A Loran-type electronic timing apparatus serves to measure the time difference between, say, the second and eleventh spiral turns for a given mass. Comparisons of these times for several ions constitutes a relative mass measurement.

With our magnetic field of 600 gauss, the time in microseconds between the second and eleventh orders is approximately ten microseconds per mass unit. Our timer can measure these periods to within 0.01 microseconds, giving a theoretical accuracy of ±1 milli-mass-unit, or about 1 Mev, over the entire mass range. We may thus use the accurate values for the C and H masses obtained on deflection-type machines to provide standard hydro-carbon masses with which to evaluate our scale factor and any nonlinearity.

The accuracy actually achieved has been in the range plus-or-minus one to two milli-mass-units. This figure represents three to four times our statistical probable error, which has therefore ranged from about 0.0003 to 0.0007 mass units, but we prefer to quote the more conservative estimates. These results apply in the mass range 50 to 250 mass units.

There are two important limitations on the present design. First, due to the low magnetic field required to obtain long times, the ion energies are very low (25 v for mass 100). The ions are thus easily

---

[1] Brookhaven National Laboratory, Upton, N. Y., under contract with the A. E. C.
[2] Phys. Rev. **84**, 824 (1951); **85**, 630 and 1065 (1952).
[3] Design by E. U. Condon and J. A. Hipple and generously loaned to us by Westinghouse Research Laboratories.
[4] L. G. Smith, Rev. Sci Instruments, **22**, 166 (1951).

influenced by surface-potential fields arising from traces of dirt on the vacuum-chamber walls. This effect has been reduced by employing a gold-plated liner which must be periodically cleaned. This has reduced the effects to the point where the nonlinearity correction is never more than 5 milli-mass-units. Secondly, to obtain still longer times, and hence greater accuracy, it would be necessary, for the reasons just given, to employ spiral orbits of a great many turns. Geometry considerations then require an impractically large volume of magnetic field.

The present machine will therefore be used only to obtain a few mass values of possible immediate interest; in view of improvements to be expected in the future, we do not plan any extensive program of mass measurements. It is felt that the present investigation has shown that time-of-flight methods offer particular advantages in precision measurements of heavy masses.

16. The Mass Synchrometer

By Lincoln G. Smith [1]

1. Introduction

The instrument just described was an outgrowth of a discussion at Brookhaven in April 1948 held at my suggestion to undertake mass measurement work there by mass spectroscopic methods. At this conference the virtues of the crossed field instrument were ably described by Professor Bleakney and Dr. Thomas of Dr. Hipple's group. It was the consensus of the participants and others concerned: (1) that it would be desirable to do mass measurement work at Brookhaven; (2) that a large crossed-field spectrometer seemed then to offer the best possibility of attaining the desired precision of at least 1 part in 10^6; but (3) that because of the high cost of such an instrument, work should be undertaken to develop, if possible, a less costly instrument capable of such precision. It was the belief of some of us that a method of measuring masses in terms of frequencies offered the best hope.

In the method proposed by Dr. Goudsmit, as in the crossed-field spectrometer, use is made of the perfect focusing both in space and time of ions after n complete rotations from the source, However, the period of rotation T is measured by electronic timing of the flights of ion bunches rather than in terms of the distance from source to the nth image thereof. This method appeared at first to offer excellent possibilities of providing the desired instrument, because it did not require an extended uniform electric field normal to the magnetic field H. However, after designing and constructing the present "chronotron" in the Westinghouse spherical coil built by Dr. Hipple, I became convinced that neither adequate resolution nor accuracy could be obtained therewith. This was first because of the geometrical limitation on the number of turns ions can make and second, because of the lack of adequate homogeneity of the field. I felt that overcoming these difficulties would involve extremely difficult experimental problems.

It then occurred to me that both these difficulties could be resolved by use of a crossed electric field of small extent in space which varies in time. Thus I was led to investigate an instrument which I have called a mass "synchrometer" largely because masses are measured therein by a synchronous method.

2. Original Instrument

Figure 1 shows a diagram of the instrument as it was first assembled and described in a short report in Review of Scientific Instruments last spring.

Ions of limited mass range from source slit S_1 are focused after a half revolution on the triple slit S_2, S_3, S_4 called here a "pulser" of which S_2 and S_4 are grounded while S_3 is connected to a source of

---

[1] Brookhaven National Laboratory, Upton, N. Y.

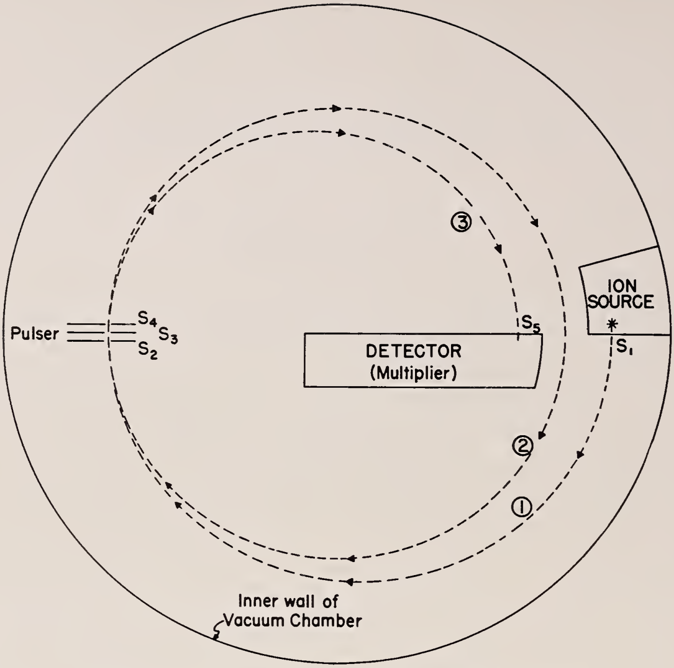

Figure 1. *Diagram of first mass synchrometer.*

potential which varies with time. Until quite recently this potential source has consisted of a pair of thyratrons each giving out negative rectangular voltage pulses of 1 microsecond duration at a repetition rate variable up to about 1,000 per second. The delay between pairs of pulses is continuously ajustable by means of a stable delay circuit.

When a pulse from the first thyratron is applied a short group of ions in the neighborhood of S_3 is decelerated sufficiently to miss the source housing on subsequent revolutions and is thus free to circulate in orbit (2) until all the ions are lost by scattering or the action of stray fields. If before this occurs, a pulse from the second thyratron is applied at a measured time later equal to nT, the remaining ions of this group can be made to enter slit S_5 of the detector, a 15-stage magnetic electron multiplier using dynodes of beryllium copper.

The metal vacuum chamber is placed in the 2 in. gap of an electromagnet with poles 15 in. in diameter. The diameter of the central orbit (2) is 10 in. and all slits are ⅛ in. wide by ⅝ in. high. A photograph of an early arrangement is shown in figure 2. Here we see the ion source consisting of a tungsten ribbon filament from which electrons are drawn along the magnetic field into a nichrome box whence ions are drawn through slit S_1 transversely. The pulser and multiplier are also shown as are electrodes designed to produce focusing in the direction of the magnetic field and two enclosed regions about the central orbit at about 270° and 360° from the source where adjustable electrostatic fields can be applied if necessary to compensate effects of stray fields.

With this arrangement and at a field of 850 oersteds, ion bunches of mass 28, formed in the residual gas at a pressure of 10^{-5} mm Hg

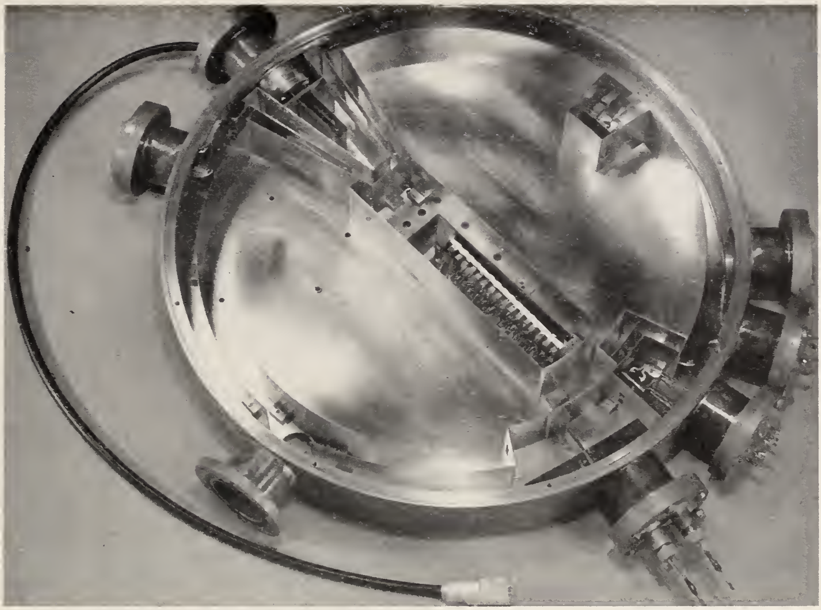

Figure 2. *Photograph showing interior of first mass synchrometer.*

and accelerated to an energy of 250 v, have been observed after going as many as 90 revolutions (72 meters) between applied voltage pulses. It is found that the length of a bunch which is here about equal to its width (3 mm) does not increase appreciably even after 90 turns so that the resolution (half width) here is $M/\Delta M = (72{,}000/3) = 24{,}000$. However, intensity after so many turns is extremely low so that the peak of average ion current versus time interval between pulses is very far from smooth.

This difficulty of intensity represents a serious fundamental drawback of time-of-flight spectrometers like this and the chronotron, first because the "duty cycle" or fraction of the time that ions are being collected is extremely low ($\sim 0.01\%$ or less to date) as compared with conventional mass spectrometers, and second because a considerable loss in intensity occurs after many turns. This occurs despite some success we have had in preventing spreading along H by electrostatic focusing. In the synchrometer some improvement in duty cycle seems possible by starting new bunches before old ones are detected, but since it does not seem practical to have more than about 10 bunches circulating at any time, an upper limit of about 0.1 percent seems required for the duty cycle.

In recent studies by Dr. Beth and myself with the aid of Mrs. Marylin McKeown it has been found that after about 20 turns the number of ions per bunch falls exponentially with the number of turns at a rate corresponding to a free path of about 15 meters (at 10^{-5} mm Hg) while below 20 turns it falls at a faster rate with increasing n.

These experiments were performed with a modified pulser in which the gap between S_3 and S_4 was increased from $\frac{3}{16}$ in. to $1\frac{1}{2}$ in. and electrodes were introduced between S_2 and S_3 so as to maintain the potential for $1\frac{1}{4}$ in. behind S_3 at the same (pulsed) potential as S_3.

At the same time a slit S_6 was placed around orbit 2 in the same plane as S_1 and S_5. Originally designed to put less stringent requirements on the rise times of the applied voltage pulses, this arrangement allowed production of bunches of length proportional to the pulse height which could be made less than a slit width. It was found that these bunches also did not increase in length so that resolution could be increased by raising pulse voltage, and a resolution of 14,000 corresponding to a bunch length of about 1 mm has been observed after 20 turns for mass 28 where the intensity was sufficient to give fairly smooth peaks.

This observation led to the conclusion that, so long as intensity is proportional to bunch length (ΔL) but falls exponentially with n while resolution is proportional to $^1/\Delta L$ and to n, then, for a given resolution, one obtains the greatest number of ions per bunch by working at a path length of one free path. Further reflection reveals however, that since increasing the number of turns (i. e., the free path) lowers the duty cycle, the maximum number of ions per unit time would be obtained for given resolution by working at only one turn between applied pulses. This consideration immediately brought up the impossibility of pulsing thyratrons at the required high rate and led at once to the consideration of using radio-frequency voltage on the pulser, now more appropriately called a modulator.

3. Recent Modifications

Therefore let us now consider the effect of using r-f on a modulator such as the triple slit arrangement shown in figure 1. In the approximation that one can neglect differences in transit times through the modulator; the velocity modulation of ions emerging therefrom is an harmonic function of the phase of the r-f as they pass any particular plane. Thus the diameter of their subsequent orbits are modulated with a similar harmonic function of phase. If the amplitude of diameter modulation (ΔDm) is greater than the distance between S_1 and S_6, then S_6 will select two bunches per cycle whose effective length is very much less than the distance traveled in a cycle. On their next transit through the modulator both of these bunches can be made to enter the detector if the applied frequency is an exact multiple of the cyclotron frequency. Since ions travel only one turn between transits through the modulator, the original bunch length would have to be $\frac{1}{20}$ as great. However, the duty cycle is now raised from 0.01 to about 5 percent and a loss of ions in going 20 turns of about a factor of 100 is avoided so that, for the same resolution, an increase in intensity of about 2,500 should be possible over the former method.

More recently it occurred to me that if the detector were placed on the original orbit (1), say just behind the source, then not only ions which passed through slit S_6, but in fact all ions which miss the source (if S_6 were removed) would be returned to the detector if they arrived at the modulator $n+\frac{1}{2}$ cycles after they left it the first time. Thus a still larger duty cycle would be possible. In fact, if one either allowed the ions to spiral two turns from the source to a detector placed above or below it as in the chronotron or displaced the orbits transversely as in the crossed field instrument, the duty cycle could be made 100 percent: i. e., at the peak of current versus frequency the current is the full current that would travel as a d-c beam from source to detector.

Calculations show that when all ions are accepted, the half width of a peak is $\frac{1}{4}$ $(w/\Delta Dm)$ of an r-f cycle, where w is the slit width. This fraction is $\frac{1}{64}$ if $w=\frac{1}{8}$ in. and $\Delta Dm=2$ in. The resolution is $(n+\frac{1}{2})$ divided by this fraction so that if each ion goes once around in 100 cycles (the present ratio of orbit circumference to modulator thickness is about 100) a resolution of 6,400 should be available. Moreover, by reducing w by a factor of 3 and the separation of modulator plates by the same factor, one should be able to increase the resolution by a factor 9 to about 60,000 with only $\frac{1}{3}$ loss in peak intensity.

To test these ideas the instrument has been greatly simplified as shown in figure 3. The multiplier has been removed and replaced by a simple collector plate in a Faraday cage connected to a vibrating reed electrometer while the central modulator plate is connected to an r-f oscillator and amplifier giving up to 100 v at from 2.5 to 6 megacycles. Here we accept only ions which are decelerated enough to miss a baffle in the plane of S_1 whose inner edge is about 1 in. from the center of S_1, i. e., about 30 percent of the ions for $\Delta Dm=2$ in. Under these conditions the theoretical half width is $\frac{1}{3}$ $(w/\Delta Dm)$ and the resolution expected is 4,800.

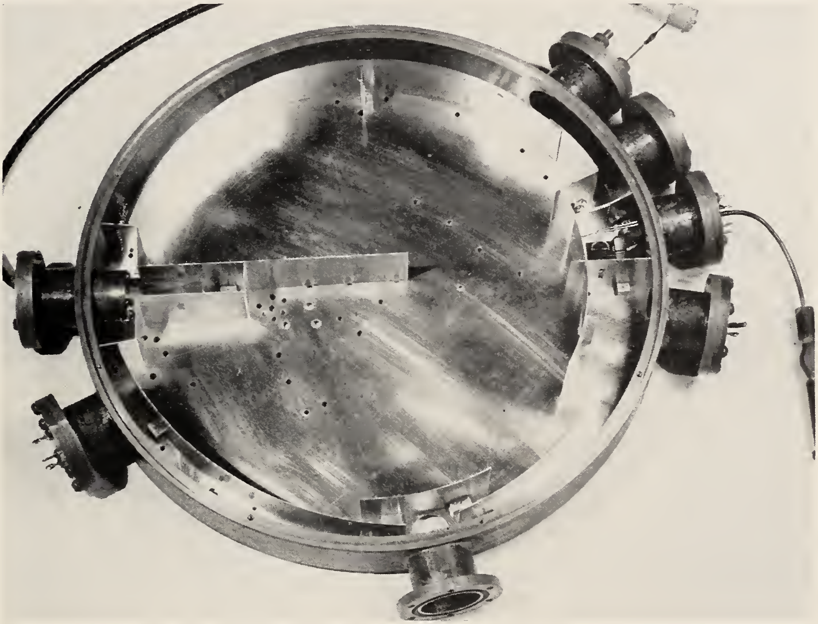

FIGURE 3. *Modified mass synchrometer using r-f modulation.*

The equipment in this form has been in reasonably reliable operation only over the past weekend so we don't know all its idiosyncrasies. However, I can report that we get peaks of intensity nearly 10 percent of the d-c current (which goes around only once) on mass 28, which peak intensity is about 10^{-10} amp, and that the resolution is about 1,200, $\frac{1}{4}$ the theoretical value. My present best guess as to the reason for this low observed resolution is that the equipotential surfaces between the modulator electrodes are not sufficiently plain. Refinements such as the use of grids over the slits are being considered.

In conclusion I should like to express my sincere gratitude to Dr. Richard A. Beth for his invaluable assistance in the developments of the past summer and to Mrs. Marylin McKeown for painstaking care in constructing and maintaining equipment. I should also like to thank Drs. Hipple and Sommer for their suggested possible modification of the synchrometer and to suggest that they might consider the above modification as an improvement of the crossed-field instrument.

17. Work on Cyclotron Resonance at the National Bureau of Standards

By J. A. Hipple and H. Sommer [1]

In considering the topics to be covered in this presentation we had expected to describe the omegatron and include some brief remarks on our current work here on cyclotron resonance. We have come to realize that the emphasis should be changed because most of you will see our equipment during the symposium. The omegatron equipment is small and furthermore a detailed description has appeared recently [1]; [2] on the other hand, the larger equipment you will see in our laboratory cannot be ignored during your visit, and we believe you will be more interested in having us take all the limited time available to describe our plans for it, even though one much prefers to talk about an experiment after some success has been attained.

Our analyzer consists of crossed uniform electric and magnetic fields in which the ions follow a trochoidal path [2] of five cycles. To refresh your memory, figure 1 illustrates the desirable focusing properties of this instrument. A beam of ions of one particular value of m/e forms an astigmatic image of the source slit independent of the initial energy or direction of motion of the ions in passing through the source slit. The figure shows the foci corresponding to two different values of m/e. We were interested in exploiting this focusing principle as well as the linear mass scale for precision mass measurement and undertook the construction of an instrument for this purpose. A trochoidal path of five cycles was planned with a distance

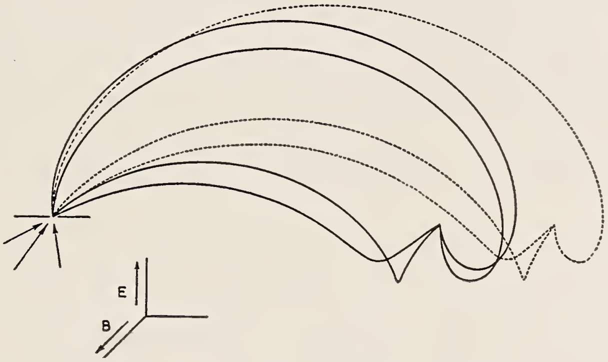

Figure 1. Trochoidal mass spectrometer.

The foci obtained for ions of two values of m/e are independent of initial conditions of velocity and direction (focusing in the plane perpendicular to B). The time for one trochoid is determined by the cyclotron frequency and is also independent of the initial conditions.

---

[1] National Bureau of Standards, Washington, D. C.

[2] Figures in brackets indicate the literature references on p. 126.

of two meters between the source and the final focus and provision for either electrical or photographic recording.

The major components, with the exception of details in the analyzer, were completed and assembled into an integrated unit last spring. A workable vacuum was obtained, the magnetic field was regulated by means of proton resonance, and the maximum variation in magnitude over the area to be used (225 cm by 48 cm) was determined to be ±0.01 percent.

Many persons, no longer connected with the project, had made major contributions up to this point. H. A. Thomas was an active collaborator since the early planning, soon after the inception of the project at the end of 1946, and he reported on the status of our design and construction at a Brookhaven conference in April 1948 when a similar project was being considered there. The project itself was initiated under the sponsorship of the Office of Naval Research in collaboration with Westinghouse Research Laboratories and the National Bureau of Standards. After completion of the components for the major subassemblies, the sole responsibility for the continuation of the project was transferred to the National Bureau of Standards and progress was delayed for a considerable period because of administrative details involved in this transfer. The Westinghouse personnel who made a major contribution to the engineering design and completion of the large subassemblies were W. M. Brubaker, R. E. Fox and D. J. Grove. Many others were helpful although participating less directly.

Last spring a reorientation in our plans occurred with the decision to convert to a time-of-flight instrument based on cyclotron resonance. Before describing this new approach we would like to recall for you the relation between the trochoidal and the time-of-flight instruments. The ions in the crossed-field instrument follow circular paths on a coordinate system moving with a uniform velocity $v=E/B$ (independent of the m/e or initial conditions) where E is the electric field and B the magnetic. The period for the ions to traverse one complete circle of 360° is given by the cyclotron condition and is unaffected by E. The result is that the usual trochoidal instrument is essentially a time-of-flight instrument with the time for one cycle being given in terms of the distance the moving coordinate system moves while the ions turns through 360°. This was well-known at the time we started this project. The direct timing of the flight by electronic means was discarded at that time because an effective method was not then apparent, although this possibility did provide an additional argument for choosing the trochoidal instrument. A cogent reason for the change in our initial plans is the stimulation received by the success and indications of success of various cyclotron resonance methods. [3, 4, 5, 1.].

Our method is illustrated in figure 2. The ions, after traversing one cycle, pass through a pair of small, closely spaced electrodes to which a radio frequency voltage is applied. At present these electrodes consist of a pair of copper wires of 0.6 mm diameter with a gap between them of 1.0 mm. The r-f voltage applied to these wires will in general deflect the beam in the direction of the magnetic field and consequently the ions are unable to reach the gap between a second similar pair of wires four cycles later. However, if the ions pass through the first r-f pair at the time when the r-f voltage is approximately zero, they will be undeflected and can pass through the analyzer in the usual manner until they reach the second r-f pair. Similarly, the ions will be undeflected by the second r-f pair and pass onward to the ion collector outside the magnetic field only if they pass through this r-f pair during the brief interval of time when the r-f voltage is approximately zero. Since the two sets of deflectors are connected to the same source of r-f voltage, the frequencies ν that will permit the undeflected passage of the ions through the instrument are related to the cyclotron resonance frequency by the relation indicated in figure 2.

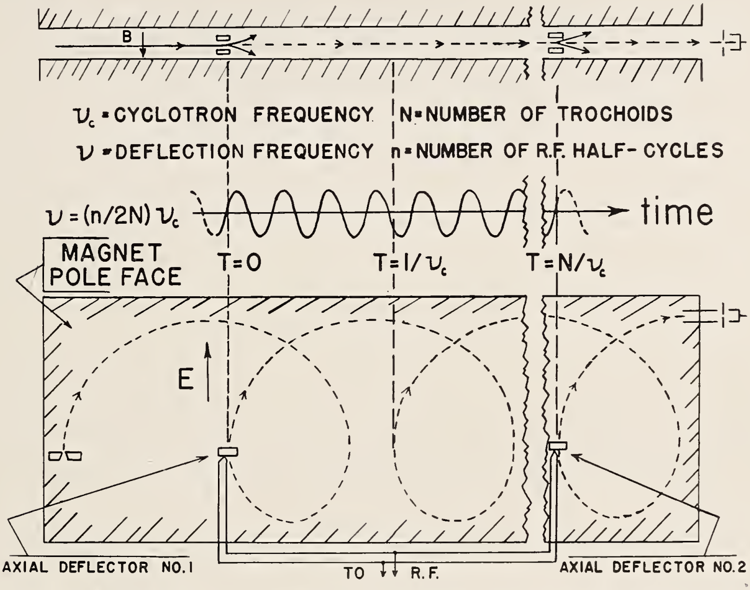

FIGURE 2. *Modification of conventional trochoidal instrument to permit accurate timing of the flight of ions during multiple cycles of the trochoid.*

Several reasons can be presented for the conversion to the time-of-flight operation. One immediately evident is the ability to use crystal oscillators for control of the two basic parameters involved in the measurement of m/e—the flight time and, by means of proton resonance, the magnetic field. Another advantage is the replacement of the photographic plate by electrical detection. The method of electrical detection is not otherwise so readily adaptable to the trochoidal instrument for accurate mass measurement. The requirement on the stability of the electric field E in the analyzer is greatly eased since this does not appear in the cyclotron relation; similarly, since the magnetic field appears in this relation in the first power rather than the second as in the customary crossed-field instrument, the tolerable limit in the stability of the magnetic field is doubled.

You undoubtedly expect an opinion on the performance we anticipate. We prefer not to attempt a prediction of the ultimate resolution, but simply to give an example of possible operating conditions for ions of mass 200; time will tell whether this was a reasonable target at which to shoot. Our magnet is already regulated at 3400 gauss and for this the transit time for four trochoids will be 150 microseconds. For these conditions it seems reasonable to expect that geometrical limitations will not be too serious at 5 megacycles which is approximately the 750th harmonic of the fundamental corresponding to four trochoids. We are interested in working at the highest harmonic possible, because, in the operating range, the resolution increases linearly with frequency with no loss in intensity. For the above conditions there would be 1,500 "pulses" in transit at any instant. On the other hand, an increase in r-f voltage will increase the resolution at the sacrifice of intensity. If a voltage of amount V_L is just sufficient to block passage of the ions through the instrument and V is the r-f peak voltage, then if we take $(V/V_L)=100$, the pulse of ions would have a spread of approximately 1/300 of a cycle or in our case 600 micromicroseconds. The resolution in this case would be $[150/(2)(.0006)]\approx 125{,}000$. Other factors quite possibly may limit the resolution to a lower value, but this does appear to be a goal that is attainable on the basis of intensity of the beam at the detector. Neglecting admittedly important factors such as the spreading of the beam in the direction of the magnetic field during transit and also other geometrical considerations, an elementary calculation indicates an intensity for the r-f operation of 0.003 compared with the ordinary d-c operation. A somewhat greater factor than this should be tolerable with the use of an electron multiplier and a slit of considerable width in the direction perpendicular to both fields.[2]

The high harmonic that is employed would cause trouble with overlapping orders except for the fact that the crossed-field instrument with its dispersion of 20 mm for 1 percent mass difference serves the function of an optical prism to sort out the "monochromatic" beam (in this case one value of m/e) for the precision measurement by the "interferometer", the analogous role performed by the timing electrodes.

The main modifications in the equipment were the additions of the timing electrodes, the electron multiplier, and a series of deflectors to bring the beam out of the magnetic field to the multiplier. As this symposium began, we had completed the assembly and were starting to look for an ion beam.

In talking to one another we initially called this new device a crossed-field, time-of-flight mass spectrometer. We were not able to endure this string of nouns very long and at this point recalled a proposal [6] made some years ago in which the path of ions reminded one of the yo-yo. In fact, we used this name in our own discussions. Consequently we are now using the name "yo" because the path is so similar to half of that in the yo-yo.

[1] H. Sommer, H. A. Thomas, and J. A. Hipple, Phys. Rev. **82**, 697 (1951).
[2] W. Bleakney and J. A. Hipple, Phys. Rev. **53**, 521 (1938).
[3] S. A. Goudsmit, Phys. Rev. **74**, 622 (1948); E. E. Hays, P. I. Richards, and S. A. Goudsmit, Phys. Rev. **84**, 824 (1951).
[4] F. Bloch and C. D. Jeffries, Phys. Rev. **80**, 305 (1950); C. D. Jeffries, Phys. Rev. **81**, 1040 (1951).
[5] L. G. Smith, Phys. Rev. **81**, 295 (1951); Rev. Sci. Instruments **22**, 115 (1951).
[6] J. A. Hipple and H. A. Thomas, Phys. Rev. **75**, 1616 (1949).

---

[2] Several months after the symposium, a resolution of 12,000 at half maximum was attained with xenon ions on the 270th harmonic of the fundamental corresponding to the flight time of 100 microseconds between the pairs of timing electrodes. There are indications that higher resolution should result from changes in electrode structure and use of a higher frequency when the equipment became available.

Discussion for Papers 15, 16, and 17

MATTAUCH: I am sure now many of you will have questions to ask. Do you have questions on any of the three papers?

DELFOSSE: I did not quite get what Dr. Hipple meant by over-voltage.

HIPPLE: We have this applied sine wave on the deflecting electrodes. There is a certain minimum voltage required; that is, if we apply no voltage, the ions will go straight through. As we increase the radio frequency voltage, there is some value at which we begin to lose ion current; the ions are deflected and lost. Voltage greater than this we have called over-voltage.

BLEAKNEY: I would like to ask, do you plan when you scan, that is when you are looking for something, do you vary the frequency and the electric field simultaneously?

HIPPLE: No, we vary the electric field to pick out the component we want. We shut off the r. f. at this time and get the desired ions centered properly on the exit slit. After turning on the r. f. and measuring this component of the doublet, the r. f. is turned off once more and the other component of the doublet is focused on the exit before this is measured with the r. f. Thus both components are made to pass through the same magnetic field.

BLEAKNEY: The attempt is to get each component to go through the same path.

HIPPLE: Yes.

BLEAKNEY: It seems to me also that in both these last two modifications they are hardly time-of-flight instruments any more, since you are again matching frequencies against multiples. You don't call the omegatron a time-of-flight instrument, do you?

HIPPLE: Yes, we do. Wouldn't you, Smith?

BLEAKNEY: Well, it is a matter of opinion.

SMITH: Goudsmit has always made a distinction between time instruments and measurement instruments.

When you adjust the resolution of the first half turn of the synchrometer it is adequate to select the first mass number. When one has a doublet which is not separated the situation is more involved, but, of course, I didn't have time, really, to go into much detail on these things. It is true that even some of those which do go through to the detector are of no interest. Those which get no deflection are always going in. This is a small fraction. One has this rather small background against which he sees rather sharp peaks.

EWALD: Is there any focusing in the direction of the magnetic field?

HIPPLE: Focusing by the r. f. field?

EWALD: No, by the constant electric field.

HIPPLE: No, there is no axial focusing in the direction of the magnetic field.

EWALD: These lines are going a little upward?

HIPPLE: They would drift out as an astigmatic focus.

DUCKWORTH: Dr. Hipple, as I understand it, this project to try on a grand scale the mass spectrometer is being abandoned as such.

HIPPLE: No, this instrument will operate with the trochoidal method but we have a choice now of which method it would be so we put our effort on the first. It is our opinion that the thing that we should stress is the time-of-flight operation.

Duckworth: You would have to take out these deflection electrodes in order to test as a straight trochoidal instrument, is that right?

Hipple: They are small. They should not bother us very much. The final pair are simply on a photo plate holder so we can remove them. The others we can't remove but we don't need to put the r. f. voltage on them. It would cut down the range of masses we could record on a photographic plate. I don't know exactly how much, maybe 25 percent of the range would be cut out but the rest is still free.

Duckworth: If the instrument is used as a straight trochoidal instrument, what resolution might you expect then? That is, what do you compare to the 125,000?

Hipple: Well, that figure was not a prediction. It is just an illustrative example.

Duckworth: Well, have you a number you could pick?

Hipple: I think this would be like a news release before the event.

Duckworth: Well, this was.

Hipple: I will answer you this way, it may be this high. It depends on how well it works. I don't know.

Nier: A question related to Dr. Duckworth's last one. This perhaps will orient us a little bit in this thing. How large a slit did you plan to use as your initial slit or final slit in the source—perhaps call it the final slit in the source?

Hipple: Well, we thought we could use slits comparable to what other people have used.

Smith: Which other people?

Hipple: Professor Mattauch, Professor Ogata. I will show you. The resolution is given by the equation $(M/\Delta M)=D/\Delta D$ where D is the distance from the source slit along the focal plane to the final image—in our case approximately 2,000 mm. For photographic detection ΔD is simply the width of the entrance slit to the analyzer. What should I use for ΔD, Dr. Mattauch?

Mattauch: You should be able to use slits of 0.01 mm.

Nier: Well, isn't it a factor then in the new scheme that you could use quite a wide slit there and compensate for your loss in intensity in the duty cycles? Isn't this an important factor?

Hipple: Oh, yes, this could be very wide. This does not affect the time. Providing we put the r. f. electrodes on the focal plane, we could vary the "E" field and get the same answer, if the magnetic field is perfectly uniform. It is very uniform but we would prefer to use a rather small part of the magnetic field.

Bleakney: It seems that Dr. Smith has pushed the duty cycle way up at the sacrifice of some resolving power. It isn't quite clear to me how much.

Smith: Well, again I did not quite finish that. I should have mentioned the resolving power that we should get with our present instrument. The slits are one-eighth of an inch wide and the theoretical resolving power is, for 30 volts on the r. f., about 30,000, providing we had 100 cycles around the circle. The peak width in fractional part of a cycle in our case turns out to be one-quarter of the slit width divided by the modulation and if you divide by the number of cycles around you get the resolving power. The base of our electrode now is about three-eighths of an inch. You want to make this the distance of about one cycle of the r. f. We can use about 100 cycles. Theoretically you get a resolution of 6,400.

Now, if you cut the slit width down to about 1 millimeter we can get three times as many cycles in and also reduce the fraction of a cycle by one third and get nine times the resolution with 1 millimeter slits at one-third reduction in intensity. The implication of this, if you go a little further, is that we might also get a resolution of three or four hundred thousand with still enormous intensity but I don't like to stick my neck out too far.

BAINBRIDGE: I want to point out on this problem of resolution and accuracy, that nature provides a requirement in the problem of measuring the mass of tritium against helium 3. This is an experiment that would be nice to do, and the resolving power, if it is going to be done with one exposure of both beams, would have to exceed one in 150,000. If you wanted an accuracy of a kilovolt, then you would need an accuracy of measurement of one in 3,000,000. Here is a natural aiming point on resolution and accuracy.

DUCKWORTH: I would like to ask Dr. Smith the same sort of a question I asked Dr. Ewald yesterday, namely whether or not during the experiments this summer he has had an opportunity to observe if the doublet spacing varies much under pressure.

SMITH: No, I have not. We have not done very much about precision mass measurements at all. We are still interested in developing the instrument.

18. Present Status of Isotopic Abundances

By Alfred O. C. Nier [1]

In 1933 when Aston published his book on isotopes, the relative abundances of isotopes in about 50 of the elements had been measured, most of them by Aston who used his mass spectrograph. In the 18 years which have elapsed, the mass spectrometer has gradually superseded the mass spectrograph as a means for measuring isotopic abundances.

The techniques employed by Dempster, Smyth, Kallmann, Bleakney, Tate, Smith, and others in the late 1920's in the studies of impact on gases by electrons were soon applied in isotopic abundance studies. In 1932 Bleakney and his coworkers began reporting isotopic abundance measurements with an instrument using a common magnetic field for collimating the electron beam and making a mass analysis of the ions produced by electron impact. The use of this type of instrument was extended by others so that by 1942 when the last edition of Aston's book appeared, 48 of the elements had been measured by electrical means.

During the war years few isotope abundance measurements were made, but by the end of 1950, electrical abundance measurements had been made for 78 of the 83 "naturally" occurring elements. Only fluorine, aluminum, yttrium, ruthenium and thorium remain uninvestigated by the electrical method.

Because of the high sensitivity attained in most of the investigations and the rather thorough search for rare isotopes in the neighborhood of the known abundant ones, it is not likely that more than a very few naturally occurring isotopes remain undiscovered.

Most isotope abundance ratios are now known to one percent or thereabouts. In some cases the ratios are known more accurately. In most instances of extremely rare isotopes the accuracy may be somewhat less. Also, in cases of elements covering a wide fractional mass range, the accuracy may be lower due to instrumental discrimination depending upon mass.

Instrumental discrimination depending upon mass may be eliminated, or at least minimized by calibration of the instrument by use of synthetic isotope mixtures. About a year ago we at Minnesota made some very accurately determined argon mixtures by mixing known amounts of nearly pure A^{36} and A^{40}. The large fractional mass difference (10 percent) and the relatively high accuracy to which the abundance ratios were known (a few tenths of a percent) made it possible to obtain in 10 common elements, abundance ratios which we believe to be quite accurate. This work has not been extended because of the pressure of other matters.

With the rather good knowledge of the natural occurrence of stable isotopes and the relatively satisfactory information on relative abundances of isotopes, our greatest interest at present in isotope abundance ratios lies in special problems which may be solved by measuring isotope abundance ratios.

---

[1] University of Minnesota, Minneapolis, Minn.

In the field of geochemistry and geophysics the surface appears hardly to be scratched. Historically, the accurate measurement of lead isotope abundance ratios has contributed much to our knowledge of geological age. Further measurements on both radiogenic and common lead will provide the geologists for years to come with fundamental research problems. Measurements on argon, calcium, and strontium have not as yet been exploited. Systematic studies of carefully chosen minerals containing these elements cannot help but provide the geologists with additional tools for measuring geological age.

Then there are the elements such as helium, boron, carbon, oxygen, nitrogen and sulfur where the cause of the variations reported appears to be other than radioactive decay. The careful measurement of isotope abundance ratios in these and other elements where undoubtedly variations exist which have not yet been detected will provide a fertile field of endeavor for the student of physical chemistry and geochemistry.

The use of separated stable isotopes as tracers has not been fully appreciated. While the use of heavy hydrogen, nitrogen and carbon in biochemical studies has been well established, the availability of separated isotopes of other elements is making possible tracer studies in these elements.

I have touched on but a few applications of isotope abundance measurements. The program which follows will give other examples. Let us turn now to some of the new work.

19. A Mass Spectrometer for the Measurement of Small Differences in Isotope Abundance Ratios

By S. Epstein [1]

It is the object of this talk to report on some work that has been done by a group headed by Harold C. Urey at the University of Chicago. This research requires the use of a mass spectrometer which measures small differences in isotopic abundance ratios. Some results are presented as an illustration of the performance of the mass spectrometer.

The considerations which led to the initiation of the research have been described by Urey.[2] Consider the isotopic equilibrium system

$$\tfrac{1}{3}\mathrm{CO}_3^{=16}+\mathrm{H_2O^{18}}\rightleftarrows\tfrac{1}{3}\mathrm{CO}_3^{=18}{}_{5}+\mathrm{H_2O^{16}}$$

The equilibrium constant can be expressed as

$$K=\frac{(\mathrm{CO}_3^{=18})^{\frac{1}{3}}}{(\mathrm{CO}_3^{=16})^{\frac{1}{3}}}\bigg/\frac{\mathrm{H_2O^{18}}}{\mathrm{H_2O^{16}}}$$

Urey calculated the equilibrium constant from spectroscopic data for a free carbonate ion. McCrea [3] also considered the lattice motion of the crystal and arrived at values for K: at 0°, $K=1.02548$; at 25°, $K=1.02058$. From these $\Delta K/\Delta T=0.0002/°\mathrm{C}$. In the case of the oceans where the carbonate concentration is low, the change in the equilibrium constant will, for practical purposes, be due to a change in $\mathrm{O^{18}/O^{16}}$ ratio of the carbonate only. If marine animals lay down their calcareous shells in isotopic equilibrium with the surrounding water, it should be possible to measure the temperature, within 1 deg C, at which a marine animal lives by determining the relative $\mathrm{O^{18}/O^{16}}$ ratio of the $\mathrm{CO_2}$ extracted from the $\mathrm{CaCO_3}$ in its shell to an accuracy of approximately 0.02 percent. These were the foundations of the problem of measuring temperatures of oceans in geologic time.

The mass spectrometer used for this research was the one described by Nier,[4] with some modifications essential for its application to this problem. Detailed descriptions of all the units have been published.[5] Substitution of the vibrating-reed electrometer for the d-c amplifier for measuring the small variation in ion beam of mass 46 was very helpful. This was done by adapting the ion beam balancing circuit of Nier, Inghram, and Ney [6] as shown in figure 1.

The input resistors R_1 and R_2 are 1.5×10^{11} and 1.5×10^{10} ohms respectively. The voltages developed across these resistors are approximately 750 mv and 18 v respectively. The short range fluctuations of the output of the vibrating reed itself are less than 0.1 mv and are 0.15 mv for the output of the balancing circuit.

---

[1] University of Chicago, Chicago, Ill.

[2] H. C. Urey, J. Chem. Soc. 592 (1947).

[3] J. M. McCrea, J. Chem. Phys. **18**, 849 (1950).

[4] A. O. Nier, Rev. Sci. Instruments **18**, 398 (1947).

[5] C. R. McKinney, J. M. McCrea, S. Epstein, H. A. Allen, H. C. Urey, Rev. Sci. Instruments **21**, 724 (1950).

[6] A. O. Nier, M. G. Inghram. E. P. Ney, Rev. Sci. Instruments **18**, 294 (1947).

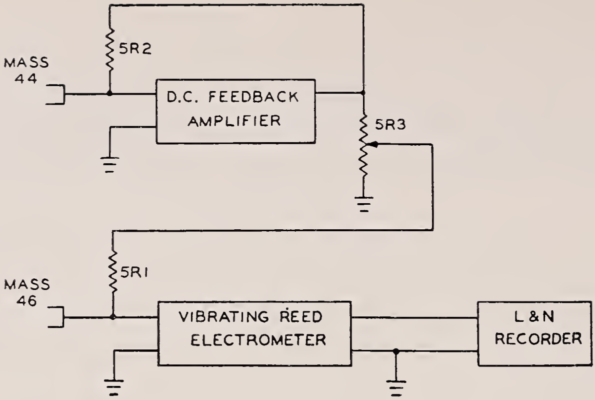

FIGURE 1. *Ion beam balancing circuit.*

Slow variations with time of conditions in the ion source cause variations in the absolute determinations of the ratio which are much larger than those we wish to detect. Since the research only required measurements of changes in the ratio of masses 46/44, these measurements were made with reference to an arbitrarily chosen reference carbon-dioxide gas.

Two complete gas feed systems, mercury leveling reservoirs and capillary leads of the type described by Nier were attached to the mass spectrometer through a magnetically operated valve (fig. 2)

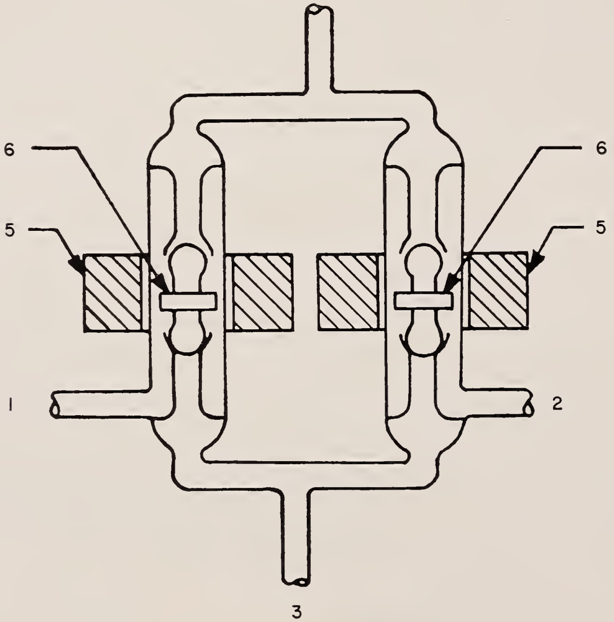

FIGURE 2. *Valve for reversing samples.*

1, inlet for sample 1; 2, inlet for sample 2; 3, outlet to waste vacuum; 4, outlet to mass spectrometer; 5, coil windings; 6, soft iron washer on glass valve.

delivering one sample to the mass spectrometer and the other to a waste vacuum. In this way the flow of the two samples could be reversed rapidly. Since the valve is on the low pressure side, there is a very small lag in changing from sample to sample. The memory effect of each gas is very small since the samples are all of nearly identical isotopic composition.

Figure 3 illustrates the traces of the balance circuit output. Trace 2 represents the null point of the standard gas and trace 1 represents the deviation from the null point by a decrease of 0.63 per mil in the intensity of the ion beam of mass 46. If the deviation from the null point is large, part of the increase or decrease is taken up by changing the setting on the balancing system. Straight lines are drawn through the irregular traces and extended to the point where the samples were changed, and the differences are read at these points. The displacement on the chart is readily calibrated in terms of the dial settings in the resistance panel. The average of some seven readings is then used to correct the ratio read from the resistors.

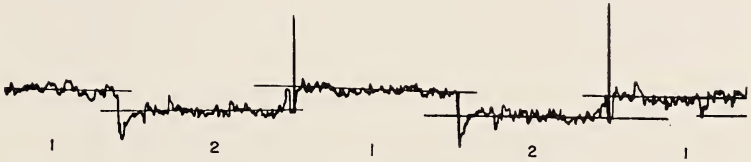

FIGURE 3. *Sample potentiometer record.*

Examples of check analyses are given in table 1. The recorded figures are the differences in per mil of the normal ratio between the sample and the standard working gas, and are calculated by the formula:

$$\delta O^{18}=\left(\frac{R_{\text{sample}}}{R_{\text{standard}}}-1\right)1,000,$$

where R_{sample} and R_{standard} are the ratios of $CO^{16}O^{18}/CO^{16}O^{16}$ for the unknown sample and reference gas respectively. The errors in duplication also include the experimental error due to the preparation of the samples, except sample 3 for O_2 gas. Many hundreds of analyses have established this limit of duplications.

TABLE 1.

CO_2 gas				O_2 gas		
Sample	$\delta(O^{18})$	$\delta(C^{13})$	Date	Sample	$\delta(O^{18})$	Date
1	−0.53	0.42	12/13/49	1	17.11	12/7/49
	−.59	.50	1/4/50		16.77	12/8/49
2	−2.98	1.95	12/20/49	2	0.23	2/10/50
	−2.99	1.75	1/3/50		−.10	2/13/50
	−3.00	1.58	1/3/50			
3	−3.87	1.30	12/12/49	3	.00	2/10/50
	−3.83	1.35	1/3/50		.00	2/11/50
					−.20	2/13/50
4	−2.30	2.30	12/13/49	4	.44	2/10/50
	−2.56	2.46	1/4/50		−.02	2/11/50
					−.14	2/13/50
5	−2.18	1.73	12/22/49			
	−2.22	1.90	1/4/50			

I should now like to present a few of the results we have been able to obtain by means of the mass spectrometer.

Figure 4 shows the variation of O^{18}/O^{16} ratio in marine waters. The samples of water were furnished by Dr. H. Pettersson[7] who collected them on the Albatross expedition. The samples were collected from various depths in the temperate and equatorial zones. The O^{18}/O^{16} ratios of the waters were determined by equilibrating the water with CO_2 and analyzing the CO_2. The O^{18} of the water varies over a range of 2 ppm. If the O^{18} content of the water is plotted against the salinity of the water, a direct relationship between O^{18} content and salinity is obtained. This is as expected since evaporation and condensation processes will affect the two in a parallel manner.

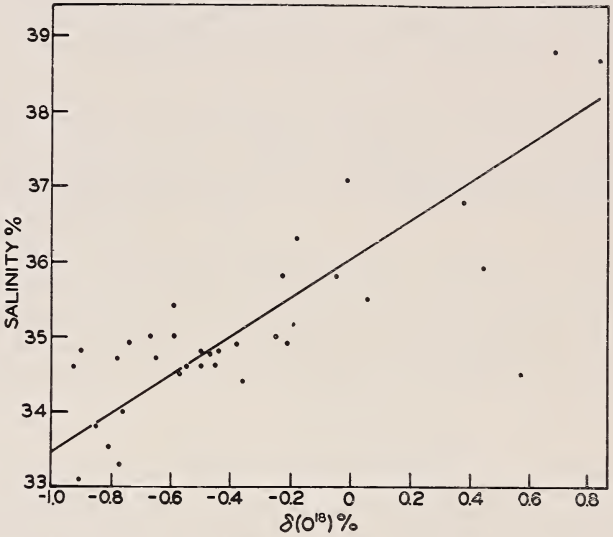

FIGURE 4. *Plot of salinity versus relative O^{18} content for ocean waters.*

Figure 5 shows a plot of O^{18} content of the surface and near surface waters versus temperature. The variation of O^{18} content of ocean water introduces sources of error in measuring absolute paleotemperatures since this variation will be superimposed on the effects of temperature on the O^{18} content of the calcium carbonate. This difficulty can be eliminated by determining a temperature scale based on the $PO_4^{\equiv}-H_2O$ system. From the combination of the two temperature scales it is possible to determine the relative O^{18} content of the ocean waters which then will not only facilitate a correction for variation of relative O^{18} content of ocean waters, but will also provide information regarding magnitude of evaporation and condensation processes of the oceans and degree of uniformity of temperatures on the surface of the oceans. Since fresh water analyzes ≈6.0 percent less O^{18} than marine water, it should also be possible to locate mouths of rivers that existed in the past.

Figure 6 shows the experimentally determined temperature scale. Samples of shells generated by marine animals while living in tanks

---

[7] H. Pettersson, Endeavor 8, 182 (1949).

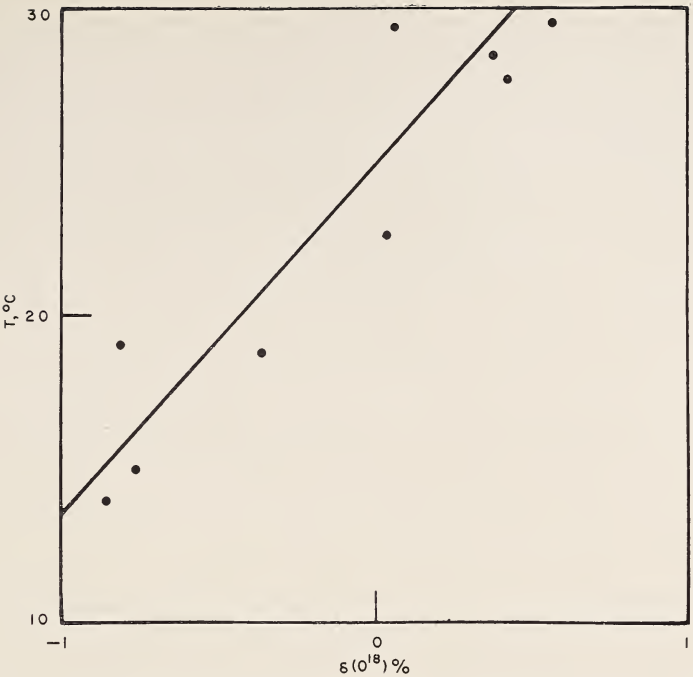

FIGURE 5. *Temperature of the water versus variation δO^{18} of surface ocean water.*

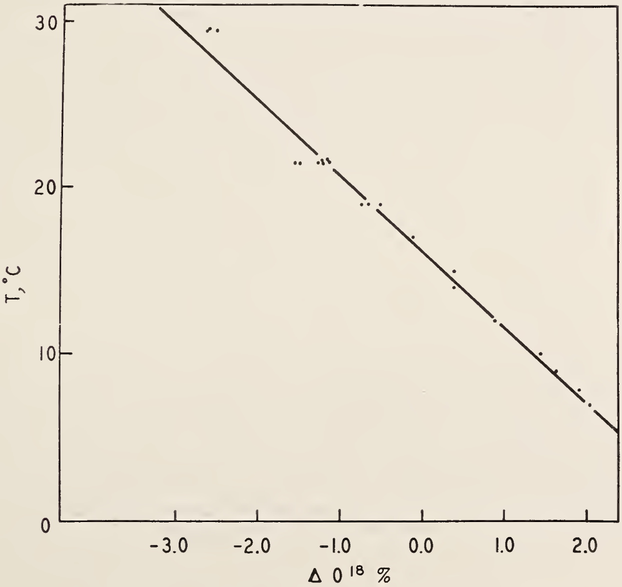

FIGURE 6. *Experimentally determined temperature scale.*

at controlled temperatures or in areas where temperatures of the water are well known were powdered and roasted at 475° C for approximately 45 minutes in an atmosphere of helium. The carbon dioxide was released by reacting the powder with 100 percent H_3PO_4 in which was dissolved about 5 percent P_2O_5 and the gas was analyzed mass-spectrometrically. The points at 29.5°, 21.5°, and 18.9° C were determined using shells grown in thermostated water tanks. The rest of the points were determined by analyzing consecutive growth layers of marine shells found in their natural location and matching the maximum and minimum 46/44 ratio with that of the average minimum and maximum temperature of the location. The relationship represented by the temperature scale may be expressed as $T°C=16.2-4.6\delta O^{18}$.

The subject for the first paleotemperature determinations was a Jurassic Belimnite, an extinct marine animal which flourished in the Mesozoic era, about 120 million years ago. The guard of this marine invertebrate is well preserved, compact, and in many cases growth rings are preserved. To determine whether the oxygen isotopic composition of the original $CaCO_3$ is preserved over this long period of time successive samples were ground off parallel to the growth rings from a disc representing a cross section of the guard. The CO_2 extracted was analyzed mass-spectrometrically.

Figure 7 shows the variation of the temperatures (as calculated from the temperature-δO^{18} relationship) with distance from the center of the disc. This variation is taken to be due to seasonal variations in temperature and indicates with some certainty the preservation of the original $CaCO_3$.

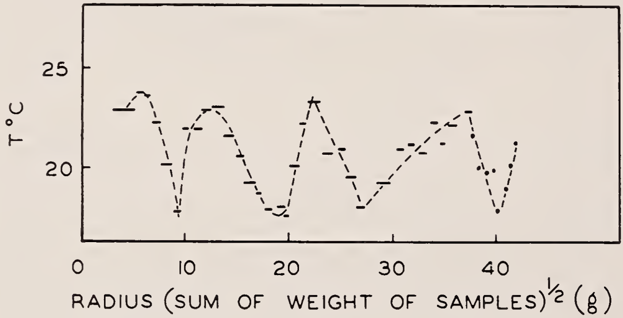

FIGURE 7. *Seasonal variation of jurassic belemnite.*

Figure 8 shows the determined average temperatures of the seas which covered areas in the listed countries during the Upper Cretaceous times plotted against the chronologically ordered cretaceous subdivisions. There is indicated an association of low temperature with beginning and ending of the period and a warmer temperature in the middle of the period. One can attach some significance to these data since endings of periods are designated by drastic changes in both faunal records and topography of land surfaces.

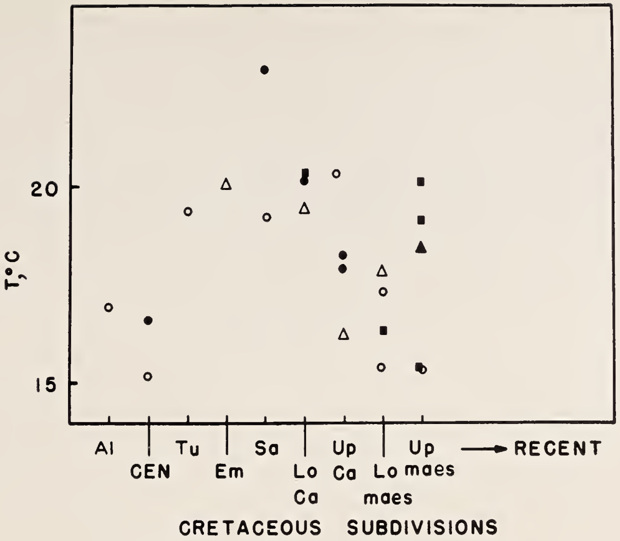

FIGURE 8. *Cretaceous temperature.*

●, England; ○, Denmark; △, Sweden; ■, Holland; ▲, southeastern United States.

Discussion

A. O. NIER: It has been suggested that when other methods for measurement come along we may be looking for other occupations. I would like to ask Dr. Urey and Dr. Epstein how useful it would be to develop high resolution instruments for this type of work you are doing. You mentioned the problems of impurities, for instance. With the exception of the work going on now at Consolidated Engineering in connection with their separating some very close masses, no one has really seriously considered this. We would just stop and say, "This isn't interesting any more and let's work on something else." That has been the attitude in our laboratory.

I would like to know how useful it would be to take the double-focusing mass spectrometer and apply that to the measurements you are doing and have an instrument that has a resolving power of 2,000, 3,000 or 4,000, something like that.

H. C. UREY: I would say, since Dr. Epstein asks me to answer this, that it would be exceedingly useful. The most difficult part of this problem was the chemistry. Dr. Epstein deserves credit for solving this problem. It required months and months to get rid of the impurities. If you have an instrument that will separate carbon dioxide from nitrogen oxide, or whatever it was that gave it its impurity, it would solve a great many chemical problems. I think it would be very interesting to work on nitrogen in nature, but this work will be bothered by carbon monoxide. If you could separate them it would solve a great many problems. I am a chemist, but there is nothing I dislike so much as doing chemistry. If you could find any way to avoid it, I would be very glad.

20. Instrumental Problems Encountered in Mass Spectrometer Isotope Analysis of Water Samples

By H. W. Washburn, C. E. Berry, and L. G. Hall[1]

1. Introduction

The determination of deuterium concentration in water samples is becoming an increasingly important factor in biological tracer studies. In the past it has been necessary, in the majority of cases at least, to convert the water sample by some chemical process to hydrogen gas which was analyzed on the mass spectrometer for the ratio of deuterium to total hydrogens. If this conversion process could be eliminated by running the water samples directly on the mass spectrometer, it would have the advantage of simplicity, and what is more important in biological work, very small samples could be used.

Due to these advantages, it was suggested that the possibility of analyzing water samples directly be investigated. This was done on two instruments which had been designed to perform water-alcohol analyses. One instrument was the Consolidated Engineering 21–103 and the other was an experimental instrument employing the same ion source as the 21–103 in a modified 180° instrument having a 2½ in. ion path radius. This instrument differed from the conventional apparatus in that the air gap is widened at both ends of the analyzer in order to accommodate physically the source and collector assemblies. This laboratory instrument was equipped with a pen-and-ink recorder, and the spectrum was swept by varying the ion accelerating voltage.

It was found that on these two instruments it was possible to determine differences in concentration of $D/(H+D)$ as low as 0.0006 mole percent when the concentrations of $D/(H+D)$ were in the neighborhood of that existing in normal water. The accuracy of determining $D/(H+D)$ by analyzing the water sample directly is therefore as good as or better than the accuracy obtained when the water is first converted to a gas sample. This was a bit of a surprise as previously published data indicated errors about 300 times as large as this.

The remainder of this paper will be devoted to: first, a brief review of the problem of water-alcohol analyses and second, a discussion of the design features and procedures necessary to make deuterium concentration analyses by running water samples directly on the mass spectrometer.

2. Water-Alcohol Analysis

The problems encountered in making mass spectrometer analyses of water-alcohol mixtures are mainly those of adsorption and elution. Adsorption exhibits itself by the extra long time required to pump

---

[1] Consolidated Engineering Corporation, Pasadena, Calif.

out a sample. Elution is observed when a sample of different composition from previous samples is run. Even when the previous sample has been pumped out for a long time and practically no background exists, when the second sample is introduced it will adsorb on the walls and the previous sample will be eluted as shown by the appearance of its spectrum. For example, if a sample of ethyl alcohol is run until the apparatus comes to equilibrium with it and then is pumped out until only a very small background remains, the introduction of methyl alcohol will cause the ethyl alcohol spectrum to appear to a degree depending upon how well the apparatus is designed to minimize the elution effect.

Both the adsorption and elution effects may be minimized by (1) using a high differential pumping, (2) moving the leak close to the ion source, and (3) using a procedure of flushes rather than long pumpouts. The advantages of using these three features are perhaps best shown by the results of some simple experiments. The first experiments performed were designed to locate the surfaces on which most of the adsorption was taking place. The gas flow system in the mass spectrometer on which these experiments were performed is shown schematically in figure 1. The sample to be tested was first placed in the sample bottle at a pressure of about 100 microns and allowed to flow through the leak, ion source, and into the cold trap and diffusion pump for a period of about 30 minutes. The sample bottle was then evacuated through a pumping system not shown and the height of one of the major peaks of the sample recorded as a function of time. This result gives a measure of the adsorption on all surfaces.

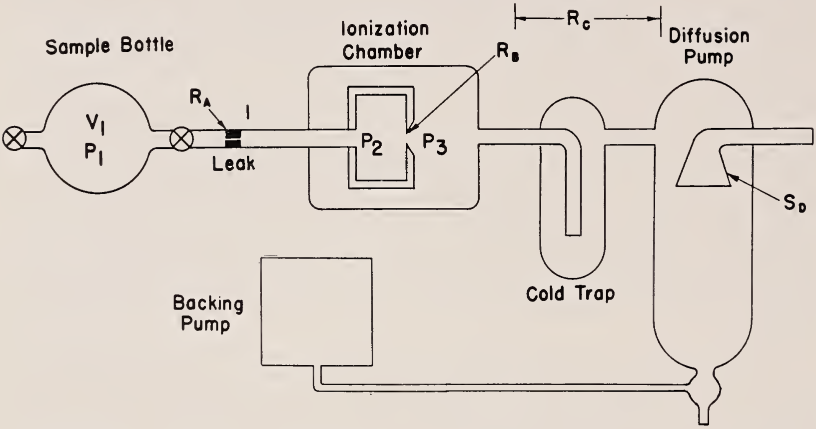

FIGURE 1. *Schematic drawing of gas flow system in the mass spectrometer.*

In order to determine what fraction of the adsorption takes place on the walls of the analyzer tube the sample was introduced directly into the analyzer tube (the region designated by P_3 in figure 1) at a pressure of about 10^{-6} mm which corresponds to the pressure which exists in the region when the sample is flowing from the sample bottle through the leak in a normal manner. The pressure P_2 in the ionization chamber under these conditions is the same as that in the analyzer tube and is only about 1/20 of the pressure which normally exists in the ionization chamber. Any adsorption effects observed in this experiment would therefore be those normally due to adsorption on the walls of the analyzer tube plus a small fraction of those normally due to adsorption in the ionization chamber. The adsorption effect was determined by stopping the gas flow into the analyzer tube and recording the peak height of one of the major peaks as a function of time. The results of this experiment showed that the adsorption on the analyzer tube was negligible compared to the total adsorption observed in the first experiment. This result is due to the high differential pumping factor employed.

In order to determine how much of the adsorption occurred in the sample bottle a sample was admitted to the sample bottle only, at the standard pressure of 100 microns and allowed to remain there for 30 minutes. During this time the stopcock between the sample bottle and the leak remained closed. The sample bottle was then evacuated and at the end of one minute the stopcock between the sample bottle and the leak was opened and the height of one of the major peaks recorded as a function of time. This experiment showed that the adsorption in the sample bottle was small as compared with the overall effect. Since the effect in both the sample bottle and the analyzer was small, it was concluded that the major cause of long pumpouts was the adsorption on the surfaces between the leak and the ionization chamber and in the ionization chamber itself.

The surface area of the line between the leak and the ionization chamber was much larger than that of the ionization chamber and so it was decided to see if heating this line would reduce the adsorption effect. The result of heating this line to around 200° C is shown in figure 2, which gives the peak height as a function of time with the inlet line cold and with it heated. It is seen that an improvement

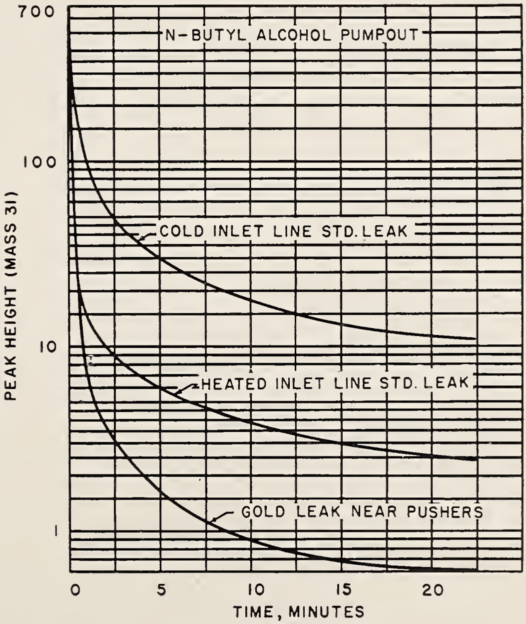

Figure 2. *Peak height as a function of time with the inlet line cold and heated.*

of about a factor of 4 was obtained by heating the line. It was believed that minimizing the area of this line might be even more effective than heating it and so the leak was moved as close to the ionization chamber as possible. The result of moving the leak is also shown in figure 2 as an improvement by another factor of 4. It is seen that with the leak near the ionization chamber, butyl alcohol was pumped down to about 0.2 percent in five minutes time which is satisfactory for most applications.

Similar experiments were then performed to determine the offending surfaces as far as elution is concerned. These experiments again showed that the offending surface was that between the leak and the ion source. The results of one of the experiments performed after the leak had been moved close to the ion source is shown in figure 3, which gives the elution of ethyl alcohol by methyl alcohol. At zero time on the graph the inlet sample bottle then containing ethyl alcohol was evacuated, and it is seen that the pumpout is quite fast. At the time of six minutes methyl alcohol was introduced into the envelope at normal envelope pressure (about 10^{-6} mm). It is seen that the amount of elution from the envelope is negligible. At ten minutes time the methyl alcohol was introduced through the ionization chamber in a normal manner and it is seen that the ethyl alcohol is eluted to the extent that its spectrum is between 1 and 2 percent of its normal value. This is quite good, but it is desirable for some analyses to reduce this figure still further. Table 1 shows how the effect of elution can be minimized by repeated introductions and thus getting rid of the previous sample by successive elutions rather than by long pumpouts. It is seen from table 1 that after three introductions the

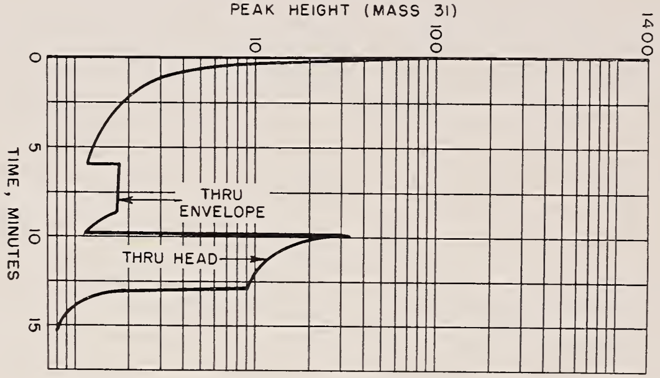

Figure 3. *Elution of ethyl alcohol by methyl alcohol.*

Table 1. *Ethanol eluted by methanol*

Methanol introduction number	Percent eluted
1	0.55
2	.08
3	.01
4	.01

cross contamination as a result of elution has been reduced to 0.01 percent, which is quite satisfactory for water-alcohol analysis.

It may be concluded from these experiments that satisfactory analysis of water-alcohol mixtures can be made provided the adsorption and elution effects are minimized by employing high differential pumping, placing the leak close to the ion source, and by using a procedure of successive elutions rather than long pumpouts.

3. Measuring $D/(H+D)$ in Water Samples

In measuring the deuterium concentration in water samples the same problems are encountered as were encountered in water-alcohol analysis and in addition there are two other effects which must be minimized. The first of these is the exchange of deuterium and hydrogen atoms in the sample with the deuterium and hydrogen atoms in the water adsorbed upon the walls of the apparatus. This exchange will exhibit itself in the same way as does elution, and it is found that apparatus designed to minimize elution gives a satisfactorily small exchange or memory effect.

The second phenomenon which causes trouble in determining the deuterium concentration is the formation of large numbers of ions having a specific mass of 19 which are not HDO^+ ions. Measurement of the concentration of these is desired. These spurious ions of mass 19 are observed to have an abundance which is proportional to the square of the pressure. This indicates that they are formed by some secondary process. They are believed to be H_3O^+ ions which are formed by the collision between an H_2O^+ ion and an H_2O neutral molecule.

Before any changes were made to minimize the formation of these H_3O^+ ions, their abundance was several times as great as the HDO^+ ions obtained when normal water is run. By considering the method of analysis, it is seen that their presence in such large quantities may cause serious errors in the determination of $D/(H+D)$. The normal way of analyzing an unknown sample is to run an unknown and then a standard and take the difference in the 19/18 ratios in these two runs. Since the H_3O^+ ion abundance is pressure sensitive, if the pressure at which the unknown sample is run differs from the pressure at which the standard sample is run an error would be made in the determination of the HDO^+ concentration. Before steps were taken to reduce the H_3O^+ formation a pressure difference of 10 percent would cause a 5 percent error in the determination of $D/(H+D)$ for samples having a composition near that of normal water. This error is larger than can be tolerated for many applications.

The way in which the abundance of the H_3O^+ ions can be reduced is illustrated by figure 4 which shows the ratio of the 19/18 peaks as a function of pressure for various repeller voltages. It is seen that all of these curves intercept the Y axis at approximately the same value of 19/18 ratio. This intercept gives the 19/18 ratio when there are no H_3O^+ ions present as presumably none could be formed at zero pressure. The height of any point on the curves above the intercept gives the abundance of the H_3O^+ ions under the particular conditions of pressure and repeller voltage. It will be observed that the ratio of the H_3O^+ ion abundance to mass 18 ion abundance increases linearly with pressure. This corresponds to an increase in H_3O^+ ion abundance with the square of the pressure since the mass 18

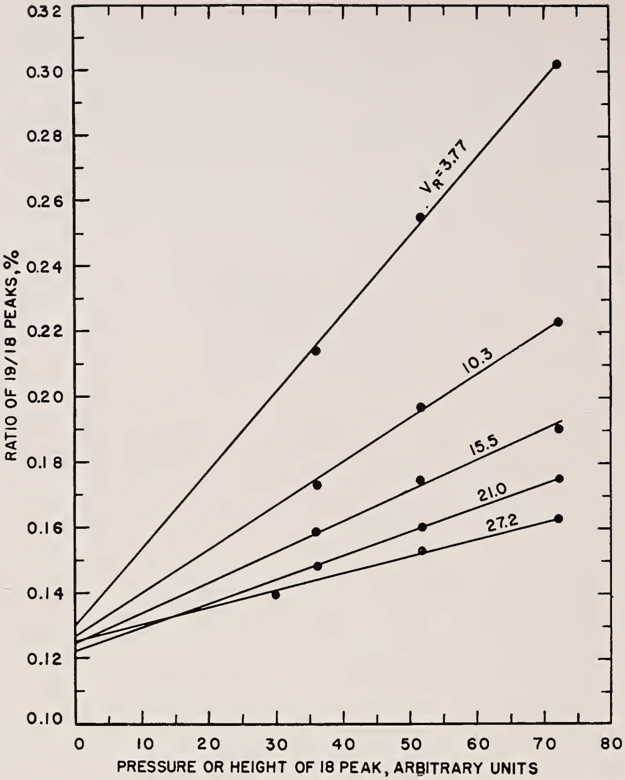

FIGURE 4. *Abundance of* H_3O^+ *ions as a function of pressure for various repeller voltages.*

Ion accelerating volts=500; V_R=repeller volts.

ion abundance is itself proportional to the pressure. It will also be observed that as the repeller voltage is increased, the formation of H_3O^+ ions is greatly reduced. Furthermore, it is found that at the higher repeller voltages it is possible to use a higher electron current without running into space charge effects. With the higher electron current a lower pressure may be used and so a further decrease in the H_3O^+ ion abundance may be realized. It was found that by increasing the repeller voltage and electron current and correspondingly decreasing the pressure, the H_3O^+ ion abundance could be reduced by a factor of between 5 and 10. The error, introduced into the D/(H+D) determination by a difference of 10 percent in pressure of the standard and unknown samples, is therefore reduced to below 1 percent, which is quite satisfactory.

It should be noted at this point that the large reduction in H_3O^+ ion abundance by increasing the repeller voltage has to date only been realized in instruments having a relatively high magnetic field at the ion source. With weak source magnet design the high repeller voltages give a lower sensitivity which in turn requires a higher sample pressure. The higher pressure would defeat the purpose since it would cause an increase in the rate of formation of H_3O^+.

It is thus seen by using a mass spectrometer having high differential pumping, locating the leak close to the ion source, and using a procedure of flushes rather than long pumpouts, that adsorption, elution, and atom exchange effects are minimized. By using a spectrometer which has a high magnetic field at the source so that the H_3O^+ ions may be minimized by increasing the repeller voltage, it should be possible to obtain accurate measurements on deuterium concentrations by running water samples directly on the mass spectrometer.

Before giving some of the results that can be obtained, it should be pointed out that for the low concentrations of deuterium the O^{17}/O^{16} and O^{18}/O^{16} ratios in the standard samples should be very nearly the same as those in the unknown sample. The closeness with which these isotope ratios should be held may be seen by referring to table 2. In a sample having $D/(H+D)=0.025$ percent, for example, the O^{17} and O^{18} contributions to the 19 peak are roughly of the same magnitude of the concentration of the HDO from which the concentration of deuterium is determined. The percentage error in the determination of deuterium concentration would be approximately the same as the percent difference in the ratios O^{17}/O^{16} or O^{18}/O^{16} in the standard and unknown samples. To obtain an accuracy in the results which is comparable to the best accuracy obtained by the instrument therefore, the ratios of O^{17}/O^{16} or O^{18}/O^{16} in the standard should not differ from those in the unknown by more than 2 percent. It will be observed in the last column the figures given for 0.2 percent of $D/(H+D)$ show that the contributions of O^{18} and O^{17} are only about $\frac{1}{10}$ of the contribution of the HDO^{16}. Relatively large differences in the standard and unknown sample O^{18}/O^{16} and O^{17}/O^{16} ratios can therefore be tolerated.

Table 2. *Contribution of various ions to mass 19 in a water mass spectrum*

Mass 19 contributions [1]	$D/(H+D)$ 0.025%	$D/(H+D)$ 0.2%
	Percent	*Percent*
HDO^{16+}	0.050	0.402
HO^{18+}	.053	.053
H_2O^{17+}	.039	.039
DO^{17+}	.000	.000
H_3O^+	.019	.019
Total 19	.161	.511

[1] Contributions are expressed as a percent of the mass-18 peak.

An example of the accuracy of the measurements which can be obtained is shown in figure 5. In obtaining the data for figure 5 a flushing technique was used which consisted of five introductions of one sample, the isotope ratio 19/18 being recorded on the fourth and fifth introductions only. The second sample was introduced in like manner and the 19/18 ratio measured on the fourth and fifth introductions. The first sample was alternated with the second sample until all data were obtained. It will be observed that the average difference of concentration determined in this manner was 0.0034 atom percent as compared with 0.0040 atom percent indicated by the synthetic composition. The difference between the experimental and the synthetic results is therefore 0.0006 atom percent. It is also of interest to note that the maximum deviation of any of the data from the average is only ±0.0005 atom percent. These results show that the method of introducing water samples directly gives accuracies in the determination of D/(H+D) as good as or better than those obtained by first converting the sample to hydrogen deuterium gas and running this gas on the mass spectrometer.

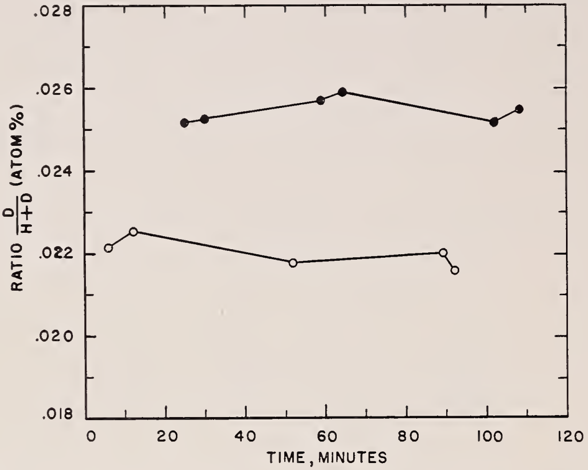

Figure 5. *Illustration of the accuracy of the analytical method.*

●, synthetic samples, 0.022 atom percent $\frac{D}{H+D}$; 0.026 atom percent $\frac{D}{H+D}$.

○, average difference, 0.0034 atom percent $\frac{D}{H+D}$.

4. Conclusion

Accurate measurements of D concentration in water samples can be made by running water directly, by the following procedures: High differential pumping, positioning of the leak close to the ion source, and flushing rather than long pumping to minimize adsorption, elution, and atom exchange effects; high repeller voltages in a source situated in a strong magnetic field to inhibit the creation of H_3O^+ ions.

5. Discussion

H. C. Urey: Dr. Mattauch, I would like to ask Dr. Washburn where he thinks the remaining adsorption occurs? Is it inside the instrument or in the connecting tubes or where?

H. W. Washburn: Mainly inside the ion source. It is also adsorbed in the analyzer, but since the pumping speed from the analyzer to the ion source is so small it would probably go out the pump, instead of into the ion source.

Urey. Do you think you are going to be able to improve this any beyond this point?

Washburn: Not very much. We have obtained quite a few results, some a little better than others.

UREY: The abundance of deuterium varies from about .014 to .015 percent. One would like to measure abundances in nature considerably better than one-third of that which is what you have.

WASHBURN: I don't quite understand; the normal is .015 and we are measuring to .0006.

UREY: It would be very nice if you could improve that by a factor of 5.

WASHBURN: I agree, but such an accuracy would be very difficult to achieve.

F. L. MOHLER: I would like to ask Dr. Washburn if you get much better sensitivity in H_2O than you do using hydrogen gas.

WASHBURN: At the very low concentrations now we are getting about the same accuracy we would get from the gas itself, providing you haven't made any error in transforming the water into the gas. At higher deuterium concentrations the accuracy with water samples is perhaps better. When in the region of 2 percent, about two-tenths of 1 percent accuracy is obtained.

21. The Mass Spectrometer as a Tool for Studying Nuclear Reactions

By Mark G. Inghram [1]

1. Introduction

Nuclear processes involve questions of what isotope undergoes what change to what new isotope. Since the mass spectrometer is a tool for studying isotopes, it follows that it is a tool for studying nuclear reactions. Applications of this type in the past, however, have been extremely limited due to the fact that the yields of most nuclear processes are extremely small. Thus the mass spectrometer did not have enough sensitivity to detect the effects. This limitation is being rapidly removed both due to the fact that new and more powerful cyclotrons, Van de Graaffs, piles, etc., are becoming available, increasing the yield; and secondly, that the sensitivity of the mass spectrometer has been improved by the use of new types of sample handling systems, ion sources and ion detectors to the point where the yields produced in a number of types of nuclear reactors are sufficient to be detected and measured. Present day sensitivities are such that 10^{-12} g of most of the elements are detectable, and in some cases, notably the alkali metals, less than 10^{-15} g are detectable.

Several laboratories have been involved in studies of the type. To mention a few there are, in addition to the group at Chicago, Prof. H. G. Thode and associates of McMaster University, Dr. F. Reynolds of the University of California, and a group at the Institute of Theoretical Physics in Copenhagen, Denmark. Due to lack of time it will be impossible to adequately cover the work of all these groups, and many interesting experiments will be left out in an attempt to illustrate the wide variety of applications which are possible.

2. Radioactive Half-Lives

In radioactive decay, for example, $Pu^{240} \rightarrow U^{236} + He$ and $Br^{82} \rightarrow Kr^{82} + \beta$, there are a number of things characteristic of the half-life of the decay process. The method of half-life measurements which has been used extensively in the past is that of using counters and counting the number of decay particles produced per unit time. However, just as characteristic of the decay process is the rate of loss of the parent isotope or the rate of increase of either the daughter isotope or the so-called decay particle. Thus, for example, if one has a sample containing Br^{81} and Br^{82}, one can get the half-life of Br^{82} simply by measuring the rate of change of the isotopic ratio. Such determinations can be completely independent of counting methods. If the half-life is long, it is preferable to measure the rate of increase of the daughter element rather than the decay of the parent. This method is preferred for long-lived isotopes inasmuch as a large change in a

---

[1] University of Chicago and Argonne National Laboratory, Chicago, Ill.

small isotope is easier to measure than a small change in a large isotope.

The first use of the growth of the daughter element for half-life determination was that of Nier [1] in which he measured the half-life of U^{235} by measuring the growth of Pb^{207} into a uranium mineral over geologically long periods. Since Nier's original indirect measurement, three series of experiments using counting methods have given values for the half-life 15 percent longer than Nier's original value. Very recently, however, two new counting results have come out which completely agree with the old mass spectrometric measurement. This illustration points out the value of the method.

A number of half-life determinations have recently been made using these methods both at Chicago and McMaster. One of the more recent determinations which was made at Chicago [2] was that of the half-life of Pu^{240}. The decay relations involved in a mixed sample of Pu^{239} and Pu^{240} are:

$$\mathrm{Pu}^{239} \xrightarrow{24{,}410\ y} \mathrm{U}^{235} \xrightarrow{7\times 10^{8}\ y}$$

$$\mathrm{Pu}^{240} \xrightarrow{\ ?\ } \mathrm{U}^{236} \xrightarrow{2\times 10^{7}\ y}.$$

Since the time necessary to complete the experiment is short in comparison to the half-lives involved, the decay can be written

$$\mathrm{U}^{235}=(\mathrm{Pu}^{239}/\mathrm{T}_{1/2}^{239})\ .693$$

$$\mathrm{U}^{236}=(\mathrm{Pu}^{240}/\mathrm{T}_{1/2}^{240})\ .693$$

dividing one equation by the other and solving for the half-life of Pu^{240} one obtains,

$$T_{1/2}(\mathrm{Pu}^{240})=\frac{(\mathrm{U}^{235})}{\mathrm{U}^{236}}\times\frac{(\mathrm{Pu}^{240})}{\mathrm{Pu}^{239}}\times T_{1/2}(\mathrm{Pu}^{239})$$

The half-life is thus determined in terms of the isotopic ratio of the plutonium, the isotopic ratio of the daughter uranium, and the known half-life of Pu^{239}.

The plutonium used in this particular experiment was chosen because it contained a relatively large amount of Pu^{240}, and because it had been purified several years earlier with respect to other heavy elements.

The calculation of the half-life involved two experimental errors: (1) The error in the half-life of Pu^{239} which is given by Westrum as ±0.3 percent, [3] and (2) the error in the mass spectrometric measurements of the isotopic ratios which is about ±0.3 percent. It should be pointed out that the usual mass discriminations inherent in the mass spectrometer cancel in the present case. Using the values obtained for the isotopic abundances and Westrum's value for the half-life of Pu^{239} gives a value of 6,580±40 yr for the half-life of Pu^{240}. This value and its limits of error are to be compared with those of 6,240±120 yr [3], 6,850±150 yr [4] and 6,650±150 yr [4] as determined by specific activity measurements.

This illustration points out some of the advantages of the daughter method of half-life determination. It completely eliminates problems of contamination with other radioactive materials, and it is easily applicable in the laboratory to half-lives of up to 10^4 yr.

MacNamara, Collins and Thode [5] have used the converse of the above method to determine the half-life of Xe^{133}. They measured the rate of decrease of the parent element by comparison with other stable xenon isotopes. In this way they obtained a value of $5.270 \pm .002$ days for the half-life of Xe^{133}.

From these two illustrations, it is clear that for long half-lives, that is, greater than a few years, the daughter-growth method gives the most accurate results. For half-lives of up to a few years, the parent decay is the more accurate. The ultimate accuracy obtainable with the parent-decay method is considerably better than the daughter-growth method. This is due to the fact that the latter requires chemical procedures to extract the daughter element.

3. Radioactive Branching Ratios

Among the stable nuclear species now known, there are 62 even-even isobaric pairs which differ in atomic number by two and which are separated by an unstable odd-odd nucleus of intermediate atomic number. According to present theories of beta decay, these intermediate nuclei are unstable with respect to both isobaric transitions $Z \rightarrow Z-1$ and $Z \rightarrow Z+1$. Hence, branching may be expected to take place in the decay schemes of these nuclei to an extent which may or may not be experimentally observable, depending chiefly on the energies available for the alternate modes of decay. Counting techniques have detected branching in only 12 of the 62 possible cases. From the counting standpoint K capture is difficult to detect in the presence of a large amount of β emission. It is probably for this reason that only twelve instances of branching are known.

Exactly as in the case of simple radioactive decay, it is possible to use the mass spectrometer to look at the daughter isotopes instead of using counters.

Hayden, Reynolds and Inghram [6] used the mass spectrometric method to measure branching in the Eu^{152} and Eu^{154}. Reynolds has used the method for branching in the isotopes of Cu^{64}, Br^{80} and I^{128}. The examples I will use for illustration are taken from the work of Reynolds.

Consider the decay of I^{128} (fig. 1).

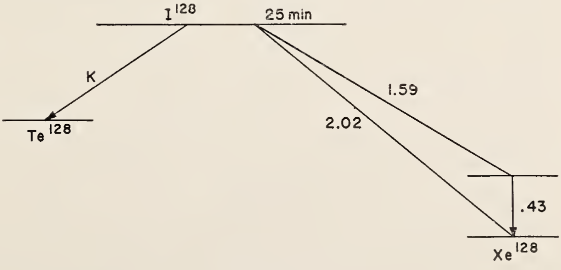

Figure 1.

If Te^{128} grows into a sample as I^{128} decays, K capture occurs. The quantitative yield can be determined by using the method of isotopic dilution. The experimental method Reynolds used was as follows. Gram quantities of reagent grade chemicals, in the above case NaI, were subjected to prolonged neutron irradiation in a graphite moderated pile. After cooling, weighed quantities of the elements of the decay products were added to the solution of the sample in a form isotopically different from the radiogenic material. After isotopic mixing had been assured, the daughter elements were isolated for mass spectrometric analysis. Using this procedure, quantitative recovery is unnecessary, and, if the tracer isotope used has a composition different from that of normal, contamination can be eliminated. The amount of branching is then determined by the isotopic dilution of the original tracer material.

The isotopic composition of the tellurium extracted from the neutron irradiated NaI sample is shown in figure 2. For comparison the spectra of the tracer Te^{130} is shown in the upper part of the figure. The marked increase in the peak at mass 128 is evidence that I^{128} decays to Te^{128}. Further, since the intensity of the Te^{130} peak corresponds to a known mass of Te^{130}, the mass of Te^{128} in the sample is known. Note also that the lack of any change at Te^{126} proves that the sample was not contaminated with normal Te.

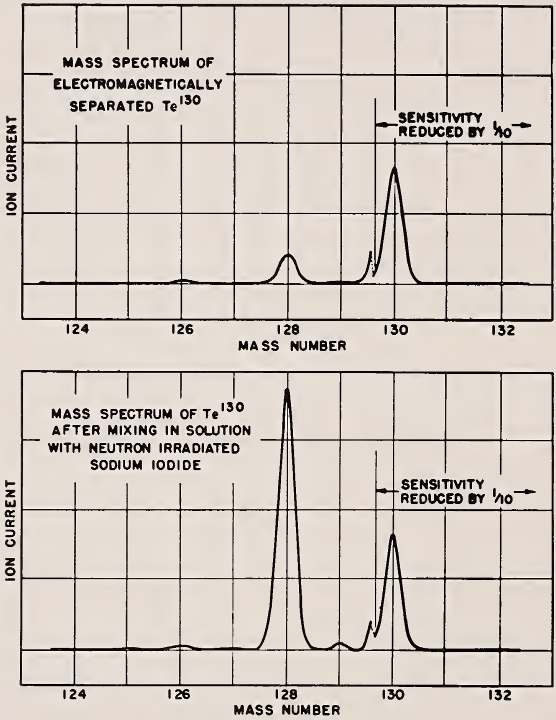

FIGURE 2. *Isotopic dilution of tellurium.*

Figure 3 shows the xenon extracted from the same NaI sample. Again the excess Xe^{128} allows a calculation of the mass of Xe^{128} formed in the original sample. The ratio of these masses is thus the ratio of branching to $Z+1$ and $Z-1$. It should be pointed out that the decay to $Z-1$ had never been detected by counting methods.

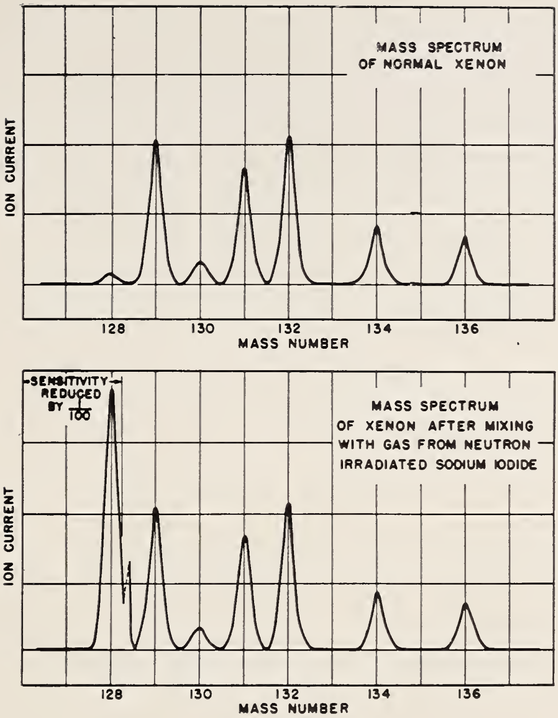

FIGURE 3. *Isotopic dilution of xenon.*

Another case studied by Reynolds is the decay of Cu^{64}. It decays by negatron emission, positron emission and K capture. The level scheme is shown in figure 4.

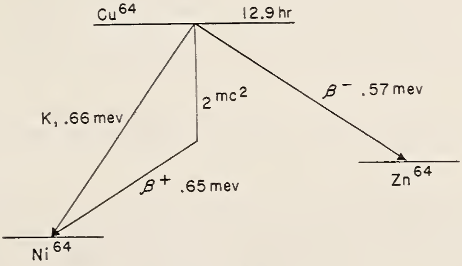

FIGURE 4.

In addition to the above, there is a weak γ ray due to a small amount of decay by K capture to an excited state. This branching is sufficiently small that it can be neglected for the purposes at hand. Both the negatron and positrons have been studied with great care and both serve as excellent examples of simple spectra with allowed distributions.

Two investigators have determined the overall β^-/β^+ ratio by integration of the spectra. Cook and Langer report a value of 2.0

negatrons per positron; Bradt et al., a value of 2.1. The value 2.05 ± 0.10 will be adopted for this quantity in the calculations to follow. This value, together with the ratio 1.62 ± 0.11 of $Z-1$ transitions to $Z+1$ transitions measured mass spectrometrically, determines the branching scheme: (a) by negatron emission, 38.2 ± 1.6 percent; (b) by positron emission, 18.6 ± 1.2 percent; (c) by orbital electron capture, 43.2 ± 2.0 percent (with 0.46 ± 0.06 percent decaying by electron capture to the 1.35-Mev state of Ni^{64} according to Deutsch.)

The K/β^+ ratio is of particular interest since it is independent of nuclear matrix elements and can be calculated from the Fermi theory. Huber, Ruetschi, and Scherrer and Bouchez and Kayas have each calculated this quantity using a formula due to Moeller and the latest value of 0.657 Mev for $E_{\max}$ for Cu^{64} positrons. They find respectively:

$$(K/\beta^+) \underset{\text{Theor.}}{Cu^{64}} = 2.08 \text{ and } 2.35.$$

The new experimental value is:

$$(K/\beta^+) \underset{\text{Exp.}}{Cu^{64}} = 2.32 \pm 0.28$$

and is in agreement with both the calculated values.

Thus from mass spectrometric data we have a test of the theory of beta decay.

4. Double Beta Decay and the Theory of the Neutrino

There are only a few phenomena where the question of the neutrino theory gives a measurable effect. One of these phenomena is the theory of the decay of a nucleus by the simultaneous emission of two beta particles. The so-called Majorana theory predicts a half-life of about 10^{15} yr for isotopes such as Sn^{124} and Te^{130}. The Dirac theory predicts a value of 10^{24} yr for the same isotopes. The group at Chicago has put considerable effort into trying to detect this effect. They give a half-life for the Te^{130} isotope for double beta decay as equal to or greater than 2×10^{21} yr. Dr. Hayden will report on these experiments in more detail in a later paper at this meeting.

5. Fission Yields From Slow Neutron Induced Fission

During the war a mass yield curve from the fission of U^{235} was determined radiochemically. As far as could be told from that data the curve was smooth. Shortly after the war Thode published some mass spectrometric results on the yields of the krypton and xenon isotopes in fission. Somewhat later the Chicago group published the relative abundances of the rare earth isotopes formed in fission. Very recently Dr. Glendenin, Dr. Hess, Dr. Steinberg and the author have made measurements on the isotopes of molybdenum and zirconium formed in fission. The work which I will summarize is all taken from a paper by these authors.

The early results of Thode et al. on Kr and Xe abundances in fission indicated abnormally high yields at masses 133 and 134 and, perhaps, in the region 83–86 as well. One would, of course, expect to find some structure in the yield-mass curve as a result of known delayed neutron effects, but these, at most, are of the order of ~0.5 percent in fission yield and cannot account for the magnitude of Thode's results. Recent radiochemical studies on Te and I fission yields have also indicated a high yield at mass 134 [7].

A proposal to account for the observed anomalies which was made by Glendenin based on the boiling off of an extra neutron from the fission fragments containing 51 or 83 neutrons appeared to be qualitatively successful. This hypothesis, however, predicts a low yield at mass 137 which has been shown not to be the case [8]. The discrepancy between observation and prediction here led Thode to propose a possible preference for an 82 neutron configuration in the fission act in addition to a neutron boil-off effect following fission. It should be noted that an extension of the neutron boil-off hypothesis to fission fragments containing three and five neutrons in excess of a closed shell would account for the observed "normal" yield of mass 137. Fission yield determinations of masses complementary to the mass region 133–137 should establish whether the fine structure observed is the result of a preferential mode of fission or of phenomena following fission.

In the present work some interesting effects have been noted in the isotopic abundances of Mo and Zr produced in the fission of uranium. These data, together with normalized data on fission Xe and Kr (Thode) and Nd (Inghram), are presented in figure 5 where they are compared with the smooth radiochemical fission yield-mass curve.

Since the results obtained from these investigations are relative abundances, the data of one element must be fitted to those of another

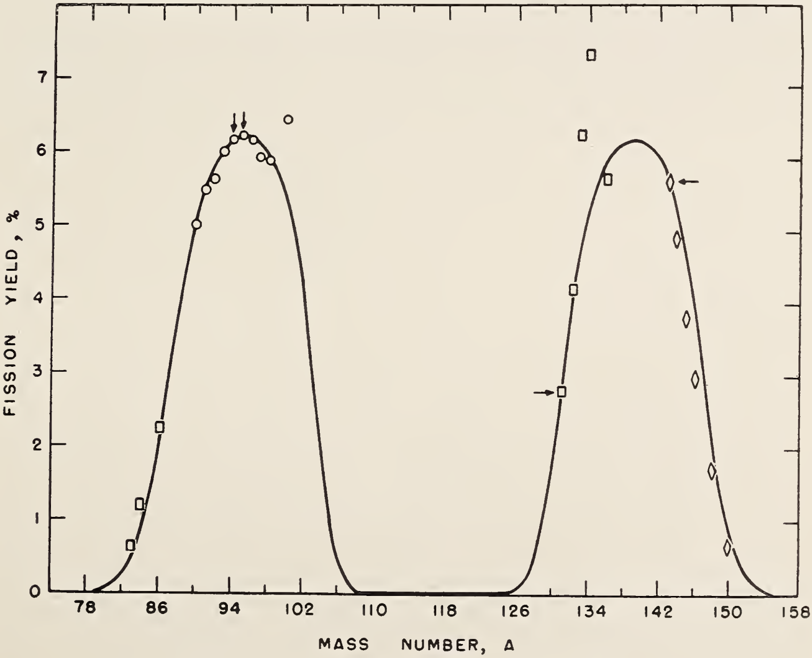

FIGURE 5. *Fission yield from uranium 235.*

—, smooth radiochemical yield-mass curve; ○, present investigation (Zr, Mo); □, Thode et al. (Kr, Xe); ◇, Inghram et al. (Nd); →, indicates points of normalization.

in some, as yet arbitrary, manner. For the present we have normalized the Xe data to the radiochemical yield-mass curve at mass 131(=2.8 percent). Since the ratio of total Xe to Kr was obtained in Thode's work, this also fixes the Kr yields. Likewise, the Nd data were normalized to the radiochemical curve at mass 143(=5.7 percent), Zr was normalized at mass 94=6.20 percent and Mo at 95=6.25 percent. Experiments are in progress to establish absolute abundances of Zr, Mo, and Ru in fission by the method of isotopic dilution and thus obviate some of the difficulties of normalizing the relative abundance data.

It should be noted, however, that whatever normalization is employed, the present data for Mo indicate an abnormally high yield in the mass region 98–100. The anomalies in the mass 133–136 region are also quite evident on this linear plot. The original Kr^{86} and Xe^{136} data have been corrected for known delayed neutron emission. Thus, the data are corrected for the significant changes known to take place after fission. If a value of 2.5 for the number of neutrons per fission is taken for U^{235}, the data may be plotted as in figure 6 with the heavy group reflected over the light group such that the masses of complementary fission products sum to 233.5. In such a "folded" curve the coincidence of the anomalies at masses 98–100 versus 133–136 becomes obvious. Although neutron boil-off effects may be operating in the 133–137 mass region (the region in which 82 neutrons are present), there does not appear to be any reasonable basis for this effect in the region of mass 100. The high yield at Mo^{100} then suggests a preference for this mass in the fission act, perhaps as the complement of a preferred 82 neutron shell in the heavy fragment.

In addition to an enhanced yield due to some preferential mode of fission, delayed neutron and neutron boil-off effects from the fragments after fission could affect the yields in the 133–136 region further.

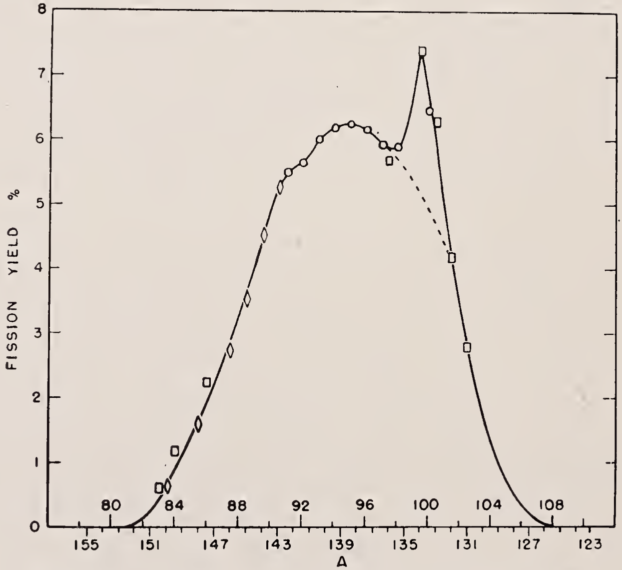

Figure 6. *Folded curve for fission yield of uranium 235.*

○, Zr+Mo; □, Kr+Xe; ◇, Nd.

Evidence supporting the latter effects is provided by the abnormally low yield of Xe^{136} (and of I^{136}) determined radiochemically [9]. However, the existence of a short-lived isomeric state could account for the observed result in the case of I^{136} and perhaps faulty normalization in the case of Xe^{136}.

A treatment of beta-decay systematics by Suess [10] indicates that the observed energies of Zr^{93} and Zr^{95} are much lower than expected. This may be an indication of a shell at 40 protons. Recent mass measurements by Duckworth and Preston [11] also indicate extra stability for a 40 proton configuration. If this is true, the high yields near mass 100 may also be the result of a preference in fission for a 40 proton configuration. In any event, it appears that the only reasonable explanation for the anomalous yield at Mo^{100} is a nuclear structure preference in the fission act.

The data also indicate a dip in the curve at mass 92 which is unexplained at present. Since low binding of closed shell plus 3 and 5 neutrons seems probable from published data on neutron binding energies, [12] boil-off of the 55th neutron (at Rb^{92}) is perhaps prominent here.

6. Discovery and Assignment of Mass to Radioactive Isotopes

The use of mass spectrometers as a small scale isotope separator has aided a great deal in the assignment of mass number to known radioactive isotopes. In addition, a number of new radio isotopes have been discovered by this method. The first use of this method was that of Smythe, Rumbaugh and West [13] in their determinations of which of the isotopes of potassium and rubidium were responsible for the naturally occurring radioactivities. It has since been used extensively among others by the groups in Chicago, Berkeley and Copenhagen, Denmark. I will use the work of Lewis and Hayden [14] in Chicago to illustrate the method.

The small scale isotope separator used by these investigators is shown in figure 7. In this unit, ions of the activated element are formed in the source by surface ionization or electron bombardment, accelerated through a potential of 8,000 v and resolved with a conventional direction focusing 60° analyzer. The resolved ion beams are collected on a photographic plate. Two methods are available for locating the position of the activity on the plate. These methods are illustrated in figure 8. The first involves placing the plate under a counter, and defining the portion of the plate which can see the counter by a heavy lead slit. In this way a plot of the activity as a function of position can be made. By developing the plate to locate the normal isotopic spectrum, the location of the activity is correlated with mass number. In the second method of analysis shown in the lower part of this figure, a second photographic plate is placed face to face with the original plate containing the activities. Thus the radioactive decay particles emitted by the radioactive deposit give developable images on the transfer plate. Upon development, comparison of the two plates gives the location of the activities. For short-lived activities the counter method is to be preferred; for half-lives of greater than one to two hours, the transfer technique is preferred. The transition between the two methods does not occur at the point where theoretically it should, i.e., 10^5 decay particles give a line and

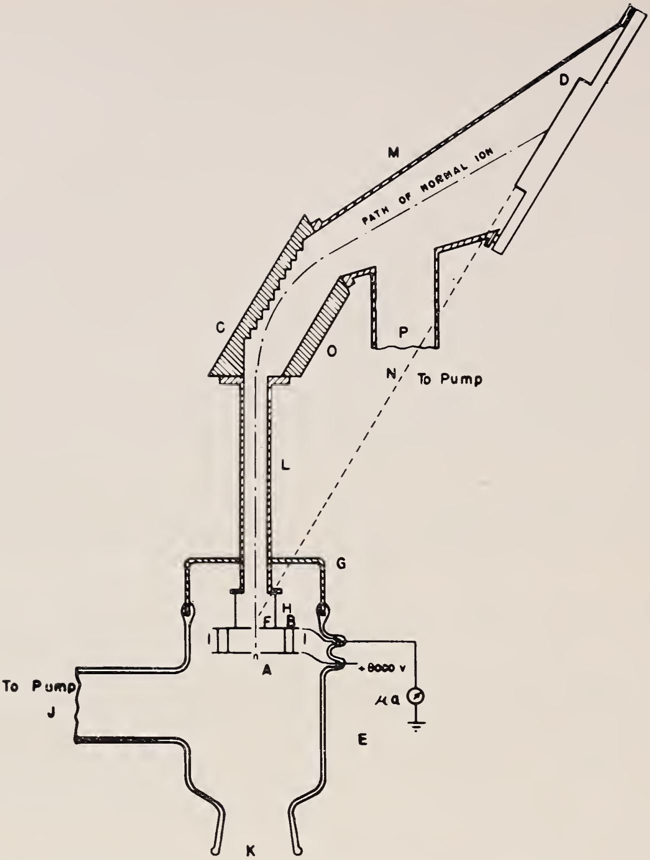

Figure 7. *Small-scale isotope separator at Chicago.*

A. Filament.
B. Grounded disc.
C. Pole pieces.
D. Photographic plate.
E. Glass tube.
F. Ion beam defining slit.
G. Kovar cup.
H. Glass spacer.
I Glass spacers.
J. Pumping lead, filament region.
K. Ground glass joint.
L. 1-inch copper tube.
M. Trapezoidal brass box.
N. Center of curvature for normal ion.
O. Brass pole spacers.
P. Pumping lead, plate region.

5 disintegrations per minute can be detected counterwise. This results from practical considerations of the rate at which the plate can be scanned.

For half-lives of less than ten minutes, neither of the above methods is satisfactory and recourse to a third technique is necessary. In this technique the isotopes are separated before activation and one simply activates the separated isotopes. This technique has grown to rather mammoth proportions in the gross separation of isotopes by the calutrons at Oak Ridge.

The usefulness of these techniques is illustrated by table 1, which tabulates a number of results which have been obtained with the micro-separation technique. This list is by no means complete since a complete list would require a number of slides for presentation. This data serves as a backlog for a number of other experiments.

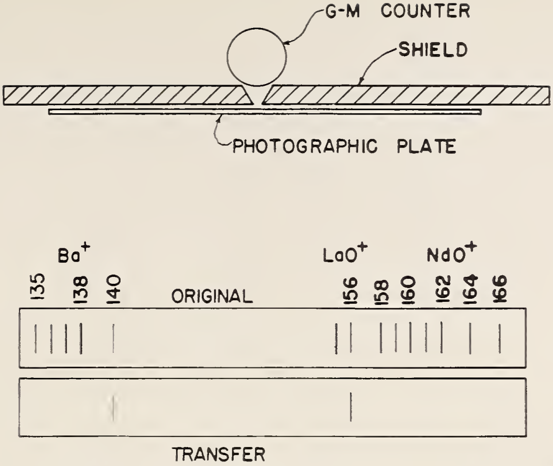

FIGURE 8. *Detection of radio isotopes deposited on a photographic plate.*

For example, several of the fission yields were uncertain until assignments of mass had been made by the mass spectroscopic method.

TABLE 1. *Mass determinations of radioactive isotopes.*

Half-life	Isotope	Mass	Previous certainty of assignment (Seaborg)
55 d	Sr	89	A
30 y	Sr	90	B
105 d	Y	88	B
57 d	Y	91	B
10^6 y	Tc	99	------------
1 y	Ru	106	D
13 h	Pd	109	C
33 y	Cs	137	------------
12.8 d	Ba	140	A
40 h	La	140	A
28 d	Ce	141	A
275 d	Ce	144	D
13.8 d	Pr	143	B
17 m	Pr	144	D
3.7 y	61	147	------------
5.3 d	61	148	------------
55 h	61	149	------------
>72 d	Sm	145	------------
~20 y	Sm	151	------------
~46 h	Sm	153	D
9.2 h	Eu	152	B
long	Eu	152	------------
long	Eu	154	B
2 to 3 y	Eu	155	------------
15.4 d	Eu	156	------------
>72 d	Gd	153	F
72 d	Tb	160	A
27.5 h	Ho	166	B
102 h	Yb	175	C
6.6 h	Lu	177	C
2.3 h	Re	186	B
18 h	Re	188	B
60 d	Ir	192	C
19 h	Ir	194	C
1.25 m	Dy	165	F

Table 1. *Mass determinations of radioactive isotopes*—Continued

Half-life	Isotope	Mass	Previous certainty of assignment (Seaborg)
2.6 h	Dy	165	D
2.5×10^6 y	Be	10	A
2.6 h	Ni	65	C
10 y	Kr	85	------------
40 s	Ag	107	C
40 s	Ag	109	C
6.7 h	Cd	107	C
158 d	Cd	109	C

7. Nuclear Cross Sections

A number of slow-neutron cross sections have been determined mass spectrometrically. The first technique to suggest itself is that of preparing separated isotopes and measuring the cross section of the pure isotope. This procedure in general requires large amounts of separated isotopes and hence large apparatus. Dempster was the first to use the change in isotopic abundance as a measure of cross sections. His first work was done using the elements Sm and Gd, each of which has very large slow-neutron cross sections. By irradiating samples of these elements in a pile, he was able to show from the change in isotopic abundances that the large slow-neutron cross section of samarium is due to the isotope Sm^{149} and the large slow-neutron cross section of gadolinium is due to the combined cross sections of Gd^{155} and Gd^{157}. Since his original work, measurements have been made on 10 elements by the Chicago group and several other elements by the McMaster group.

For illustration of the technique figure 9 shows the change in the isotopic composition of mercury due to neutron irradiation. The left-hand spectra shows the abundances obtained for normal mercury, and the right-hand that of neutron irradiated mercury. In both cases, the mercury was obtained by heating mercury sulfide near the ion source. The large change in the isotopes at 196 and 199 is immediately apparent. The loss from 199 appears at the 200 position. The loss at 196 goes to a short-lived mercury activity at 197 and decays to gold. For this reason the loss at 196 does not appear at 197.

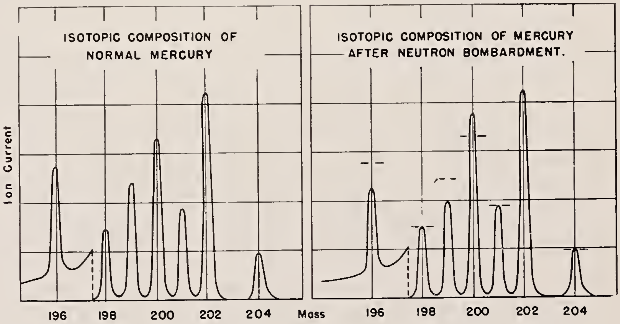

Figure 9. *Change in isotopic composition of mercury from neutron irradiation.*

Table 2 shows the calculated results. The largest cross section in mercury is clearly Hg^{196}. However, in normal mercury, due to the small abundance of this isotope, it contributes only 1 percent to the total cross section.

TABLE 2.

Mass number	Abundance normal	Abundance bombarded	Net Change	Isotopic cross sections in 10^{-24} cm^2	Contribution to total section in 10^{-24} cm^2
	Percent	*Percent*			
196	0.155	0.120	-0.035 ± 0.002	3100	4.8
197	<0.001	<0.001	------------	--------	--------
198	10.12	10.17	$+0.05 \pm 0.05$	--------	--------
199	17.01	13.78	-3.23 ± 0.07	2500	425
200	23.21	26.52	$+3.31 \pm 0.03$	<60	<15
201	13.15	13.11	-0.04 ± 0.07	<60	<8
202	29.66	29.63	-0.03 ± 0.15	<60	<18
203	<0.001	trace	+trace	--------	--------
204	6.69	6.68	-0.01 ± 0.03	<60	<4
205	<0.001	<0.001	-----------	--------	--------

In addition to work on slow-neutron cross sections, a number of other nuclear cross sections can be measured. For example, a quite practical bombardment by high-energy protons can produce of the order of 10^{-11} g of spallation products. Thus since the mass spectrometric sensitivity for a number of elements is 10 to 1,000 times greater than this, it is quite feasible to measure the spallation excitation functions by measuring isotopic abundances of the spallation products.

8. The Internal Conversion Process

An isotope which decays by K capture always emits a gamma ray. This gamma ray can be internally converted emitting one or more electrons. Theoretical calculations can be made as to the resultant charge on the atom after the conversion process has taken place. In some cases resultant charges as high as plus six are expected in appreciable yield. No good experimental evidence, however, has been obtained to check these calculations. It is, however, feasible to use a mass spectrometer to measure the distribution of charge from this process. The usual procedure is to introduce a highly activated gas into the usual electron bombardment source. Operating the source with the ion beam on permits setting the spectrometer to the particular charge in question. Turning the electron beam off removes all ionization from the source except that due to radioactivity; hence the charge distribution can be measured. Experiments of this type can be performed only with electron multiplier detection. Only very crude results have so far been obtained in this experiment. However, it shows promise, and the results will be immediately applicable to problems of radiochemistry, that is, what happens to an atom chemically when it undergoes a nuclear process.

9. Conclusions

These illustrations point out only a few of the many applications in which the mass spectrometer can aid in the understanding of nuclear processes. It is apparent that the use of the machine as a tool for general nuclear research is a very large field and will be worthy of a great deal of effort.

10. References

[1] A. O. Nier, Phys. Rev. **55,** 153 (1939).
[2] M. G. Inghram, D. C. Hess, G. Pyle, and P. Fields, Phys. Rev. **83,** 1250 (1951).
[3] E. F. Westrum, Phys. Rev. **83,** 1249 (1951).
[4] S. G. Thomson, K. Street, A. Ghiorso, and F. L. Reynolds, Phys. Rev. **84,** 165 (1951).
[5] J. Macnamara, C. B. Collins, and H. G. Thode, Phys. Rev. **78,** 129 (1949).
[6] J. H. Reynolds, Phys. Rev. **79,** 789 (1950).
[7] A. C. Pappas and C. D. Coryell, private communication; L. Yaffe, private communication.
[8] L. E. Glendenin, Phys. Rev. **75,** 337 (1949).
[9] C. W. Stanley and S. Katcoff, J. Chem. Phys. 653 (1949).
[10] H. E. Suess, private communication.
[11] H. E. Duckworth and R. S. Preston, Phys. Rev. **82,** 468 (1951).
[12] K. Way, Phys. Rev. **75,** 1448 (1949).
[13] W. Smyth, H. Rumbaugh, and S. S. West, Phys. Rev. **45, 724** (1934).
[14] R. J. Hayden, Phys. Rev. **74,** 650 (1948).

11. Discussion

W. E. Stephens: I will call for discussion on this paper.

H. G. Thode: I am very much interested in your high fission yield result for molybdenum 100. This would seem to be the mirror image of mass 134 in the heavy group which has a very high fission yield. Undoubtedly this "fine structure" in the mass fission yield curve is related to closed shell effects in atomic nuclei. The mass chains involved all have members with 82 neutrons and there are two possible effects. First, a nuclide with 82 neutrons might be favored in primary fission, as Dr. Inghram has suggested; secondly, nuclides with 83 neutrons, one more than a closed shell, might have sufficient energy as primary fission products to boil out one neutron. In this way one mass chain would have a low yield and the adjacent chain a high yield. (This later process is known to happen for Xe^{137} and Kr^{87}.)

I note that Dr. Inghram did not suggest that asymmetric fission is due to the stability of closed nuclear shells. However, it is curious that all the fission fragments cluster around the numbers 50 and 82.

Recently we investigated the fission yields of products involved in the fast fission of U^{238}. It was found that the fine structure in the mass yield curve is shifted 1 to 2 mass units toward the lighter masses as compared to U^{235} fission.

H. C. Urey: Dr. Inghram, you folded these back on each other on the assumption that there are two and one-half neutrons. Of course there aren't two and one-half. There may be two or three or four. Would some of the irregularities disappear if you tried folding it at some other position?

M. G. Inghram: No, it would shift Professor Thode's values only very slightly in comparison with ours. Even if there were five neutrons emitted, the two peaks would still coincide within the experimental error.

Urey: I was thinking about where you had an irregularity you didn't know how to explain. Part were produced from a nucleus with one number and part from a nucleus that had a different number. Then the irregularity might be accounted for. That is all I was thinking.

Chairman Stephens: I would like to ask, do you have any estimate of the sensitivity with which you could detect carbon 14, and does this compare with the radioactivity method?

Inghram: No, it does not compare with the radioactivity method. Carbon 14 is relatively difficult.

22. Electromagnetic Separation of Noble Gas Isotopes and Their Use in Some Nuclear and Spectroscopic Experiments

By Jørgen Koch [1]

1. Introduction

At the end of the thirties, when accelerators for carrying out nuclear disintegration experiments became available at the Institute for Theoretical Physics in Copenhagen, the demand for using pure isotopic samples soon arose. Among the known methods of isotope separation some sort of mass spectroscopic techniques seemed to be most promising for our purposes. Several methods of ion beam analysis were in principle considered possible. Special attention was paid to the possibility of using either the difference in time of flight of monoenergetic ion bunches or the dispersion resulting from the passage of a monoenergetic ion beam through a magnetic field. Finally the last method, the electromagnetic method, was chosen, since it seemed to show most promise for separating the isotopes of any element at a reasonable rate of separation.

In the years 1940–1942 preliminary experiments [1][2] were carried out especially with the purpose of finding a suitable source for the production of atomic ions and of developing a lens system for the formation of an ion beam. The application of high acceleration voltages was aimed at in order to reduce the effects of space charges and to decrease the angular spread among the ions. In the years which followed, a larger isotope separator [2] was developed, having a resolving power appropriate for separating isotopes even of heavy elements. Since that time only a few constructional changes have been made and the apparatus has been in almost continuous operation in connection with research carried out at the Institute.

In what follows I should like to give a brief report on the construction of the isotope separator at its present stage of development and in addition a survey of experiments, carried out with the separated isotopes, especially isotopes of the noble gases. In this survey I have also incorporated the work which was carried out by other members of the scientific staff of the Institute, as is cited below in the text (references are given at the end of the paper). Instead of going too much into detail concerning the physical results obtained in the course of this work, I believe it to be in harmony with the purpose of this conference to present especially such features of the experiments which throw light on the performance of the isotope separator, the techniques of ion collection, and the manifold possibilities of using the isotopic samples.

---

[1] Institute for Theoretical Physics, University of Copenhagen, Denmark.

[2] Figures in brackets indicate the literature references on p. 178.

2. Construction and Operation of the Electromagnetic Isotope Separator

A general view of the isotope separator is shown in figure 1. At the present time the apparatus is being removed from its old site to a new laboratory and at the same time a few improvements in the construction[3] are being made according to figure 2. As is seen, the ion source and associated equipment are enclosed in a large corona screen and mounted on a heavy glass plate, insulating these parts of the apparatus, which are kept at the accelerating voltage of 60–80 kv. The ion source is a low voltage arc of the capillary type developed for

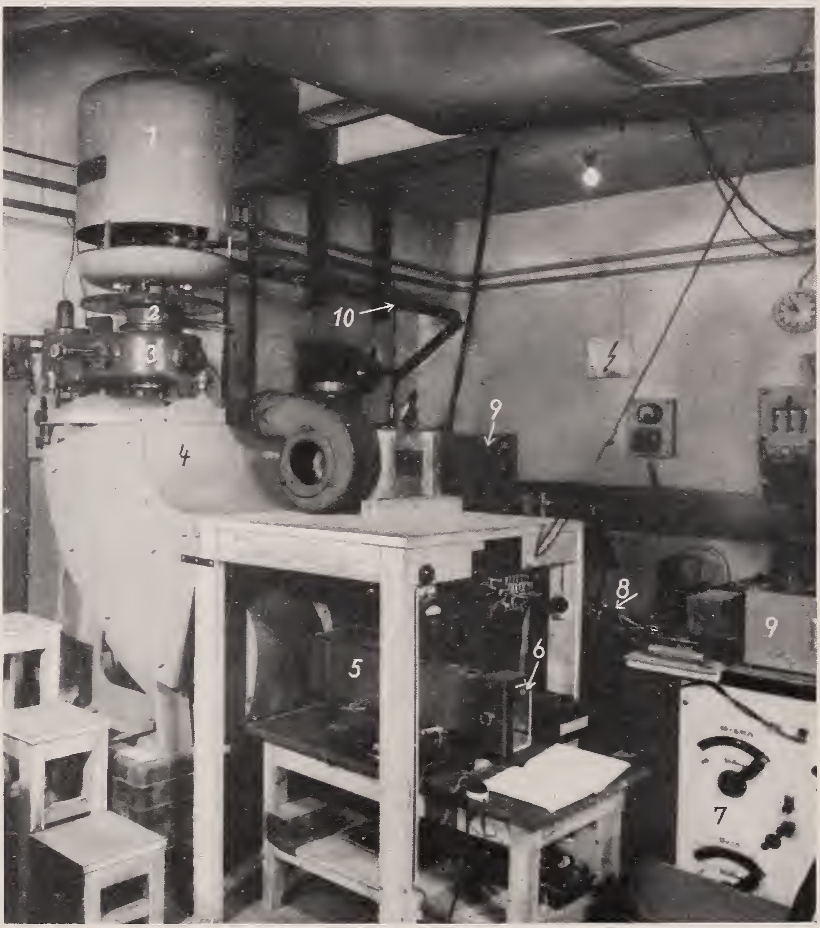

FIGURE 1. *Isotope separator at the Institute for Theoretical Physics, Copenhagen*

1, Corona screen with ion source, gas containers, etc.; 2, electrostatic lens system; 3, chamber carrying diffusion pumps; 4, magnet; 5, analyzing chamber; 6, fluorescent screen and collector arrangement; 7, regulation of magnetic field; 8, regulation of acceleration voltage; 9, compensator; 10, power supply for ion source. Power stack and high voltage plant are placed in the adjacent room.

---

[3] This work is being carried out together with K. O. Nielsen, C. E., who is presently in charge of the reconstruction of the isotope separator.

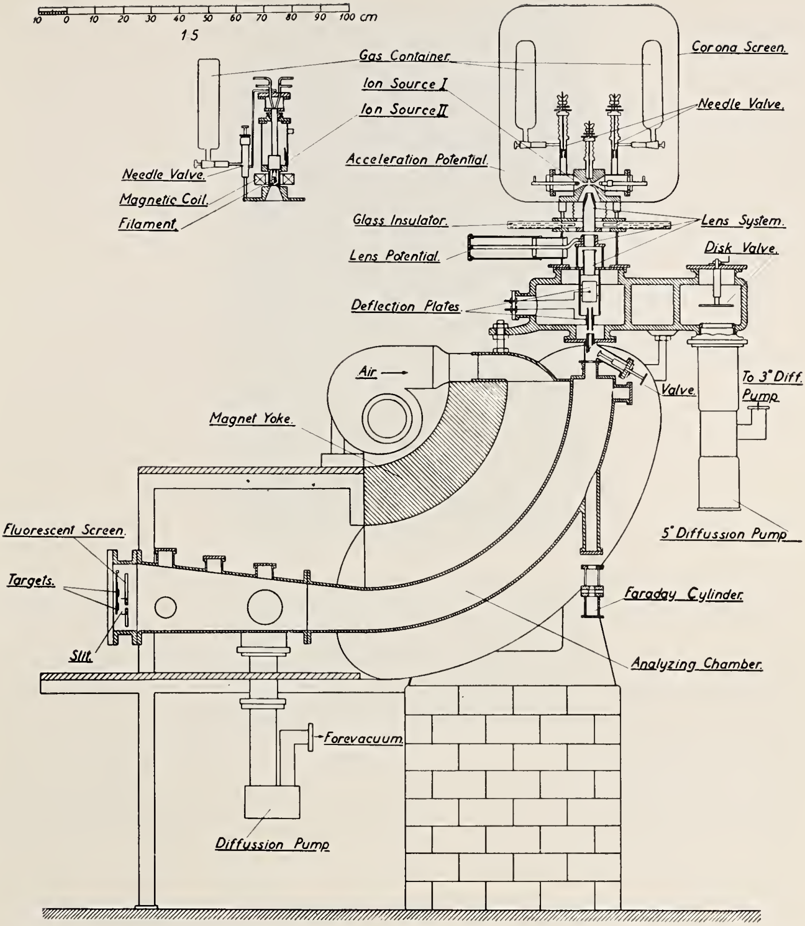

Figure 2. *Constructional details of isotope separator.*

Ion source I is the low voltage capillary arc described in the text. Ion source II works with a vertical electron beam collimated by a magnetic field (footnote 7). The undeflected ion beam may be observed and measured in the tube mounted below the electrostatic lens. For the change of collectors, the valve at the entrance to the analyzing chamber can be closed.

the production of hydrogen ions at the Massachusetts Institute of Technology [3]. When running the source with noble gases the pressure lies between 2×10^{-3} and 6×10^{-3} mm Hg and the arc current varies from 0.2 to 0.8 amp. The ions of the plasma are emitted through the small aperture in the wall of the capillary and are accelerated in the space between the ion source and the grounded cylindrical electrode below. The slightly divergent beam is focused by means of a unipotential lens, operating with a decelerating voltage of about two-thirds of the acceleration voltage. The shape of the beam is shown in figure 3, which is a photograph of the faint light being emitted when the beam traverses the main chamber having a pressure of a few 10^{-5} mm Hg. The beam current may be raised to several hundred microamperes.

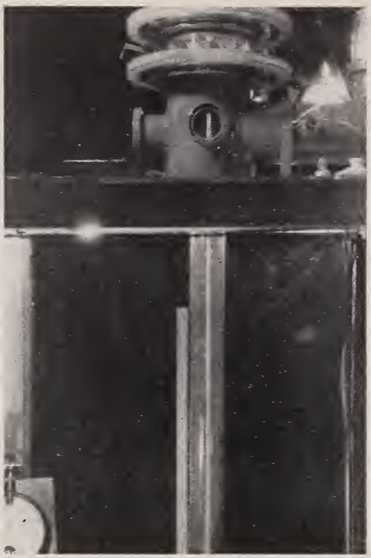

FIGURE 3. *Ion beam passing a field-free space.*

The lens system (not the same as in fig. 2) is mounted on top of the apparatus. The beam is first seen in a glass window and later in a long glass tube. Distance from lens to collector at the bottom about 110 cm.

For magnetic analysis the almost parallel beam is deflected by 90 degrees in a homogeneous, wedge-shaped field, having a mean radius of curvature of 80 cm (width of pole pieces 15 cm, spacing 6 cm). A magnetic field strength of about 8,000 gauss can be maintained for the deflection of heavy ions at the energies in question. A fluorescent screen for visual observation of the mass spectra and equipment for the collection of isotopes are mounted at a distance of 80 cm from the edge of the pole pieces where maximum resolving power is obtained.[4] For accurate current measurements deep Faraday cups are used in order to prevent the escape of secondary electrons. For the collection of isotopes such precautions are in general not necessary and a plane metal collector is used, mounted behind a slit to avoid isotopic contamination.

A general impression of the resolving power of the isotope separator may be obtained from figure 4, showing photographs of some mass spectra as they appear on a fluorescent screen (glass covered with ZnS). The black stripes across the pictures originate from molybdenum wires stretched over the surface in order to prevent the accumulation of electric charges, which would give rise to disturbing flickering effects. In the photographs only the most abundant isotopes appear, but if a very thin coat of fluorescent material is used even faint isotopes may be visually observed. If the vacuum is good (about 10^{-5} mm Hg) the edges of the beams are quite sharply defined, which easily may be checked by using a pure (uncovered) glass plate as a fluorescent screen. The line breadth is mainly governed by the angular spread of the ions before entering the analyzing field. Since the angular spread in turn is dependent on the initial

---

[4] It was expected that the focus would lie at the edge of the pole pieces, and it is not fully explained why this is not the case. The effect was, however, welcome, since the resolving power was hereby strongly increased.

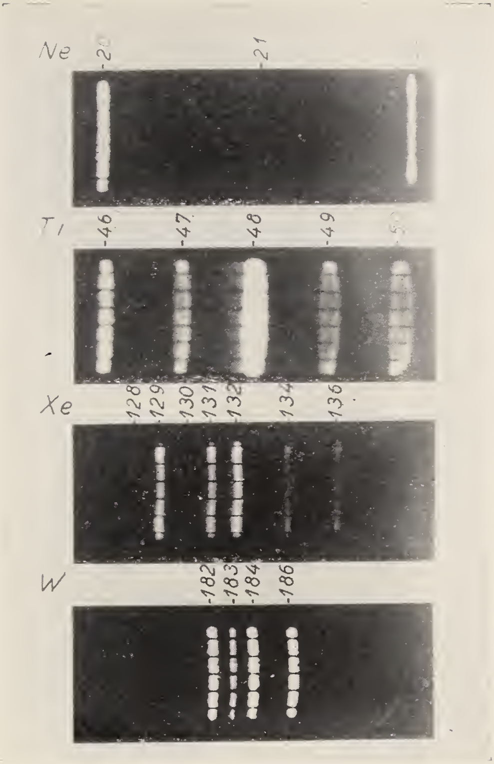

FIGURE 4. *Mass spectra of neon, titanium, xenon, and wolfram.*

Atomic ions of Ti and W were obtained by running the arc with TiCl$_4$ or WF$_6$, respectively. The addition of a noble gas generally helped to stabilize the arc. Ions of metals may also be produced by means of an externally heated oven, mounted in the source. (Scale 1/2.)

ion energy, this quantity may be calculated from the exposures. The initial energy of ions from this source turns out to be only a few tenths of one electron volt.

In the preparation of isotopic samples for nuclear research it may be of importance to have the isotopes uniformly distributed over an area which is larger than the breadth of lines of figure 4. This may be accomplished in different ways. If the distance between two neighboring lines is large enough, the isotopic beams may either be defocused by varrying the lens potential, or they may be electrically swept over the collector surface by putting an alternating voltage on the lower pair of deflection plates, which is inserted just below the lens system as shown in figure 2. If the lines lie close together, the collector may be moved mechanically behind the slit, which limits the ion beam.

During the time of collection of isotopic samples a very steady operation of the apparatus is, of course, important. A constant magnetic field is obtained by running the magnet from a large bank of storage batteries. Since a variation of the high voltage of 1 part in 10^4 will give rise to a displacement of the spectrum of about 0.1 mm special equipment is necessary to meet the demand for constancy. Although some sort of voltage stabilization might be adequate, a device for compensating the effect of voltage fluctuations was worked out [4], which is shown schematically in figure 5. Before entering the magnetic field the ion beam passes through a pair of deflection plates (lower pair of fig. 2). One of the plates is grounded, while the other plate is supplied with a potential E, which is proportional to the fluctations from the average accelerating voltage V. If V increases by ΔV the ion beam will be slightly deflected from its original direction and enter the magnetic field at a. From here the ions continue on a circular path with a radius of curvature, which is somewhat larger than ρ belonging to the central beam. At a' the ions continue tangentially to the point of focus F. A general discussion of this type of focusing is given elsewhere [5].

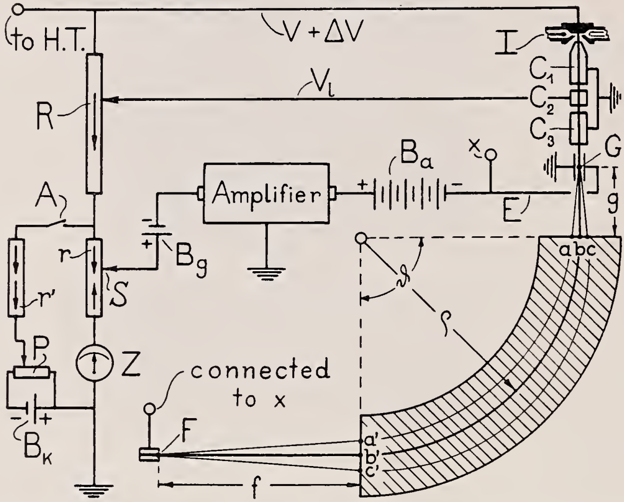

FIGURE 5. *Schematic diagram of device for the compensation of fluctuations of the accelerating voltage.*

Despite the precautions mentioned above, it may happen by some irregularity (e. g., sparking across the insulator) that the mass spectrum is displaced, which may seriously affect the purity of the collected sample. In order to avoid such isotopic contamination, another pair of deflection plates is inserted (upper pair of fig. 2), with the following purpose: As soon as the ion current reaching the collector differs slightly from its maximum value, the beam will automatically be swept sideways (in the longitudinal direction of the lines) onto a fluorescent screen for visual observation by applying a potential on the deflection plates. When readjustment of the apparatus is achieved, the beams will again sweep backward onto the collector. A mechanical shutter is also inserted in front of the slit as a further safety precaution.

3. Experiments With Separated Stable Isotopes

It was feared that the well-known difficulties arising in the electromagnetic preparation of isotopic samples, due to the sputtering action of the impinging ions, might be seriously increased by using the high energies of the present experiments. On the other hand, it was known from the theory of N. Bohr [6] on the penetration of atomic particles through matter, that ions of medium mass and of the energies in question would penetrate a metal surface, as for instance silver, to a depth of about one hundred atomic diameters. It appeared to be possible to load a collector surface with the impinging particles, provided they would not diffuse too rapidly to the surface and escape from there.

In the first experiment to test this point a silver surface was exposed to a beam of fluorine. This element was chosen since its chemical affinity to silver is large and since very small amounts might be identified by studying the radiative proton capture process with the electrostatic generator of the Institute. The result of such an experiment was that the well-known resonances of the $^{19}\mathrm{F}(p,\gamma)^{20}\mathrm{Ne}$ reaction could easily be recognized indicating a considerable concentration of fluorine in the silver surface.

Encouraged by this result an attempt was made to collect the isotopes of neon (^{20}Ne, 90%. ^{21}Ne, 0.3%. ^{22}Ne, 9.7%)[5] and the prepared samples were subsequently bombarded with protons [7]. The results for the $^{22}\mathrm{Ne}(p,\gamma)^{23}\mathrm{Na}$ reaction are shown in figure 6. In the energy interval from 0.5 to 1.5 Mev about twenty resonances were found. The sharpness of the resonance peaks was limited by the fluctuations of the acceleration voltage (±5kv), since the stopping power of the silver layer, in which the neon atoms were collected, was very small. In a similar experiment with ^{20}Ne only one resonance was found between 0.5 and 1.3 Mev. The 23 sec β-activity of the

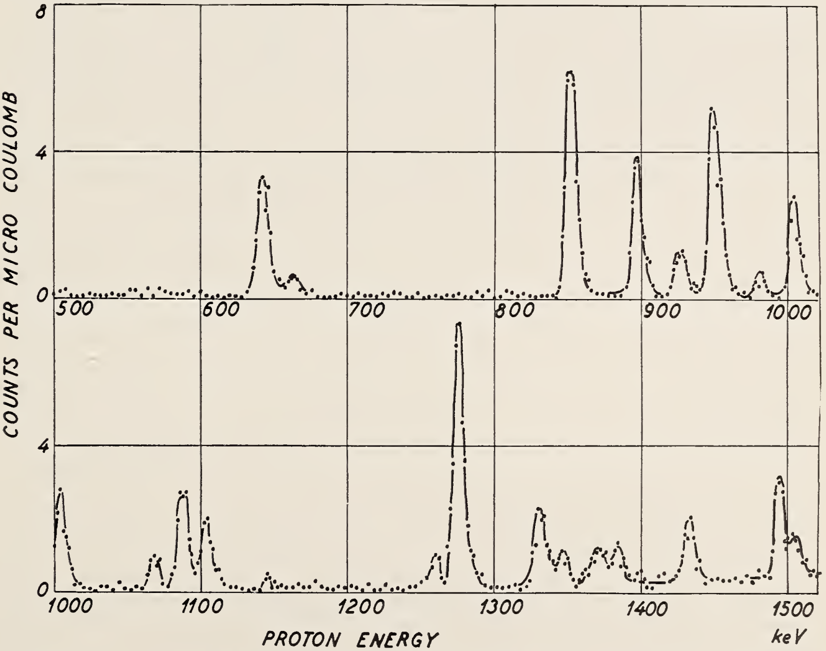

FIGURE 6. *Gamma-ray intensity from ^{22}Ne bombarded with protons of energies between 0.5 and 1.5 Mev.*

---

[5] The abundances given in this article are only approximate values for general orientation.

produced ^{21}Na isotope could be detected. By using ^{21}Ne targets several resonances were found in accordance with the general expectation that the ^{21}Ne spectrum would resemble that of ^{22}Ne rather than that of ^{20}Ne.

The silver targets used in these experiments were bombarded with about 6×10^{16} ions per cm^2 which corresponds to the collection of 2 micrograms of neon per cm^2 if all the atoms remain in the surface. In the preparation of ^{22}Ne targets the ion current density was 5 to 20 μa/cm^2 and the time of collection accordingly 40 to 10 min. Measurements of the height of a certain (p,γ)-resonance with targets, which were bombarded by different numbers of ions, showed that the concentration of neon in the silver surface gradually approached a maximum value, characterized by the data given above. Considering the line breadth of the (p,γ)-resonances one may estimate that the relative concentration of neon to silver atoms in the surface of such "saturated" targets is at least 1 to 10, but probably considerably higher. It is believed that the effect of saturation is mainly due to the influence of sputtering of the collector surface.[6] It was shown that noble gas targets may be stored for months without losing a noticeable fraction of the atoms imbedded in the surface. However, when exposed to proton bombardment the neon content gradually decreased. Appropriate corrections for this decrease were made by referring all measurements to a certain resonance, which was frequently checked.

Neon targets, which were prepared as described, also proved useful for examining the Ne(d,p)Ne reactions by means of an electrostatic generator using nuclear emulsion plate techniques for measuring the range of the emitted protons [8]. For the abundant isotopes ^{20}Ne and ^{22}Ne a convenient number of tracks was obtained by bombarding with 1–2 millicoulomb of 1.5 Mev deuterons (7.5 millicoulomb for ^{21}Ne). From analysis of the histogram of figure 7, new Q-values were found for the processes concerned. Finally I want to mention that the emission of γ-rays from proton-bombarded argon isotopes (^{40}A and ^{36}A) has been investigated [9]. Using only a few targets containing ^{40}A (99.6%) five resonances were found in the energy interval 0.5 to 1.8 Mev. The above-mentioned saturation effect was also found in this case. The experiment with ^{36}A (0.3%) showed no resonances.

Due to the great interest in carrying out optical hyperfine structure measurements with pure isotopes of the noble gases, experiments were set up in order to prepare the quantities required [10]. Targets of silver 6 by 2.5 cm in size, were first strongly degased in vacuo by high-frequency induction. After a target was mounted in the isotope separator, its surface was exposed, a portion at a time, to a heavy bombardment of $^{20}Ne^{+}$-ions so that saturation with neon atoms in the entire surface was ensured. Subsequently the target was removed from the apparatus and installed as an electrode in a discharge tube (fig. 8). After being evacuated and degased the tube was sealed off. Sometimes He gas was admitted at a pressure of 5–10 mm Hg in order to obtain the most favorable conditions for exciting the small amounts of neon. The neon-bombarded electrode was now heated by high-frequency induction to a dull red glow, at which temperature the neon atoms (and also some remaining impurities, mainly CO_2 and H_2O)

---

[6] The degree of saturation may be followed by observing the emission of secondary electrons, which decreases during the time of collection approaching a constant value. This effect may partly be due to the removal of absorbed gas on the collector surface as well as the accumulation of atoms in the outer surface yaer.

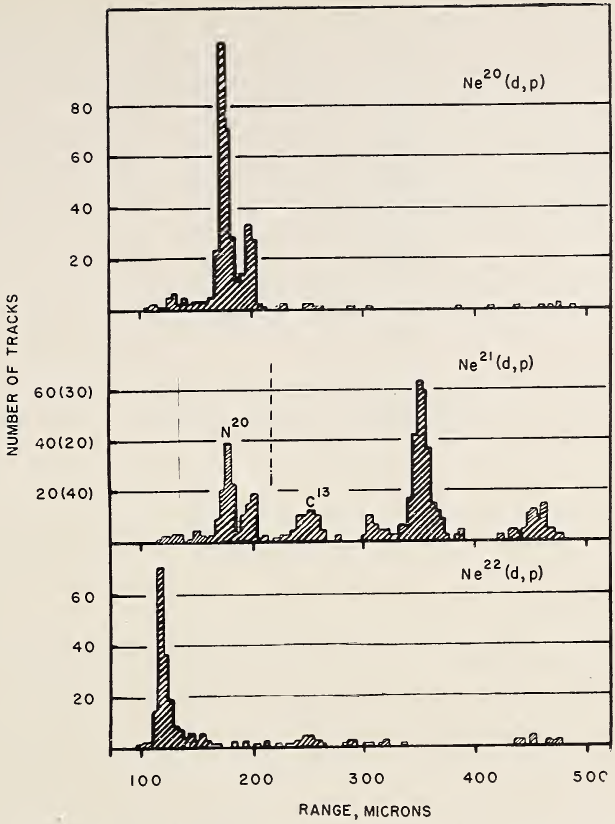

FIGURE 7. *Distribution of track lengths in the photographic emulsion after bombardment of the different neon isotopes by 1.5 Mev deuterons.*

were rapidly released. After running for a short time the discharge tube, which was dipped in liquid air, a pure neon spectrum was observed, and, of course, the helium spectrum was also observed if this gas was present. Similar experiments were carried out with neon-bombarded targets of Al, Ni and W. No marked difference in the ability of collecting the ions was found. The noble gases He, A, Kr and Xe could also effectively be collected in the different metals. Aluminum was, however, generally preferred as collector since this metal, when subsequently used as an electrode in a discharge tube, suffers only slight sputtering, which would tend to clean up the gas. If it were desired to prepare large isotopic samples it may be advisable to study in more detail the influence of the collector material and the ion energy on the ability of retaining the impinging ions, in order to increase the yield. Also the temperature of the collector during the time of separation may play an important role.

The technique described above was used in an investigation of the hyperfine structure and nuclear spin of ^{83}Kr and ^{21}Ne [11]. With a tube containing about 2 microgram atomic weight of ^{83}Kr (11%)—collected in a four hours run—interferograms were photographed with a Fabry-Perot etalon, showing the structures of the 1*s*–2*p* com-

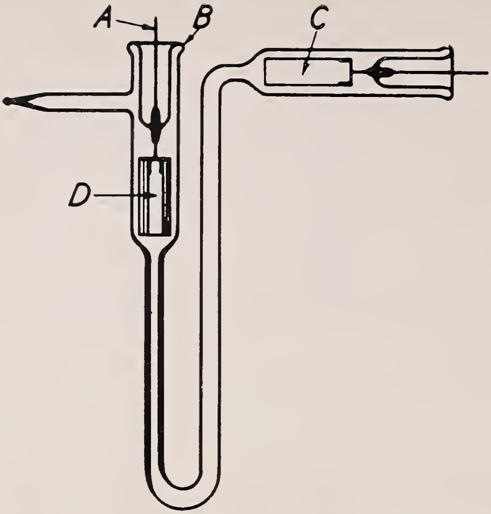

FIGURE 8. *Discharge tube for spectroscopic investigation of isotopic samples of the noble gases (scale 1/2).*

The bombarded electrode D is mounted on the tungsten wire A and the tube is fused together at B. C, ordinary Al electrode.

binations in the infrared. From measurements of the components of the line 8059 A the spin value $\frac{9}{2}$ was found by means of the Landé interval rule. Furthermore by comparing interferograms taken alternately on the same plate with ^{82}Kr (11%), and ^{84}Kr (57%) an isotope shift was detected which is due to the mass dependence of the Rydberg constant. Since the isotope shift was smaller than the natural line breadth, these measurements strongly emphasized the importance of working with isotopic samples of highest purity. For isotopes which differ by only one mass unit the greatest difficulty arises from the formation of hydrides. In the present experiments the ratio KrH/Kr for a given isotope was about one per cent. In the experiment with ^{21}Ne (0.3%) the hydride formation was especially disturbing due to the high abundance of ^{20}Ne (90%). Most favorable conditions were obtained by running the ion source for cleaning for some hours before starting the separation. In the finest sample the amount of ^{20}Ne was nearly the same as that of ^{21}Ne. With a tube containing about 0.2 microgram atomic weight of ^{21}Ne, collected in a ten-hour run, it was found that the magnetic moment of this isotope is negative and the spin $\frac{3}{2}$ or possibly greater.

For the interferometric investigation of xenon [12] six tubes were prepared containing the following isotopes in high purity (>99%): ^{129}Xe (26%), ^{130}Xe (4%), ^{131}Xe (21%), ^{132}Xe (27%), ^{134}Xe (10%), and ^{136}Xe (8.95%). Interferometric exposures of one of the even isotopes (132) and of the two odd isotopes (129, 131) are presented in figure 9. From these experiments not only the spin values for ^{129}Xe ($\frac{1}{2}$) and ^{131}Xe ($\frac{3}{2}$) were established beyond any doubt, but also a small isotope shift was revealed among the even isotopes, which is due to a nuclear volume effect. A more detailed study [13] of the hyperfine structure of ^{129}Xe and ^{131}Xe permitted the determination of the ratio of the magnetic moments μ^{129}/μ^{131} ($=-1.131\pm0.005$). In addition deviations from the Landé interval

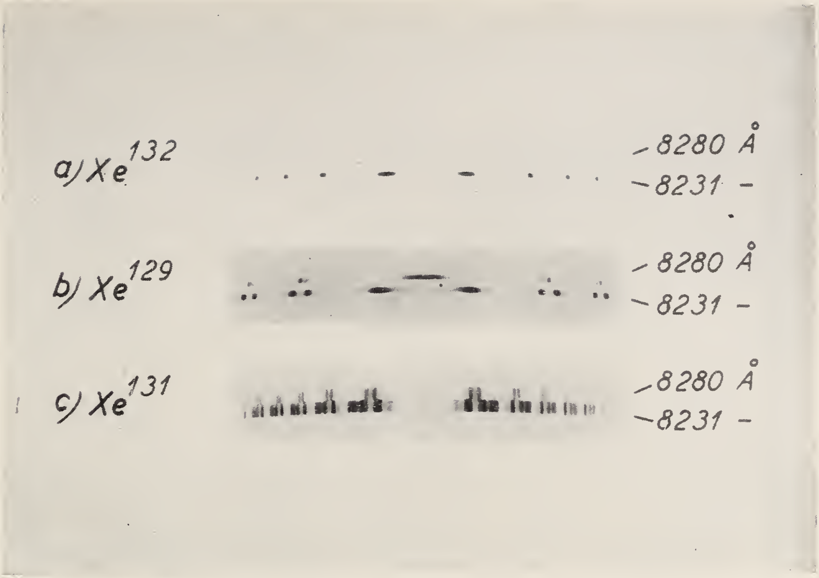

FIGURE 9. *Interferometer exposures of the infrared lines 8231 A and 8280 A.*

The lines for ^{132}Xe are single. For ^{129}Xe the lines 8280 and 8231 have two and four components, respectively. For ^{131}Xe the line 8280 has three components of which the two outermost are not resolved due to a quadrupole effect. The line 8231 shows at least six components.

rule permitted an estimate of the quadrupole moment of ^{131}Xe (-0.12×10^{-24} cm^2).

It may be added that the preparation of ^{84}Kr on a more industrial scale may be of importance for use in spectroscopic light standards [14]. Some experiments for the construction of a suitable tube using only krypton 84 gas in the discharge have been carried out in cooperation between the Institute for Theoretical Physics (Copenhagen), The National Physical Laboratory (Teddington), and the General Electric Company (London).

4. Experiments With Separated Artificial Radioactive Isotopes

The isotope separator under consideration has also proved useful for the separation of radioactive isotopes. This is due to the high yield of ionization in the ion source and the relatively large currents, which may be passed through the apparatus. The separation of radioactive isotopes not only permit an unambiguous assignment of half-lives to the different mass numbers, but also offers the possibility of a closer study of the β- and γ-rays emitted from definite isotopic species.

As an example may be mentioned the separation of some long-lived, radioactive krypton isotopes [15]. In these experiments ten kilograms of uranium oxide were heavily irradiated for some hours with slow neutrons produced by our cyclotron. The noble gases resulting from fission, which emanated together with some carrier gas, were pumped off by means of a Toepler pump and concentrated in a volume of about 100 cm³. After having added an adequate amount of normal krypton for providing a mass scale, the gas mixture was introduced to the ion source. The mass spectrum of krypton could easily be recognized and fixed by observing the beams from the stable isotopes on a fluorescent screen. As collector a stack of brass plates was used, which divided the mass range into fifty steps (fig. 10). This arrangement simplified the investigation of the radiation from the individual parts of the collector without disturbing effects from neighboring active deposits. In front of the collector a shutter was inserted, which was opened magnetically, as soon as good operating conditions were established. After running the isotope separator for about one hour, the collector plates were quickly removed in order to study the active deposits. The distribution of radioactivity along the stack of collector plates is shown in figure 11. From visible marks on the collector plates, due to the sputtering action of the stable isotopes, the peaks could be assigned to the isotopes ^{85}Kr, ^{87}Kr, and ^{88}Kr. The radioactivity was intense enough for following the decay over a number of periods. The following half-lives were measured with an accuracy of about 2 percent: $\tau_{85}=4.36^h$, $\tau_{87}=1.30^h$, and $\tau_{88}=2.77^h$. A determination of the maximum β-energies was carried out by absorption measurements. From the shape of the absorption curve of ^{88}Kr it seemed permissible to deduce that the β-spectrum of this isotope is complex. This could definitely be demonstrated when ^{88}Kr was separated from its daughter substance ^{88}Rb (being a γ-emitter) by induction heating of the target. The liberated gas showed an emission of γ-rays having an energy of about 2 Mev.

Experiments with the short-lived krypton isotopes could not be carried out by means of the slow procedure described above. However, by using an improved technique for the introduction of the radioactive gas into the ion source it was possible to extend the investigations to comprise the isotopes ^{89}Kr, ^{90}Kr and ^{91}Kr and their daughter substances [16, 17]. The uranium container, which was located close to the neutron source of the cyclotron, was connected to the ion source

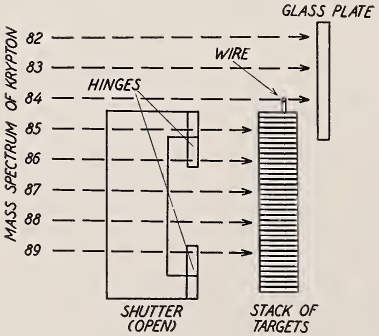

Figure 10. *Arrangement for the collection of radioactive noble gas isotopes.*

Thickness of each target 1.5 mm.

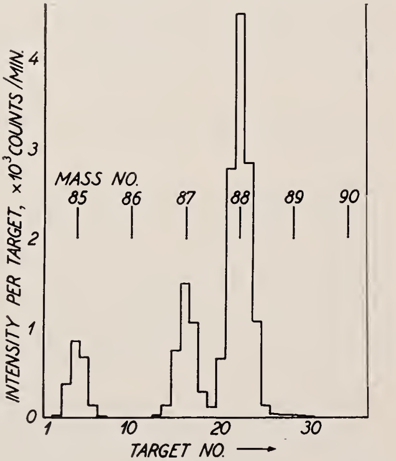

Figure 11. *Mass spectrum of some radioactive krypton isotopes.*

The counting rate of each target (fig. 10) is given as function of target number.

of the isotope separator through a ten-meter-long evacuated tube. By means of a liquid air trap mounted directly in front of the ion source, the carrier gas together with the radioactive noble gas was pumped through the tube, but only the noble gas proceeded by diffusion to the source. Here it became mixed with normal krypton gas which acted as a mass marker. In the actual experiment the cyclotron and the isotope separator were operated simultaneously. As a collector of the separated isotopes, a thin aluminum foil was used in such a way that the β-particles from the active deposit could pass through the foil and enter a counter mounted behind it. Counting began immediately after having stopped the machines. The radiation characteristics were studied by absorption measurements. The lack of a β-spectrometer prevented a closer study of the decay schemes. Some of the results are summarized in table 1.

Table 1. *Observed radiations.*

Isotope	Half-life	Radiation	$E_{\beta}^{\max}$	Spectrum
			Mev	
Kr^{89}	3.18 min	β^-, γ	4.0	Complex.
Kr^{90}	33 sec	β^-, γ	3.2	Do.
Rb^{90}	2.74 min	β^-, γ	5.7	Do.
Kr^{91}	10 sec	β^-, γ probable	~3.6	Do.
Rb^{91}	100 sec	β^-, γ	4.6	Do.
Rb^{91}	14 min	β^-, γ	3.0	Do.

In the preparation of this survey I decided to confine myself to the description of experiments carried out at the Institute for Theoretical Physics. It would, however, be incomplete to present a survey of experiments with electromagnetically separated isotopes of the noble gases without at least bringing to the attention of the audience the fine investigations which have been carried out by my colleagues with the isotope separator of the Nobel Institute in Stockholm [18].[7] Experiments carried out with this apparatus have especially been devoted to the study of the radiations from active isotopes of krypton and xenon by means of the various β-spectrometers of the Institute. The preparation of β-spectrometer samples by means of the isotope separator proved most satisfactory, since such samples contain only one isotope, they are carrier free, without any covering substance and extremely thin. The use of thin collector foils reduces the effect of back-scattering. An exhaustive description of the applied technique has recently been published in articles on the isomers of Kr and Xe [19] and on the decay of ^{88}Kr [20].

5. Conclusion

When work on the preparation of isotopic samples for nuclear research was started in Copenhagen, it was the impression that the main difficulty would be to obtain a rate of separation which was sufficient for nuclear experiments. As shown today a number of experiments may be carried out with the present equipment although no special effort has been made to achieve large ion currents. Of

---

[7] These authors made use of an ion source construction in which electrons from a filament are collimated by a vertical magnetic field. The ion source II of figure 2 is a modification of their construction. This type of ion source works at a lower pressure than the capillary arc and the yield of ionization is larger. These facts make the source more favorable for the production of ions of metals evaporated from an oven. It is, however, doubtful whether the initial energy of the emitted ions is as small as that mentioned earlier which would give rise to an increase of the width of the mass spectrum lines and would make it more difficult to prepare very pure isotopic samples.

course, some day the demand for larger samples will arise, but I am convinced that a somewhat more efficient ion source may by constructed without too much trouble. The intensity problem to be dealt with in the preparation of pure samples of rare isotopes may partly be overcome by using a starting material in which the rare isotope is somehow enriched by other methods. The main aim in the construction of an isotope separator for use in the laboratory should be to make it flexible enough to switch from one element to another and at the same time to ensure the preparation of extremely pure samples.

6. References

[1] J. Koch, Electromagnetic Isotope Separation, thesis, University of Copenhagen (1942).
[2] J. Koch and B. Bendt-Nielsen, Dan. Mat. Fys. Medd. **21,** No. 8 (1944).
[3] E. S. Lamar, E. W. Samson, and K. T. Compton, Phys. Rev. **48,** 886 (1935).
[4] J. Koch, Phys. Rev. **69,** 238 (1946).
[5] J. Koch, Dan. Mat. Fys. Medd. **24,** No. 7 (1948).
[6] N. Bohr, Dan. Mat. Fys. Medd. **18,** No. 8 (1948).
[7] K. J. Brostrøm, T. Huus, and J. Koch, Nature **160,** 498 (1947).
[8] J. Ambrosen and K. Marck Bisgaard, Nature **165,** 888 (1950).
[9] K. J. Brostrøm, T. Huus and J. Koch, Nature **162,** 695 (1948).
[10] J. Koch, Nature **161,** 566 (1948).
[11] J. Koch and E. Rasmussen, Phys. Rev. **76,** 1417 (1949).
[12] J. Koch and E. Rasmussen, Phys. Rev. **77,** 722 (1950).
[13] A. Bohr, J. Koch and E. Rasmussen, Anniversary volume for Professor M. Siegbahn (1951). Arkiv f. Fysik 4, No. 29 (1952).
[14] H. Barrell, Nature **164,** 599 (1949).
[15] J. Koch, O. Kofoed-Hansen, P. Christensen and W. Drost-Hansen, Phys. Rev. **76,** 279 (1949).
[16] O. Kofoed-Hansen and K. O. Nielsen, Phys. Rev. **82,** 96 (1951).
[17] O. Kofoed-Hansen and K. O. Nielsen, Dan. Mat. Fys. Medd. **26,** No. 7 (1951).
[18] I. Bergstrøm, S. Thulin, N. Svartholm and K. Siegbahn, Arkiv f. Fysik **1,** No. 11 (1949).
[19] I. Bergstrøm. Anniversary volume for Professor M. Siegbahn (1951). Arkiv f. Fysik 5, No. 14 (1952).
[20] S. Thulin. Anniversary volume for Professor M. Siegbahn (1951). To be published in Arkiv f. Fysik in the near future.

7. Discussion

QUESTION: You mentioned that you can store gases for long periods of time. Do you have an estimate of some of the diffusion times for various gases?

J. KOCH: No; I am sorry. We have started a little of this work, but it is not quite simple to carry out. If you have a limited number of people working, you have to decide to take the most interesting problem. In any case the diffusion is very slow and you must consider that the target during the time of collection is very hot, in the order of 300° or 400° C. Since it can be collected at that temperature it must stay at a lower temperature awhile.

QUESTION: You say the gas can be collected without cooling?

KOCH: Yes; it can be. We don't make any cooling during the time of collection.

F. J. NORTON: In the case of the neon hydride there are two means by which you might try to get rid of it. Add an excess of oxygen and in the competition for the hydrogen the oxygen might win out. You might flush out the excess with deuterium so you would get your neon deuteride.

23. A High-Intensity Electromagnetic Isotope Separator

By J. Kistemaker and C. J. Zilverschoon[1]

We constructed at Amsterdam a 180-degree type mass spectrometer with a main radius of 100 cm for separation purposes. The object is to separate all elements at the highest possible intensity. One of the most essential things is a good focusing at the target side. A homogeneous magnetic field cannot be used as it gives only first order radial focusing. To get a high intensity we must permit a large radial opening angle Θ at the source and the image is determined by $R\ \Theta^2$. Taking $\Theta=15$ degrees or ¼ of a radian, we find $R\ \Theta^2 \approx 60$ mm, whereas the separation for one mass unit at $m=250$ is only 4 mm. We therefore had to profile our pole shoes to get a magnetic field according to Beiduk and Konopinski, giving high order radial focusing after 180 degrees.

The shape of the 40 ton magnet was such that we could enter the vacuum chamber between the pole shoes from nearly all sides. This shape required a heavy shimming, however. The field is in accordance with the Beiduk-Konopinski field within 1 percent, rotational as well as radial.

The height of the pole gap is 17 cm, the maximum size of the beam 30 cm, limited by a baffle at 90 degrees. This baffle is necessary to intercept the ion beams which have been shot into the magnet chamber

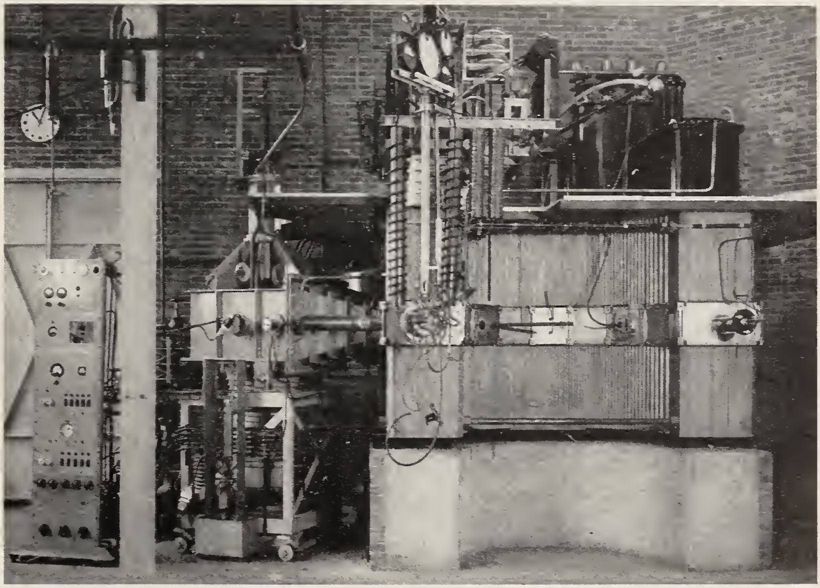

Figure 1. *General photo.*

---

[1] Laboratorium voor Massaspectrografie, Amsterdam, Nederland.

under too large axial angles with the median horizontal plane. Magnetic fields are used from 250 to 4,000 Gauss, with a constancy of 1 in 10^4.

The high tension is up to 30 kv positive, with a constancy of 1:2500 and can take 100 ma. We can superimpose a sweeping voltage which is about 10 percent of this stabilized voltage to observe the spectrum and the shape of the beams on an oscilloscope.

Another very essential part of this apparatus is the ion source, which you see in figure 4, together with the acceleration slit.

This source is situated between the pole tips, in the magnetic field. We can make the electrons oscillate in the source by choosing the electrode potentials carefully. Then we have a source of the type such as Heil developed in Germany 10 years ago. It is also very easy to have the discharge burning as a d-c arc, however. We try both. The gas and electrical efficiency of the oscillating type is much better. Some data are: Filament current 130 amp; arc current 0.1 to 3 amp, arc voltage 50 to 200 volts; arc pressure $10^{-3}-10^{-2}$ mm Hg of air; ion output in total about 10 ma to 20 ma with 20 kv between source and acceleration electrode; distance source to acceleration slit 10 mm; slit in the ion source 100×2 mm^2. The use of gas is about 100 mm^3 of 1 atm/sec. The source and filament holders are water-cooled.

We are still studying the behaviour of the beam. In this way we got rather well focused positive-ion beams of N^{14} and N_2^{14} each of 3 ma. The half width of these beams at the focusing point was from 5 to 7 mm. Of argon we got even higher currents. If we reduce the ion intensity in these beams, e.g. by reducing the filament current in the ion source, then we can go up with the resolving power. It looks as if we shall be able to separate 150 and 151 with a degree of purity of some percent.

For the higher elements we are still fighting the "hash" as our biggest enemy. This hash is a kind of noise superposed on the beam intensity. We frequently observed hash intensities of the same

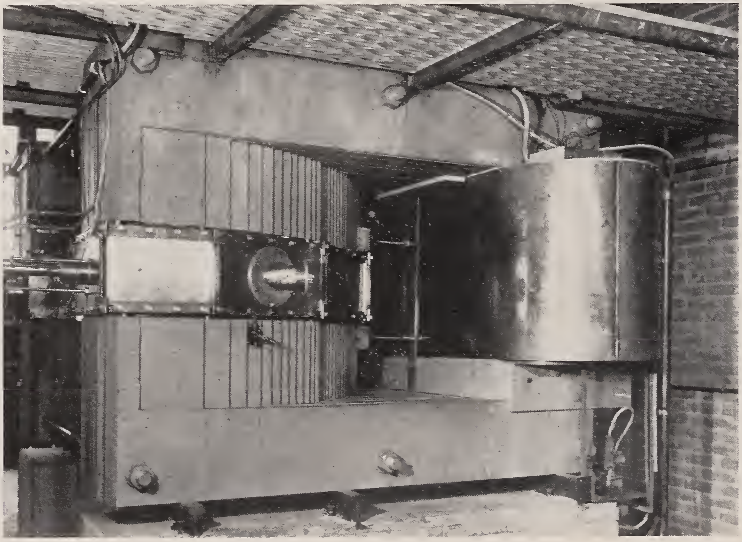

FIGURE 2. *Side view of the coil.*

intensity as that of the beam. This is a very bad thing as the hash has a rather high-frequency character. You will know that these heavy loaded positive-ion beams can only exist with space charge compensation from electrons. These compensating electrons are probably created in the gas in the magnet chamber and the process of building up a beam therefore takes some time. If the frequency of the hash is too high, it can happen that the beam does not get the time to build up. In this way the beam intensity is strongly reduced. The hash originates from the ion source itself, from false electromagnetic corona discharges between the positive-ion source and earth and perhaps from the beam itself. In the suppression of the corona hash we had some success with well shaped screening caps around the ion source.

The hash from the ion source is much stronger with the Heil source than with the arc source; the beam from the latter is better focused. Important factors for the focusing seemed to be: pressure in the vacuum chamber; stability of the high tension and the circumstances in the ion source: voltage, current and pressure.

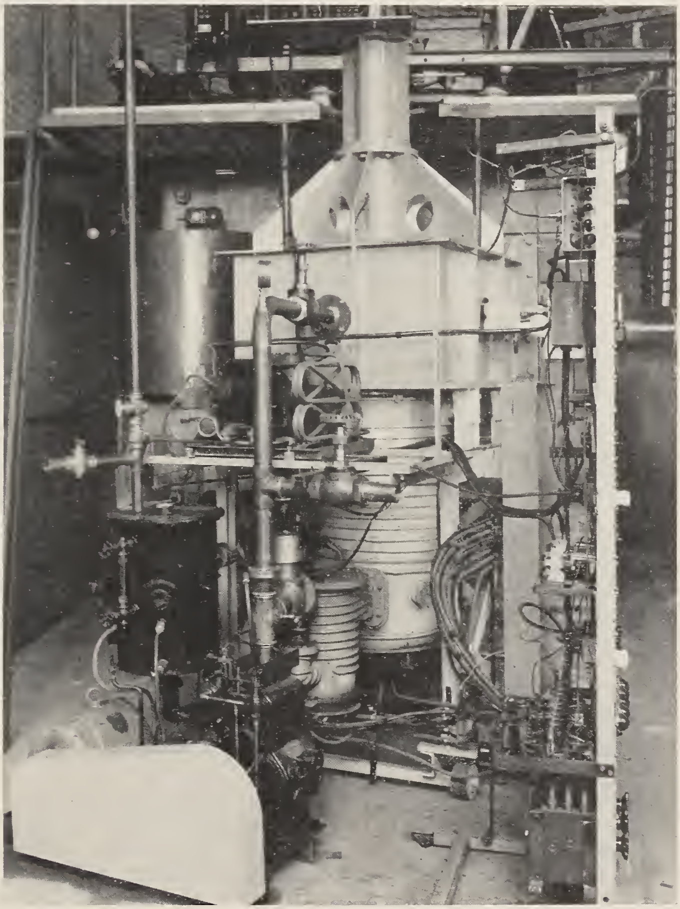

Figure 3. *The vacuum system.*

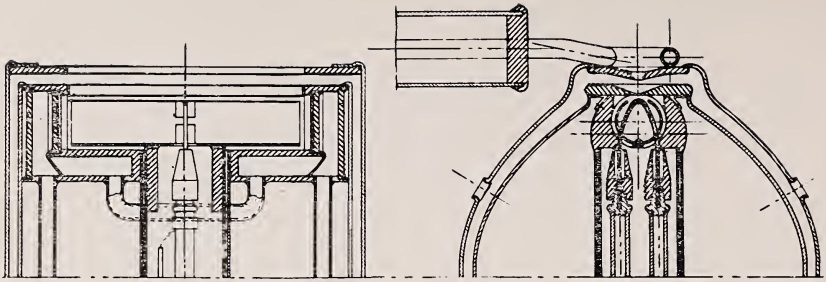

Figure 4. *The ion source.*

Discussion

H. C. Price: I would like to ask, did you measure how closely you were able to attain the divided field?

J. Kistemaker: Yes, we have an agreement with the theoretical Konopinski field of 1 per mil in the radial direction and the field is constant in the ϕ direction at any particular radius, also within 1 percent. We have the impression that this is satisfactory.

Price: Were the pole faces machined with sharp corners as shown on the slides?

Kistemaker: Yes.

K. T. Bainbridge: I just wanted to say about that field distribution, that Walter Brown and E. M. Purcell achieved that field distribution in the construction of a magnet of the type that Cockroft made many years ago for alpha studies.

Price: At Indiana University a semi-circular 15 cm radius beta spectrometer has been built using this Konopinski-Beiduk field.

J. Koch: I should like to ask whether you have any suggestions as to the energy spread of the ions.

Kistemaker: We have the impression that it is certainly not more than five or ten volts. It depends on the situation, but in general I can say that we have an anode potential to the order of 100 volts.

Koch: It is not possible that it is much smaller?

Kistemaker: Perhaps.

Koch: We have the impression that the energy spread is much less than one electron volt. There is an angular spread of the beam; then it comes out that the energy is much less. This is not in agreement with experiments of Compton.

Kistemaker: I think your source is in this respect very favorable, more favorable than these sources of the Finkelstein type that we are using here.

Question: Can you give a figure for the angular spread in the vertical direction?

Kistemaker: No, I have no idea. There are many things which I do not understand at this moment.

Question: It is known to some extent?

Kistemaker: You may know much more about that than I do, but I can only say that experimentally I have observed that when there is an acceleration of 30 kv the beam is nearly horizontal. It is a beam like that—I can illustrate that on the board—but when you go down to 10 kv you clearly see that it is more diverging. It depends, of course, on the acceleration. You may think about it.

24. Measurement of Trace Quantities of Uranium and Lead in Minerals and Meteorites

By David C. Hess, Harrison Brown, Mark G. Inghram, Clair Patterson, and George Tilton [1]

The analysis of minerals and meteorites for traces of uranium and lead permits deductions of the ages of these substances and, in the case of meteorites, gives information about the cosmic abundances of elements and isotopes. Age measurements in the past have all been made on ore deposits. Since low concentrations of three to ten parts per million (ppm) of lead and uranium in igneous rocks have precluded direct age measurements on them, their ages have been inferred from ore data obtained on deposits within the igneous structure. Table 1 shows the relative sensitivity of some methods of analysis for uranium. The addition of the techniques of mineral separates, isotopic dilution, and surface ionization has removed this limitation so that it is now possible to make age determinations directly on igneous substances.

Table 1.

Method	Sensitivity of U	Sensitivity of U	Accuracy
	Micrograms	*ppm*	*Percent*
Optical spectra	0. 5	1000	5
Optical spectra with chemistry	. 5	25	5
Mass spectra hot spark	. 003	3	2 to 3
Isotope dilution with chem	. 0000002	10^{-6}	1 to 2
Isotope dilution	. 0000002	------------	2 to 3

Gram quantities of several minerals including zircon, perthite and sphene were separated from about a hundred kilograms of a pre-Cambrian granite of the Canadian shield from Essonville, Ontario. The separation was done by E. S. Larsen of the U. S. Geological Survey, using flotation and magnetic processes followed by final selection under the microscope. The separated minerals were cleaned, weighed, and dissolved: the zircon and sphene by fusion in borax followed by hydrochloric acid dissolution, the perthite by hydrofluoric acid treatment followed by perchloric acid.

For the lead analysis, the sample was divided into a large and a small aliquot. The smaller portion was equilibrated with about twenty-five micrograms of lead enriched in lead 208, while the larger portion was not "spiked". These two aliquots and an amount of the enriched lead equal to that used to spike the smaller aliquot were processed to separate the lead. This processing was simultaneous for a given mineral in order to produce similar exposure to the laboratory atmosphere which appears to be the principal cause of contamination. The entire process consisted of extractions of lead dithiozonate into chloroform and decompositions of the dithiozonate.

---

[1] Argonne National Laboratory and University of Chicago, Chicago, Ill.

No precipitation process was used, and the yield should not depend on the smallness of the sample. The few micrograms of lead obtained were dissolved in nitric acid and some borax "flux" added. The solution was evaporated on a wolfram strip 0.75 by 8 mm and this filament placed in the mass spectrometer.

The uranium analysis involved two different weights of sample, which were spiked with the same amount (usually about thirty micrograms) of uranium enriched in uranium 235. These were processed with the same amounts of reagents so that contamination could be taken into account. The principal uranium separation was accomplished by extraction of the uranyl nitrate into methyl isobutyl ketone (hexone) from a solution salted with nitrate ion. Again the solubility product does not enter so that small samples may be used. The tens of micrograms obtained were dissolved in nitric acid, and a few micrograms evaporated onto a tantalum filament the same size as that used for the lead. It was not necessary to use a flux for the uranium analysis.

The small amounts of material obtained from reasonable samples precludes the use of the usual electron bombardment source which may require several milligrams of sample for an analysis (even though much of this may be recovered later). Therefore, surface ionization was used in a 12 in. radius, 60° magnetic analyzer. An electron multiplier proved necessary for good lead anlyses and resulted in a marked increase in sensitivity for uranium.

Figure 1 shows a summary of the procedure given above. The calculation is for a contribution from the sample approximately equal to the amount of tracer. In this case, it is possible to ignore the amount of uranium 235 from the sample and the amount of uranium 238 from the tracer. When the contribution of the sample is markedly different from this, equations can be set up which account for either the uranium 235 from the sample or the uranium 238 from the tracer. By utilizing the results from two samples of different weight, the amount of contamination introduced by the chemical treatment can be taken into account.

Because of the wide variation of natural lead, it is necessary to measure the isotopic composition of the lead without tracer. Then the measurement with added tracer when combined with the indicated contamination (which is assumed to be "average" lead) obtained from the measurement of the tracer which was processed simultaneously with the other samples will yield the amount of lead present in the original sample.

<table>
<tr><th>PROCEDURE</th><th colspan="3">SAMPLE CALCULATION</th></tr>
<tr><td rowspan="5">1. WEIGH SAMPLE.
2. DISSOLVE SAMPLE.
3. ADD KNOWN WEIGHT OF ISOTOPIC TRACER OF THE ELEMENT IN QUESTION.
(4) EXTRACT ELEMENT IN QUESTION CHEMICALLY.
5. MEASURE THE CHANGE IN THE ISOTOPIC COMPOSITION, DUE TO DILUTION OF THE TRACER WITH THE NORMAL FROM THE SAMPLE</td><td colspan="3">WT. OF SAMPLE - GRAMS = W
WT. OF TRACER - μGRAMS = M
PPM OF IMPURITY (U) = X</td></tr>
<tr><td></td><td>235</td><td>238</td></tr>
<tr><td>U - FROM TRACER</td><td>M</td><td>—</td></tr>
<tr><td>U - FROM SAMPLE</td><td>—</td><td>XW</td></tr>
<tr><td colspan="3">$\left|\frac{238}{235}\right| = \frac{WX}{M}$
$X = \left|\frac{238}{235}\right| \frac{M}{W}$ PPM</td></tr>
</table>

Figure 1. *Summary of method of isotope dilution.*

Table 2 gives the results obtained for uranium analyses. It should be noted that the zircon and sphene contain most of the uranium in the rock while all the other minerals hold only a minor fraction.

TABLE 2.

Mineral	Mineral abundance	U (ppm of mineral)	U (ppm of rock)
	Percent		
Zircon	0. 04	2614±25	1. 02
Sphene	. 40	299±3	1. 20
Apatite	. 02	93. 3±0. 9	0. 019
Magnetite	. 40	4. 12±. 13	. 016
Perthite	50	0. 22±. 02	. 11
Plagioclase	18	. 20±. 01	. 036
Quartz	29	. 13±. 01	. 038
Hornblend	2. 0	----------	-----
Calcite	. 40	----------	-----
Pyrite	. 02	----------	-----

Table 3 shows the total lead for the two minerals and Table 4 shows the separation into radiogenic and nonradiogenic. This was accomplished by setting the composition of the lead in zircon and sphene at the time they were formed equal to that of the perthite. This is reasonable since the small uranium content of the perthite indicates that its lead has not changed in isotopic composition. With this distribution, the values are normalized at 204 and the amount of nonradiogenic lead for the minerals calculated. The ages of the minerals are calculated and are shown in table 5.

TABLE 3.

Mineral	Mineral abundance	Pb (ppm of mineral)	Pb (ppm of rock)
	Percent		
Zircon	0. 04	451±10	0. 18
Sphene	. 40	230±5	. 92

TABLE 4. *Lead isotopes in minerals.*

Mineral	204	206		207		208	
		Non-radiogenic	Radiogenic	Non-radiogenic	Radiogenic	Non-radiogenic	Radiogenic
	µg/g	*µg/g*	*µg/g*	*µg/g*	*µg/g*	*µg/g*	*µg/g*
Zircon	0. 146	2. 6	374. 8±9. 0	2. 32	28. 27±0. 7	5. 94	36. 93±1. 0
Sphene	1. 66	29. 67	35. 86±1. 8	26. 37	2. 50±0. 7	67. 54	66. 46±3. 5
Perthite	0. 086±0. 010	1. 557±0. 18		1. 362±0. 16		3. 488±0. 42	

TABLE 5. *Ages of minerals in millions of years*

Mineral	Pb^{206}/U^{238}	Pb^{207}/U^{235}	Pb^{207}/Pb^{206}
Zircon	1000±30	1020± 30	1100± 20
Sphene	850±40	860±150	930±150

There are two controversial viewpoints about the origin of the granite which was the source of these minerals: one is that the rock mass is of magmatic origin, i. e., all of the minerals were crystalized at the same time from molten magma; the other is that of metasomatic origin, i. e., recrystallizations, replacements, etc., of a solid or of sediments. The general spread in ages for the different minerals would tend to support the metasomatic origin theory. However, more data are necessary for a satisfactory interpretation.

The uranium content of stone meteorites was also measured by the isotopic dilution technique. The results are shown in table 6. Figure 2 shows a typical trace from the mass spectrometer in the analysis of a meteorite. Earlier values of uranium content of stone meteorites deduced from their radon contents run from a few hundredths ppm to about 1 ppm. This table also shows the results of measurement of the purity of one of the reagents. It shows the power of the method.

TABLE 6.

Solid studied	U
	ppm
Norton County stone meteorite	0.0054 ±0.0002
Modac stone meteorite	.0105 ± .0003
Ammonium nitrate	.000075± .000004

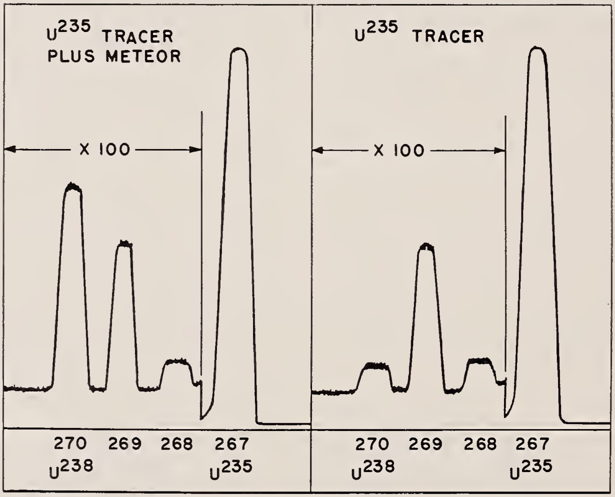

FIGURE 2. *Mass spectrometer record in the analysis of a meteorite.*

Discussion

Question: I was wondering about this lead contamination from the atmosphere. Have you made separate studies of the lead in the atmosphere?

D. C. Hess: No, the uranium contamination is not as bad for the atmosphere as the lead. Various samples were run of different amounts of reagent. There was no correlation. The only thing that did appear was the amount exposed to the atmosphere.

Question: I was just wondering if there was that much there.

Hess: The results I have shown are some of the better results. Contamination for example in the zircon was negligible.

Question: The lead you get from the atmosphere—if somebody cleans off the tables there is lead; it isn't really atmosphere lead, just dust. Would you care to say anything about the possibility of differential leakage from different minerals which might result in the same thing? What information do you have in regard to leakage from different minerals?

Hess: That is a rather involved problem and I didn't want to get stuck with it. I am not a geologist either. The slide I showed indicated a difference in age. Since you would expect there was less leakage of lead, the lead age should be a truer age. We calculated lead-lead and uranium-lead. If there was a different amount of leakage of lead in uranium, you would expect the lead-lead age to be considerably different from the uranium-lead. That was the way we first interpreted it.

Question: What half-life do you use for U_{235}?

Hess: Approximately Dr. Nier's value. The late work at Argonne has supported that value; I think it is 7×10^8. I can give you an exact value later if you want it.

Question: Could you elaborate somewhat on the reason you get better emission of lead ions when you add lead borax?

Hess: No, that is difficult.

Question: Does it give you higher ion currents?

Hess: I don't know. On the filament we bring the temperature up gradually. We did find that by adding the borax you can slow down the emission and spread it out. It may be more involved.

Question: Sometimes the filament sort of spurts out all at once. Borax spreads it out.

Hess: Yes. From the present apparent theory you would not expect lead to ionize at all, and it does not very much. That is why you need the multiplier.

25. Further Results on the Double Beta Decay of Te^{130}

By Richard J. Hayden and Mark G. Inghram [1]

One of the few instances where the difference between the Majorana and the Dirac theories of the neutrino predicts different conceivably measurable effects is the case of the simultaneous emission of two beta particles. The reactions involved in the two cases are:

$$Z \rightarrow (Z+2)+2\beta(\text{Majorana})$$

$$Z \rightarrow (Z+2)+2\beta+2n_0(\text{Dirac})$$

The half-life, according to the Dirac theory, is much longer than that predicted by the Majorana theory. Fireman [2] has, by means of coincidence counting detected activity in tin which he ascribed to double beta decay of Sn^{124}. He assigned a half-life of 4 to 9×10^{15} yr, a result in rough agreement with the Majorana theory. Later counting results indicate that his activity probably came from another source. Inghram and Reynolds [3,4] measured the Te^{130} double beta half-life by extracting Xe from an old tellurium mineral and measuring the isotopic composition of the Xe with a mass spectrometer. Knowing the amount of Xe^{130} extracted, the amount of Te^{130} in the sample, and the geological age of the sample, the double beta half-life may be computed. Inghram and Reynolds (table 1) found excess Xe^{130} (after normal had been subtracted by means of Xe^{132} peak) which gave Te^{130} a half-life of 1.4×10^{21} yr. For allowed transitions with 1.6 Mev available energy, the Majorana theory predicts a half-life of 6×10^{14} yr, and the Dirac theory a half-life of 10^{24} yr. Combining the theories would allow any intermediate half-life to be predicted.

One difficulty with the Inghram-Reynolds experiment was that in addition to the excess Te^{130} large quantities of excess Xe^{129} and Xe^{131} (10 to 20 times the amount of Xe^{130}) were found. They explained these isotopes as being due to neutron absorption in tellurium (the particular ore used was taken from the neighborhood of uranium

TABLE 1. *Xenon extracted from 70-percent* Bi_2Te_3 *deep mineral*

Mass	Bi_2Te (#4)	Normal	Difference	Difference normalized
124	<0.004	0.0005	<0.0035	<0.29
126	$<.005$	.0005	$<.0045$	$<.38$
128	$<.014$	.011	$<.003$	$<.25$
129	$\equiv1.000$	.1525	.8475	71.99 ± 0.7
130	.0652	.0236	.0416	$3.48\pm.17$
131	.4088	.1235	.2853	$23.90\pm.3$
132	.1566	$\equiv.1566$	$\equiv.0000$	$\equiv.00$
134	.0651	.0611	.0040	$.33\pm.25$
136	.0562	.0519	.0043	$.36\pm.16$

2.6×10^{-7} STP Xe

---

[1] Argonne National Laboratory, Chicago, Ill.

[2] E. L. Fireman, Phys. Rev. **75**, 323 (1949).

[3] M. G. Inghram & John H. Reynolds, Phys. Rev. **76**, 1265 (1949).

[4] M. G. Inghram & John H. Reynolds, Phys. Rev. **76**, 822 (1950).

deposit) but their abundance ratio was not in accord with what is predicted from neutron cross sections. Another difficulty in their work was inherent in their method of measuring the absolute amount of Xe^{130} in the rock. A 100 percent recovery of Xe through the purification set up was assumed and the amount was measured using the ionization efficiency of the mass spectrometer as a standard. A sample of Xe thousands of times the size of the unknown was used to calibrate the instrument and source efficiency as a function of sample pressure was not studied.

To correct these difficulties, a determination was carried out on another sample of telluro bismuthite, obtained from the Mångfallberget mine through the generous cooperation of Dr. Erland Grip. According to Dr. Grip there were no uranium deposits in the neighborhood of this sample. To measure the absolute amount of Xe^{130} formed an Xe^{128} tracer was used. The tracer used contained $1.286 \times 10^{-7} \pm .064 \times 10^{-7}$ cc at STP Xe^{128} and no other observable Xe. The preparation and measurement of this tracer was a fairly critical task. Xe^{128} was formed by a long irradiation by slow neutrons of NaI in an evacuated quartz tube. This tube was broken open in another evacuated quartz tube which was connected to a gas purification system very similar to that of figure 1. After purification the gas was collected in charcoal at liquid nitrogen temperature. After a preliminary breakdown by a factor of 400, the Xe^{128} was introduced into the apparatus shown in figure 2. Twenty sample tubes were sealed on the system.

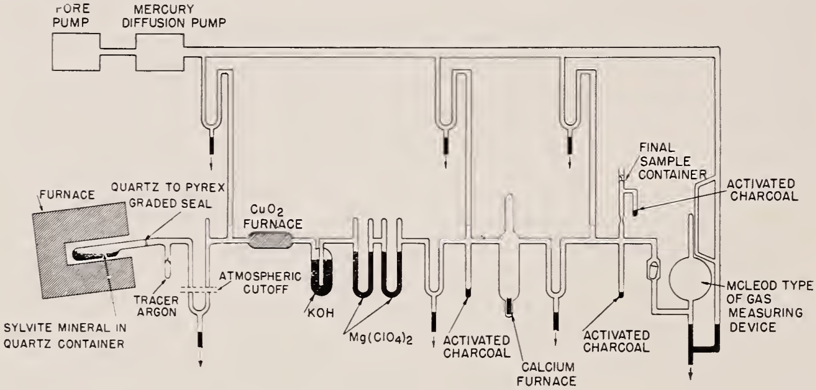

FIGURE 1. *Gas purification system.*

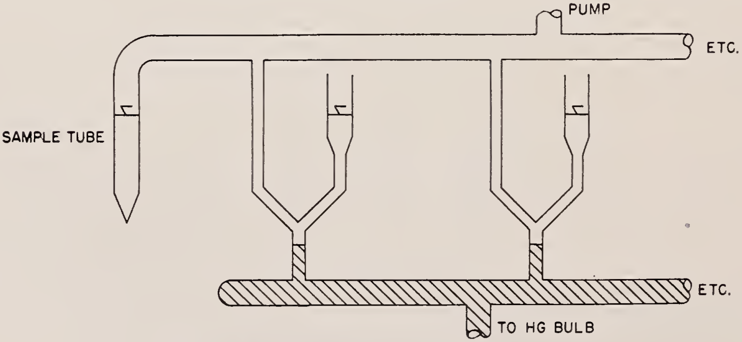

FIGURE 2. *System for preparing samples.*

After pumping out and sealing off the pumping lead, the tracer was broken out of its tube and allowed to equilibrate into the twenty tubes of known volume. Then the mercury level was raised to isolate the tubes and finally the tubes were sealed off. To determine the Xe^{128} pressure in the tubes, one of the tubes was mixed with a measured amount of spectroscopically pure Xe. In practice it is difficult to physically measure out less than 10^{-3} cc at STP normal Xe. Even this must be done in a capillary McLeod with a breakoff on top of the capillary to minimize Xe adsorption on the walls of the vacuum system. Because of the low normal abundance of Xe^{128} 10^{-5} cc at STP Xe^{128} gives a 40-percent change in the 128/129 ratio when mixed with 10^{-3} cc at STP normal Xe. Thus about 10^{-5} cc at STP Xe^{128} is needed for calibration. The tubes intended for calibration were made about 100 times larger than the standard tubes. The total volume of the sample system was chosen so as to make the amount of gas roughly 10^{-5} cc at STP in the calibrating tubes and 10^{-7} cc at STP in the standard tubes. The mixing and measuring of several calibrating tubes then gave an average value for the amount of Xe^{128} in each of the other tubes. The major source of error lies in the measurement of the 10^{-3} cc at STP normal xenon and in the different percentage gas adsorption on the walls of the big and little tubes.

The xenon from the telluro-bismuthite was purified in the same system as used by Inghram and Reynolds. This system was similar to that shown in figure 1. The tracer was added near the furnace at the time when most of the gas was coming out. After mixing and purification, the xenon was introduced into a sample system similar to that shown in figure 3. Measurement showed small, roughly equal peaks at masses 129, 130, 131 and 132. They are about .2 percent of the height of the 128 peak. If the 130 were due entirely to double beta emission from Te^{130}, the half-life would be 3.3×10^{21} years. This value is based on an assumption of 1.5×10^{9} years as the Xe age of the mineral. That this value is not far out of line is shown by the fact that the argon extracted from the rock with the xenon is mostly radiogenic and is present to an amount which, when coupled with the potassium content of the rock, gives an argon age of about 2×10^{9} yr. No tracer was used for this determination. It was assumed that the gas present after final purification was 30 percent argon, a figure which was determined after noting mass spectrometrically that argon and carbon monoxide were the principal gases present.

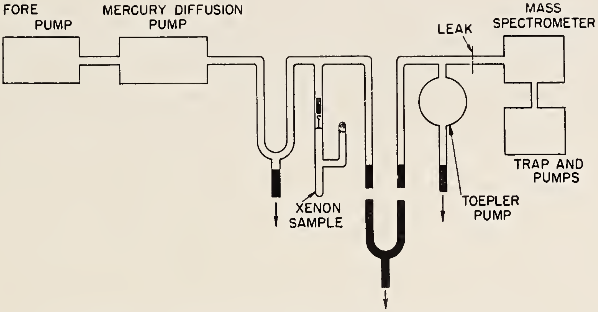

FIGURE 3. *Sample system for mass spectrometer.*

These results are not inconsistent with the Inghram-Reynolds data. In fact, they clarify these data. The great drop in the amounts of Xe^{129} and Xe^{131} observed indicate that these peaks are not due to spontaneous processes in tellurium. The 129, 131, 132 and a very small 134 peak that also appears are approximately in normal abundance, and probably are caused by normal xenon. The excess 130 still remains. The difference in the two half-life observations is not too large to be explained by calibration errors in the Inghram-Reynolds experiment. In any event 3.3×10^{21} yr is a fairly good lower limit for the Xe^{130} double beta half-life. The major uncertainty in this experiment now lies in the fact that the tellurium content of the ore has just been estimated at 10 percent; after a chemical analysis of the melted ore has been performed, a final value will be arrived at.

Discussion

W. E. Stephens: Are you so sure that argon has not leaked out that you can say this is a lower limit and not an upper limit?

R. J. Hayden: Well, you are not certain but you know that argon does not leak out too much. I mean, argon gives you 15- or 20-percent error when it leaks, and you would not think this would leak quite as much.

M. G. Inghram: The argon age was determined. It runs on the order of between 1½ and 2 billion years. If argon has not leaked out, why should I assume that xenon has?

Stephens: Any other discussion?

Question: How hot did you have to heat the ore before you made sure you got out all the xenon? How hot did you heat the sample?

Hayden: It was heated to a temperature of about 1,000 degrees centigrade. During the heating the metal could be seen distilling out onto the cooler pumping lead where it condensed and ran back into the furnace proper. At the conclusion of the run, the major portion of the metal solidified as a pool at the bottom of the furnace.

26. Ionization by Electron Impact

By Homer D. Hagstrum [1]

Ionization is only one of several processes which can occur when electrons of sufficient energy strike gas molecules. It is an important collision, however, because its products can be detected electrically. For this reason, ionization processes are grouped together and discussed together.

The study of ionization by electron impact has a long and venerable history. It goes back practically to the turn of the century when Lenard [1][2] in Germany for the first time attempted to measure an ionization potential by electron impact. The history of the field since those very early days records three important strides forward. The first of these was the application by Dempster [2] in 1916 of positive ray analysis to the detection of the collision fragments. The second was the attempt by Smyth [3] in 1922 to measure appearance potentials of ions observed in his mass spectrometer. The third occurred in the late 1920's in Professor Tate's laboratory with the development of instruments having the transverse magnetically collimated electron beam with which we are all now familiar. This type of ionizing electron beam arrangement was used in three types of apparatus: one for the measurement of total ionization by Jones [4] and Smith [5]; another for the determination of kinetic energy of dissociation products by Lozier [6]; and the third, Bleakney's [7] incorporation of this type of ion source into the mass spectrometer. With these instruments it was possible for the first time to demonstrate unambiguously that a molecule can be dissociated and ionized in a single collision. This marked the beginning of the "modern era" in the field during which investigations have become more or less reliable.

Since the development of basic apparatus and technique the study of ionization by electron impact has been developed in a number of directions: In the direction of studying more and more complicated molecules, in the direction of attempting to determine bond dissociation energies, of improving the measurement of appearance potentials, of recognizing the formation of metastable ions, and in other directions no further catalog of which will be attempted here. The remainder of this paper, rather, will concern itself with the making of a few comments about the nature and theory of ionization processes which can occur in molecular gases on electron impact.

First, consider the nature of ionization processes induced by electron collision. The types possible for electrons of energies greater than a few electron volts are four. The first process, A, called simple or direct ionization, is that in which the molecule loses one or more electrons only, no other change occurring. The second category, B, is one of three which involve dissociation and thus can occur in diatomic or polyatomic gases only. Here the molecule is first ionized by the incident electron and then dissociates into an ion and one or more

---

[1] Bell Telephone Laboratories, Murray Hill, New Jersey.

[2] Figures in brackets indicate literature references on p. 199.

neutral fragments. In process C the molecule is first excited to one of the excited states of the neutral molecule where it finds itself unstable and dissociates into a positive and a negative ion and possibly another neutral fragment. Finally, in process D the bombarding electron can, under certain conditions, be captured into the electronic structure of the molecule forming a negative ion which, in turn, is unstable and falls apart into fragments one of which is negatively charged. Processes C and D are possible only in gases which contain an electronegative atom or radical.

In discussing these processes it is well to bear in mind the nature of the energy transformations involved. The energy absorbed by the molecule from the translational energy of the bombarding electron could conceivably be of four types: electronic, and nuclear vibrational, translational, and rotational energy. One can dispose of the last two readily on the grounds of the disparity of mass between the electron and the nuclei. This leaves electronic and vibrational energy changes to be accounted for. It is clear that each of the above processes involves electronic changes. Processes for molecules having two or more constituent atoms may include vibrational energy changes in processes of each of the four categories. In dissociative ionization processes (B, C, D) vibrational energy lying in one of the dissociation continua is imparted to the molecule.

The vibrational energy changes which can occur on electron impact are governed by the well-known Franck-Condon principle. It also follows from the small ratio of electronic mass to nuclear mass, and states that neither the position nor momenta of the nuclei can be changed appreciably during the electronic change which accompanies electron impact. It provides the key to understanding many features of dissociative ionization. We shall discuss its application here in terms of the potential energy diagram in figure 1 for a representative diatomic molecule. Curve 1 is the potential curve for the ground state, curves 2 and 3 for states of the molecular ion XY^+ dissociating to the fragments X^+ and Y. The square of the ground state vibrational eigenfunction [ψ^2] is shown and the vertical dashed lines bound the classical Franck-Condon region. Curves 4 and 5 represent probability of transition as a function of total kinetic energy of the products.

In terms of transitions from the potential curve of one electronic state to that of another in figure 1, the Franck-Condon principle requires vertical transitions, those from the ground vibrational state lying essentially between the two vertical lines placed at the classical turning points of the motion in the ground state and defining the so-called classical Franck-Condon region. Thus the portions of the potential curves of the upper electronic states to which transitions can take place lie within this region. The subsequent behavior of the molecule is intimately connected with the form of the upper potential curve and, in particular, the position of the curve in the Franck-Condon region with respect to its asymptote or dissociation limit. The intersection of the potential curve, for example 3 in figure 1, with the boundaries of the Franck-Condon region gives the approximate limits of the total kinetic energy which the dissociation fragments can possess. Ions of zero initial energy can be formed only in processes which involve transitions to curves which cross their asymptotes inside the Franck-Condon region (curve 2 of figure 1).

One can determine an approximate distribution function for kinetic energy of the fragments in dissociative ionization by use [8] of the so-

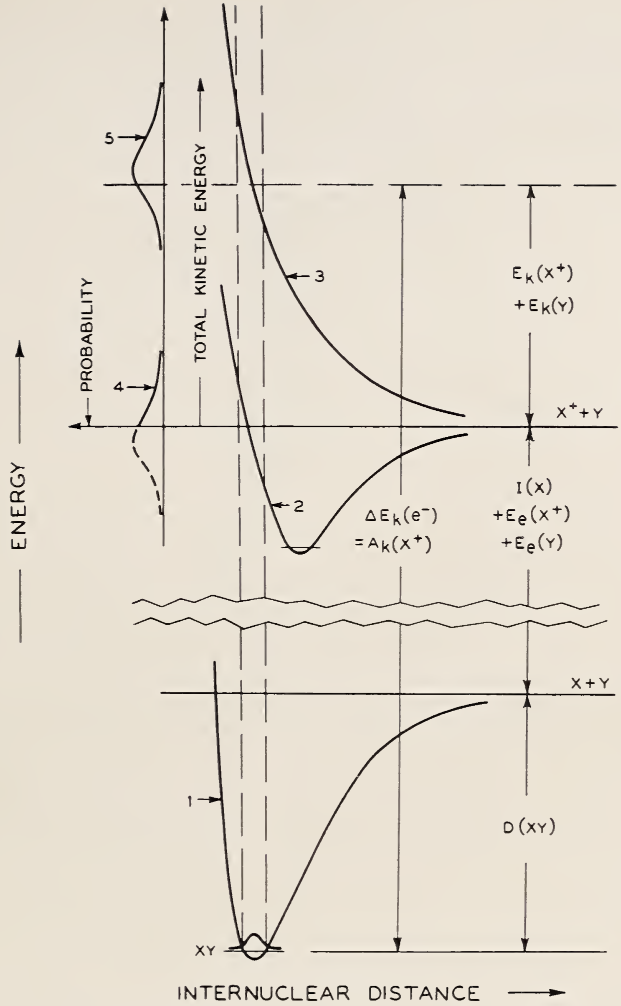

Figure 1. *Diagram of potential energy versus nuclear separation for a typical diatomic molecule XY.*

called reflection method developed for the interpretation of continuous absorption spectra. According to it, the relative probability of the process yielding fragments of given total kinetic energy is determined by the probability of finding the nuclei in the ground state at the value from which transition vertically will reach the desired energy level on the upper potential curve. The whole probability curve is thus determined by reflection of the function ψ^2 for the ground vibrational state in the upper potential curve. Curves 4 and 5 of figure 1 are examples of such curves obtained by reflection of ψ^2 in curves 2 and 3, respectively.

In addition to the function giving probability of producing fragments of given kinetic energy there is another function descriptive of the process, namely, the relative probability of its occurrence as a function of kinetic energy of the bombarding electron. This is the familiar ionization efficiency function which is zero below the threshold, rises steadily above this potential, passes through a maximum and declines monotonically to higher energies. It is instructive to combine these functions into a three-dimensional plot as in figure 2. This

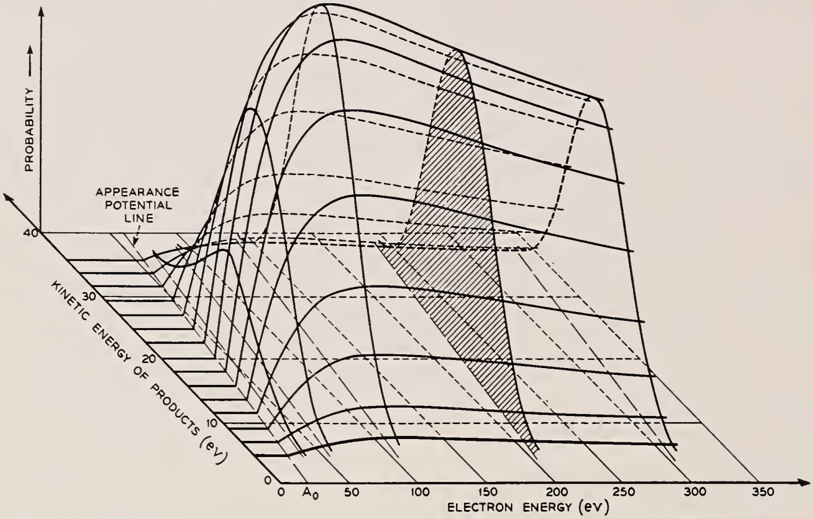

Figure 2. *Surface giving the efficiency of a non-capture dissociative ionization process as a function of electron energy and total kinetic energy of the dissociation products.*

yields a surface which prescribes the efficiency or cross section of the process yielding fragments of a given total kinetic energy at a given value of incident kinetic energy of the bombarding electron. In figure 2 the sections through the surface parallel to the electron energy axis yield the efficiency function versus electron energy. Sections parallel to the so-called appearance potential line are the Gaussian curves of the types obtained by the reflection method described above. The surface rises from zero along the appearance potential line, the slope of which line is dictated by the conservation of linear momentum between the fragments on dissociation. The surface of figure 2 pertains to a process for which the upper potential curve is situated as is curve 3 of figure 1. How the surface changes for a potential curve situated as is curve 2 of figure 1 is readily envisaged.

The variation of cross section with kinetic energy of the dissociation products has been seen to follow directly from the Franck-Condon principle and the form of the probability in nuclear separation of the molecule in its ground state. An explanation of the form of the dependence on electron energy is not as straightforward. Clearly the bombarding electron must have at least the energy of the transition which must be induced in the molecule for the process to occur at all. Hence the cross section is zero up to this energy value. Similarly one can get a simple physical picture for the decrease of cross section with energy at high energies. Here it is convenient to think of the molecule as a resonant system which is subjected to a pulsed disturbance generated by the passage of the bombarding electron. The probability that the molecule absorbs energy sufficient for ionization is then determined by the magnitude of the Fourier component in the pulse which is in resonance with the energy change in the molecule. As the bombarding electron becomes faster the pulse narrows and the magnitude of the lower frequency components in it decreases. Thus the efficiency of the ionization process decreases with increasing electron energy as is indeed found experimentally to be the case.

The form of the dependence of cross section on electron energy immediately above the threshold is of considerable interest both experimentally and theoretically. A knowledge of the form of the curve in this region is of importance in discovering ultra-ionization potentials and is basic to some methods of determining onset potentials accurately. All experimental data, even with velocity selected electron beams, show the cross section rising with finite slope. Lawrence, [9] however, at one time concluded that the ionization cross section in Hg vapor sets in abruptly at a finite value at each of a series of critical potentials and decreases above these values. The observed rising curve then was to be construed as the sum of a series of such curves. The problem is at best a difficult one experimentally.

Considerable progress has been made in the theoretical prediction of the form of the cross section near the threshold. In an early work, Blackett [10] discussed the efficiency of excitation on the basis of a classical theory involving conservation of angular momentum on collision. He concluded that the efficiency of the process should rise steadily above the threshold as the cross section available to an inelastic collision obeying the conservation of angular momentum increases with excess energy above the threshold. Blackett pointed out that the theory could say nothing concerning the efficiency of ionizing collisions, however, since the freed electron if it were to escape the Coulomb attraction would retain an angular momentum comparable to $h/2\pi$, the whole angular momentum of the atom.

It appears now that the escape of the slowly moving electron or electrons in both excitation and ionization processes is the factor which alone dictates the form of the cross section of the process immediately above threshold. Wigner [11] has shown by quantal methods that the relative variation of the cross section near threshold is in fact independent of the reaction mechanism and depends only on the long-range interaction of the product particles. Wigner's conclusions apply only to processes involving two particles before and after collision and so for the ionization processes of interest here predicts a cross-section variation only for dissociative ionization of the type C in which the primary electron collision excites the molecule. Wigner gives a dependence on the square root of the excess energy for the interaction of neutral particles.

Wannier [12] has considered ionization processes (three bodies after collision) and concludes that direct ionization of the parent gas (process A) should proceed with a cross section above the threshold depending on the 1.127 power of the excess energy above the threshold value. Bates, Fundaminsky, Leech, and Massey [13] have recently applied the Born approximation to the calculation of cross sections near the threshold obtaining gratifying agreement with Wigner's theory for two body processes. The theory is applied to ionization and detachment processes as well, yielding for ionization of a neutral particle a cross section depending on the first power of the excess energy above that of the threshold.

Thus, one must conclude that the efficiency of each of the ionization processes rises monotonically with electron energy above the threshold and that Lawrence's proposal of a finite cross section immediately above the threshold can no longer be entertained. This conclusion is not altered by the interpretation of the ultra-ionization potentials as indicating the onset of ionization by Auger processes, the first stage of which is double excitation of atomic electrons. The results of Wigner and of Bates, et al, do, it is interesting to note, predict a finite cross section at threshold for one type of process, namely, the two-body reaction of particles between which there is a Coulomb attraction. A process of this type is the excitation of an ion by electron impact.

We have yet to discuss in more detail the nature of dissociative capture processes (type D) yielding negative ions. The distinctive features of this process arise from the requirement that the bombarding electron possess exactly the energy to be given to the atomic or molecular structure when the bombarding electron is absorbed. Thus the possible electron energies at which dissociative capture can occur are those given by the transitions from the molecular ground state to the available points on the potential curve of the negative molecular ion in the Franck-Condon region. The efficiency of the process as a function of electron energy should then be of the same form as the distribution in kinetic energy of the dissociation products (curves like 4 and 5 of fig. 1). The efficiency "surface" analagous to that of figure 2 collapses to the space curve shown in figure 3 placed above the appearance potential line. Its projections on the efficiency-kinetic energy and efficiency-electron energy planes are of the Gaussian form demanded by the theory. Figure 3 shows clearly the characteristic interdependence of electron energy and kinetic energy for these processes and that an efficiency curve versus electron energy of finite width can be observed only if ions of differing kinetic energy are being collected.

An ionization process once identified is completely specified by efficiency surfaces of the types shown in figures 2 and 3. Simultaneous measurement of appearance potential, cross section, and kinetic energy are essential it would seem [14]. Identification of the process involves not only specification of the dissociation products and their state of ionization but their residual electronic (and possibly vibrational) energies as well. There is no hope of measuring these latter quantities directly at present. Comparison of threshold energies for a number of dissociative ionization processes in one gas or related gases has made possible, particularly for diatomic gases where residual vibrational energy can play no role, the unambiguous identification of all processes observed [14].

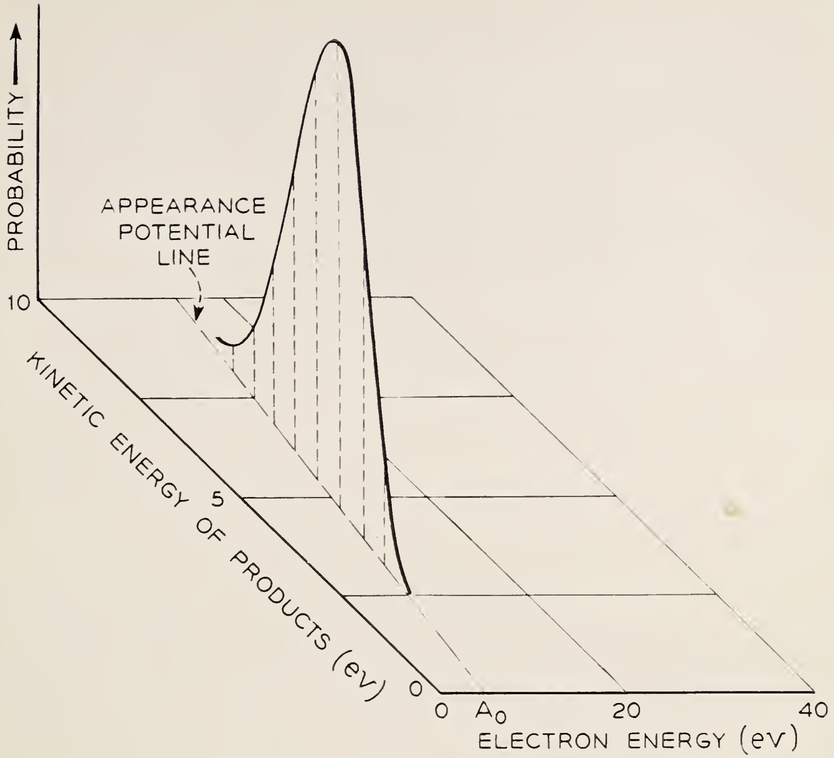

FIGURE 3. *Efficiency "surface" for the resonant dissociative capture process (D of fig. 1).*

The "surface here" is a space curve situated above the so-called appearance potential line.

---

[1] P. Lenard, Ann. Physik [4] **8,** 149 (1902).
[2] A. J. Dempster, Phil. Mag. **31,** 438 (1916).
[3] H. D. Smyth, Proc. Roy. Soc. [A] **102,** 283 (1922).
[4] T. J. Jones, Phys. Rev. **29,** 822 (1927).
[5] P. T. Smith, Phys. Rev. **36,** 1293 (1930); **37,** 808 (1931).
[6] W. W. Lozier, Phys. Rev. **36,** 1285 (1930).
[7] W. Bleakney, Phys. Rev. **34,** 157 (1929); **35,** 139, 1180 (1930).
[8] H. D. Hagstrum and J. T. Tate, Phys. Rev. **59,** 354 (1941).
[9] E. O. Lawrence, Phys. Rev. **28,** 947 (1926).
[10] P. M. S. Blackett, Proc. Cambridge Phil. Soc. **22,** 56 (1924).
[11] E. P. Wigner, Phys. Rev. **73,** 1002 (1948).
[12] G. H. Wannier, private communication.
[13] D. R. Bates, A. Fundaminsky, J. W. Leech, and H. S. W. Massey, Phil Trans. Roy. Soc. London [A] **243,** 93 (1950).
14] H. D. Hagstrum, Revs. Mod. Phys. **23,** 185 (1951).

27. Mass Spectrometer Effects at Higher Pressures

By Francis J. Norton [1]

There are some interesting effects to be observed at pressures higher than normal operating conditions in the mass spectrometer, and two will be discussed. One is the case of high partial pressure of hydrogen with another gas; and the other is high absolute pressure of a single gas.

The case of the hydrogen molecular ion, H_3^+, has been discussed in the literature in some detail. The ion formed by hydrogen and helium, HeH^+, has been investigated by Bainbridge,[2] Beach,[3] and Hiby.[4]

Not much has been reported on other molecular ions with hydrogen as a constituent.

The mass spectrometer used was the Nier type, 60° single focussing with 6 in. radius of curvature. It is made by the General Electric Company. The pressures given were measured on a DPI ion gage (type VGIA) at the tube exit, with argon calibration. The pressure in the ionizing region was about tenfold higher.

When argon-hydrogen mixtures are run, even with a few percent hydrogen, peak 41 appears, due to AH^+. The height of this relative to the argon 40 peak increases as the proportion of hydrogen increases (table 1).

TABLE 1. AH^+ *peak 41 behavior*

Argon	Hydrogen	Ion gage pressure	Peak 40	Peak 41
Percent	*Percent*	*mm*		
100	0		100	0.01
90	10	1.2×10^{-5}	100	.115
10	90	7.5×10^{-6}	100	1.65
0.75	99.25	6×10^{-6}	100	14.3
.04	99.96	2.5×10^{-5}	100	50

It will be observed that as large hydrogen excess is added, the 41 peak can go to large fractions of peak 40. There is an added effect of pressure as such, shown by the 0.75 percent argon in hydrogen mix (table 2).

TABLE 2. AH^+ *peak 41 in 0.75% argon, 99.25%* H_2

Ion gage pressure	Peak 40	Peak 41
mm		
5.0×10^{-5}	100	26
8.5×10^{-6}	100	16
6.0×10^{-6}	100	14.3
2.8×10^{-7}	100	8.5

---

[1] General Electric Research Laboratory, Schenectady, N. Y.

[2] K. T. Bainbridge, Phys. Rev. **43**, 103 (1933).

[3] J. Y. Beach, J. Chem. Phys. **4**, 353 (1936).

[4] J. W. Hiby, Ann. Phys. **34**, 473 (1939).

If deuterium gas is added to argon instead of hydrogen, peak 42 appears, AD^+, instead of 41.

Hydrogen excess will give this hydride ion with the other rare gases and with mercury. The situation with oxygen is more complicated and needs further work. Here as excess hydrogen is added, peaks 33 and 34 both increase, with 34 peak higher than 33, as though $O_2H_2^+$ were formed. At higher hydrogen pressures, peak 33, O_2H^+ is larger.

In the case of a single gas at high pressure going through the mass spectrometer tube, there is a most interesting appearance of a peak at double the mass of the normal peak. This effect was noted by Mattauch and was explained by him in a paper by Mattauch and Lichtblau.[5]

They give for the apparent mass M_B, the equation

$$M_B = \frac{M_1^2 \cdot No}{Mo \cdot N_1^2}$$

where No is the original charge on the molecule, N_1 is the final charge, Mo is the original mass and M_1 is the final mass. The peaks at double mass arise when an ion originally doubly charged loses one charge between the acceleration region and the magnetic deflexion region of the spectrometer. In the case of argon 40, for example, there is no change of mass, and if at high pressure where there are secondary electrons, A^{++} changes to A^+ in transit, then $M_1 = Mo = 40$, and $No = 2$, $N_1 = 1$ and

$$M_B = \frac{(40)^2 \times 2}{40 \times (1)^2} = 80$$

Hence, there will appear a peak at mass 80. Mattauch also showed that, due to magnetic fringing effects, this double mass peak should be displaced toward the lower masses. Figure 1 shows this for argon with a hydrocarbon background.

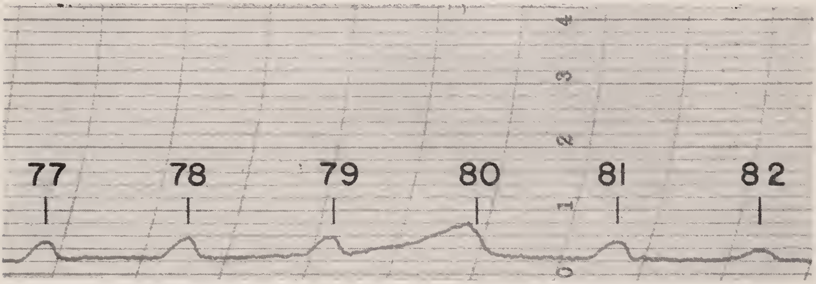

Figure 1. *Mass spectrum record showing the unsymetrical double mass 80 peak of argon.*

The pressure range for the appearance of peak 80 in argon is shown by table 3.

The fact that A^{++} is involved in the appearance of peak 80 is shown by the fact that as ionizing potential is changed, peak 80 abundance parallels A^{++} peak 20.

Peak 80 appears above the double ionization potential of argon, 27.76 volts, and below its triple ionization potential of 40.75 v.

---

[5] J. Mattauch and H. Lichtblau, Physik. Zeits. **40** 16 (1939).

TABLE 3. *Peak 80 in argon*

Pressure ion gage	Peak 80 current
mm	*amps.*
1.2×10^{-5}	23×10^{-13}
9.6×10^{-6}	14 "
5.0×10^{-6}	3 "
2.6×10^{-6}	1 "

To observe the mercury double mass peaks, a container holding mercury was connected directly to the mass spectrometer through a tube 100 cm long and 8 mm in diameter. Then by controlling the temperature of the liquid mercury its vapor pressure was controlled and known, and an estimate could be made of the pressure in the ion chamber at the end of the connecting tube. The height of peak 404 is given for these pressure conditions in table 4.

TABLE 4.

Temp. °C	Mercury equilibrium vapor pressure	H_g pressure in ion chamber	Ion gage pressure	Peak 404 positive ion current
	mm	*mm*	*mm*	*amps.*
25	2×10^{-3}	2×10^{-5}	4×10^{-6}	80×10^{-13}
0	2×10^{-4}	6×10^{-6}	6×10^{-7}	2×10^{-13}

Figure 2 shows the normal mercury isotope peaks 198–204 and the double mass peaks 396–408. There is a tapering off of this high mass group toward lower masses, and this extends over 10 or 12 mass units.

Similar double mass peaks were observed for N_2 in the mass 56 region at ion gage pressures of 2.5×10^{-5}, and for xenon in the same pressure range.

No double mass peaks were found for hydrogen or deuterium, and neon double mass is obscured by possible traces of argon.

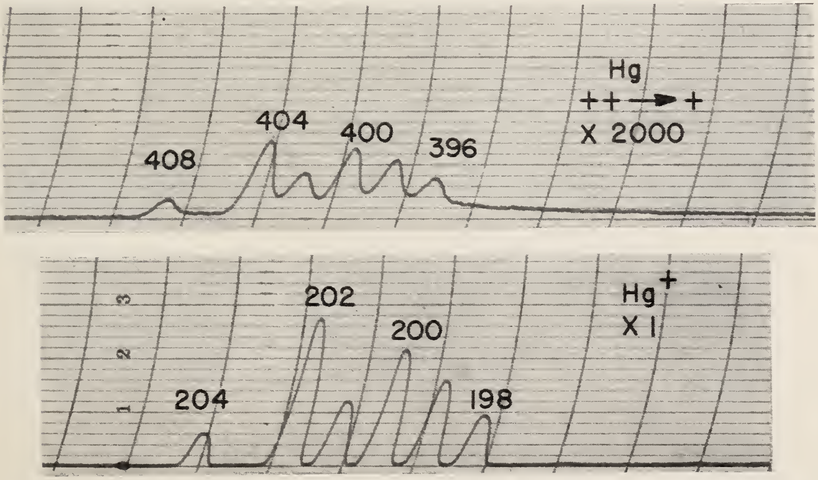

FIGURE 2. *Double mass peaks of Hg+ and of the double mass spectrum at a pressure of 10⁻³ mm.*

All of these double mass peaks occur at pressures where the normal peak height is departing from linearity with pressure, and at the region where the response starts back down with further pressure increase, about 10^{-4} to 10^{-3} mm ion gage pressure at tube outlet.

Discussion

M. G. Inghram: Facts similar to these have been studied in about three different laboratories. In addition to the effect which Norton suggests there is one other effect which we have observed and which Nier has worked with, this is the molecular state of argon.

For example, if you plot the intensity of the mass 80 peak, as a function of electron energy, it is a curve which rises to a sharp maximum a few volts above the threshold and if we plot the atomic argon, that curve rises less steeply to a flat maximum in the usual conventional curve which Dr. Hagstrum was talking about.

If we take an argon atom and bombard it with an electron, we get an excited state. This argon excited state upon collision with another argon atom, gives 80^+, plus an electron, which is the origin of the charge. All you need to do to get this mass is to put it in an excited state. In addition, the shape of this curve is about the shape of the curve that you would predict for the excitation function, to a P level. The final proof comes from using a mixture of argon 36 and argon 40 in equal parts. If it is a molecular peak the molecules will show peaks at twice the first mass which is 72, at the sum of two masses which is 76, and at 80. On the basis of Dr. Norton's suggestion you would not expect to see this, and the intensities of these for equal amounts is 1, 2 and 1, which are exactly what you would expect. The same thing carries over to xenon. The krypton does the same thing. You can get cross molecules with any of them. There are several other things which need study here. These complicate tremendously this type of spectrum.

F. J. Norton: I think the pressure distribution, if there is any differential pumping, will determine which one of these might appear. We had no differential pumping, and the argon and mercury in our case did not appear until we got up to the potential for double ionization. It appeared below the triple ionization potential.

Inghram: The change in charge from 2 to 1 does occur, but in this case if you bring it below the state where you can form the double charge you still get the mass 80 peak.

Norton: That did not occur in my case.

Question: That effect would be hidden when you have that much energy.

D. C. Hess: This would be swamped by the change of charge process. Also this is a function of pressure.

H. E. Duckworth: We have noticed that there is this trailing off that Dr. Norton mentioned. If the peak is symmetrical it would be A_2. If it trails off, it would be a change of charge.

28. Observation of Ion Dissociation in a Parabola Spectrograph

By A. Henglein and H. Ewald [1]

The primary ions coming from the ion source can undergo changes by dissociation and charge exchange on their way through the mass spectroscopic apparatus. The dissociations occur in part spontaneously without external influences. Certain types of primary ions may be formed in metastable states with life times of the order of magnitude of the time of flight of the ions through the apparatus. These processes were observed in 1946 by Hipple, Fox, and Condon in highly evacuated mass spectrometers, and they have been thoroughly examined since that time.

Secondary dissociation and charge exchange may also occur by collisions of the primary ions with residual gas molecules in the vacuum space. Hints of such processes were found as early as about 1915 in research with the parabola spectrograph. In the mass spectrographs of Aston, Dempster, Bainbridge and Jordan and of Mattauch and Herzog secondary ions formed in this manner were observed. Mattauch and Lichtblau have undertaken a very thorough examination of these processes.

If the dissociations occur in the field-free space between the electric field and the magnetic field of these apparatus, then the secondary fragment ions will be focused on the photographic plate. There they will give rise to lines which are somewhat diffuse and which may lie at fractional effective mass numbers. These effective mass numbers, M_{eff}, may be calculated from the following relation:

$$M_{\mathrm{eff}}=\frac{M_1^2}{M_0}\frac{n_0}{n_1^2}$$

where M_0 and n_0 give the mass and charge of the primary ions and M_1 and n_1 pertain to the secondary ions. It is an experimental fact that the collisions will occur without appreciable transfer of kinetic energy. The initial kinetic energy of the primary ion is distributed among the fragment ions in proportion to their masses. The collision itself does not change the direction of flight of the fragment ions but, in the dissociation, repelling forces of the fragments may give them energies of a few electron volts. In this manner small changes in the directions of flight of the ions may result.

We have found these dissociation processes can best be observed in a parabola spectrograph in combination with an electron impact ion source. We have constructed an ion source of the type described by A. E. Shaw (Phys. Rev. **75**, 1011, 1949). We tested this source with a parabola spectrograph built for this purpose (fig. 1). It is planned to make doublet measurements with this source on the precision mass spectrograph to study elements which cannot easily be studied with a canal-ray ion source.

---

[1] Max Planck Institute für Chemie, Mainz, Germany.

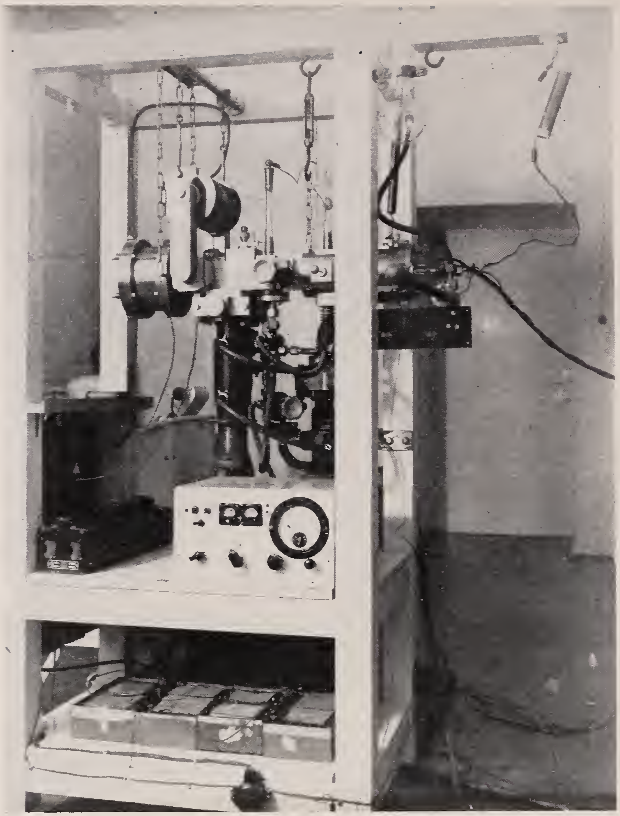

FIGURE 1. *Parabola mass spectrograph.*

An electron impact ion source gives ions very homogenous in energy as compared to the canal-ray tube. These ions of homogeneous energy but of different masses do not give rise to large segments of parabolas on the photographic plates but only to definite points on these which all correspond to the same deflections of the ions by the electric field. These points, called principal points, are observed with great intensity on the plates. Figure 2 shows these points all lying on the same abscissa X_0.

With increased pressure in the ion source and, therefore, in the whole apparatus, these points receive weaker prolongations in the direction of the parabolas. That means, that besides the primary ion formation in the ion source chamber an additional ion formation is initiated by secondary processes along the acceleration path of the ions. The ions so formed have less energy than the primary ones. Therefore, they reach points of the parabolas which correspond to greater deflections by the fields.

Furthermore, a great number of secondary points are observed with considerable intensity superposed on the weaker prolongations. They correspond to dissociations and charge exchanges which the primary ions undergo in the field-free space between the acceleration and deflection fields by collisions with gas molecules. The secondary ions

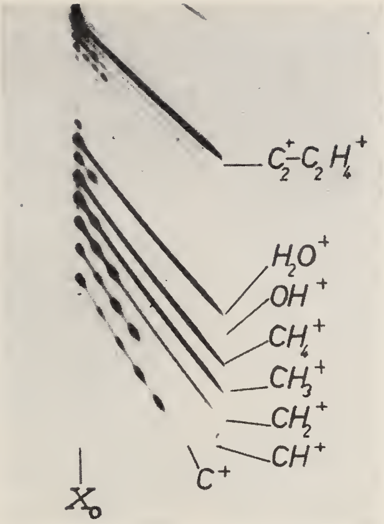

FIGURE 2. *Dissociation spectrum of components of illuminating gas.*

Abscissae give electric deflection and ordinates give magnetic deflection.

so formed have a smaller energy than the primary ones because the initial kinetic energy is distributed between the fragments in proportion to their masses. The deflection of such ions by the electric field is given by the relation

$$X_1 = X_0 \frac{M_0 n_1}{M_1 n_0}$$

where X_0 is the deflection for singly charged primary ions of mass M_0 and charge n_0, and M_1 and n_1 give the mass and charge of the secondary ions.

The results of Mattauch and Lichtblau can now be confirmed and extended in several directions by our parabola spectrograms, because they give directly from the position of the secondary points on the plates the true mass number and the energy of the secondary ions and from this we derive the processes of dissociation. It is found that every gaseous chemical compound has a characteristic dissociation pattern analogous to the well-known characteristic patterns of the organic molecules in mass spectrometry.

Figure 2 shows a part of the parabola spectrogram of the compounds of illuminating gas. The parabolas of mass numbers 12, 13, 14, 15 in addition to the principal points of deflection X_0 corresponding to the primary ions C^+, CH^+, CH_2^+ and CH_3^+, show respectively 4, 3, 2, and 1 secondary points. These points represent part of the dissociation pattern of methane. For instance, the C^+ ions which give rise to 4 secondary points on the mass-12 parabola are formed by dissociation from the primary ions CH^+, CH_2^+, CH_3^+, and CH_4^+

$$\begin{aligned} CH^+ &\rightarrow C^+ + H \\ CH_2^+ &\rightarrow C^+ + 2H \\ CH_3^+ &\rightarrow C^+ + 3H \\ CH_4^+ &\rightarrow C^+ + 4H \end{aligned}$$

The secondary point on the mass 17 parabola shows the formation of OH^+ from H_2O^+ primary ions. On the parabolas of mass numbers 24 to 28 are seen the dissociation points of ethylene.

Figure 3 gives the same dissociation group in pure ethylene. Figure 4 shows the dissociation of heavy hydrogen ions from heavy acetylene. These points come from the processes:

$$\begin{array}{cc} C_2D_2^+ \rightarrow D^+ + C_2D & X_1 = 14X_0 \\ DO^+ \rightarrow D^+ + O & X_1 = 9X_0 \\ CD^+ \rightarrow D^+ + C & X_1 = 7X_0 \end{array}$$

The D^+ ions from these processes have very small energies corresponding to their small masses. For instance, the energy is 1 to 2 kev in the first process.

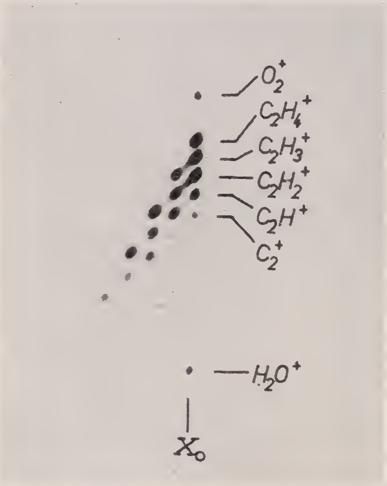

FIGURE 3. *The C_2 part of dissociation spectrum of ethylene.*

FIGURE 4. *Slow deuterium ions from C_2D_2.*

Figure 5 shows the pattern of carbon dioxide. In parentheses are given the primary ion followed by the secondary ion for each secondary point.

Figure 6 shows negative ions from the compounds of illuminating gas. There are negative products of dissociation and charge exchange from water and methane. Intensity ratios are strikingly different from those of the positive parabolas of figure 2. For instance, primary ions H_2O^- and presumably CH_4^- are absent.

Figure 7 shows negative ions from ethane and figure 8 those from ethyl chloride. The negative ions which are observed in astonishing variety have about a hundredth of the intensity of the positive ions.

Furthermore, there are ions which have been accelerated as doubly charged ions and then undergo charge exchange and dissociation by collision. If the secondary ions are singly charged, then they will acquire half of the electric deflection, $X_0/2$, of the primary singly charged ions. Charge exchange and dissociation here again give rise to extended groups of secondary points.

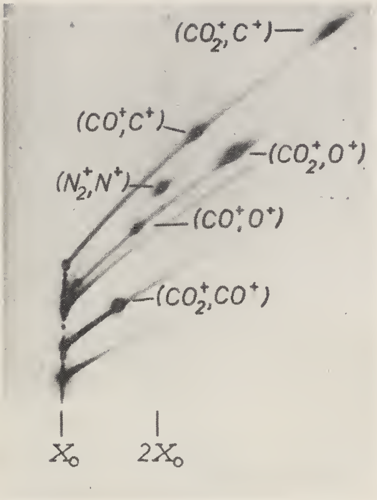

FIGURE 5. *Dissociation spectrum of CO_2.*

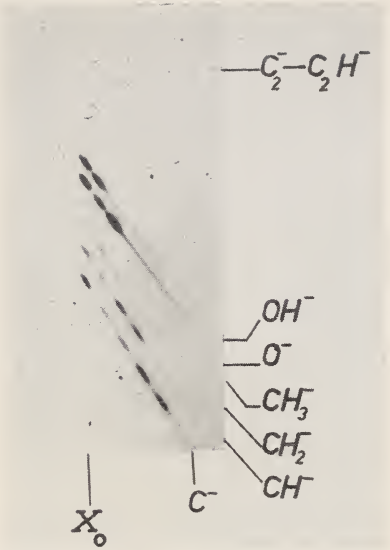

FIGURE 6. *Negative ions from illuminating gas.*

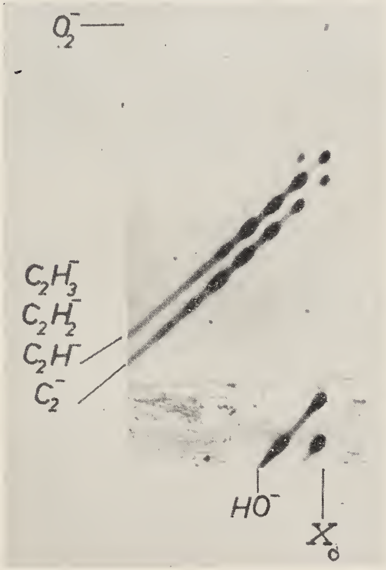

FIGURE 7. *Negative ions from ethane.*

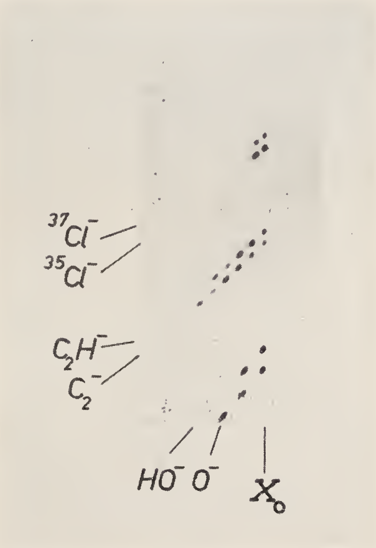

FIGURE 8. *Negative ions from C_2H_5Cl.*

Figure 9 shows singly charged fragment ions from doubly charged ethylene ions. A striking feature is the absence of three of the points showing that the ions C_2^{++} and C_2H^{++} are not formed primarily, but only the doubly charged ions with more than one hydrogen atom.

Figure 10 shows singly charged ions from doubly charged ethane ions. Again primary ions C_2^{++} and C_2H^{++} are not seen. Moreover, the doubly charged molecular ion $C_2H_6^{++}$ is not formed. The variation of intensity from point to point is noteworthy. From it one can deduce that primary doubly charged ions with an even number of hydrogen atoms are produced with greater intensity; a conclusion which has also been given by Mohler, Bloom, Lengel, and Wise from mass spectra.

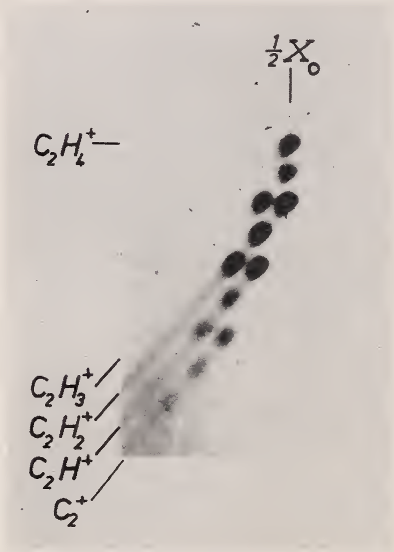

FIGURE 9. *Fragments from doubly charged ethylene ions.*

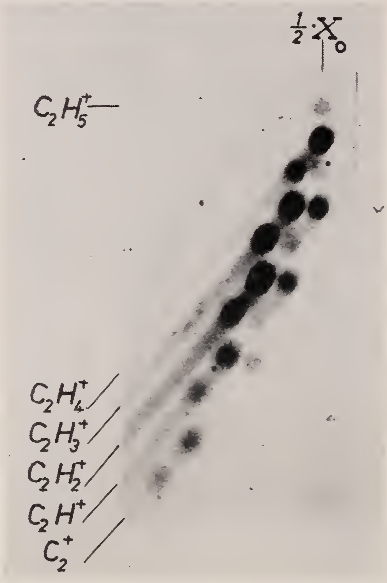

FIGURE 10. *Fragments from doubly charged ethane ions.*

29. Direct Measurement of Appearance Potential and Ionization Probability Using a Mass Spectrometer

By R. E. Fox, W. M. Hickam, T. Kjeldaas, Jr., and D. J. Grove [1]

Many studies [1–7] [2] have been made for determining the minimum energy of electrons capable of producing ionization in a particular gas and the manner in which the ionization cross section varies with the electron energy. A typical curve of such measurements showing the ion current observed as a function of electron accelerating voltage, in general, consists of a straight line portion with tailing near the appearance potential over an energy range of the order of 1.5 electron volts. A large part of the tailing has been attributed to the energy spread in the electron beam; this spread originating from thermal energies, voltage drop across the filament, space charge, contact potentials, and the cross field used for initial ion acceleration. Under the disturbing influence of these factors, it is difficult to determine the true ionization probability curve (P_i) near the appearance potential. Furthermore, a primary standard of known appearance potential is required for establishment of the electron energy scale. The work of Nottingham [8] on mercury clearly shows the many advantages to be gained when a nearly monoenergetic beam is used.

The method to be described enables measurement of ions formed in a field-free region by an electron beam monoenergetic within an arbitrarily small limit and of known energy. It provides an absolute measurement of appearance potential and a method for obtaining the P_i curve near the appearance potential. This is accomplished in part by the use of retarding potentials. In figure 1a is shown a

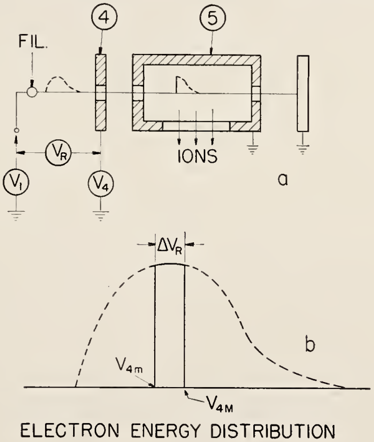

Figure 1. a. *Simplified electron gun illustrating the effect of the retarding potential in preventing low energy electrons from entering ionization chamber.* b. *Electron energy band of width* ΔV_R *utilized in obtaining the* P_i *curves.*

---

[1] Westinghouse Research Laboratories, East Pittsburgh, Pa.

[2] Figures in brackets indicate the literature references on p. 216.

simplified electron gun. Electrons leaving the filament are accelerated into the ionization enclosure by the potential V_i. The intermediate or retarding electrode is maintained at a negative potential with respect to the filament. This removes the low-energy electrons from the distribution and changes the original energy distribution to that shown in the ionization chamber. The minimum energy of the electrons in the ionization chamber is just eV_4. Since these electrons had near zero energy at the retarding electrode, this permits location of the electron energy scale. The difference in the observed ion current for the given distribution in the ionization chamber and that obtained when V_4 is changed by ΔV_R, keeping V_i fixed, is the ion current produced by the electrons within the ΔV_R band. In figure 1b is shown the electron energy band of energy spread ΔV_R which was selected from the original distribution to yield the difference ion current. Since the difference ion current is produced by electrons in a narrow energy band, one may for convenience think of the electrons as actually possessing this distribution. V_{4M} is the largest in absolute value of the two V_4 settings. V_{4m} is the smallest in absolute value of the two V_4 settings. If the difference in ion current is plotted versus V_{4M}, the current will go to zero at the appearance potential. It may be advantageous to use a-c voltage on the retarding electrode to provide the ΔV_R and thus permit measurement of the difference ion current with an a-c amplifier. At present d-c amplification is used. Since the energy scale is determined by the voltage between the retarding electrode and the ionization chamber, a contact potential between the filament and these electrodes would not influence the energy of the electrons responsible for the difference ion current. The electrode structure has been gold-plated to reduce or eliminate those contact potentials which could alter the results. Preliminary measurements have indicated no errors from this source.

Figure 2 illustrates the shape of the curve one would theoretically expect for a case where the ionization cross section varies linearly with energy. At values of V_{4M} greater than the appearance potential plus ΔV_R, one expects a linear curve. At smaller values, the curve is essentially parabolic since the difference-ion current is proportional

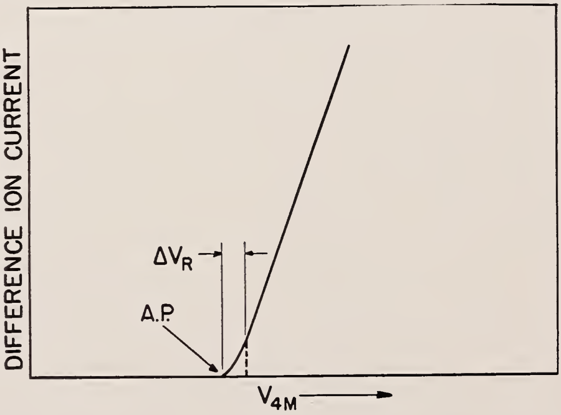

FIGURE 2. *Theoretical P_i curve for the case in which the ionization cross-section is a linear function of the electron energy and the electron energy band is of width* ΔV_R.

to the product of the number of electrons and the ionization cross-section. In the measurements to be described, ΔV_R was 0.1 v, and usually no points were taken inside the curved region. This amounts to extrapolation over the small region ΔV_R. It may be proven that this will give a value too high by ½ ΔV_R. To compensate for this, the experimental curves are plotted versus the average value of V_4 instead of the maximum.

Up to now, no mention has been made of the action of a retarding potential on the velocity component normal to the electron beam. If plane electrodes are used, the retarding potential alters the velocity component normal to the electrode and causes little change in the velocity component parallel to the electrode. Since a magnetic field is used for focusing the electrons, spiralling of the electrons takes place making possible an appreciable velocity component normal to the electron beam. A theoretical study shows that, if these large velocity components were present for the electrons in the ion chamber, tailing would be obtained on the ion difference curve comparable to one-half that obtained using the conventional method. Our measurements are in agreement with the theoretical curve obtained assuming no large transverse velocity component. Tailing is observed only over the interval ΔV_R as one would expect if the distribution in transverse velocity component is not significant. The general agreement of our results with the spectroscopic values indicates this component to be near zero. Possibly the multiple slit structure serves to reduce the transverse energy of the electrons entering the ionization chamber.

Conventionally an energy spread is introduced in the electron beam by the application of a cross field for accelerating the ions. Some workers have eliminated this effect by measuring the appearance potential as a function of the ion draw-out field and extrapolating to zero field [2]. Figure 3 is a schematic drawing of the electron gun used, showing the path of the electrons and the removal of ions from the ionization chamber. Electrons leaving the filament are accelerated by 3, retarded by 4, accelerated by 5, and collected by 6. Initial ion acceleration is accomplished by applying a potential between 5 and 7. To enable ion formation in a field-free region, a pulse generator capable of producing two synchronized pulses at a fixed repetition rate is used. The one pulse is applied to the electron retarding electrode 4 and the second pulse is applied to 7 for accelerating the ions. During the production of ions the pulse signals are zero; the condition of a field-free region in the ionization chamber is thus established. A negative voltage pulse is then applied to V_4 of such magnitude as to prevent all electrons from entering the ionization chamber. A fraction of a microsecond later, a positive pulse of shorter time duration is applied to 7 for ion removal. Requirements for accomplishing this are greatly simplified since the ion source is operated at ground potential in a manner described by Hipple, Fox, and Condon [9].

Another problem commonly encountered in this work is that of electron space charge yielding a potential depression. This factor is particularly serious in this application because of the slow velocity of the electrons in the vicinity of the retarding electrode. Figure 4 shows the shift found in the appearance potential associated with various total electron emissions. This curve has been used to correct for space charge in the preliminary data which will be shown. As further refinements are made, it is expected to improve the accuracy of this curve

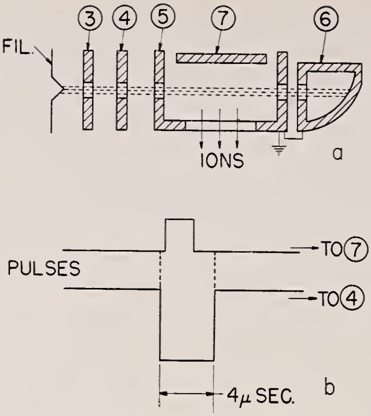

FIGURE 3. a. *Electron gun assembly.* b. *Pulses employed to insure that the ionization takes place in a field-free region.*

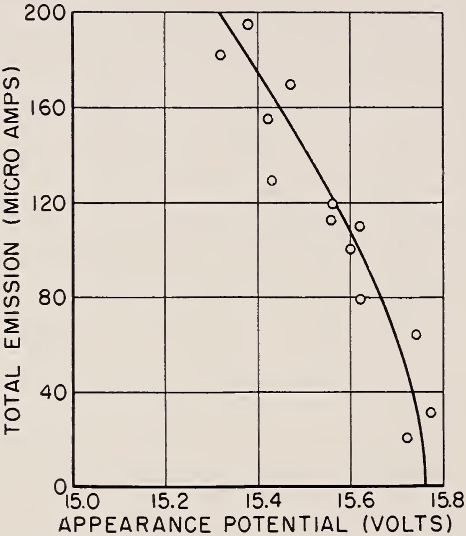

FIGURE 4. *Space charge effect on measured appearance potential of argon.*

and identify second order effects. Possibly, sufficient ion sensitivity can be obtained so that no significant correction will be necessary.

Included in the preliminary results obtained by the method described are the shape of the P_i curves near the appearance potential and the measured appearance potentials for argon (40^+), krypton (84^+), nitrogen (28^+), and carbon monoxide (28^+). First, let us examine the argon (40^+) curves shown in figure 5. Runs 1 and 2 are the ion currents observed by the conventional method using two different amplifier sensitivities. Run 3 demonstrates the improvement obtained by narrowing the energy spread of the electrons entering the ionization chamber. In run 4, ions are formed in a field-free region by an electron beam of narrow energy spread. This shows that the P_i

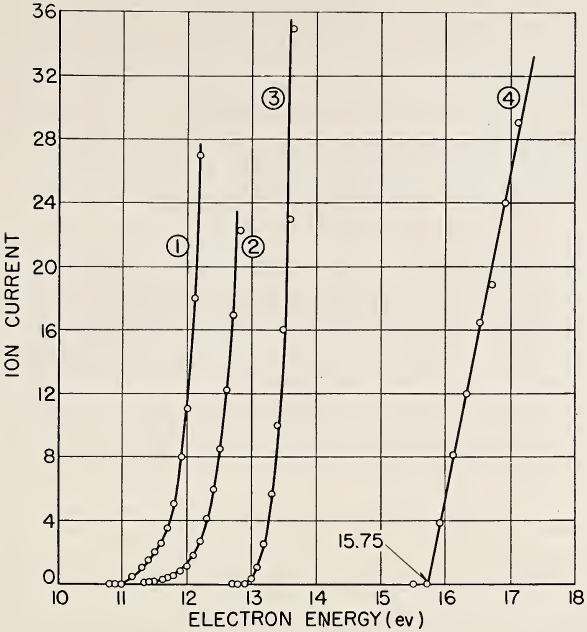

Figure 5. *Effect of electron energy spread on the observed shape of the ionization curve for argon 40^+.*

Run 1, Conventional method; run 2, Conventional method with 1/10 sensitivity; run 3, Using retarding on electrons but with ion-draw out field of 3 volts; run 4, Using retarding on electrons and pulsing fields on ions and electrons.

curve is essentially a straight line for argon near the appearance potential and yields an appearance potential of 15.75 v when corrected for space charge.

Similar curves were obtained for krypton (84^+), nitrogen (28^+), and carbon monoxide (28^+) and the measured appearance potentials as compared to the spectroscopic values are given in table 1. Some experimental curves for krypton indicated a slight break at 0.7 v above the appearance potential, which could be caused by the doublet ground state of this ion.

Table 1. *Observed appearance potentials and spectroscopic values of krypton, nitrogen and carbon monoxide.*

Ion	Appearance potential	Spectroscopic value
	Volts	*Volts*
Kr(84^+)	13.99	14.00
N_2(28^+)	15.51	15.58
CO(28^+)	13.92	14.01

The method outlined, as indicated by the preliminary results obtained, provides an approach to many problems which could not be answered when a large spread in electron energy was tolerated. We are at present making refinements with hopes of obtaining higher accuracy and are planning to study a large number of gases. Since the method provides measurement of ion formation by a nearly monoenergetic electron beam of high intensity, it should be possible to observe fine structure which has been overlooked in the past and to locate the fine structure to high accuracy. Establishment of the true P_i curves will do much to help evaluate the appearance potential methods used in the past.

The authors wish to acknowledge the contributions of Dr. T. Holstein in the development of the method presented.

[1] D. P. Stevenson and J. A. Hipple, Phys. Rev. **62,** 237 (1942).
[2] R. E. Honig, J. Chem. Phys. [2] **16,** 105 (Feb. 1948).
[3] J. J. Mitchell and F. F. Coleman, J. Chem. Phys. [1] **17,** 44 (Jan. 1949).
[4] H. D. Hagstrum, Phys. Rev. **72,** 947 (1947).
[5] Thomas Mariner and Walker Bleakney, Phys. Rev. [9] **72,** 807 (Nov. 1947).
[6] R. H. Vought, Phys. Rev. [2] **71,** 93 (Jan. 1947).
[7] V. H. Dibeler, J. Research NBS **38,** 329 (1947).
[8] W. B. Nottingham, Phys. Rev. **55,** 203 (Jan. 1939).
[9] J. A. Hipple, R. E. Fox, and E. U. Condon, Phys. Rev. [7 and 8] **69,** 347 (April 1 and 15, 1946).

30. Mass Spectra of Heavy Hydrocarbons

By M. J. O'Neal [1]

Analytical mass spectrometry has been successfully applied to the analysis of many light hydrocarbons and other low-boiling organic compounds. Its use has been entirely limited to materials exhibiting at least a small vapor pressure (about 0.5 mm) at room temperature. The low resolving power of most commercially available instruments, the lack of an adequate heated inlet system, and the anticipated complexity of spectral interpretation have been discouraging factors to the extension of the method to molecules above 200 molecular weight.

It was thought that if the experimental difficulties could be overcome, the mass spectra of higher molecular weight molecules would be of some value in the study of molecular structure. The possibility existed that spectral variation with molecular structure might be more systematized for heavier molecules than has been observed for the lighter ones.

A standard Consolidated model analytical mass spectrometer was modified in order to scan satisfactorily and resolve the mass scale up to about mass 600. The ion-slit and exit-slit widths were both decreased. The loss of sensitivity thus incurred was compensated for by increasing the amplifier sensitivity. The magnet coils were heavily insulated to withstand the higher temperatures accompanying continuous operation at higher magnet currents. Additional filter stages were added to increase the stability of the ion accelerating voltage, and the critical components of the magnet power supply were increased in size to supply the higher currents for the magnet.

The inlet system was of considerable importance. After considerable experimentation the inlet system design as shown in figure 1 was used. The apparatus consists of a glass vapor reservoir with a molten gallium Y-tube cut off isolating the pumping system from the inlet system. The gallium-covered sintered disk allows for sample introduction in the same manner that mercury-covered disks have been used. The entire sample introduction line is heated, including that portion inside the envelope up to the ionization chamber.

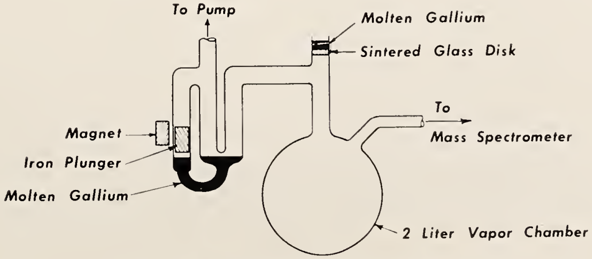

Figure 1. *Diagram of inlet system.*

---

[1] Shell Oil Company, Houston, Texas.

The resolution as obtained from the modified instrument is illustrated by a partial mass spectrum in the *m/e* 600 region of a heavy oil as shown in figure 2.

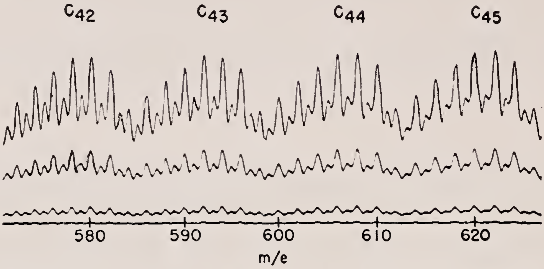

FIGURE 2. *Partial mass spectrum record of a heavy oil.*

The mass spectra of a few pure compounds will be shown in order to illustrate the type of dissociation mechanisms occurring under an electron impact. Figure 3 shows the mass spectrum of *n*-hexadecane in which relative intensities of the various ions produced under electron impact are shown relative to the mass scale. The mass spectra of the *n*-alkanes are very similar one to another in regard to type and intensity of the ions produced. In all cases a relatively large parent peak is obtained. Ions equivalent to "chain breaking" are small in the C_{15} and less region but gradually increase in intensity with decreasing carbon number. Very large ions are obtained in the region of C_2–C_6 with the maximum peak obtained at mass 57 or equivalent to the

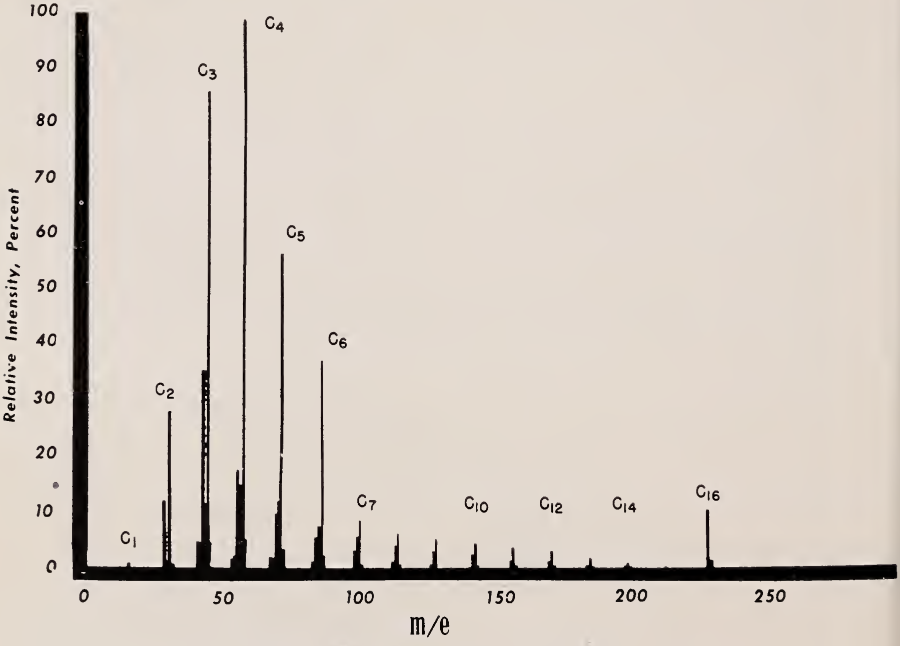

FIGURE 3. *Mass spectrum of n-hexadecane.*

butyl ion, $C_4H_9^+$. Figure 4 shows a comparative plot of all C_nH_{2n-1} fragments as well as the parent peaks for each of 3 *n*-alkanes: *n*-C_{16}, *n*-C_{24}, and *n*-C_{32}. The C_nH_{2n+1} relative intensities of these compounds are identical up to fragments within three carbon numbers of the parent compound. Thus, it becomes a simple matter to predict unknown spectra by constructing a family of curves relating relative intensities to carbon number for the various fragmentation peaks. The lower intensity peaks, C_nH_{2n}, C_nH_{2n-1}, C_nH_{2n-2}, etc., in the *n*-alkane spectra appear to increase in relative magnitude with the molecular weight of the compound.

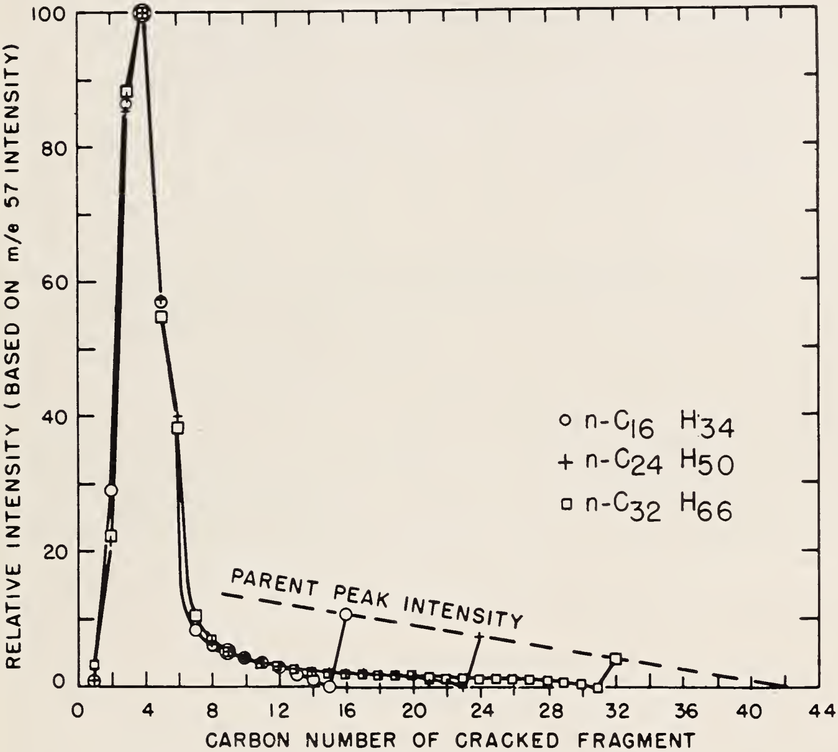

Figure 4. *Superimposed mass spectra of three n-paraffins.*

The mass spectra of isoalkanes have a general spectral appearance similar to that of normal alkanes with large peaks due to the fragmentation of the alkyl branches superimposed thereon. Figure 5 shows the spectrum of 7-*n*-propyltridecane. The parent peak of this compound is very small compared to that of *n*-hexadecane. Several interesting features in regard to fragmentation are apparent. As in the case of *n*-hexadecane, the largest peaks occur in the region of the C_4 fragment and decrease in intensity with increasing carbon number. However, two prominent peaks are noted in contrast to that of *n*-hexadecane, one at C_{10} due to loss of the C_6 alkyl fragment, and the other at C_{13} due to the loss of the C_3 alkyl branch. Thus, it is apparent that branching in a pure compound is easily detected from the dissociation pattern in the mass spectrometer. The mass spec-

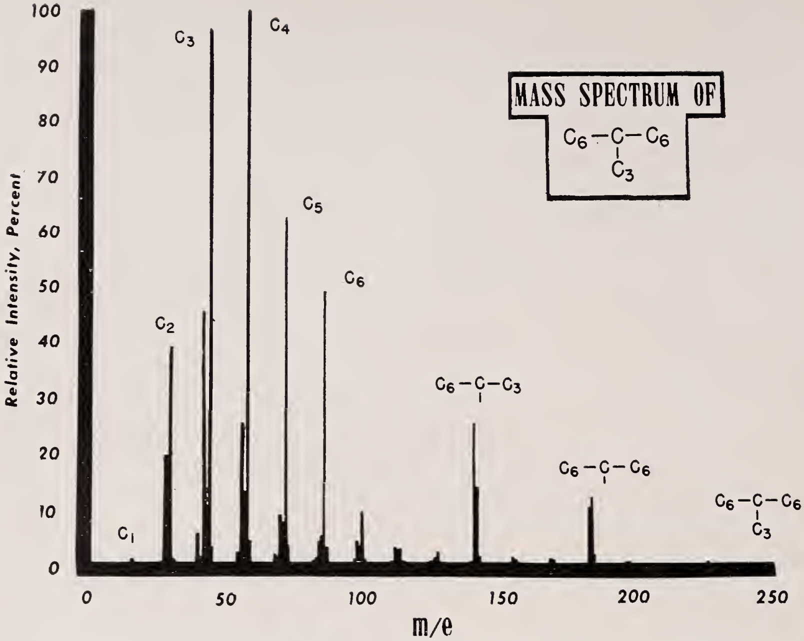

Figure 5. *Mass spectrum of 7-n-propyltridecane.*

trum of 5-cyclohexyleicosane is shown in figure 6. In addition to the basic saturate pattern as was shown for the normal and isoalkanes, large ion fragments are obtained due to the cyclohexyl ions. Large ions are produced due to the branching in the structure in the same manner as the isoalkane. The parent peak of this compound,

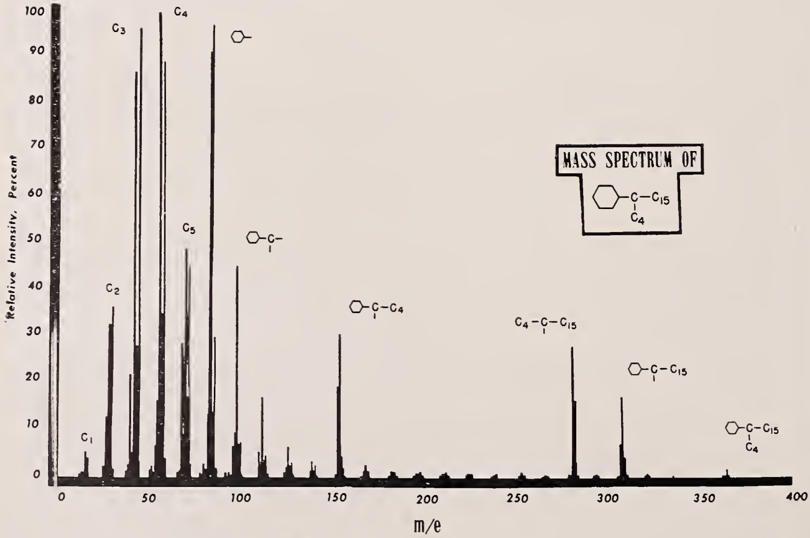

Figure 6. *Mass spectrum of 5-cyclohexyleicosane.*

although smaller than the corresponding n-alkane, is considerably larger than that of the corresponding isoalkane (n-hexyl group replacing the cyclohexyl ring). Although the parent peak intensity varies considerably depending upon the branching, in general the naphthenic compounds have larger parent peaks than the corresponding alkane of the same degree of chain branching.

Figure 7 shows the spectrum of a polyaromatic hydrocarbon. In this compound relatively few peaks are obtained compared to that of the nonaromatic compounds previously shown. A very large parent peak is obtained which is due to the highly aromatic nature of the molecule. In general aromatics have a greater intensity parent peak ion than the corresponding cycloalkyl derivitives. In addition, the parent peak sensitivity increases with the number of aromatic rings, assuming the same chain branching. The dissociation mechanism in aromatics is quite different from that of the cyclic naphthenes. In cycloalkyl rings the dissociation of alkyl substituents occurs at the ring, but in the aromatic molecules the break occurs on the carbon-carbon bond conjugated with the aromatic ring. Thus, in the spectrum of the molecule shown, the largest peak occurs at C_{19} which is the aromatic nucleus with one methylene group attached. No appreciable fragments are obtained in other ring splitting. As compared to the saturate compounds previously shown, only small peaks are obtained in the region of C_3 to C_4. The spectrum of this aromatic molecule is relatively simple although the structure is generally regarded as chemically complex.

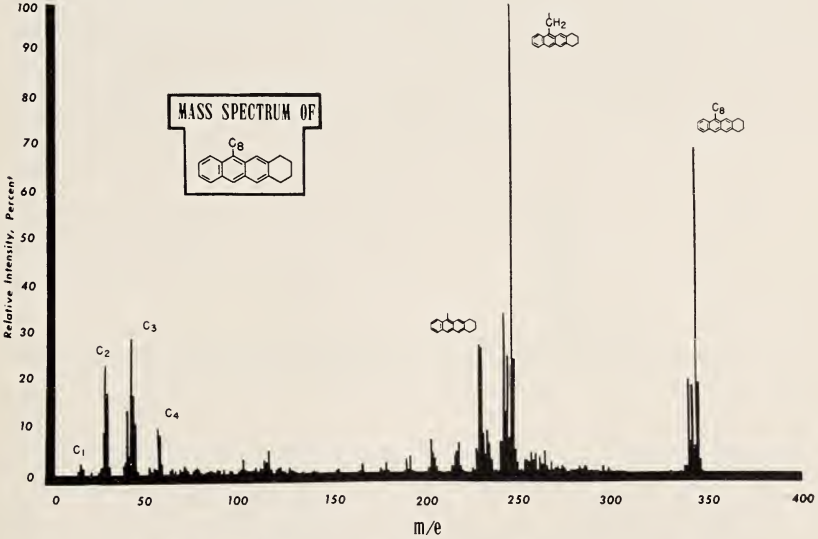

FIGURE 7. *Mass spectrum of a polyaromatic hydrocarbon.*

In the spectra just discussed, attention has been paid principally to the mechanism of the dissociation of the molecule under electron bombardment. Although simple molecular dissociation is quite an important feature of the spectra of heavy molecules, the molecular rearrangements that occur are also important and quite interesting. Some of the important fragmentation peaks of tricyclohexylmethane are shown in figure 8. The parent mass of this compound is at mass 262 and is quite small due to the branched nature of the molecule. The simple dissociation of a cyclohexyl ring will produce a large peak at mass 179 which shows up quite strongly in the spectrum. However, the loss of two cyclohexyl groups should produce a peak at mass 96 due to the ion containing a cyclohexyl ring with a C–H substitution.

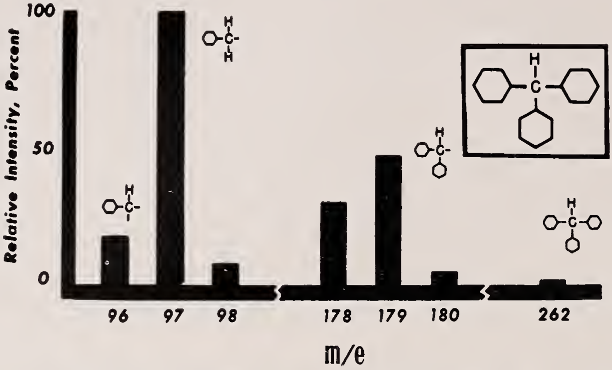

Figure 8. *Part of mass spectrum of tricyclohexylmethane showing the cycloalkyl rearrangements.*

Actually the peak at mass 96 is fairly small relative to the peak at mass 97, which is the largest peak in the spectrum. The only manner in which this peak can be explained is that hydrogen rearrangement produces a cyclohexyl ring with a CH_2 group substituted thereon. Thus the base peak in this spectrum can be explained only by the molecular rearrangement. A similar molecular rearrangement is noted in the spectrum of many aromatic molecules. Figure 9 shows the

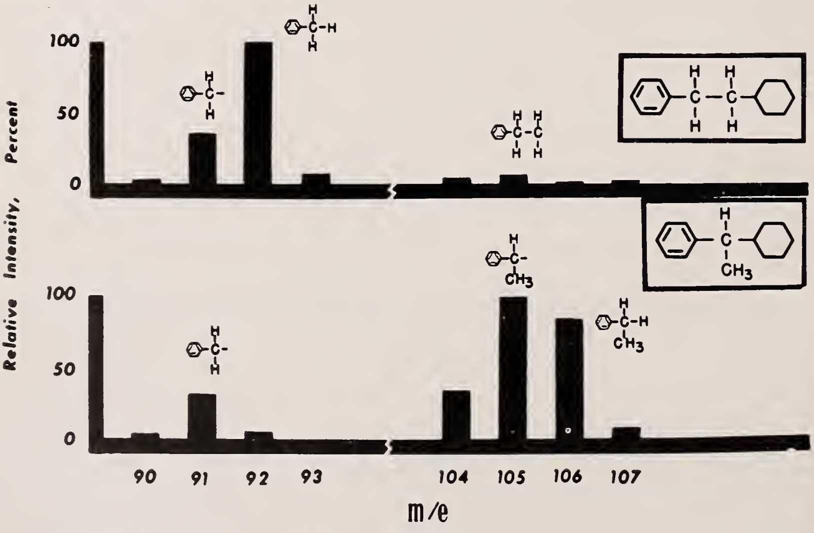

Figure 9. *Part of mass spectra of 1,2 phenylcyclohexylethane, and 1,1 phenylcyclohexylethane showing aromatic rearrangments.*

comparison of certain important peaks in the spectrum of two similar aromatic molecules. In the one case (1,2 phenylcyclohexylethane), an ion at mass 91 would indicate a simple dissociation between the carbon atoms of the ethyl group to produce an ion fragment containing an aromatic ring with a CH_2 attached. Although a peak is in evidence at mass 91, a still greater peak, in fact the largest peak in the spectrum, is obtained at mass 92. The mass 92 peak can be explained only by hydrogen rearrangement to produce an ion equivalent to methyl benzene. In the other case (1,1 phenylcyclohexylethane), a dissociation occurs not between the alkyl carbons but between the alkyl and cycloalkyl tertiary carbon atoms to produce ions in the mass 105 and 106 region. Here, a simple dissociation would produce a fragment at mass 105, which does occur and is the largest peak in the spectrum. However, a peak at mass 106 is obtained to the extent of 80 percent of the base peak. Again, such a peak can be explained only by a molecular rearrangement with a hydrogen atom becoming attached to the carbon which was previously attached to the cyclohexyl ring. These rearrangement peaks have been observed in practically all types of molecules: alkanes, cycloalkanes, and aromatics. However, the rearrangements generally occur in a very specific manner which can be predicted and utilized in many analytical applications.

In conclusion, it has been shown that the spectra of several heavy hydrocarbons indicate some interesting and useful relationships between the mass spectra and molecular structure. These relationships help to reduce the complexity of analytical mass spectroscopy as applied to heavier molecules, and the continued development of such techniques should materially improve the ability to define complex molecular structures.

31. Space Charge and Error in Mass Spectrometric Measurement

By E. W. Becker and W. Walcher [1]

The influence of space charge in a mass spectrometer has been investigated theoretically for special cases.[2] There is also a paper concerning this subject in sector shaped fields [3] as they are commonly used today (e. g., in the Nier type spectrometer) but that investigation deals with a ribbon shaped beam of infinite extension. Recently this computation was extended to finite beam extension. It was found that in isotope ion beams of 10^{-10} amp no influence of the space charge on the focusing properties is to be expected, whereas for currents larger than 10^{-9} amp the space charge becomes effective. Experiments confirm these theoretical results.

First a qualitative discussion of the space charge influence to be expected is given without detailed computations. A description of the experimental results follows and the errors produced by the space charge are presented. Detailed computations together with further results will be published in the Zeitschrift für Physik.

1. Discussion of the Space Charge Influence

In a customary mass spectrometer of the Nier type an image of the object slit M is formed by the sector shaped field II at M′ in figure 1, where the image forming bundle is represented by solid lines. For a bundle of infinite extension at right angles to the drawing plane, the image displacement can easily be found. In space I the paths of the ions are not straight lines any more, but they are parabolas. Their parameter is given by the field resulting from the space charge. The field can be characterized by a "space-charge-constant" k which is fundamental for all computations. The bundle entering the sector field appears to come from M_{I}. If the space charge in II and III had no effect on the particles, the image of slit M would be formed at M'_{I} rather than at M′. If we consider the space charge effect in II we get the image at M'_{II}. If, finally, we consider the space charge in III, then the ion paths are no longer straight lines but parabolas and we get the image of the slit or, strictly speaking, the cross section of least confusion at M'_{III}. The corresponding displacements $\Delta f'_{\mathrm{I}}$, $\Delta f'_{\mathrm{II}}$, and $\Delta f'_{\mathrm{III}}$ (fig. 1) can be evaluated relatively easily using the space charge constant k. The total displacement is the sum of these three partial displacements.

Corrections have to be applied to these calculations for the following reasons: The bundle is of finite extension; the bundle is, from the start, divergent in the direction perpendicular to the plane of the drawing. This divergency is increased by the space charge.

Further investigation is needed for the case of two isotopes of unequal abundance.

It can be shown that the above effects can be handled by the intro-

---

[1] University of Marburg, Marburg, Germany.

[2] L. P. Smith, W. E. Parkins, and A. T. Forrester, Phys. Rev. 72, 989 (1947). C. F. Robinson, Rev. Sci. Instruments 20, 745 (1949).

[3] W. Walcher, Z. Physik 121, 719 (1943).

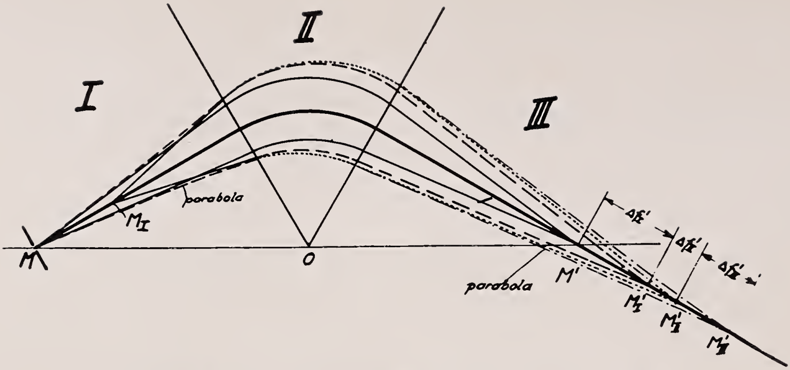

FIGURE 1. *Image displacement due to space charge.*

duction of an effective space charge constant k_{eff} instead of k. The value of the effective space charge constant will be smaller than that of k, since with a rectangular beam cross section part of the lines of force leave the side walls. It decreases in the direction of beam propagation, since the space charge decreases on account of the lateral divergence. The net effect of all these corrections is a diminution of the image displacements $\Delta f'$ previously mentioned.

If the beam contains isotope ions they are split up in the sector field into separate beams. With isotopes of different abundance we get different current intensities and the space charge effect in the separate beams is different, which means that the image displacements are different.

To sum up, we get the following effects of the space charge: With a fixed collector slit, as in most mass spectrometers, we find a greater line width and a lower peak intensity, i. e., we get a lower resolution. Since with isotope bundles of unequal intensity the shape of the lines is changed in a different manner for the two isotopes, there is an error in the relative abundance.

2. Experimental Setup

For examining the space charge effects a mass spectrometer as shown in figure 2 was used.[4] It was operated with argon (^{36}A=0.34%, ^{40}A=99.6%) at an acceleration voltage of 1,350 volts. The magnet could be moved along its line of symmetry and the displacement P (see fig. 2) was measured relative to a reference point. For testing the above considerations two experiments had to be done: (1). The shift of the image M'_{III} with increasing bundle intensity had to be proved; (2) the changing of the measured value of the relative abundance with increasing bundle intensity had to be proved.

The location of the image was determined by measuring the line width (fig. 3 and 4). For this purpose the line was moved across the collector slit by means of small variation ΔU_B of the acceleration voltage U_B at different positions of the magnet. For each position the line width at ⅕ of the peak value was measured. In figures 3 and 4 these line widths expressed in terms of $\Delta U_B/U_B$ are plotted against the position of the magnet. The minimum of the resulting curve corresponds to the location of the image.

---

[4] E. W. Becker, E. Dörnenburg, and W. Walcher, Z. angew. Phys. **2**, 261 (1950).

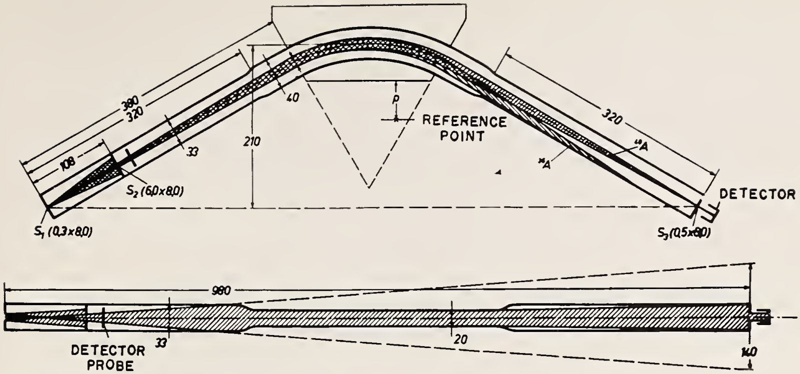

Figure 2. *Experimental arrangement for investigating the effect of space charge.*

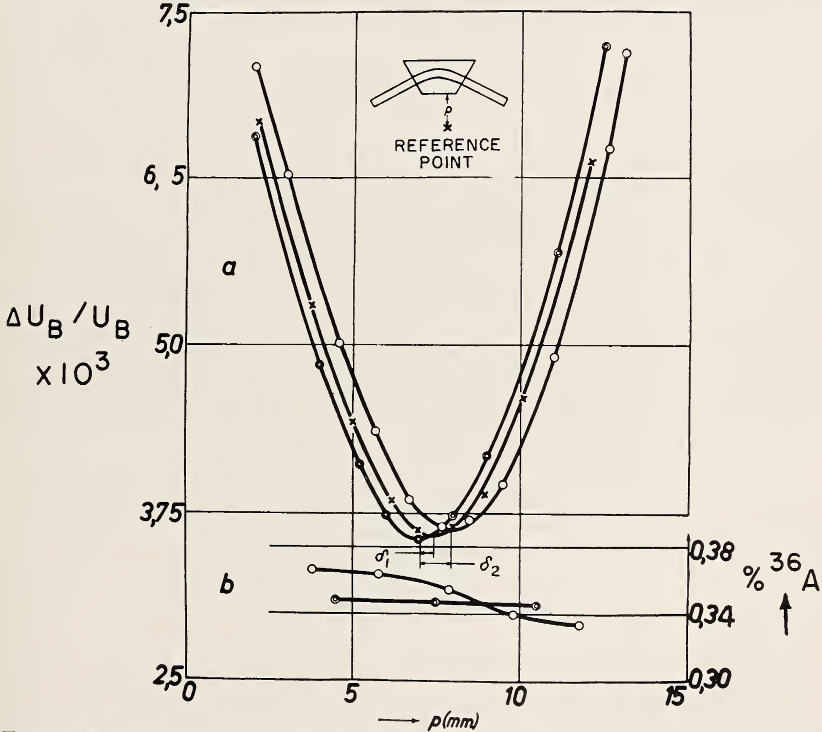

Figure 3. (a) *Relative line widths versus* p *showing the displacement of image due to space charge.* (b) *Effect of space charge on measured abundance of* A^{36}.

For testing the geometry of the beam a testing collector was mounted behind slit S_2 (fig. 2). The current measured at this point was 17.5 times the current through the collector as it should be in accordance with geometry, as illustrated in figure 2.

3. Measurements

The result of the measurements is given in figure 3. The curve with double circles corresponds to a collector current of 4×10^{-10}

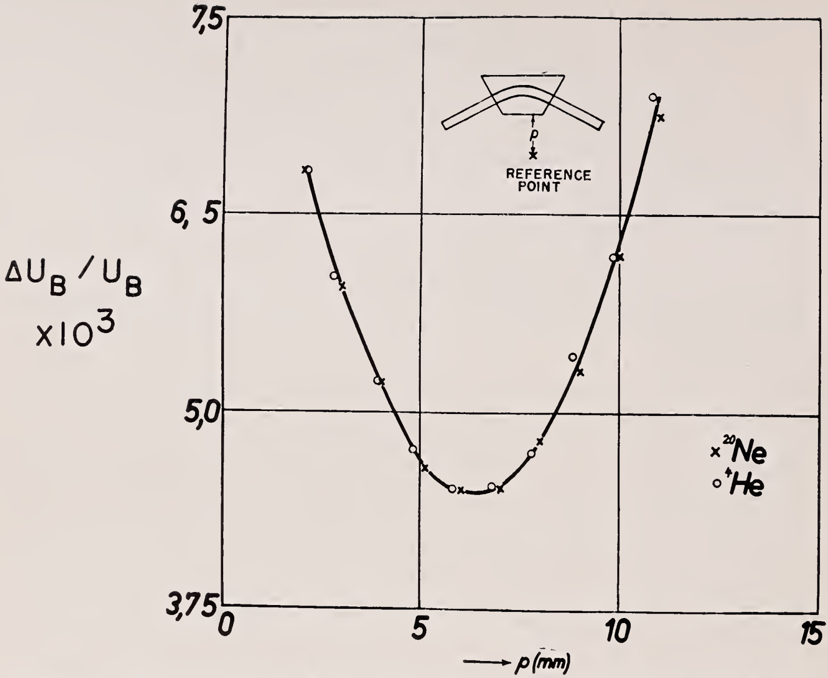

FIGURE 4. *The image for* Ne^{20} *and* He^4 *coincide, demonstrating that there is no mass aberration.*

amp (behind slit S_2 7×10^{-9} amp), the one with crosses to 2×10^{-9} amp and the one with single circles to 1×10^{-8} amp. It can be seen from figure 3a that the minimum of the curves moves to the right with increasing current intensity, which corresponds to an increasing image distance.

In figure 3b the values of the relative abundance, as measured at different currents, are also given. At a collector current of 4×10^{-10} amp the relative abundance is independent of the position of the magnet, whereas at 10^{-8} the obtained values vary up to 10 percent with the position of the magnet. The relative abundance was measured as the ratio of peak heights with an opening of 0.5 mm at the collector slit.

Finally, we want to show that the dependence of the relative abundance on the position of the magnet, as represented in figure 3b, does not originate from an effect that is produced by the different masses of the isotopes. For this purpose the image position curves were measured for ^{20}Ne and ^{4}He. Figure 4 shows that they coincide within the experimental error. It should be pointed out that there are circumstances under which these curves do not coincide, i. e., the mass spectrometer has a mass aberration. This will be the subject of another paper.

4. Discussion

L. T. ALDRICH: Is there any discussion?

A. E. CAMERON: Mr. Chairman, I was very interested in this because about five or six years ago I attempted to calculate this. We concluded we were safe at 10^{-10}, and I am glad to see that confirmed.

32. Mass Spectrometric Studies in Solids

By R. H. Plumlee [1]

The interest in mass spectrometry at RCA is derived from the application of mass spectrometric techniques to the study of electronically active surfaces and solids. Materials such as photo-surfaces, secondary emitters, and thermionic emitters must in general be studied in a high vacuum environment and hence are, in principle, well suited to examination via the mass spectrometer. Surface analyses of these materials detecting as little as one thousandth of a monolayer and bulk analyses detecting as little as one part in 10^8 are desirable. The experiments which we have performed thus far, though loosely aimed at developing techniques for performing such analyses, are best described as employing the spectrometer to detect or produce small changes in the composition of such sample materials.

There were indications from various sources at the time our project was begun, that electron bombardment might be a useful tool for stripping off surface monolayers for mass spectrometric analysis. Accordingly a series of experiments (summarized last year [2]) was conducted. They disclosed no detectable erosion of targets of (BaSrCa)O, ZnO, and several metals by incident electrons having energies as high as 1,400 v, the maximum employed. Whereas gas molecules offer cross sections of about 10^{-16} cm^2 for electron impact ionization, all targets tested showed erosion cross sections not larger than 10^{-23} cm^2, the minimum detectable. From these experiments it was concluded that electron bombardment does not, in general, give sufficient erosion and material transport from solids to be a useful analytical tool.

There were found, however, specific cases of substantial erosion produced by electron bombardment. All those noticed were of the category of foreign contaminant elements being stripped off metal substrates. The most prominent example of this category was the removal of O^+ ions from a presumably clean Mo target. Figure 1 shows a decay-recovery sequence for this erosion, the O^+ ions formed by the bombarding beam being drawn directly through the spectrometer. With the bombarding beam biased off, the sample recovered quickly so that a large O^+ peak height could always be produced after a short period of no bombardment. The same data are replotted on a semi-log scale in figure 2. The two straight-line portions of each decay curve indicate two separate rate processes (both first order) with half-lives of about one minute and 20 minutes. From data for other sample temperatures, it was found (1) that the half-lives for both processes were temperature independent, (2) that the peak height increased with temperature as shown in figure 3, and (3) that the peak height increase at high temperature was due to the increase in the contribution from the fast-decay type of oxygen sites.

---

[1] RCA Laboratories, Princeton, N. J.

[2] J. Applied Phys. 21, 811-819 (1950).

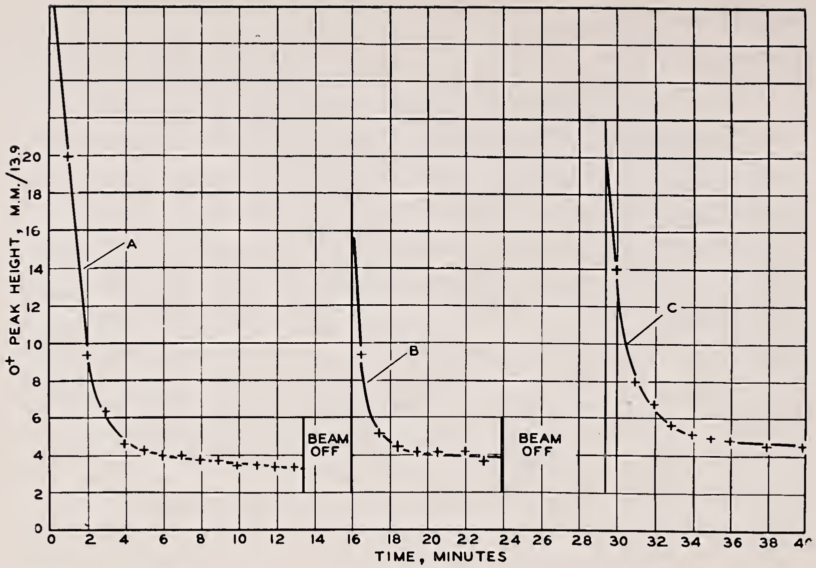

FIGURE 1. *O^+ from Mo by electron bombardment (4 ma/cm ^{2}, 300 v) (1473° K) decay-recovery sequence.*

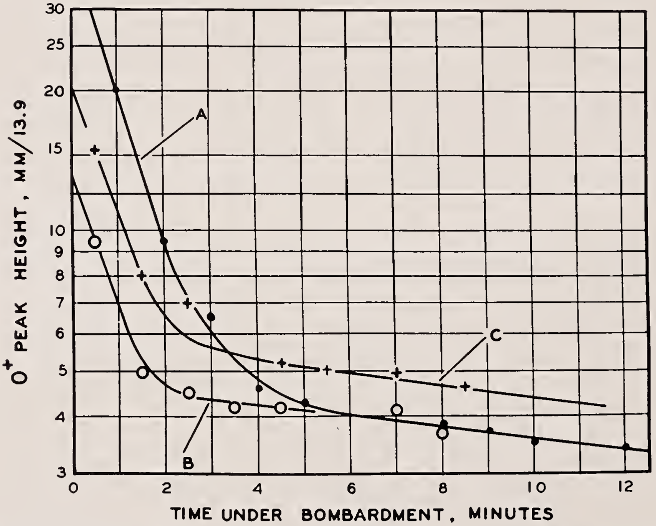

FIGURE 2. *O^+ from Mo by electron bombardment (4 ma/cm ^{2}, 300 v) decay sequence at 1473° K.*

In this experiment the current density of particles eroded was very much smaller than that of the bombarding beam. This condition together with that of temperature independent half-lives allows the conclusion that the increase in yield (O^+ peak height) with temperature could result only from an increased number of removable oxygen sites.

The fraction of Mo sites covered by removable oxygen was then computed to be about 10^{-6} at 1,000° K and 10^{-4} at 1,475° K for the

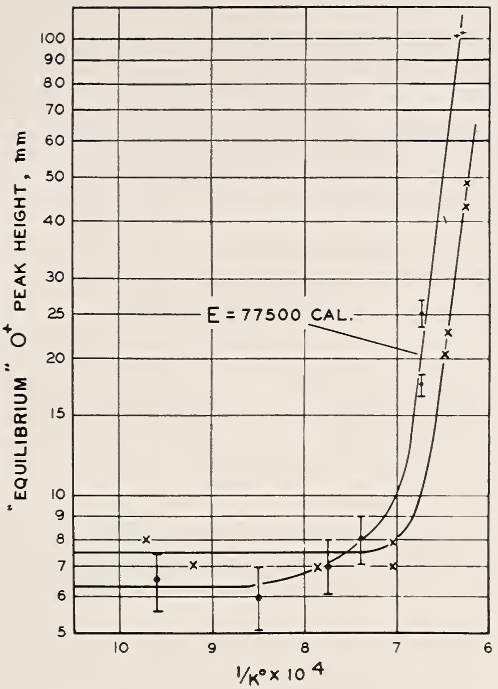

Figure 3. *O^+ from Mo by electron bombardment (4 ma/cm^2, 300 v).*

fast decay type of oxygen sites. For the slow decay type of oxygen sites, the fractional coverage was about 10^{-5} and temperature independent. The erosion cross section was computed to be 10^{-18} cm^2 for the fast-decay type and 10^{-20} cm^2 for the slow-decay type.

Without speculation about the circumstances in the vacuum system which will produce such oxygen sites on the Mo, these results are presented as an example of the type of information which may be obtained by bombardment experiments conducted in the spectrometer, the spectrometer serving merely as a sensitive device for detecting the composition changes produced by the bombardment.

We expect to continue making some electron bombardment studies of targets of practical interest to the electronics industry and hope to improve somewhat the instrumental sensitivity for detecting bombardment induced erosion. The biggest impediment to obtaining higher sensitivity in these experiments is the miscellaneous background spectrum. More refined processing of analyzer and sample components before assembly of the ion source can be expected to give some improvement. In addition we have started development of an analyzer tube with high current electron guns on side arms so that the heater power is dissipated in areas remote from the sample. This allows, if needed, differential pumping so that material evolved from the guns does not clutter up the sample region. However, a model having only one electron gun has been constructed and operated. The electron beam was focused and alined by solenoids rather than an iron magnet. Ionizing electron beam currents of several milliamperes (at current densities around 100 ma/cm^2) were obtained across the source region. Figure 4 shows a schematic diagram of the source end of another tube under construction. The sample holder and guns are made "demountable" by induction heating of the kovar rings to facilitate the sealing and opening procedures. This general design allows also the use of schemes for mounting several samples on a movable wheel so that they may be compared directly during and after controlled processing schedules.

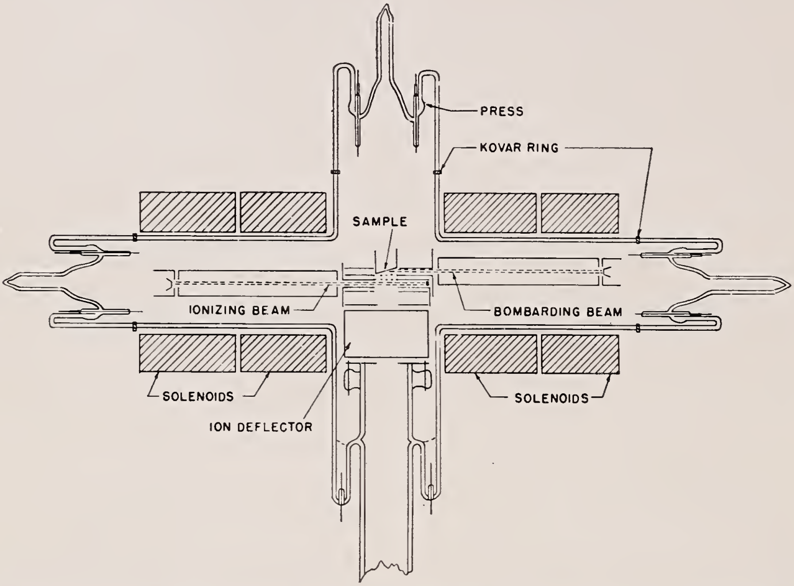

FIGURE 4. *Schematic diagram of mass spectrometer ion source for bombardment erosion of solids.*

The experiments thus far described have all employed electron bombardment as an eroding agent. The use of positive ions rather than electrons to sputter off surface material is now being undertaken by R. E. Honig in our laboratories.

For this purpose he has designed an experiment employing the double 180° analyzer shown in figure 5. Ions are formed in one analyzer by a suitable source, accelerated, then separated and directed against the target sample to be studied. Sputtered material, whether neutrals, ions, or both, is then analyzed in the second analyzer. Whether an analytical tool for the complete analysis of surfaces will result remains to be seen. In any event, considerable information about the nature of sputtering processes should be derived from these experiments, and this will be of interest in itself.

Another type of experiment which we have under way employs the spectrometer as a separator for depositing known chemical species on prepared sample targets. For the first experiment an oxide cathode has been selected as a target and placed behind the exit slit of the analyzer as in figure 6 so that it can collect the separated beams. The sample is indirectly heated and both front and back surfaces are coated. While the front surface is exposed to the ion beam, the rear surface is utilized as the cathode of a reference diode. Platinum

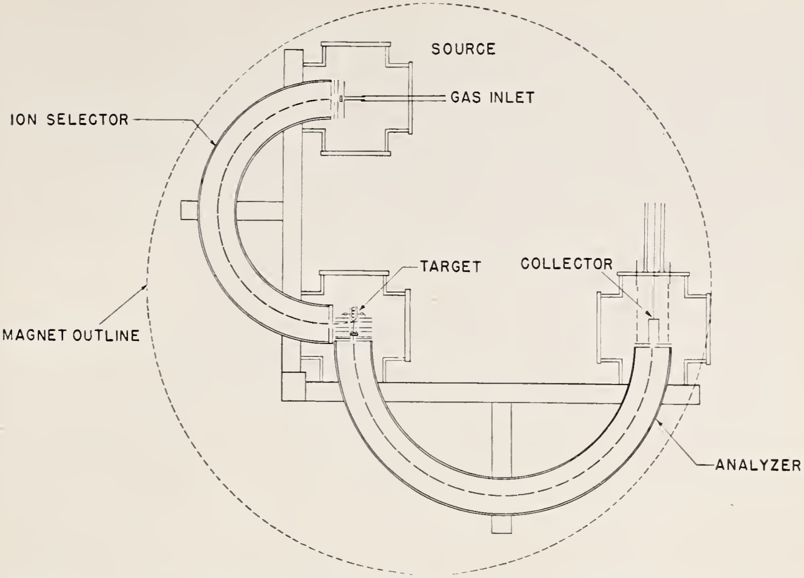

FIGURE 5. *Schematic of proposed spectrometer for the bombardment of solids by positive ions.*

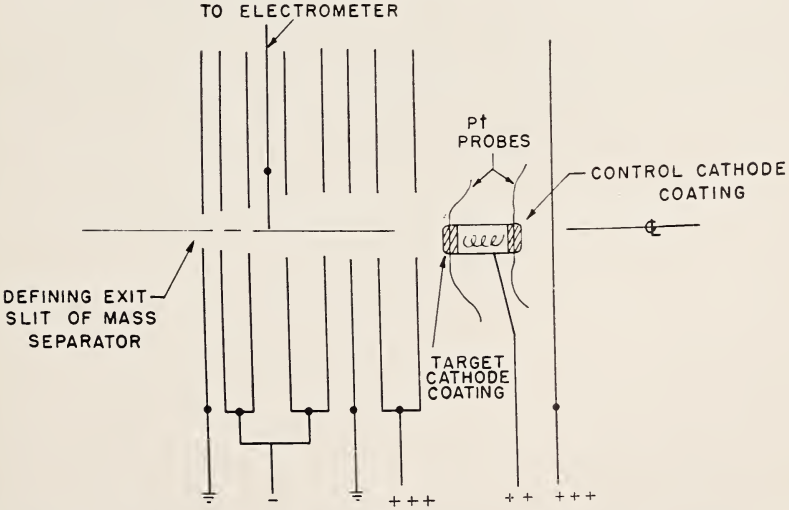

FIGURE 6. *Schematic receiver assembly for selective deposition of poisoning and activating agents on sensitive surfaces.*

probes are buried in the coatings to measure the potential distribution and resistance of the coatings. Electron emission and coating resistance can then be measured as functions of the kind and amount of activating or poisoning agent deposited by the analyzer.

This experiment is being undertaken in collaboration with L. S. Nergaard and R. M. Matheson whose measurements on thermionic emission suggested its practicability. They found indications that cathodes are activated when exposed to what is presumed to be Ba vapor at a partial pressure of about 10^{-12} mm produced by a simple evaporator. The question was raised whether Ba is the sole activating agent. For a target of .05 cm.^{2} it is computed that an analyzer ion current of 10^{-16} ampere would give the same deposition rate as direct exposure of the target to a Ba vapor pressure environment of 10^{-12} mm. It is thus apparent that an ordinary mass spectrometer can be used for depositing known quantities of specific poisoning and activating agents on such sensitive surfaces. Until we have completed the experiment, however, we will not know whether the target is actually as sensitive as preliminary measurements indicate.[3]

Discussion

J. Koch: Did I understand you correctly that this solid surface analysis had not been made as yet? (Fig. 5.)

R. H. Plumlee: No, it is in the process of being geared up.

Koch: Don't you think it would be very difficult to analyze because of the energy distribution of the eroded particles? Possibly a Thompson parabola instrument would be better if the intensities are large enough.

Plumlee: That may well turn out to be the case, but there is some information in the literature which indicates that this material has a characteristic temperature of the order of 1,000° K. If you are right, however, we will have to do something else. That is one reason the analyzer is designed this way, so we can actually measure the distribution of energies of this material as well as its mass numbers.

---

[3] Note added in proof: Confirming results of this completed experiment have been described in part in a paper by Nergaard, Plumlee, and Matheson in the Report, Twelfth Annual Conference on Physical Electronics, March 27–29, 1952, Mass. Inst. Tech., p. 38–46.

33. The Distribution of S^{34} in Nature

By H. G. Thode and J. Macnamara [1]

1. Introduction

It has been known for some little time that the isotopes of the elements differ in their chemical properties. In the mid-thirties Professor Urey [1a] and his coworkers showed that these differences did exist and demonstrated that the isotopes of the light elements could be separated by chemical means. Since isotopes do differ in their chemical properties one would expect isotope fractionation in chemical reactions, whether in the laboratory or in naturally occurring processes.

Actually, wide variations in the abundances of the isotopes have been reported. A study of these variations provides a means for tracing out reactions or processes, which occurred in nature many millions of years ago. Investigations in our laboratory in the past three years have shown that relatively large variations in the abundances of the sulfur isotopes occur in sulfur samples of terrestrial origin.[2] On the basis of this evidence, it is reasonable to assume that fractionation of the sulfur isotopes has occurred in natural biological and geological processes owing to differences in the chemical and physical properties of isotopic sulfur compounds.

Figure 1 shows the distribution of S^{34} in nature. This diagram represents an accumulation of data obtained over a period of several years. It is seen that the S^{34} concentration varies by as much as 7 percent, depending on the source of the sulfur. There are a number of interesting features about this distribution of the sulfur isotopes in nature. Although the isotopic concentration varies for each group of samples, over a certain range, it is seen that, in general, sulfates are enriched in S^{34} whereas sulfides and hydrogen sulfide samples are depleted in the heavy isotope. The S^{34} concentration varies over a wide range in samples of pyrite collected from different parts of the earth. It is interesting to note, however, that one pyrite sample differed widely from all others. It was found that this sample had been procured from the Franklin New Jersey furnace, an unique deposit in which are found some ten or twelve minerals not found anywhere else in the world. As this sample has a S^{34} content, very nearly that of the most enriched sulfate, one might conclude that this pyrite was formed at high temperature under reducing conditions by the reduction of secondary deposits of sulfate.

2. Meteoritic Sulfur

Some twelve samples of meteorites collected from different parts of the earth and involving both iron and nickel and stony meteorites were examined.[3] These samples were found to have identical isotopic

---

[1] Hamilton College, McMaster University, Canada.

[1a] H. C. Urey and L. J. Greiff, J. Am. Chem. Soc. **57**, 321 (1935).

[2] H. G. Thode, J. Macnamara, and C. B. Collins, Can. J. Research **B27**, 361 (1949).

[3] J. Macnamara and H. G. Thode, Phys. Rev. **78**, 307 (1950).

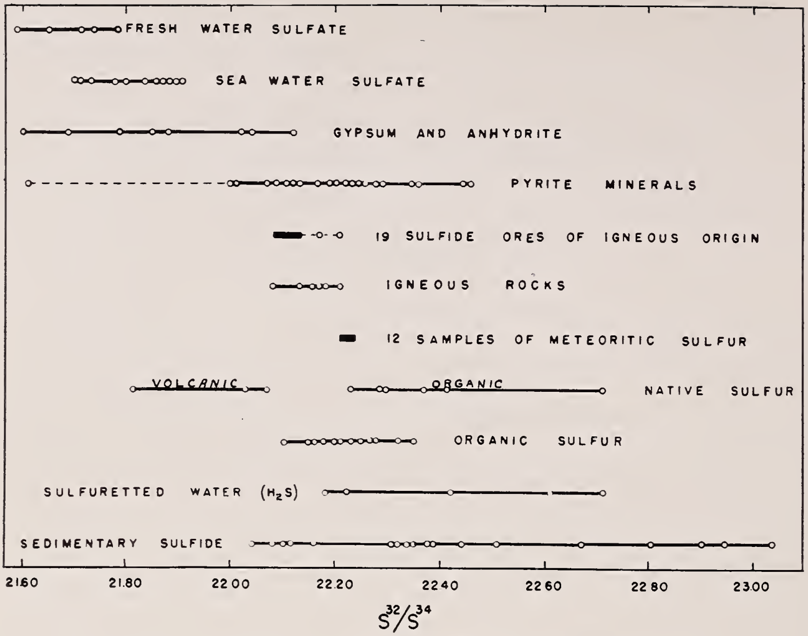

FIGURE 1. *Distribution of S^{34} in terrestrial and meteoritic sulfur.*

ratios. The small spread in concentration shown on the diagram is indicative of the fluctuations obtained from day to day. Actually, it was found that when the precision was increased on any one day the spread between samples was even less than that shown. These results indicate little or no variation in the abundances of the sulfur isotopes from meteoritic origin. This is a striking contrast to the wide variation found by Professor Nier in the abundances of the carbon isotopes from meteoritic samples.[4]

A comparison of the isotopic ratios obtained for meteoritic and terrestrial sulfur illustrated in figure 1, suggests that at the time the earth was formed the isotopic content of sulfur was the same as that now found from meteoritic sulfur, but that fractionation has occurred since in biological and geological processes thereby spreading out the ratios above and below the base value. The remarkably constant isotopic ratios found for meteorites, however, indicate that meteoritic sulfur has not been subjected to the same fractionation processes as have sulfur samples of terrestrial origin.

3. Igneous Sulfur

Igneous sulfur is probably the nearest that we can come to sulfur which has been unaltered isotopically since the formation of the earth's crust. Both igneous rocks and sulfides of igneous origin have been investigated. It is seen from figure 1 that the isotopic composition of igneous sulfur is constant within 0.5 percent and that the S^{32}/S^{34} ratios agree more closely with the value found for meteoritic sulfur than that of the sulfur in any other group. Since the sulfur

---

[4] B. F. Murphey and A. O. Nier, Phys. Rev. **59**, 771 (1941).

in igneous rocks accounts for the greater part of igneous sulfur, one might expect that its isotopic content would remain essentially unchanged from the primordial abundance and probably have an isotopic ratio very nearly the same as that for meteoritic sulfur. Of the six samples investigated, the isotopic ratios of five agree within 0.2 percent and the values overlap with those for meteoritic sulfur. The close agreement between S^{32}/S^{34} ratios for the sulfur in igneous rocks and meteorites is further evidence in favor of the theory that meteorites and the earth had common origin. In this connection H. C. Urey has found that the isotopic compositions of igneous and meteoritic oxygen are identical.

4. Theoretical Considerations

It is clear from theoretical and experimental evidence that the variations in the abundances of the sulfur isotopes are due to fractionation that occurs in biological and geological processes due to differences in the chemical properties of isotopic molecules. Using the well-known methods of statistical mechanics, equilibrium constants for many isotopic exchange reactions involving sulfur have been calculated.[5] The results of these calculations are given in table 1. It is seen that in the exchange of sulfur isotopes between H_2S and $SO_4^=$, S^{34} will be favored in the sulfate ion by 7.4 percent at 25° C, (see column 6, row 2, of table 1). It is not surprising, therefore, to find variations in the abundances of the sulfur isotopes amounting to 7 percent. Table 2 gives partition function ratios for the various isotopic species for various molecules containing sulfur. It is seen that the partition function ratio increases for S^{34}/S^{32} species as we go from sulfide ion to sulfate ion. This means that in chemical processes there will be a tendency for S^{34} to concentrate toward the sulfate ion. Professor Urey has made similar calculations for the chlorine isotopes and there,

Table 1. *Equilibrium constants for sulfur exchanges*

	$\frac{S^{34}O_4^=}{S^{32}O_4^=}$	$\frac{S^{34}O_3}{S^{32}O_3}$	$\frac{S^{34}O_2}{S^{32}O_2}$	$\left[\frac{CS_2^{34}}{CS_2^{32}}\right]^{\frac{1}{2}}$	$\left[\frac{S_2^{34}}{S_2^{32}}\right]^{\frac{1}{2}}$	$\frac{H_2S^{34}}{H_2S^{32}}$	$\frac{S^{34=}}{S^{32=}}$	Temperature
								°C
$\frac{Q_2}{Q_1}$	1.101	1.096	1.053	1,021	1.015	1,015	1.000	0
	1.088	1.084	1.045	1.019	1.013	1.013	1.000	25
$\frac{S^{34}O_4^=}{S^{32}O_4^=}$	1.000	1.005	1.046	1.078	1.085	1.085	1.101	0
	------	1.004	0.041	1.068	1.074	1.074	1.088	25
$\frac{S^{34}O_3}{S^{32}O_3}$	------	1.000	1.041	1.073	1.080	1.080	1.096	0
	------	------	1.037	1.064	1.070	1.070	1.084	25
$\frac{S^{34}O_2}{S^{32}O_2}$	------	------	1.000	1.031	1.037	1.037	1.053	0
	------	------	------	1.026	1.032	1.032	1.045	25
$\left[\frac{CS_2^{34}}{CS_2^{32}}\right]^{\frac{1}{2}}$	------	------	------	1.000	1.006	1.006	1.021	0
	------	------	------	-------	1.006	1.006	1.019	25
$\left[\frac{S_2^{34}}{S_2^{32}}\right]^{\frac{1}{2}}$	------	------	------	-------	1.000	1.000	1.015	0
	------	------	------	-------	-------	1.000	1.013	25
$\frac{H_2S^{34}}{H_2S^{32}}$	------	------	------	-------	-------	1.000	1.015	0
	------	------	------	-------	-------	------	1.013	25
$\frac{S^{34=}}{S^{32=}}$	------	------	------	-------	-------	------	1.000	0
	------	------	------	-------	-------	------	------	25

---

[5] A. P. Tudge and H. G. Thode, Can. J. Research **B28**, 567–578 (1950).

TABLE 2. *Partition function ratios for chlorine and sulfur compounds*

Chlorine						
	$\frac{Cl^{37}O_4^-}{Cl^{35}O_4^-}$	$\frac{Cl^{37}O_3^-}{Cl^{35}O_3^-}$	$\frac{Cl^{37}O_2}{Cl^{35}O_2}$	$\left[\frac{Cl_2^{37}}{Cl_2^{35}}\right]^{\frac{1}{2}}$	$\frac{HCl^{37}}{HCl^{35}}$	$\frac{Cl^{37-}}{Cl^{35-}}$
$\frac{Q'_2}{Q'_1}$	1.097	1.055	1.036	1.009	1.005	1.000
Sulfur						
	$\frac{S^{34}O_4^=}{S^{32}O_4^=}$	$\frac{S^{34}O_3}{S^{32}O_3}$	$\frac{S^{34}O_2}{S^{32}O_2}$	$\left[\frac{S_2^{34}}{S_2^{32}}\right]^{\frac{1}{2}}$	$\frac{H_2S^{34}}{H_2S^{32}}$	$\frac{S^{34=}}{S^{32=}}$
$\frac{Q'_2}{Q'_1}$	1.101	1.096	1.053	1.015	1.015	1.000

too, Cl^{37}, the heavy isotope of chlorine, tends to concentrate in the highest valence state.[6]

Although these calculations would predict an enrichment of S^{34} in sulfates and a depletion of S^{34} in H_2S as indicated by the exchange reaction,

$$H_2S^{34}+S^{32}O_4^= \rightleftarrows H_2S^{32}+S^{34}O_4^=$$

$$K=1.074 \text{ at } 25° \text{ C}$$

the question arises as to how this isotopic exchange is brought about in nature. A lot of energy is required to reduce sulfate ion, and sulfates will not exchange their sulfur with hydrogen sulfide under normal conditions. It has been suggested that isotopic equilibrium or partial equilibrium might be established in the well known sulfur cycle in nature.[7] The part of the cycle that is of interest here is illustrated in figure 2. Preliminary experiments under controlled laboratory conditions have already been carried out to determine what fractionation, if any, occurs in the different parts of this cycle. For example, hydrogen sulfide produced by the bacterial reduction of sulfate was found to be depleted in S^{34} over that of the sulfate medium from which it was produced. In the same way organic sulfur in plant leaves was found to be depleted in S^{34} over that of the sulfate nutrient in which the plants were grown.

5. Native Sulfur

Recently we received samples from Dr. K. R. Butlin of Teddington, England, of sulfur and sulfate from a lake in Africa, the native sulfur being formed by the bacterial reduction of sulfate. The isotopic content of these samples has been investigated and the results are given in table 3. Although the 3.2-percent fractionation in the sulfur isotopes found is only about half that expected if isotopic equilibrium were obtained, it is nevertheless much higher than the preliminary value obtained under controlled laboratory conditions. Finally the results found for native sulfur samples in Texas and Louisiana indicate that here, too, the sulfur is depleted in S^{34}. Unfortunately, we have not examined sulfates of the sulfur deposits in

---

[6] H. C. Urey, J. Chem. Soc. 562, 1947.

[7] A. Szabo, A. P. Tudge, J. Macnamara, and H. G. Thode, Science 3, 464 (1950).

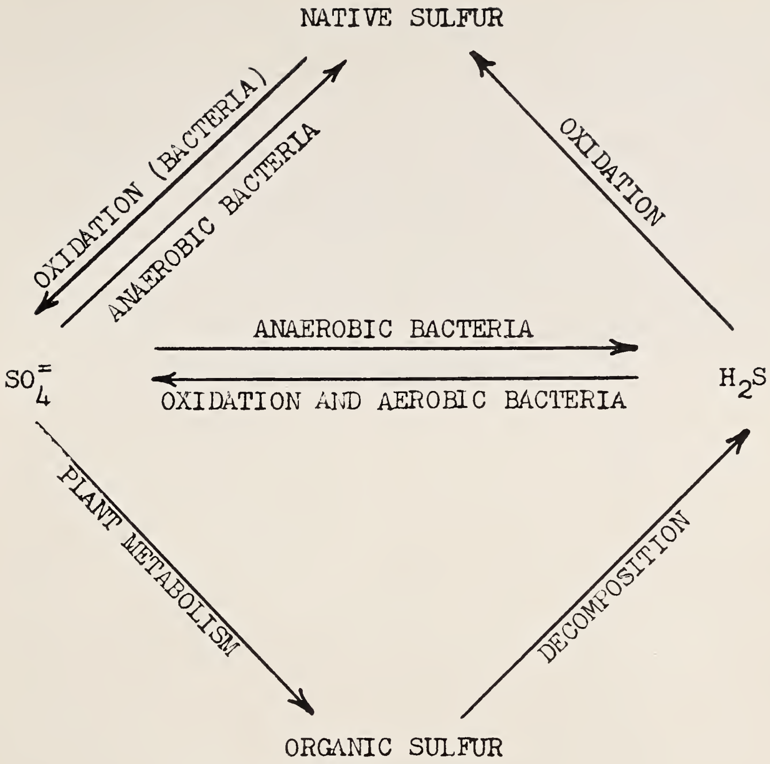

Figure 2. *Sulfur cycle in the sea.*

Table 3. *Isotope fractionation in the bacterial production of native sulfur from sulfate*

Sample	S^{32}/S^{34} ratio	Isotope fractionation factor
Native sulfur [a]	22.57	1.032
Sulfate	21.88	
Average sea sulfate	21.80	

[a] Native sulfur and sulfate from Lagoon in Cyrenaica, Africa.

question; however, if we compare the isotopic ratios of these native sulfur samples with the average present-day sea-water sulfate we obtain a factor of 1.025. This is very nearly that obtained in the bacterial reduction of sulfate reported in table 2 and thus it seems likely that these deposits were formed by the bacterial reduction of sea-water sulfate. A systematic study of isotopic abundances in core samples from sulfur wells should, therefore, give information as to the origin of these deposits.

The well-defined isotopic separations between the sulfur samples of volcanic and organic origins shown in figure 1 may provide a method of determining the origin of various natural deposits which have been interpreted in numerous ways by geologists. For example, the famous sulfur deposit near Gergenti in Sicily has been regarded by some writers as volcanic in origin and by others as having been formed through the reduction of gypsum by organic matter. Certainly the S^{32}/S^{34} ratio found for Sicilian sample would suggest that this sample is of volcanic origin.

6. Isotope Abundances and Geological Age

The isotopic ratios for sulfide and sulfates of marine origin have been determined and have been plotted in figure 3 against geological age. A rather startling correlation is found. It would appear that little or no fractionation occurred between sulfates and sulfides up until 800 million years ago, the isotopic content being at a "base level," or, the same value as that for meteoritic and igneous rock

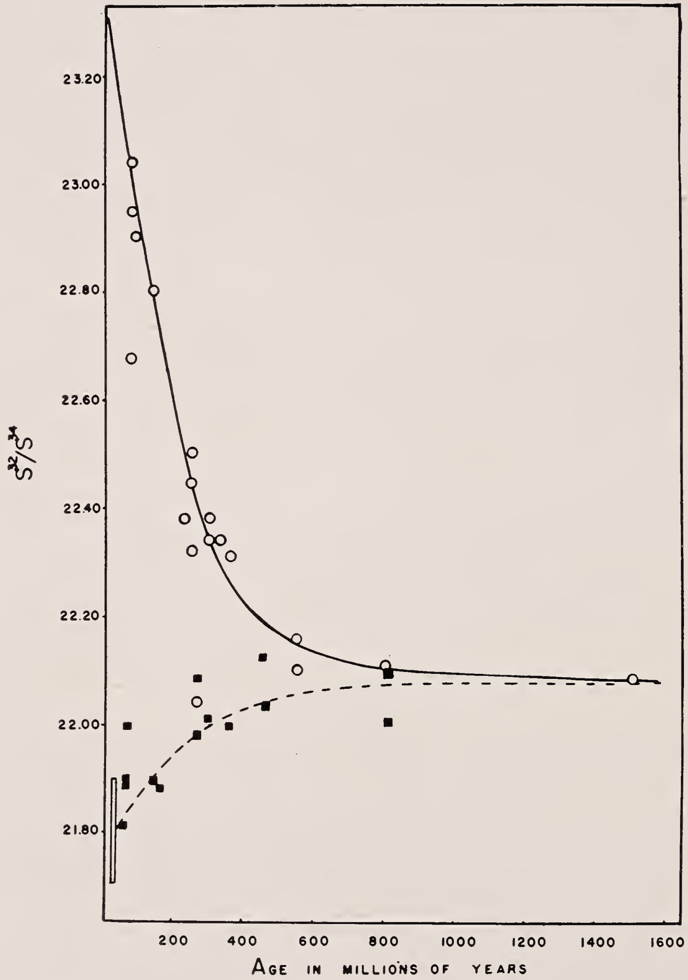

FIGURE 3. *Distribution of S^{34} in sedimentary sulfides of marine origin and sulfates as a function of age.*

○, sulfide; ■, sulfate in limestone; ▭, sea water sulfates.

sulfur. From that time forward isotopic exchange has taken place more rapidly and for the more recent samples the spread is about 7 percent. These results strongly suggest that life involving the sulfur isotopes became abundant about 800 million years ago when isotopic exchange between sulfate and sulfide began, the process becoming more and more rapid.

One objection to this suggestion is that life began much earlier than 800 million years ago. Geologists have evidence of fossils in the late pre-Cambrian period, and there is evidence of fossils even in the early pre-Cambrian (1.2×10^9 yrs.). However, if life processes began on the earth under more reducing conditions than we now have, as suggested by H. C. Urey, it is possible that in Archean times much of the sulfur was in the form of sulfides and early anaerobic life would not involve the reduction of sulfate to hydrogen sulfide to any extent.

34. The Influence of Fractionizing and Viscosity Effects in Mass Spectrometric Gas Handling Systems

By J. Kistemaker [1]

In making a gas analysis or isotope ratio determination with a mass spectrometer, it is necessary to know the relation between the gas composition in the ion source and the composition in the sample. Here we will consider especially the "viscous" or mass-flow leak, which is mostly used for isotope analysis. We did this work with a special reference to high precision isotope ratio determinations as, e. g., Urey's $O^{16}-O^{18}$ determination.

I studied the fractionizing and viscosity effects in a viscous leak, using the relations governing the flow of gas in the intermediate pressure region. I used Knudsen's simplified relation for cylindrical tubes,

$$Q=\frac{\pi}{8}\frac{1}{\eta}\frac{r^4}{l}\bar{P}(P_2-P_3)+\frac{4/3\sqrt{2\pi}}{\sqrt{\rho_{id}}}\frac{r^3}{l}(P_2-P_3)\text{ dyne cm sec}^{-1} \tag{1}$$

and partially Halsted and Nier's notation,

$$Q_a=v\left(\frac{P_{a2}}{P_2}\right)\bar{P}_{23}(P_2-P_3+\frac{k}{\sqrt{M_a}}(P_{a2}-P_{a3}), \tag{2}$$

which is more apt to describe general phenomena.

I consider the gas inlet system described schematically in figure 1.

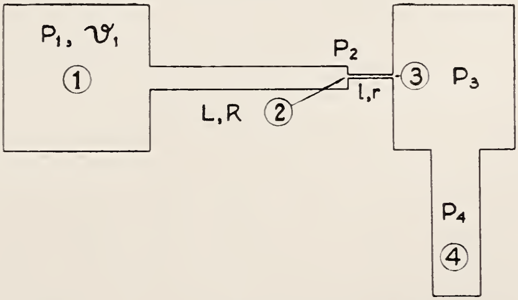

FIGURE 1. *Schematic diagram of the gas flow system.*

$P_1 \approx P_2$; $P_3 \approx 10^{-4}$ mm Hg; $P_4 \approx 10^{-6}$ mm Hg; P_1 1 to 100 mm Hg V_1 is the container; (L,R) is a capillary tube and (l,r) the "leak". P_3 is the pressure in the ion source, and P_4 in the oil diffusion pump. All calculations have been done, assuming speed of 0.2 L/sec in the ion source, with a pressure $P_3=10^{-4}$ mm Hg. As happens also in practice

---

[1] Laboratorium voor Massaspectrografie, Amsterdam, Nederland.

we had to choose the dimensions of the leak, such that this pressure P_3 and this pumping speed could be maintained with a given gas mixture at a certain pressure P_1 in the sample container. We always considered it in this way: (1) A leak consisting of one cylindrical tube ($N=1$), and (2) a leak consisting of N cylindrical tubes, with a radius a factor ten smaller than the above. As indicated already, we took the number N so large that the total quantity of gas Q, flowing through the leak, is the same in both cases. This study is of importance as the fractionizing in a gas mixture strongly depends on the number of N, or better said on the radii of the tubes r. The case of $N=1$ is more or less ideal. In practice a leak such as described by Nier, Ney, and Inghram, or a glass filter is always used. In these practical cases we never know the exact dimensions, but by a schematical consideration, taking r a factor ten smaller than for $N=1$, we get a qualitative impression of what happens.

Whereas Halsted and Nier gave the relation between the isotope ratios in the sample container and the ion source, I tried to go into details here and there. This work was partially done to get an idea about the fundamental limitations to the accuracy in isotope ratio determinations, with a given gas handling system.

I. *The actual fractionizing at 2* (fig. 1), the place where the big capillary ($L,R,$) ends and the constriction (l,r) begins. The isotope ratio at 2 depends on the gas flow for each component from 2, through the constriction (l,r), and to 2 through the tube (L,R). The flow through the constriction is characterized by a viscous and a molecular term (see equation (2)) and therefore we must expect an influence of the mass ratio of both components, which means fractionizing. On the other hand the flow through (L,R) is only viscous. The velocity of mass flow along this relatively wide tube can be so small, however, that the diffusion flow for each of the components is of importance. This diffusion current tries to eliminate the concentration gradient for each of the components along the tube (L,R). It is possible to calculate the stationary state. I calculated $(P_{b2}/P_{a2})_\infty(P_{a1}/P_{b1})$ for many mixtures.

In table 1 there are some results for $O^{16}-O^{18}$, although there are many more impressive results.

TABLE 1. *Values of* $\left(\frac{P_{b2}}{P_{a2}}\right)_\propto\left(\frac{P_{a1}}{P_{b1}}\right)$ *for* $O_2^{16}-O^{16}O^{18}$ and $P_1=P_{a1}+P_{b1}=100$ mm Hg.

Tube (L, R)	$l_{23}=1$ cm $r_{23}=1.10^{-3}$ cm $N=1$	$l_{23}=1$ cm $r_{23}=1.10^{-4}$ cm $N=2,600$
$L=$ 10 cm; $R=0.5$ cm	1.000024	1.00006
$L=100$ " ; $R=0.5$ "	1.00024	1.0006
$L=100$ " ; $R=0.1$ "	1.0042	1.010
$L=$ 10 " ; $R=0.01$ "	1.011	1.025

Especially the third row is interesting, as it is a generally used copper capillary. We see that the fractionizing of the gas mixture increases if the same quantity of gas passes per second through a larger number N of smaller tubes. Moreover long, rather narrow tubes (L, R) give the largest fractionizing.

In figure 2 the behaviour of $\left(\frac{P_{b2}}{P_{a2}}\right)_\propto\cdot\left(\frac{P_{a1}}{P_{b1}}\right)$ for H_2-O_2 is given as a function of the pressure. There is a maximum.

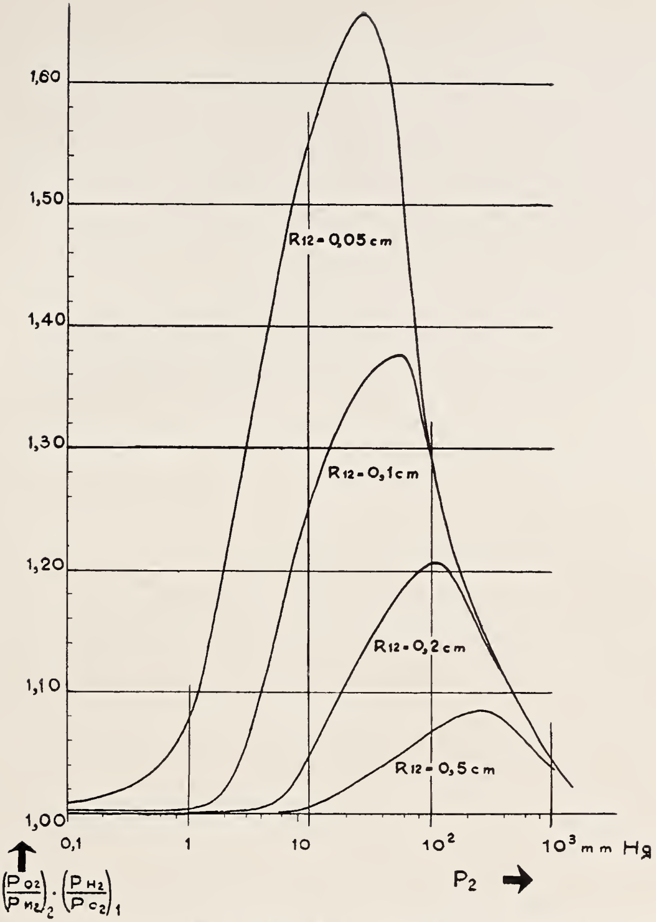

FIGURE 2. *The fractionizing phenomenon according to equations (1) and (2).*

II. *The variation of* $\left(\frac{P_{b2}}{P_{a2}}\right)$ *as a function of time.* After the gas mixture which we want to analyze has been admitted to the leak system, the ratio P_{b2}/P_{a2} will increase with the time t, until at last the stationary state is approached more and more. Realizing this we ask: How long does it take before 90 percent of the stationary state has been reached? Also this problem has been solved for many cases. In table 2 we see the values of t for $O^{16}—O^{18}$, assuming 90 percent to be reached, and for corresponding conditions as in table 1.

TABLE 2. *Values of* $t(90\%)$ *for* $O_2^{16}—O^{16}O^{18}$ and $P_1 = P_{a1} + P_{b1} = 100$ mm Hg.

Tube (L, R)	$l_{23}=1$ cm $r_{23}=1.10^{-3}$ cm $N=1$	$l_{23}=1$ cm $r_{23}=1.10^{-4}$ cm $N=2{,}600$
	sec.	*sec.*
$L=10$ cm; $R=0.5$ cm	76	76
$L=100$ " ; $R=0.5$ "	7,500	7,400
$L=100$ " ; $R=0.1$ "	5,200	4,900
$L=10$ " ; $R=0.01$ "	13	12

We observe from this table that long tubes give much larger values of t than do short tubes. Moreover, the value of t is independent of N, which means that t is independent of the character of the constriction, if the number of liters per second flowing through it is the same.

A consequence of this changing value of (P_{b2}/P_{a2}) is that the ratio of the partial pressures in the ion source changes proportionally, and therefore the intensity ratio of the ion currents in the mass spectrometer (I_b/I_a) also. This may result in serious mistakes if an analysis is started too quickly after the gas has been introduced. I think especially of the general tendency in isotope analysis to increase the accuracy of determination of the isotope ratio. A typical and brilliant example is the high precision mass spectrometer developed by Urey and his coworkers. They profess to have an accuracy of 0.02 percent in the O^{16} to O^{18} ratio. From tables 1 and 2 it will be clear that the design of the gas leak as well as the speed with which analyses are made are of utmost importance. If a copper tube with $R=0.1$ cm is used in connection with the Nier leak, an error of 0.2 percent can easily occur. In H_2—HD analyses the error can easily be of the order of 0.5 percent.

III. *The fractionizing of the gas sample* depends on the ratio of the mean mass flow and the back diffusion in the tube (L, R) as well as on the volume V_1 of the sample container and the concentration gradient in the tube (L, R). If we accept a certain time, necessary to do the analysis, we can calculate the minimum volume V_1 to give a fractionizing less than, say, 0.01 percent. In table 3 these values are given for $O^{16}—O^{18}$.

TABLE 3. *V_1 minimum for* $O_2^{16}—O^{16}\,O^{18}$ with $P_1=P_{a1}+P_{b1}=100$ mm Hg and $t=3{,}600$ sec for an accuracy of 0.01 percent.

Tube (L, R)	$l_{23}=1$ cm $r_{23}=1.10^{-3}$ cm $N=1$	$l_{23}=1$ cm $r_{23}=1.10^{-4}$ cm $N=2600$
	cm ^{3}	*cm* ^{3}
$L=10$ cm; $R=0.5$ cm	103	260
$L=100$ “ ; $R=0.5$ “	103	260
$L=100$ “ ; $R=0.1$ “	72	170
$L=10$ “ ; $R=0.01$ “	19	42

If a sample holder has 100 cm^3, we see that we can not measure for longer than half an hour to be sure that the fractionizing in the sample is below 0.01 percent.

IV. *The influence of the pressure in ratio analysis* is demonstrated in table 4. We calculated this in the same way as Halsted and Nier did, using the relation $P_{a3}/P_{b3}=FP_{a2}/P_{b2}$, where F is a function of P_2.

TABLE 4. $F=(P_{a3}/P_{b3})\ (P_{b2}/P_{a2})$ *for* $O_2^{16}—O^{16}\,O^{18}$.

P_2	$l_{23}=1$ cm $r_{23}=1.10^{-3}$ cm $N=1$	$l_{23}=1$ cm $r_{23}=1.10^{-4}$ cm $N=2600$
mm Hg		
10	0. 9962	0. 9996
50	. 9875	. 9980
100	. 9825	. 9962
150	. 9798	. 9946

A practical difficulty is that we never know exactly the size of r_{23}. We can consider 1.10^{-3} cm as the worst practical case, however, which can be used with a mass spectrometer. In that case a pressure difference of 10 mm Hg between the standard sample and the sample under investigation (with $P_2=100$ mm Hg), already gives a deviation in the observed isotope ratio of 0.08 percent.

Conclusions. The examples from tables 1 to 4 show how easily erroneous $O^{16}-O^{18}$ isotope analyses are done. False observations of the isotope ratio, up to 0.2 percent, are very probable if special precautions in dimensioning of the gas handling system are neglected.

To make an $O^{16}-O^{18}$ ratio analysis with an accuracy of 0.01 percent we must therefore take care that:

(1) $L\approx 10$ cm and $R>0.5$ cm;

(2) $l_{23}\approx 1$ cm with $r_{23}=1.10^{-4}$ to 1.10^{-3} cm if correspondingly $N=2{,}600$ to 1 (this corresponds to a glass filter or a Nier leak);

(3) the volume of the sample container $V_1\approx 100$ cm^3, corresponding with a time of analysis t: 2 min $<t<$30 min; and

(4) the pressure differences between the samples are not more than 1 mm Hg, if the sample pressure is 100 mm Hg.

Maintaining these requirements means that we are on the safe side for $N^{14}-N^{15}$ and $C^{12}-C^{13}$ analyses; H—D analyses require special precautions, however.

Professor Urey and Dr. Epstein fixed my attention to the fact that also the use of a tube (L, R) with $R\approx 0.25$ mm is very satisfactory. This is in accordance with the fact that they can start the analysis at about 15 minutes after the introduction of the sample without finding any change in concentration.

Discussion

S. Epstein: I would like to make a comment. I would like to verify the fractionization effect. We do get such an effect lasting about a minute and I don't know what the effective radius of the tube is, but perhaps we can calculate it now from this formula. However, we foresaw other effects which may have a greater effect on our results and that we thought we eliminated by making our results comparative to a reference gas, and another thing, too, we analyze samples of our standard every so often just to make sure we don't run into such troubles.

A. O. Nier: It might be interesting, Dr. Epstein, from your recording instrument, if you could get such a curve conveniently showing the fractionization; it does read the ratio, does it not?

Epstein: We have obtained several curves which I sort of ignored. We actually get effects which I should say are about six or seven times the experimental error. Even then we did not extrapolate back to zero time. This appears in a matter of seconds.

Nier: We never went through such calculations as you have done. I felt kind of intuitively that if you had a small enough diameter there it appeared all right, but we never went through the calculation. I can always disclaim responsibility for I never intended that that apparatus should give such accuracy. It is not supposed to give that great accuracy.

I am very grateful that you went through that.

35. The Mass Spectral Patterns of Isotopic Molecules

By O. Schaeffer [1]

It has been realized for some time that when bombarded by low energy electrons, isotopic molecules do not yield quantitatively the same amounts of the various ion fragments. A careful study of these variations can yield intimate information about the nature of the electron-impact process as well as about the potential states of the molecule ions.

For diatomic molecules, it has been found that the heavier of the molecules will lead to less fragmentation. Except for hydrogen containing molecules the effect is about a 2- to 5-percent change. When hydrogen and deuterium are compared, the effect is about a factor of 2.

The electron impact process has been studied carefully, as reported by Hagstrum (see paper 26, p. 123). Reviewing briefly, most dissociations yielding positive ions are vertical transitions; that is, the internuclear separations are left unchanged during the alteration in the electronic configuration caused by the impinging electron. As a consequence, the molecule ion will dissociate in one of a particular set of ways or not, depending on the configuration of its nuclei at the instant of impact. To determine the relative probability of producing a given ion fragment, one needs to know which internuclear configurations dissociate to give this particular fragment and the probability of the nuclei being in the desired configurations. The former information may be deduced from the potential curves for the ionic states, while the latter can be obtained from the ground state vibrational wave functions for the molecule.

The simplest case to treat, and also the only one which can be calculated without resort to mass spectral data, is that of the isotopic hydrogen molecules.[2] If the electron energy is low, only the lowest state of the hydrogen molecule ion need be considered. The potential curve for this state is shown in figure 1 along with the square of the ground state vibrational wave function. It is clear that for vertical transitions those internuclear separations less than r_c (indicated by the vertical dashed line in fig. 1) will lead to H^+ while those larger than r_c will lead to H_2^+. So that the relative probability of H^+ to H_2^+ is just:

$$X^+/X_2^+=\int_0^{r_c}\psi_0^2(R)dR\bigg/\int_{r_c}^{\infty}\psi_0^2(R)dR. \qquad (1)$$

For D_2 the potential curve remains the same, but the wave function becomes more concentrated near the equilibrium value and leads to a lower value for the corresponding ratio.

The calculation can be improved by taking into account the fact that the electronic transition probability is linearly related to the excess energy of the electrons above the minimum energy required

---

[1] Brookhaven National Laboratory, Upton, N. Y.

[2] D. P. Stevenson, J. Chem. Phys. **15**, 409 (1947).

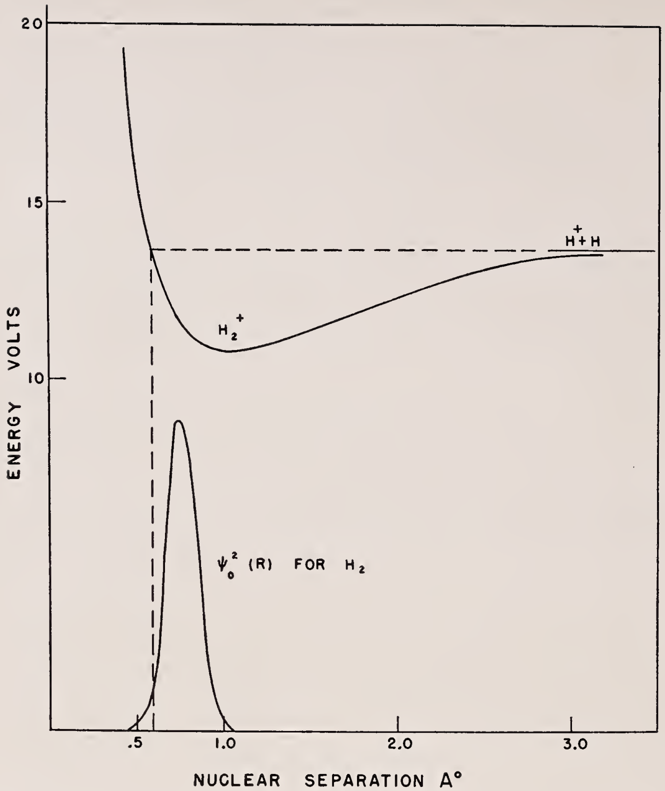

Figure 1. *Potential energy curve for the lowest state of the hydrogen molecule.*

for the process. That is, taking as the transition probability, $T(r,E)$, to the ground ionic state

$$T(r,E)=k\,[E-V(r)] \tag{2}$$

where $V(r)$ is the minimum energy required for the process (which is the potential curve of fig. 1), E is the energy of the impinging electrons and k is the proportionality constant. The above defined ratio then becomes:

$$(X^+/X_2^+)_{\text{corr}}=\int_0^{r_c} T(r,E)\psi^2(R)dR \Big/ \int_{r_c}^{\infty} T(r,E)\psi^2(R)dR \tag{3}$$

Using the anharmonic oscillator approximation to $\psi(R)$, the ratios X^+/X_2^+ are readily calculated for H_2, D_2 and T_2 which are compared with some recent observations[3] in table 1.

When other diatomic molecules are studied, it is found that the appropriate potential functions are not available. However, while it is now not possible to predict the individual ratios, X^+/X_2^+, it is possible to predict the change in the ratio due to the isotopic substi-

---

[3] O. A. Schaeffer and J. M. Hastings, J. Chem. Phys. 18, 1048 (1950).

TABLE 1. *Comparison between calculated and observed values of X^+/X_2^+ peak ratios for hydrogen, deuterium and tritium using 30 volt electrons.*

Ratio	Observed	A[1]	B[2]
H^+/H_2^+	0.013	0.0187	0.0159
D^+/D_2^+	.0070	.0083	.0072
T^+/T_2^+	.0036	.0044	.0038

[1] A. Calculated without correction for excess energy.
[2] B. Calculated with correction for excess energy.

tution. To do this, the limit r_c of the integral in eq (1) is determined so that the integral yields the observed ratio. Then the integral can be re-evaluated using the wave function for the isotopic species. A comparison between observed and predicted ratios determined in this way is presented in table 2, for several diatomic molecules.

TABLE 2. *Isotope effect on some diatomic molecules.*

Molecules	Ratio	Observed[1]	Calculated
N_2	$\frac{N^{14+}}{N^{14}N^{14+}} \Big/ \frac{N^{15+}}{N^{15}N^{15+}}$	1.10	1.06
CO	$\frac{C^{12+}}{C^{12}O^{16}} \Big/ \frac{C^{13}}{C^{13}O^{16}}$	1.06	1.04

[1] Dibeler, Mohler, and Reese, J. Chem. Phys. **18**, 156 (1950); Dibeler, Wells, and Reese, Phys. Rev. **79** 223 (1950).

In case of polyatomic molecules, the types of effects that have been observed are more diverse. Much work has been done with hydrocarbons and here it is found that there are several effects. Considering only the substitution of deuterium for hydrogen, it has been found that in a hydrocarbon containing both hydrogen and deuterium, the deuterium bonds are about half as likely to be broken as the equivalent hydrogen bonds, and the hydrogen bonds roughly 10 percent more likely to be broken than in the comparable molecule which contains no deuterium. This is the process:

$$CH_3D+e\rightarrow CH_2D^++H+2e \tag{A}$$

is about twice as probable as the process:

$$CH_3D+e\rightarrow CH_3^++D+2e \tag{B}$$

taking account of the fact that there are three hydrogens and only one deuterium in the molecule.

On the other hand, the process (A) is about 10 percent more likely than the process:

$$CH_4+e\rightarrow CH_3^++H+2e. \tag{C}$$

In order to extend the calculation to these cases, an approximation must be made. A plausible one which also allows the calculation to be made rather easily is to consider that the potential energy of the molecule is a valence type field

$$V=\frac{1}{2}\sum_j k_j R_j^2 \tag{4}$$

where R_j is a particular internuclear distance. Then to assume that those bonds will break, and only those whose potential energies, by virtue of their instantaneous R_j value, are larger than bond energies.

The ratios $C^{13+}/C^{13}O_2^{16+}$ and $C^{12+}/C^{12}O_2^{16+}$ from carbon dioxide furnish a test for the validity of this assumption. In order to produce C^+ from CO_2 both CO bonds must be less than the critical value. The symmetrical mode of vibration is the major contributing motion to achieving the desired configuration. For this mode the $C^{13}O_2^{16}$ and $C^{12}O_2^{16}$ vibrational wave functions are the same, so that to this approximation one would expect no change in the corresponding ratios.

Figure 2 shows a plot of the quantity $C^{13+}/C^{13}O_2^{16+}/C^{12+}/C^{12}C_2^{16+}$ as a function of $1/V$, V being the ion accelerating voltage. This particular plot was made so that the ratio could be extrapolated to very large ion accelerating voltages where the collection efficiencies for the ions should be more nearly equal. It is seen that the data are consistent with a zero isotope effect.

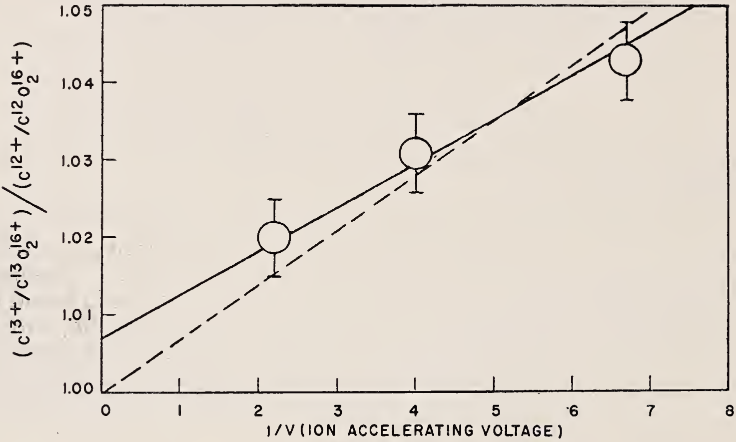

FIGURE 2. *Plot of the quantity $C^{13+}/C^{13}O_2^{16+}/C^{12+}/C^{12}O_2^{16+}$ as a function of the reciprocal of the accelerating voltage.*

The calculation has been provisionally extended to the case of acetylene. Using the three stretching frequencies as being important in the bond breaking processes, the vibrational wave function becomes

$$\psi(Q_1,Q_2,Q_3)=\exp\left(-\tfrac{1}{2}\alpha_1 Q_1^2\right)\cdot\exp\left(-\tfrac{1}{2}\alpha_2 Q_2^2\right)\cdot\exp\left(-\tfrac{1}{2}\alpha_3 Q_3^2\right) \tag{5}$$

where Q_1, Q_2 and Q_3 are the three normal coordinates for the stretching modes and

$$\alpha_i=[2\pi\sqrt{m_i k_i}/h] \tag{6}$$

The normal coordinates can be expressed in terms of the internal coordinates R by:

$$Q_k=\sum_i J_{ki} R_i \tag{7}$$

By substituting (7) into (5) one obtains the wave function in internal coordinates. If P_1 is the probability of breaking the C—H bond in acetylene, then P_1 is given by

$$P_1=\int_0^{r_{c_1}} dR_1 \int_{r_{c_2}}^{\infty} dR_2 \int_{r_{c_1}}^{\infty} dR_3 \psi(R) \qquad 8$$

with similar expressions for other bond-breaking probabilities. By using the ratio $\frac{1}{2}$ (C_2H^+)/(total ions) from C_2H_2 for P_1 and corresponding quantities for the other P's, one can evaluate critical bond distances. Then the corresponding P's can be calculated for isotopic acetylenes and compared with existing experimental results. The results of a tentative calculation are listed in table 3.

TABLE 3. *Isotope Effect on Mass Spectral Pattern of Acetylene*

Ratio	Observed [1]	Calculated
$\dfrac{C^{12}C^{12}D^+(\text{from } HC^{12}C^{12}D)}{\frac{1}{2}\, C^{12}C^{12}H^+(\text{from } HC^{12}C^{12}H)}$	1. 30	1. 05
$\dfrac{C^{12}C^{12}H^+(\text{from } HC^{12}C^{12}D)}{\frac{1}{2}\, C^{12}C^{12}H^+(\text{from } HC^{12}C^{12}H)}$	0. 66	0. 69

[1] Private communication with V. H. Dibeler.

In general, it must be admitted, that the agreement between observed and calculated ratios is not as sharp as might be desired. However, the observations are subject to various systematic errors. The kinetic energy of some of the fragments is the source of one such error. On the other hand, there are certain approximations made in the calculations which could introduce a certain amount of inaccuracy.

Discussion

A. O. NIER: Perhaps I should make remark that it is fortunate that most abundance measurements have been made on molecular ions and not on fragments. In only a few cases have they been made on fragments. I think most people did not suspect that the effect would be as large as it is.

36. Session on Experimental Methods

A. O. C. Nier (chairman): I have taken the liberty to arrange things in a rather arbitrary manner dependent on the fact that some of the participants in the conference will have to leave before the afternoon is over, men who I would like to have make some remarks. In the communications which I received and in the talks I have had with individuals here in Washington in the last two days, it appears that the greatest interest is in the use of electron multipliers as detection means in mass spectrometers and allied apparatus. Accordingly I thought we would spend perhaps an hour on this discussion. In order to give us a basis for subsequent discussion, I have asked a few individuals to make some remarks, and some of them have brought lantern slides. After that hour is up, I shall perhaps change the topic, and if you wish we can extend it or come back to it later. We will see how it goes.

The first person I have asked to make a few remarks is Dr. Lincoln Smith.

[Dr. Smith described an electron multiplier suitable for operating in a strong magnetic field. This description has appeared in Rev. Sci. Instruments **22**, 166–170 (1951).]

Nier: Perhaps we should defer discussion on multipliers until we have had several others because there will be some questions common to the several and I thought if each of the several speakers would speak about five minutes we could do that.

Smith: There is one feature which I should mention. The fact that this space focusing, you remember, is accompanied by time focusing. The electrons come off at different angles and with different velocities. Anyone interested in a very fast multiplier might consider this as a possibility.

Nier: I believe Dr. Walcher has some remarks.

[The remarks made by Dr. Walcher are contained in the following manuscript.]

The Mass Dependence of the Electron Release by Means of Isotopic Ions

By W. Ploch and W. Walcher

It is known that the ratio γ between the intensities of released electrons and impinging ions depends on the mass of the monokinetic isotope ions.[1] The recently introduced method of measuring ion beams with the aid of electron multipliers [2] will require more detailed knowledge of the dependence of the phenomenon of electron release from metal surfaces on the mass of the bombarding isotope ion. Therefore a detailed investigation was made on the dependence of γ on the atomic mass m.[3]

---

[1] M. Heala, Phys. Rev. **55**, 984 (1939); M. G. Inghram, Phys. Rev. **70**, 653 (1946).

[2] A.H.Morrish and J. S. Allen, Phys. Rev. **74**, 1260 (1948); W. T. Leland, Phys. Rev. **77**, 634 (1950).

[3] W. Ploch, Z. Naturforschg. 5a, 570 (1950); W. Ploch, Z. Physik **130**, 174 (1951).

The measurement was done with a Nier-type mass-spectrometer. A total of 32 measurements with the isotopic pairs Li^6—Li^7, Ne^{20}—Ne^{22}, K^{39}—K^{41}, with degased or not degased Pt, Mo, Be, and not degased Cu as the bombarded metal, and the accelerating potential varying between 600 and 6,000 v led to the same result that, within the limits of error of 1 percent, equal velocities of isotope ions give equal γ-values. In figure 1 a typical plot of γ versus the acceleration voltage U is given. The dotted line holds for Li^6, the solid line for Li^7. The solid points are calculated under the assumption that equal velocities correspond to equal γ-values. This simple law seems to hold generally and enables us to point out a correction formula for isotope ratio values $V=I_r/I_a$ measured with an electron-multiplier.

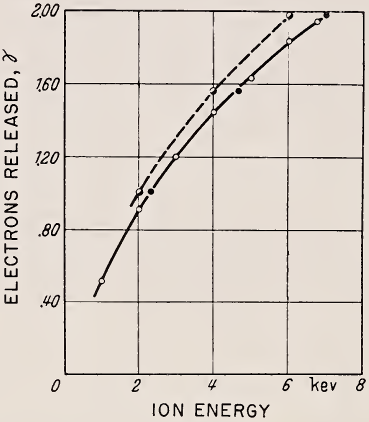

FIGURE 1. *Secondary emission ratio of Li^6 (dotted line) and Li^7 (solid line).*

We find:

$$V_{\text{real}}=V_{\text{measured}}\left(1+q\frac{m_r-m_a}{m_a}\right)$$

where

$$q=\left(\frac{\partial\gamma_a}{\partial U}\right)_{m_a}\left(\frac{U_o}{\gamma_a(U_o)}\right).$$

The subscripts a and r mean "abundant" and "rare"; U means acceleration voltages, U_o the acceleration voltage applied during the measurement, $\gamma(U_o)$ is the value of γ for the abundant isotope at the acceleration voltage U_o. The value q therefore easily may be found by measuring the multiplier current i_o of the abundant isotope at the voltage U_o, and i_o+di at the slightly varied voltage U_o+dU; then we obtain

$$q=\frac{di}{i_o}\Big/\frac{dU}{U_o}.$$

The value of q has been found to vary within the limits 1 and $\frac{1}{3}$ in the cases mentioned before; it strongly depends on the state of the surface and the energy of the ions.

For the isotopic molecules of nitrogen, e.g., the correction term may amount to about 3.5 percent in an unfavorable case. Because of the variability of q with the experimental conditions, noticeable deviations in different measurements may occur, if the result is not corrected.

NIER: Have you sent this work in for publication?

WALCHER: I have sent it in as a note.

NIER: Will it appear in the future?

WALCHER: Yes.

NIER: I will call on Dr. Inghram next, who has some similar remarks to make.

[The remarks made by Dr. Inghram are contained in the following manuscript.]

Electron Multipliers in Mass Spectroscopy

By Mark G. Inghram, Richard J. Hayden, and David C. Hess

Introduction

The use of electron multipliers in mass spectroscopy was first reported by Cohen.[1] Since that time a number of investigators have used them for a variety of applications.[2] [3] [4] It is the purpose of this paper to give a brief outline of the special problems involved in applying multipliers to mass spectroscopy. Since in this application the first important problem encountered is the conversion of an ion beam to an electron beam, this paper is concerned mainly with this process and not with details of the electron multiplier itself.

There are, in the literature, a large number of papers on effects produced when high energy ions impinge on surfaces. Many of these papers are contradictory. The fact that this can be the case is easily understood when one considers the large number of phenomena and variables involved. This paper does not purport to interpret these discrepancies. It simply states the problems which are important in the special case of mass spectrometric application, and suggests methods for their solution.

The phenomena of importance in the impact of high energy particles on surfaces are:

1. Production, energy, and angular distribution of secondary electrons.
2. Production, energy, and angular distribution of secondary negative ions.
3. Production, energy, and angular distribution of secondary positive ions.
4. Reflection of primary particles, including energy change and distribution.
5. Penetration of the primary particle into the surface.

Each of these phenomena depends to a greater or less extent on:

1. The energy of the incident particle.
2. The mass of the incident particle.
3. The electronic configuration of the incident particle.
4. The charge on the incident particle.
5. The chemical and physical composition of the surface.
6. The angle with which the incident particle strikes the surface.

---

[1] A. Cohen, Phys. Rev. **63**, 219 (1943).

[2] J. Heacock, Inghram, M. G., Nestor, O. H., NNES, Vol. **14**, Div. II (1946).

[3] W. T. Leland, Phys. Rev. **77**, 634 (1950).

[4] L. Smith, J. App. Phys. **22**, (1951).

From this list of effects and functional variations it is clear that the complete picture of the use of a multiplier for ion detection is very complex.

In the data which follows, all effects are for multiplier surfaces operated at normal temperatures. In some cases activation took place before the surface was installed in the machine, but in every case the surface had been at atmospheric pressure before use. This does not clarify the physics of the problem but is the simplest procedure for mass spectrometric use, so it was employed throughout.

Several types of multiplier configurations are possible. The linearly focused multiplier, the circularly focused multiplier, the venetian-blind multiplier, and the magnetically focused multiplier. The data reported in this paper in which a complete multiplier structure was used was taken from the linearly focused multiplier shown in figure 1. In this multiplier the beam enters the structure through the slits at the left, passes through an insulated adjustable slit which can be used to measure the primary beam intensity, through an accelerating system and onto the conversion dynode. From that point on, the electrode structure is similar to that described by Allen. It is the response of the first dynode which is of importance to mass spectrometric applications.

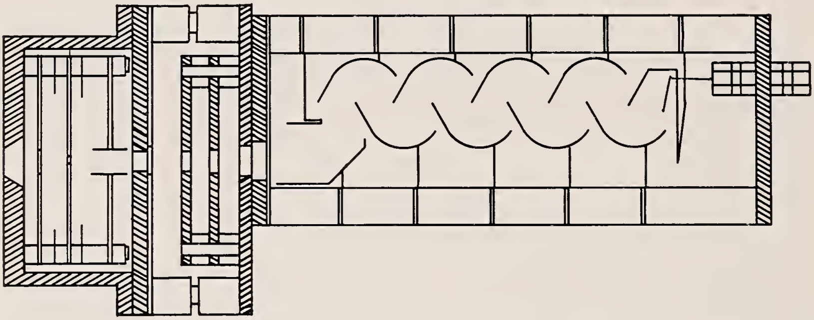

FIGURE 1. *Multiplier used for data reported in this paper.*

Secondary Electron Production as a Function of Angular Incidence

The variation of the number of negative particles produced by each particle collected on the target as a function of the angle of incidence is shown in figure 2. This curve was obtained with ions of mass 300 and 1,900 v. energy striking the target. The particular target material used in this experiment was nichrome. This data follows the form

$$\text{Gain} = (a - b \cos \theta) \tag{1}$$

This result is in agreement with the results of Oliphant.[5] It disagrees with the results of Allen [6] in which he was working with 120 Kev protons. Allen's data varied as 1/cos θ. It appears that as one increases the ion energy to the point where the ion penetration is greater than the range of the secondaries the variation is as 1/cos θ.

---

[5] M. L. E. Oliphant, Roy. Soc. Proc. **127**, 373 (1930).

[6] J. S. Allen, Phys. Rev. **55**, 336 (1939).

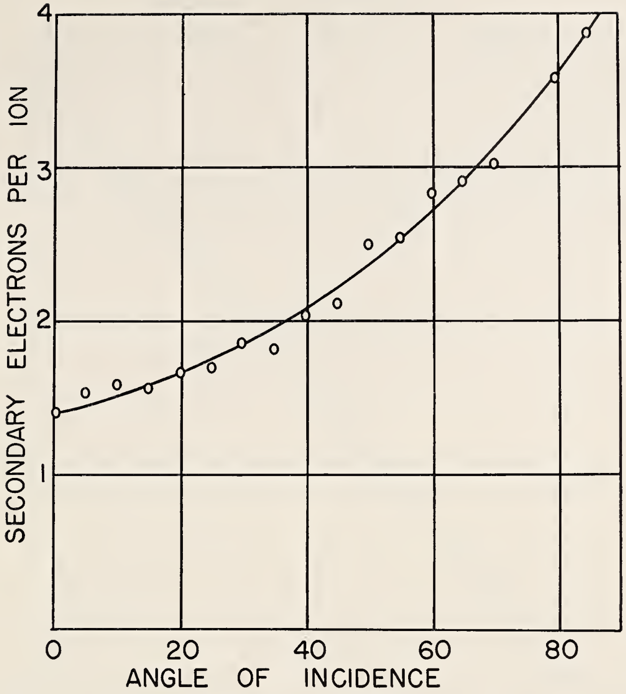

Figure 2. *Secondary electron production as a function of angular incidence.*

Conversely, if one goes to very low energy ions the term *b* in equation (1) goes to zero, i. e., there is no variation with angle of incidence. For most mass-spectrometric purposes, however, the range of energies and masses is such that equation (1) is the best approximation. A plot of this function in terms of the number of incident particles instead of the number of collected particles would decrease the slope slightly. The difference in these plots is due to ion reflection.

Ion Reflection as a Function of Angle of Incidence

The percent of the incident ion beam reflected as a function of the angle of incidence is shown in figure 3. This data is for N_2^+ ions of 1,700 v energy striking a nichrome target. Data obtained by Gurney [7] and by Sawyer [8] indicate that the percent reflection decreases as the energy increases over the range 100–1,000 v, and that there is a reflection peak at about 40 v. The fact that reflection increases more rapidly than secondary electron production, shows that there is an optimum angle for this process. At these lower energies this angle is of the order of 70°.

---

[7] R. W. Gurney, Phys. Rev. **32**, 467 (1928).
[8] R. B. Sawyer, Phys. Rev. **35**, 1090 (1930).

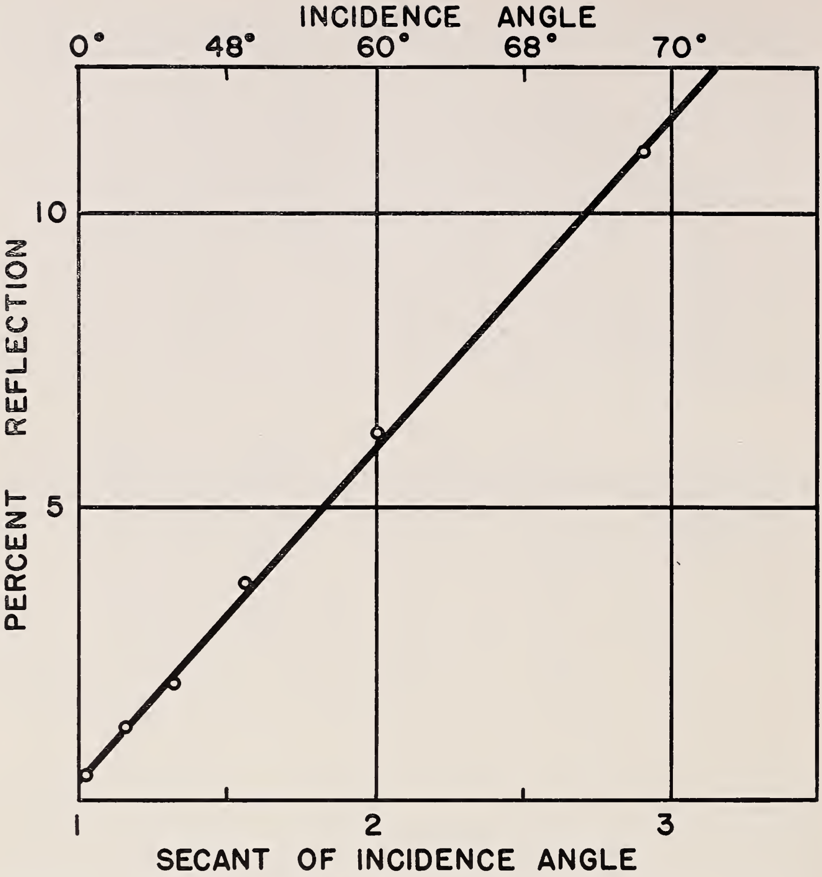

FIGURE 3. *Percent of ion beam reflected as a function of the angle of incidence (N_2^+ ions of 1,700 e. v.).*

Secondary Electron Production as a Function of Mass and Ion Energy

The number of secondaries produced by ion beams of lithium, sodium, potassium, rubidium and cesium striking the first dynode of the multiplier shown in figure 1 as a function of the energy of those ions is shown in figure 4. These data are all taken for singly charged ions striking a AgMg (1.7%) plate at a 45° angle. The important observations illustrated in the figure are:

1. For low energies the electron production is a linear function of the ion energy.
2. The range of linearity increases as the mass increases.
3. For low energies the gain decreases as the mass increases, for high energies exactly the converse is true.

A replot of the data of figure 4 is given in figure 5 in which a family of constant voltage curves is drawn. It is seen there is a portion at each voltage where the gain appears to be independent of the mass. That this apparent linearity is misleading is illustrated by the data of the next section.

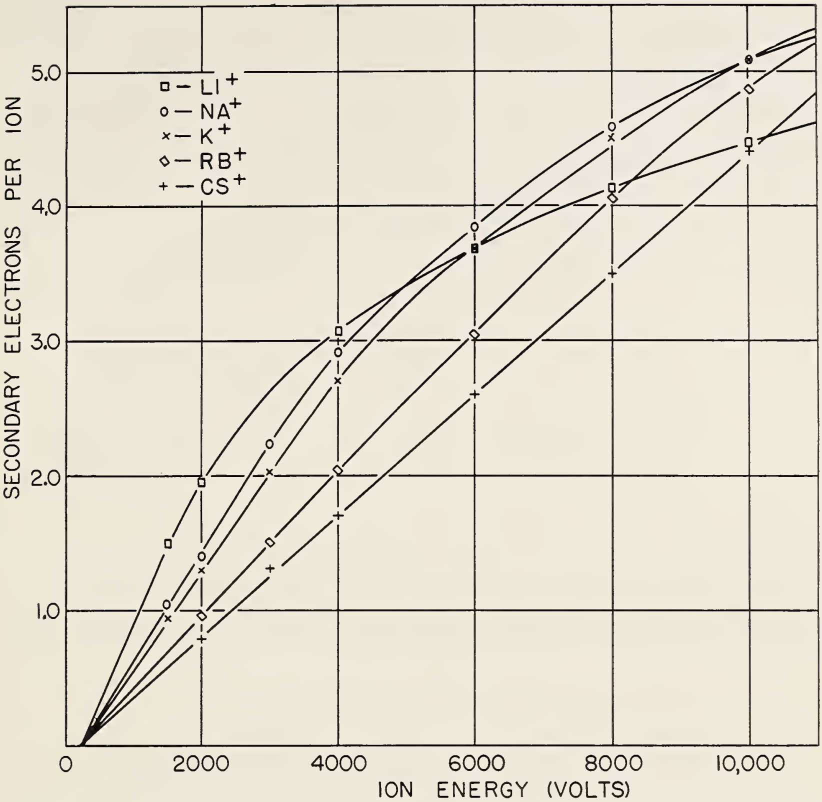

FIGURE 4. *Secondary electron emission for alkali ions at 45° incidence on Ag Mg (1.7%).*

Gain as a Function of Chemistry of the Impinging Ion

The two points shown in figure (5) for Ca^{40} and Ca^{48} illustrate that a calibration curve taken with different elements is not the same as that obtained using isotopes of the same element. This points out that the actual electronic configuration of the impinging ion is a factor in secondary electron production. The effect observed can be qualitatively understood as due to the binding energy of the last electron. As this binding energy increases, secondary electron production decreases. A similar set of curves obtained with a complete multiplier using the rare gases again shows that the gain for different isotopes of the same element varies more rapidly than that predicted using different elements. Thus an electron multiplier can be calibrated for isotopic work only by using samples of the element in question of known isotopic composition.

Secondary Electron Production as a Function of the Charge on the Incident Ion

Figure 6 shows the variation in secondary electron production as a function of mass and energy for positive and negative ions. The effective gain for negative ions is essentially that of a positive ion

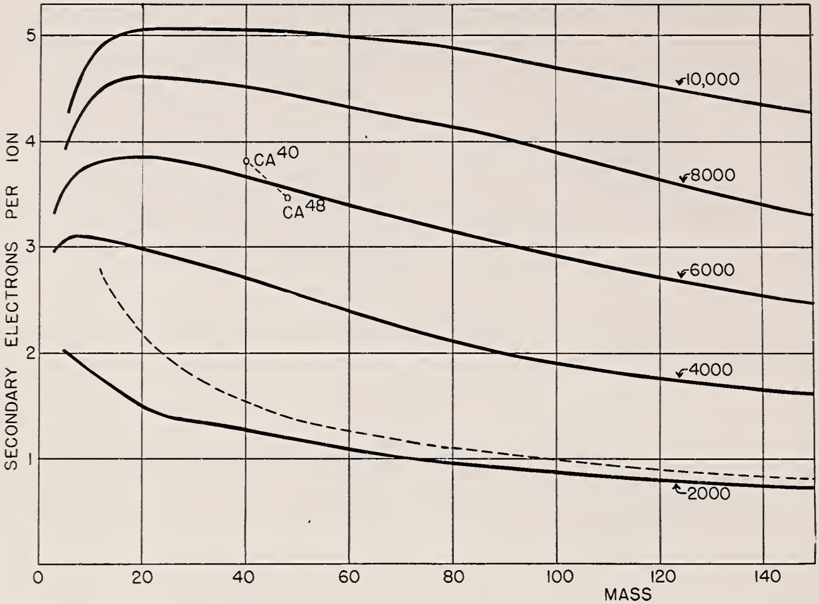

Figure 5. *Replot of delay figure 4 to show secondary emission as a function of mass at constant energy.*

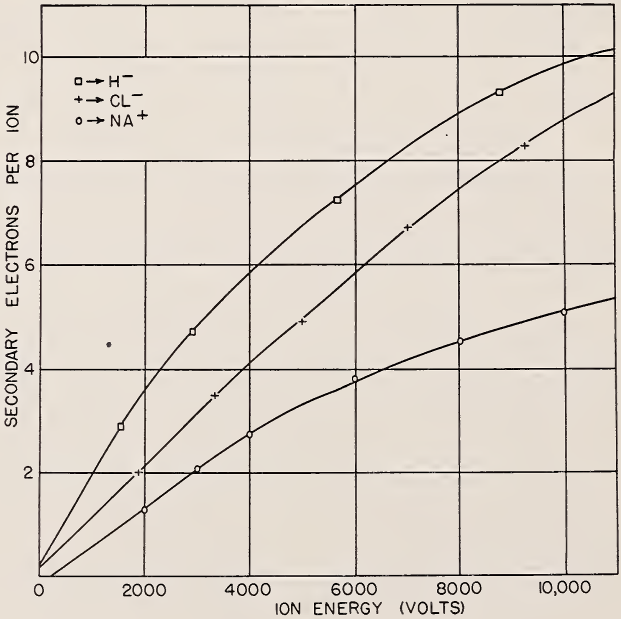

Figure 6. *Illustration of the increased secondary production by negative ions.*

plus that of an electron of energy corresponding to the velocity of the ion. This is due to the fact that on impact the ion and electron in a negative ion operate independently. Similar data for multiply charged positive ions shows that they have only slightly more gain than would be expected from a singly charged ion of energy corresponding to the multiply charged ion, i. e., Cs^{++} which has been accelerated through 5,000 v produces only a very slightly greater multiplication than Cs^{+} accelerated through 10,000 v. This is to be expected from change of charge considerations. Extrapolating to neutral particles one would predict that they would give roughy the same gain as a singly charged positive ion of the same energy. This is in agreement with the results obtained by Berry.[9]

Secondary Electron Multiplication as a Function of Molecular Form

Figure 7 shows the gain of a complete multiplier (compensated with a magnetic field to give maximum multiplication at mass 80) as a function of molecular form. This data was taken at a constant ion energy of 7,000 v. The fact that a molecule gives a greater gain than an atom of the same mass and energy is illustrated by the points due to CH, CH_2 and CH_3. This can be explained as due to the fact that the molecule breaks up on collision and acts as a group of particles of lesser energy. As long as the plot of energy versus gain is linear this effect is negligible. The effect is therefore most important for light ions at high energies.

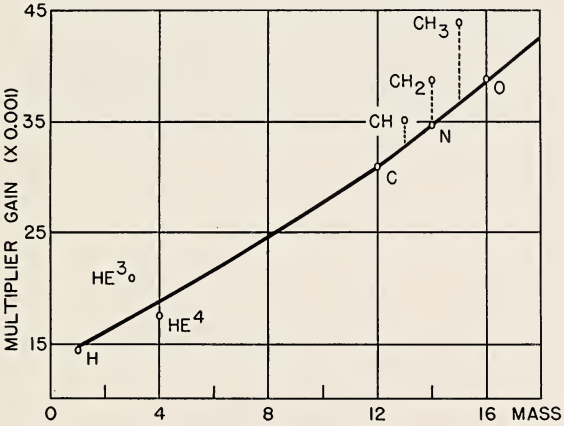

FIGURE 7. *Effect of molecular form on gain.*

Effect of Stray Magnetic Fields on Multiplier Gain

The change in gain with mass for the complete multiplier as compared to the gain for the first stage is shown in figure 8. The dotted line is the behavior as predicted from results on the first dynode, the solid line is the behaviour of the complete system. The difference in these two curves is due to the stray magnetic field from the analyzer magnet. Two methods are available for compensating for this effect.

---

[9] H. W. Berry, Phys. Rev. 74, 848 (1948).

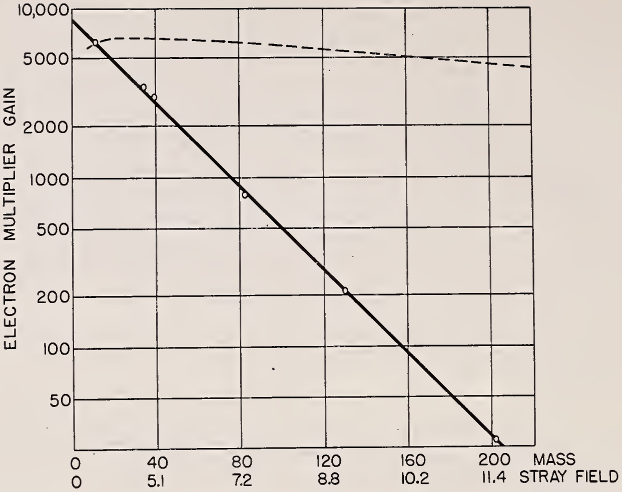

FIGURE 8. *Gain of multiplier as affected by magnetic field.*

The dotted curve shows the predicted result for negligible magnetic field.

The first is to place a magnet about the multiplier to compensate for the stray field, the second is to magnetically shield the multiplier; the authors have used both methods.

Direct Integration Recording Versus Scaler Recording

Two methods are available for recording the output of the electron multiplier. The first involves using a slow-time constant-output circuit from the multiplier followed by a d-c amplifier. The second involves amplification of the pulses obtained from the multiplier, a pulse height selector, a pulse shaper, and finally, a counting rate meter. The discriminations produced by the two methods are quite different. If a pulse height selector is used which allows all pulses to be counted, the discrimination of the over-all circuit is almost independent of the gain of the multiplier. This method of operation, however, is not practical due to noise considerations. In most cases, therefore, the pulse height selector is adjusted to detect only the major portion of the multiplier output pulses. Under these conditions the discriminations can be much more serious than in the case of direct integration.

Conclusions

Obviously in this short paper only a few of the many factors involved in optimum design of multipliers for use in mass spectroscopy have been considered. The complete unraveling of the phenomena will take a great deal of research. In spite of the briefness of the survey it is possible to draw the following conclusions: The electron multiplier can be used to increase the sensitivity of the mass spectrometer by about 1,000 times. The use of the multiplier introduces several mass discriminations not previously encountered. For isotopic work the only satisfactory method of calibration is to calibrate with a sample of known isotopic composition of the same element as that to be studied.

QUESTION: What kind of plates did you use?

INGHRAM: Silver magnesium; some of the early work was done on nichrome and some on copper.

NIER: Dr. Koch has agreed to say a few words.

J. KOCH: As a contribution to the discussion of systematic errors in the measurement of positive ion currents, I should like to report the following observation. Consider a beam of ions of high energy (60 kv) entering a deep cylindrical Faraday cup, which is closed at the bottom by a metal plate with variable potential. If the plate potential is negative (−50 v) with respect to the cylinder, the secondary electrons which are emitted due to the ion impact will leave the plate. The plate current, i_p, will be considerably larger than the current of the positive ions, i_+, entering the cup. If the plate potential is positive (+50 v), the electrons will be prevented from escaping, and one would expect to measure $i_p = i_+$. In general one finds i_p somewhat smaller than i_+, due to reflection of the positive ions. Once using a plate of tungsten we found to our surprise that i_p became negative, that is, of opposite direction of i_+. Repeated experiments showed this effect for elements such as tungsten and gold, while for aluminum and nickel the value of i_p lay between zero and i_+. The explanation which suggested itself was that the reflected ions have enough energy to liberate electrons from the wall of the cylinder. At this potential distribution, these electrons would go back to the plate and in some cases even overcompensate the incoming stream of positive ions. The reflection of ions should, in fact, be larger when the plate is made of a heavy, rather than light, metal. With an axial magnetic field, which curled up the electrons emitted from the wall of the cylinder, the plate current became positive in all cases. This same effect was observed when a cylinder with axial slots was used. The results of both of these conditions suggested the above explanation. We decided not to investigate our effect in detail at the time, since the large number of parameters may make the results difficult to evaluate. Some day we may take up the question for closer inspection. Today I just wanted to emphasize a difficulty in measuring currents of high energy ions.

COLLINS: I would like to ask Professor Bay how he prepares his multiplier plates.

Z. BAY (George Washington University): We used a four percent silver-magnesium alloy and some others used two percent. We put the plates in a vacuum at about 400° C.

QUESTION: How good a vacuum?

BAY: Not very good. It is not necessary to have a very good vacuum. It does not harm the plates. During this process the magnesium comes out to the surface and then later, in another half hour, at 430° in an oxygen atmosphere at 0.2 millimeter pressure, we oxidize this silver magnesium layer on the surface and then the plates are ready. They can be exposed to air, but I think you would be interested to know which materials or which gases spoiled such a plate. This question I cannot answer. That is an interesting question for you, but I cannot answer it. I can tell you that things are not so bad, even if you spoil the plates. You have to bake them again in vacuum, but probably you don't need to treat them again.

NIER: Would you care to comment, Dr. Bay, on the question of whether silver magnesium is to be preferred over beryllium copper?

BAY: I have never worked with beryllium copper and that is why

I cannot answer. I would be interested to know if somebody who worked with both can tell. I would be very much interested.

Question: Can someone say whether copper beryllium is better or worse than magnesium?

Inghram: We haven't found much difference between them. The silver magnesium is a little more tricky to handle. This is your procedure we are following, of course. We have a quartz system set up so we can bake these things properly at 600° C. From that standpoint the silver is a little bit harder mechanically. It is extremely soft when it is annealed. It helps some. The copper beryllium we steer clear of. It is bad from a health standpoint.

L. T. Aldrich, Carnegie Institute of Washington: I made one with beryllium copper and it worked very well. When I went to Missouri the people were interested in making one with beryllium copper. They learned from Professor Bay and the people at R. C. A. about silver magnesium, and they followed the procedure just as Professor Bay has recommended and got one the first time. This so impressed me that when we wanted one I went to Missouri, not knowing Dr. Bay was in Washington, and repeated this same process, again making a multiplier that worked the first time we tried it. The beryllium copper one I made at Minnesota worked the first time, too.

Nier: Mr. Sommer?

Sommer: I suppose this is addressed to Dr. Inghram. You showed a secondary electron ratio. On what type of target was that?

Inghram: The complete curves were for striking an activated silver magnesium target. The particular one I had was 2 per cent, not 4.

Sommer: I have one more question. You probably have one of the longest periods of experience with these. How long can you go without having to reactivate these? How often do you have to take it out?

Inghram: That multiplier has been in service, Dr. Hess—how long?

Hess: Six months, about.

Inghram: The gain in the last months—in the last four months it has not changed.

Question: Dr. Inghram, what types of ions are known for the contamination of the surface of the multiplier?

Inghram: I think Aldrich first found the worst offender in the rare gases on the surfaces. If the surface is bombarded by the rare gases, the gain drops down.

Question: Does it recover or does it stay there?

Inghram: I suppose you could recover it, but in four months the gain has not changed at all.

Question: I believe Dr. Hintenberger has made an examination.

Hintenberger: I have only made a few experiments. I have experimented with a multiplier. At first we had a great gain and then it went down. We bombard with electrons and the gain rises up, but only for electrons, not for the ions. This was only an incomplete experiment.

Nier: Dr. Bay?

Bay: Probably I could give you a suggestion in the following. It is not a characteristic of silver magnesium. For example, chromium iron can be treated in a similar manner and gives a good result, so does zinc oxide. One can use the proper material for a given spectroscopic work.

Nier: In that connection I might say that I think there really isn't a very serious contamination problem. I think that as a group mass spectroscopists have the best vacuum outside the people who make sealed vacuum tubes, for instance. They have very good vacuums and what is more, there usually isn't any opportunity for much direct bombardment because the ions go around in some angle so that there isn't a direct deposit of substance from an ion source in a multiplier.

My own feeling is that the contamination problem is not a very serious one.

Inghram: The contamination problem is only serious on the first plate of the multiplier where the ion beam hits it, and this is only a factor of a few percent. You have to calibrate and take this into account.

Nier: Dr. Aldrich?

Aldrich: I haven't learned yet, myself, but perhaps a warning that should be borrowed from the people who work with the thin films of the alkalies is that you can change the surface with sort of a layer, and if you work with these elements, you might perhaps exercise some particular care.

Nier: I believe Dr. Washburn or Dr. Berry has indicated a willingness to say a few words.

C. E. Berry: In the past, the insulating members of ion sources have usually consisted of glass or ceramic spacers and sleeves, or of more or less intricate discs or odd-shaped pieces. The problem of producing such parts is considerable, and the difficulty of obtaining accurate and stable alinement is well known.

We have recently developed a technique which is applicable to ion sources and collector systems which gets around many of the difficulties of previous methods. Briefly, the method is to use precise glass or quartz balls both as insulating spacers and for angular location of parts.

Figure 1 shows two methods of using glass balls to space and key

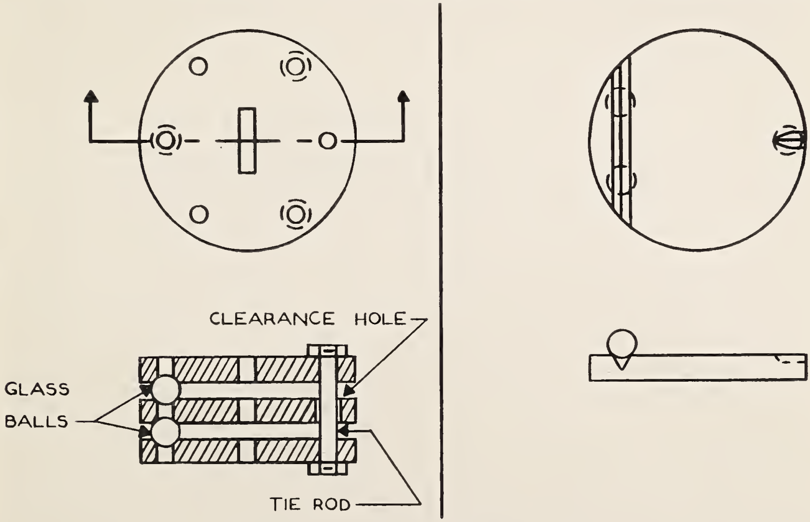

Figure 1. *Glass ball construction.*

Balls provide insulation, spacing, and axial alinement, plus easy assembly without fixtures.

together a set of plates. In the left-hand sketch, three balls are used between each pair of plates. The balls are seated in holes, the diameter of which is about 70 percent of the ball diameter. Symmetrically located with respect to the balls are three studs, which pass through clearance holes and which apply a clamping force to the structure.

Obviously, since such a system is over constrained, considerable precision must be used in the hole location and size. However, we have found that, using good tooling, this technique can be applied in either production units or experimental devices with excellent success. Basically, we are adding precision work on metal parts and eliminating precision work on fragile insulating parts, since the glass balls themselves can be purchased very inexpensively.

The right hand sketch shows a system which is not over constrained. The balls are seated in V grooves, one of which is on a chord of the disc circle and the other of which is on a diameter. The mating part, to avoid over constraint, contains no diametrical groove, but merely provides a flat surface. Two balls are placed near the ends of the chord groove, and one near the outer end of the diametrical groove. The balls can be kept from rolling in the grooves during assembly by spot welding small straps of sheet metal at the appropriate places.

There are several advantages of this method in addition to the one already mentioned. These are (1) once the system is clamped, it tends to be self-locking, so that no relative motion of parts can occur; (2) a system can be taken apart and reassembled innumerable times, without the use of fixtures, and with assurance that the alinement will be the same each time.

NIER: What kind of glass is used?

BERRY: You can get Pyrex, quartz or sapphire.

QUESTION: Do they make these balls if you furnish the glass? Will they make them from any material or are these stock items?

BERRY: I assume so. If you have only a few they will be rather expensive, perhaps a dollar apiece.

NIER: Is there any other discussion of this interesting development? Dr. Delfosse?

J. M. DELFOSSE, Universite de Louvain, Belgium: What companies supply these balls?

BERRY: The glass balls can be obtained from a number of sources. The Hartford Steel Ball Company, of Hartford, Connecticut, is a good source of supply. The balls which they produce are highly polished, are spherical to about 0.0001 in., and are graded to about 0.0001 in. on diameter. The balls can be purchased for about 20 cents apiece.

Other companies make balls of other materials such as quartz and sapphire.

NIER: Dr. Svartholm has agreed to say a few words about magnetic-field corrections, is that correct?

SVARTHOLM: I should like to mention some calculations on focusing in magnetic prisms made by Mr. R. Persson of the Atomic Energy Laboratory in Stockholm. Mr. Persson has considered various types of fields, wedge-shaped as well as circular. By the application of straight-forward methods he has constructed the locus of the foci of a point source as a function of the incident angle α. The result is shown in figure 1 in the case of a 90° sector field. To the left the distance of the focus from the field boundary is plotted as a function of α. At the value $\alpha=\alpha_0=16°$ the curve has a minimum, which corresponds to a turning point of the locus curve and represents second-order focusing. This type of focusing, which has been discussed by various authors, is known as the inflection case.

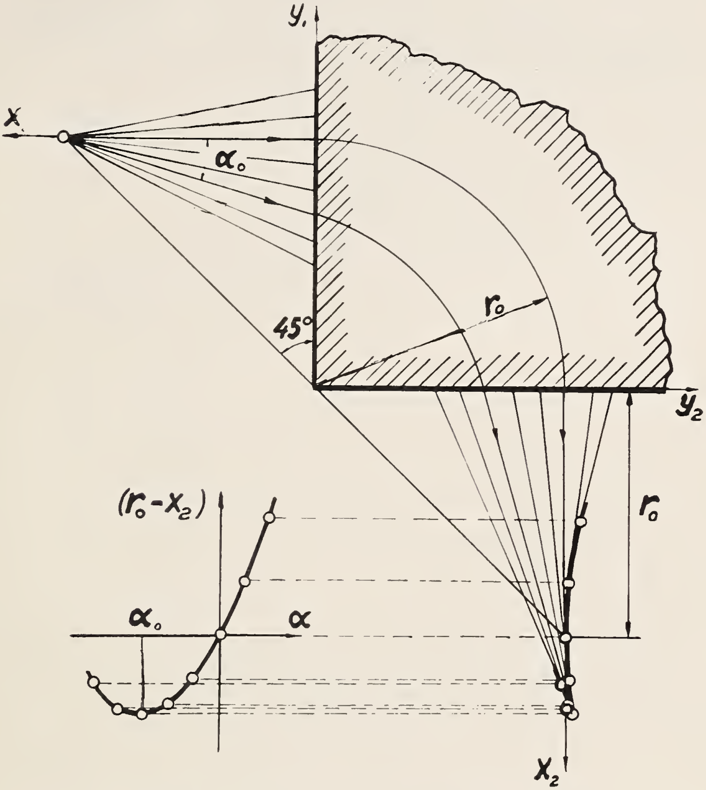

FIGURE 1. *Focusing in 90° sector field* (*Persson*).

The same graphical method applied to the case of a prism with circular boundaries gives a more symmetrical result shown in figure 2. Second-order focusing occurs now at normal incidence.

Finally, figure 3 represents a specific case of focusing in the same field and with skew incidence. The left-hand diagram indicates the occurrence of third-order focusing for $\alpha=0$.

Full details are being given by Mr. Persson in Arkiv för fysik, volume 3, number 24, 1951.

A. E. CAMERON, Oak Ridge: I wanted to ask if anybody has built an instrument using the mathematics that Kerwin published in the Review of Scientific Instruments?

INGHRAM: He built one, himself.

CAMERON: Will it work?

INGHRAM: It was published in R. S. I.

CAMERON: I built one of these, using the standard six-inch-radius tube, but with a shorter distance between source and receiver. I am not sure at the moment whether it is any better than the 60-degree.

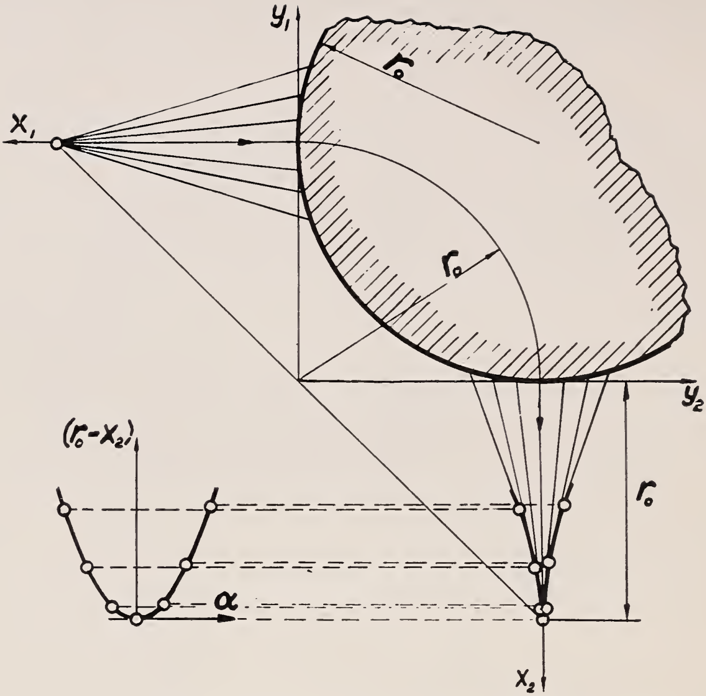

Figure 2. *Focusing with circular boundaries and normal incidence.*

I would say it is not any worse, but I am not quite happy about it. I wondered if anyone else had played with any of those.

Nier: Dr. Berry?

Berry: I have often wondered if anybody has calculated the trajectories of particles that are not on the median plane of the magnets?

Svartholm: Yes, that is being published in a paper.

Berry: Does this account for some of your descrepancies?

Svartholm: I don't know.

Nier: Dr. Herzog, you have never made calculations of that sort, the axial?

Herzog: I never made any.

Nier: Are there any other subjects that anyone would like to have discussed now?

Hayden: I had a question that perhaps some of the European people here could tell me. I have been trying to get rid of oil background in a mass spectrometer and have come to the suspicion that lots of my hydrocarbon peaks are coming from the oil in the backing pump. I am wondering if you can use another pump in back of the diffusion pump, and if so where do you get it?

Nier: Does anyone care to comment?

Question: It is not too difficult to make one.

Hayden: The thing I am worried about is a low vacuum pump.

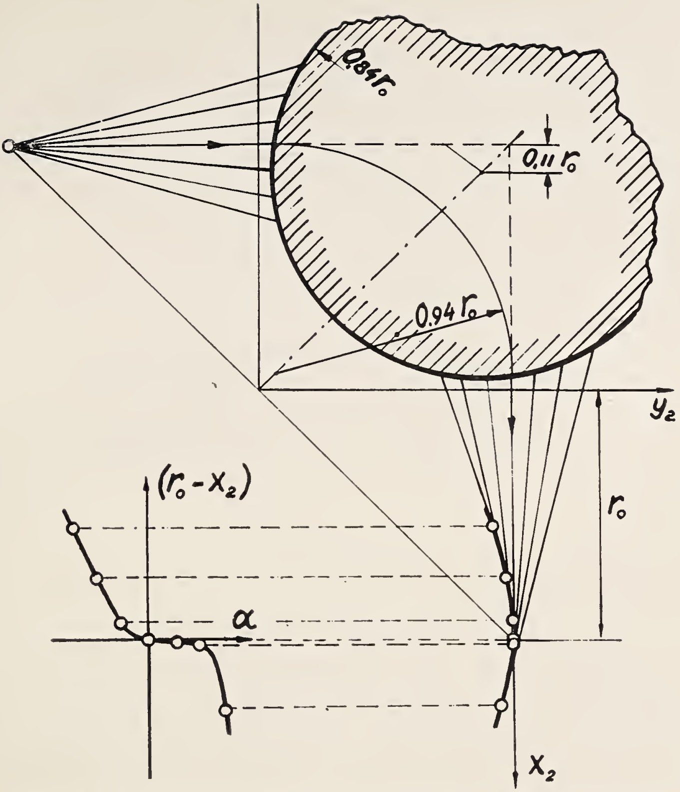

Figure 3. *Focusing with circular boundaries and skew incidence.*

Mattauch: Does anyone use molecular pumps?

Svartholm: Yes, but that has been changed.

Mattauch: It could be used for a backing pump.

Svartholm: It was used as a booster for the diffusion pump.

Delfosse: Is there anything new in the field of gasketing for high temperature?

Nier: I understand the question, but I don't know how to answer it. I know some people use gold wire.

Delfosse: That is what I know. Is there anything new?

Fox: What temperature range?

Delfosse: Well, 500 degrees.

Nier: Would anyone care to answer that question? Dr. Berry?

Berry: I don't want to answer it. I think you should repeat it for the benefit of those who did not hear it.

Nier: The question was, are there any new gasketing materials suitable for high temperatures, 500 degrees centigrade or higher.

Hintenberger: Up to 300 degrees I have used aluminum.

Nier: Dr. Inghram?

Inghram: Prof. Shaw has used gold and aluminum gaskets both up to 400 degrees. What were your results in comparison?

Shaw: We set up an experimental chamber about three inches in diameter, or three and one-half, and mounted the gaskets in this fashion and then heated the whole thing close to 400 degrees centigrade.

Walcher: Since 1941 we have been using gaskets in our mass spectrometers[1] that can be baked out. The construction is shown in figure 1. The flange *A* is furnished with a cylindrical bulge *C*, which fits into a slot *D* with a clearance of a few tenths of a mm. *C* carries a ring-shaped wedge *E*. *D* is provided with a wedge-shaped slot *F*, fitted to *E*. A silver foil (fine silver 0.1 mm. thick) is put into the slot *D*. Six or eight screws at the circumference press the silver foil between *E* and *F*, so that a high vacuum seal is attained. Even by repeated heating to 400° to 500° and cooling, the gasket remains vacuum-tight. A foil can be used 3 or 4 times. These gaskets have recently been described in detail by Hintenberger.[2] Figure 2 shows the application of the gasket to our ion source.[3]

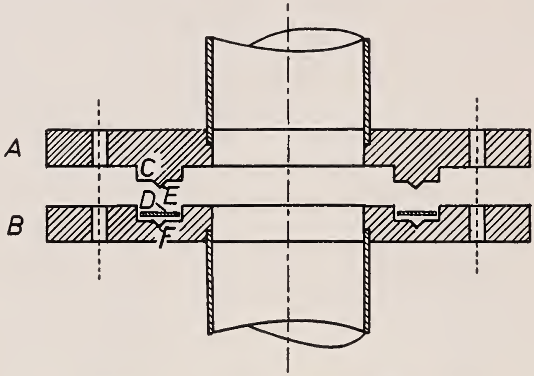

Figure 1. *Details of flange construction.*

Duckworth: Can you draw a cross section of the little piece that sticks in? Is it sharp or round?

Walcher: It is sharp.

Mattauch: It is exactly the same which Hintenberger uses with aluminum.

Walcher: That is the groove and here is the counterpart.

Question: Is that the same angle?

Walcher: The same material.

A. E. Shaw, University of Chicago: Does that work-harden?

Walcher: The silver is ductile. The silver will be pressed in between these points. If we use it a second time we can make the apparatus tighter with the screws.

Nier: How many times does it work? Three times? Four?

Walcher: Three, four or five.

Mattauch: In the case of aluminum.

Nier: Can you continue to use it?

Mattauch: Oh, no.

Nier: How deep is the dimension of that point?

Walcher: Here it is five to six millimeters and this will be 0.5 to 0.8 millimeters, I believe.

Nier: Yes.

---

[1] W. Paul, Z. Physik **124**, 244 (1948).
[2] Hintenberger, Z. Naturforsch. **6a**, 459–462 (1951).
[3] E. W. Becker, E. Dörnenburg and W. Walcher, Z. Angew. Physik **2**, 251 (1950).

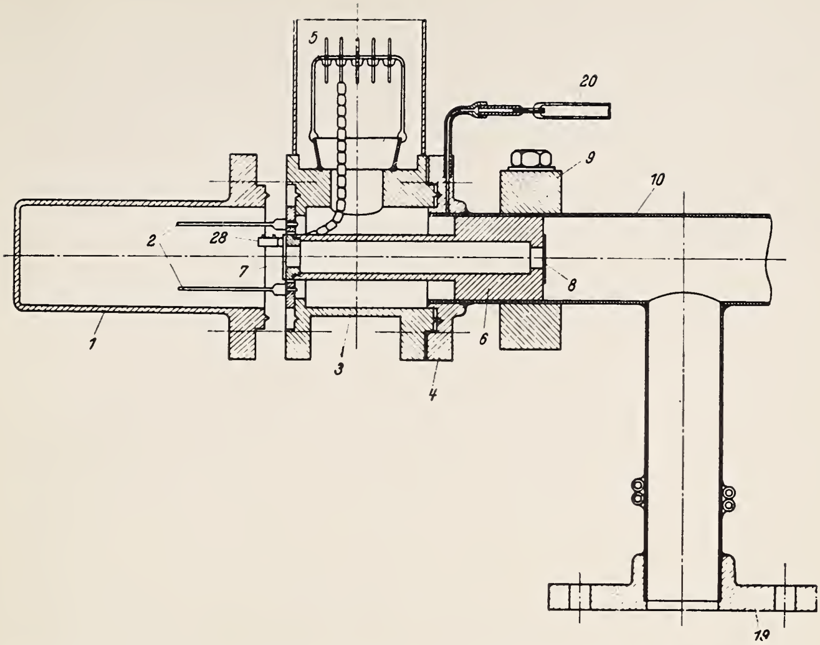

Figure 2. *Ion source housing of mass spectrometer using flange shown in figure 1.*

Fox: I would like to ask, can you take this through any number of temperature cycles? Can you take it to 500? Can you bring it back down and take it up?

Walcher: Yes. This material is resistin, copper manganese alloy.

Nier: Dr. Dibeler?

Dibeler: I was just going to say it might be practical to work out a liquid gasket. Of course, you could not turn it upside down but it is easily done with mercury. Gallium can be carried up to a high temperature and you could use that forever, I suppose.

Nier: That is interesting. Has anybody tried it?

Dibeler: We have used a glass bell jar. Very low pressures were obtained. It is no problem at all. I believe it was a gallium alloy.

Nier: I do not see Dr. O'Neal here. Oh, yes, there you are. In seeing the figures that you showed this morning, does the gallium freeze and then hold against the glass?

O'Neal: No, the gallium wets the glass. Its freezing point is about 30 degrees, I think, but it can be used as a lubricant.

Nier: I was wondering, when it cools does it expand a little so that it might seal off a glass tube?

O'Neal: We haven't tried to use it in that connection. It has been suggested that that would be an easy way to plug up a tube.

○